Impact de l'ocytocine dans le cortex piriforme antérieur et lien avec la respiration

Camille Miermon

université de BORDEAUX

THÈSE PRÉSENTÉE

POUR OBTENIR LE GRADE DE

DOCTEUR DE L'UNIVERSITÉ DE BORDEAUX

École doctorale des Sciences de la Vie et de la Santé

Spécialité - Neurosciences

Par Camille MIERMON

IMPACT DE L'OCYTOCINE DANS LE CORTEX PIRIFORME ANTERIEUR ET LIEN AVEC LA RESPIRATION

Sous la direction du : Dr. Lisa Roux
Institut Interdisciplinaire de Neurosciences de Bordeaux

Soutenue le 07 novembre 2022

Membres du jury :

M. OLIET Stéphane	DR, NCM, Bordeaux	Président
Mme. MARTIN Claire	CR, BFA, Paris	Rapportrice
M CHARLET Alexandre	CR, INCI, Strasbourg	Rapporteur
Mme MOULY Anne-Marie	CR, CRN, Lyon	Examinatrice
M. FERREIRA Guillaume	DR, INRA, Bordeaux	Examinateur
Mme MUSCATELLI-BOSSY Françoise	DR, INMED, Marseille	Examinatrice
Mme ROUX Lisa	CR, IINS, Bordeaux	Invitée

Thèse réalisée à l'Institut Interdisciplinaire des Neurosciences de Bordeaux (IINS)

146, rue Léo Saignat, 33077 Bordeaux Cedex

Equipe Olfaction et Mémoire

Impact de l'ocytocine dans le cortex piriforme antérieur et lien avec la respiration

Résumé :

La respiration est un processus hautement dynamique qui varie en fréquence et en amplitude. Ces variations sont liées à l'état émotionnel et cognitif de l'animal mais aussi au recrutement de son système olfactif pour la détection de molécules odorantes, comme c'est le cas lors d'interactions sociales entre individus. De plus, un nombre croissant de données montre que la respiration influence les rythmes neuronaux dans certaines régions du cerveau. Dans ce contexte, disposer d'un outil précis et fiable de l'activité respiratoire chez l'animal libre de ses mouvements qui soit également compatible avec des enregistrements neuronaux semble plus que jamais pertinent. Nous avons mis au point une technique d'enregistrement de la pression nasale chez la souris libre de ses mouvements et avons caractérisé ce signal en fonction de l'état de vigilance de l'animal (éveil – sommeil lent – sommeil paradoxal). Nos recherches montrent que chaque état est associé à une combinaison spécifique de paramètres caractérisant son signal respiratoire. De plus, la précision de cette technique nous a permis de mettre en évidence la présence de pauses dans ce signal (c'est-à-dire des absences transitoires de flux d'air). Ces pauses ne sont pas anodines puisque ce sont elles qui dictent la fréquence de la respiration, les autres composantes du cycle respiratoire (inhalation et exhalation) formant des unités de durée relativement fixe. Enfin, sur la base de ce signal, nous avons construit un réseau de neurones artificiels à partir de données annotées, capable de prédire l'état de vigilance d'autres souris à partir d'enregistrements de leur pression nasale.

Dans une deuxième partie de cette thèse, nous nous sommes intéressés au rôle de l'ocytocine dans le cortex piriforme au cours des comportements sociaux. En effet, l'ocytocine a été amplement décrite comme un neuropeptide pro-social qui favorise les interactions et la mémoire sociale. Chez le rongeur, l'olfaction est la modalité sensorielle principale, dont le cortex piriforme représente un substrat neuronal majeur. Le piriforme présente une anatomie semblable à celle de l'hippocampe et est impliqué dans les processus de mémoire olfactive. Parce que le cortex piriforme exprime une forte densité des récepteurs à l'ocytocine et parce qu'il reçoit des afférences

ocytocinergiques, nous avons testé l'hypothèse que l'ocytocine dans le cortex piriforme module la sociabilité et surtout la mémoire sociale. Avec une approche pharmacologique ciblée sur ce cortex, nous avons montré que l'ocytocine induit des effets subtils mais étonnants. En effet, le blocage de son récepteur entraine une augmentation sélective de certains types d'interactions sociales et semble augmenter l'attraction envers des stimuli sociaux olfactifs. Cependant, aucun effet n'a été observé dans nos conditions sur la mémoire sociale.

Enfin, dans une troisième partie nous avons commencé à disséquer les mécanismes d'action de l'ocytocine sur la physiologie du cortex piriforme. Nous montrons que l'agoniste des récepteurs à l'ocytocine entraine une diminution de la burstiness d'un sous-type de neurones excitateurs à la fois *in vitro* et *in vivo*. Nous montrons par ailleurs que l'ocytocine diminue l'entrainement des neurones du cortex piriforme par la respiration.

Mots clés :

Ocytocine, olfaction, respiration, sociabilité, mémoire sociale, piriforme

Impact of oxytocin in the anterior piriform cortex and link with respiration

Summary:

Breathing is a highly dynamic process that varies in frequency and intensity. These variations are related to the emotional and cognitive state of the animal but also to the recruitment of its olfactory system for the detection of odorant molecules, as it is the case during social interactions between individuals. In addition, a growing body of evidence shows that breathing influences brain neuronal rhythms. In this context, having an accurate and reliable tool of respiratory activity in freely moving animals that is also compatible with neuronal recordings seems more relevant than ever. We have developed a technique to record nasal pressure in freely moving mice and have characterized this signal according to the state of vigilance of the animal (awake – non-REM sleep - REM sleep). Our research shows that each state is associated with a specific combination of parameters characterizing the respiratory signal. Moreover, the precision of this technique allowed us to highlight the presence of pauses in this signal (i.e. transient absence of airflow). These pauses are not insignificant since they dictate the frequency of breathing, the other components of the respiratory cycle (inhalation and exhalation) forming units of relatively fixed duration. Finally, based on this signal, we built an artificial neural network from annotated data, capable of predicting the vigilance state of a mouse based on recordings its nasal pressure.

In a second part of this thesis, we focused on the role of oxytocin in the piriform cortex during social behaviors. Oxytocin has been widely described as a pro-social neuropeptide that promotes interactions and social memory. In rodents, olfaction is the main sensory modality, of which the piriform cortex represents a major neural substrate. The piriform has an anatomy similar to that of the hippocampus and is involved in olfactory memory processes. Because the piriform cortex expresses a high density of oxytocin receptors and because it receives oxytocinergic afferents, we tested the hypothesis that oxytocin in the piriform cortex modulates sociability and social memory. With a pharmacological approach targeted on this cortex, we showed that oxytocin induces subtle but surprising effects. Indeed, blocking its receptor leads to a selective increase in certain types of social interactions and seems to increase the

attraction towards olfactory social stimuli. However, no effect on social memory was observed under our conditions.

Finally, in a third part we started to dissect the mechanisms of action of oxytocin on the physiology of the piriform cortex. We show that the oxytocin receptor agonist leads to a decrease in the burstiness of a subtype of excitatory neurons, both *in vitro* and *in vivo*. We further show that oxytocin decreases the entrainment of piriform cortex neurons by respiration.

Key words:

Oxytocin, olfaction, respiration, sociability, social memory, piriform

Remerciements

Je souhaiterais remercier tout d'abord les membres de mon jury, Stéphane Oliet, Claire Martin, Alexandre Charlet, Anne-Marie Mouly, Guillaume Ferreira et Françoise Muscatelli-Bossy pour avoir accepté d'évaluer mon travail et pour la discussion scientifique à venir. Merci à vous.

J'aimerais dire un grand MERCI à tous les membres de l'équipe Roux passés et présents que j'ai pu côtoyer au cours de ces 4 dernières années : Edith, Pascal, Tiphaine, Aliona, Geoffrey, Giulio, Evan, Marie-Anne et bien sûr Lisa ! Un grand merci !! Je n'aurais pas pu faire cette thèse sans vous !!!!!

Je remercie Lisa d'avoir pris le pari risqué de me prendre en tant que sa première étudiante en thèse. Merci de m'avoir fait confiance ! Merci de m'avoir accueillie dans ton labo, de m'avoir soutenue, et de m'avoir appris tant de choses ! Je te souhaite plein de réussite pour la suite du labo, et vive l'ocytocine !!!

Je remercie Tiphaine très très chaleureusement. Je pense pouvoir dire sans faute que je n'aurais PAS pu faire cette thèse sans toi ! Tu as été d'un soutien sans nom, à la fois professionnellement et personnellement. Tu m'as énormément apporté et je garderais tes conseils bien en tête ! J'ai beaucoup apprécié travailler avec toi ! C'était un immense plaisir.

Je remercie Pascal, qui m'a appris une quantité de choses incroyable !! Tu as été un compagnon de bureau des plus apprécié. Je suis très contente d'avoir pu passer ces 4 ans avec toi à côté. On aura quand même bien rigolé !!!! (*C'est le clown rigolooooo*)

Je remercie Edith ! Ah mon Edith, tu manques au labo !! Pendant mes deux premières années tu as été là, et tu as aidé à façonner la scientifique que je suis aujourd'hui ! Tu m'as transmis beaucoup de ton savoir avec patience, et on a partagé beaucoup de pauses café bien nécessaires ! Je garderais en tête Paris, qui restera un de mes meilleurs souvenirs de thèse !

Je remercie Geoffrey. Couleba cousin ! Allez les bleus ! Ton énergie au labo est vraiment manquée ! On aura passé des bons moments au poste de patch. Je pense que je me rappellerais toujours de ma 1er cellule patchée ! Ton soutien scientifique et personnel est incroyable, je te souhaite vraiment que de la réussite à NY, et un beau

futur ! Après… bon courage à tes collègues qui vont subir tes chansons paillardes, et les fêtes de fin d'année qui arrivent .. Merry Xmas, Merry Xmy…

Je remercie Aliona ! Qui est toujours là 1ere à aider, et qui n'attends rien en retour. Je suis sûre que tu vas faire une excellente thèse petit padawan, et oublie pas de prendre soin de toi !! C'était un plaisir de travailler avec toi ! (Encore merci x10000 fois pour les données LMT, je t'aurais embêté avec ça !!)

I'm also thanking Giulio and Evan. The famous "Bonjour, bonjour, bonjour" of Giulio will stay with me, and I'll miss seeing Evan eat terrible salads every day. Thanks also for your support and valuable time that you gave me.

Je remercie les deux étudiantes que j'ai eu en stage : Léonie et Juliana. Vous avoir encadré a été une super expérience. Je remercie tout particulièrement Juliana, dont une partie des données sont dans ce manuscrit de thèse. Tu vois, je t'avais dit que ça serait utile ! Merci de t'être battue et d'être allée jusqu'au bout, je te souhaite pleins de bonnes choses à Toulouse.

I thank people I met from the masters to the end of this PhD and with whom I shared nice moments: Agata I, Agata N. Johannes, Giuliana, Hanna, Julio, Catherine, Anna, Tiago, Tomas, Felipe, Sylvia, Diogo, Sarah, Ashley, Marine, Dario, Aron, Sophie, Alexia, Jérémie, Valentine, Noémie, Paula, Nanci, Kjara, Urielle, Tessa...

A special thank you to Agata with whom I shared the struggles of the PhD! So happy to share my PhD day with you! I'm happy to call you my friend, and I can't wait to see what amazing life adventures are ahead of you!

I thank the gang from the Master's : Sara, Divyangana, Allison. You are brilliant ladies and I'm so proud to be your friend. You all have a bright future ahead, and you will rock it!!! Thank you for your support during this thesis.

Je remercie Remi, et les bons moments passés. Je suis désolée que le ratio livre lu / livre prêté ne soit clairement pas bon ahah, mais je te remercie pour les discussions, et le soin que tu portes aux autres ! Merci également pour tes gâteaux et tes pains délicieux !

Je remercie tout particulièrement Franck, dont les discussions nécessaires m'ont permis d'avancer dans les moments où j'étais perdue, et dont la gentillesse et les mots de sagesse restent toujours dans un coin de ma tête.

Je remercie aussi les doctorants de mon tout premier stage de Licence, Thomas et Pierre. Je ne suis restée qu'un mois dans ce laboratoire, mais j'ai appris énormément de vous, et de ce que c'était la recherche. Je me suis toujours dit que le jour où j'écrirais ma thèse, je vous remercierais ! Ce que je fais avec plaisir aujourd'hui !

Je remercie également mes amis en dehors de la science : Romain, Gabriel, Juliette, Ha-My, Léana, Elise, Anaïs, Berengère, Charlotte. Vous m'avez tous à un moment ou à un autre (voir plusieurs moments ahah) soutenue quand c'était dur. Et je suis très très fière de vous compter à mes côtés. Une petite mention spéciale pour Elise qui est en fin de thèse !! Allez Elise, si j'ai réussi à aller jusqu'à la fin, tu le peux aussi !!

Je remercie mes parents et mon petit frère, qui sont toujours là pour moi, et qui m'ont soutenue pendant ces 4 ans. Papa, maman, je vous remercie parce je n'aurais jamais pu aller si loin dans mes études si vous ne m'aviez pas soutenue dans mes choix. Cette thèse elle est aussi pour vous, et vraiment je vous remercie. Alex, ton soutien fait chaud au cœur, je te remercie pour tes petits appels et de prendre soin de moi, même à distance ! Je suis très fière d'être ta grande sœur.

Enfin, je remercie du plus profond de mon cœur Sam, sans qui je n'aurais pas fini cette thèse dans le même état…. Tu m'as supporté dans mes hauts et mes bas ces derniers mois et tu as fait preuve d'une patience infinie, je t'en suis infiniment reconnaissante. Ton aide pour la relecture a été précieuse. Tu m'apportes tellement depuis que je te connais, c'est fou ! Je t'aime très fort. Il me tarde d'avoir le temps de pouvoir profiter de toi ! J'en profite pour faire une bise chaleureuse à Céline et mamie Nicole pour leur soutien par la pensée.

A vous tous, MERCI !

Liste des abréviations

aCSF	liquide céphalo-rachidien artificiel
ADP	après dépolarisation
AMPA	α-amino-3-hydroxy-5-méthylisoazol-4-propionate
AON	noyau olfactif antérieur
AP5	acide 2-amino-5-phosphonovalerique
aPIR	piriforme antérieur
AVP	vasopressine
AVPR	vasopressine recepteur
B	cellules bitufted
BO	bulbe olfactif
BOP	bulbe olfactif principal
CA1	cornu ammonis-1
CA2	cornu ammonis-2
Ca2+	calcium
CB1	cannabinoides de type 1
CEL	cortex entorhinal latéral
DAPI	4',6-diamidino-2-phénylindole
F-I	frequence-injection
fMP	cellules multipolaires à décharge rapide
G	cellules neurogliales
H	cellules horizontales
HPC	hippocampe
HSV	valeure de saturation de l'hue
IP3	inositol-3-phosphate
I.P	injection intraperitonéale
ISI	interval entre spike
KO	knock out
LOT	tractus olfactif latéral
LCR	liquide céphalo-rachidien
LMT	live mouse tracker
mPFC	médial préfrontale cortex
MOB	bulbe olfactif principal
M/T	mitral/tufted
NaCl	chlorure de sodium
NA	noyaux accessoires
NBQX	2,3-dihydroxy-6-nitro-7-sulfamoyl-benzo-quinoxaline
NMDA	N-methyl-D-aspartate
NOA	noyau olfactif antérieur
NOSE	nez-nez
NPV	noyau paraventriculaire
NSO	noyau supraoptique
OB	bulbe olfactif
OCT	ocytocine
OCTR	ocytocine récepteur
OGEXP	orogenital de l'experimental
OSN	neurones sensoriels olfactifs
OT	tubercule olfactif

OTA	ocytocine récepteur antagoniste
OTA-L	ocytocine récepteur antagoniste L-368,899
OXT	ocytocine
OXTR	ocytocine récepteur
PFA	paraformaldehyde
PFC	cortex préfrontal
PIP_2	phosphatidylinositol 4,5-biphosphate
PIR	cortex piriforme
PKC	protéine kinase C
P-LAP	ocytocinase placentaire amino peptidase
PP	pyramidal profonde
pPIR	piriforme postérieur
PTX	picrotoxin
PV+	parvalbumine positif
PVN	noyau paraventriculaire
Ra	résistance d'accès
Ret	rétention - mémoire
Ri	résistance d'entrée
RCPG	récepteurs couplés aux protéines G
REM	sommeil paradoxal
RFID	identification radio fréquence
Rm	résistance de membrane
rMP	multipolaires à décharge régulière
ROI	région d'intérêt
RT	température ambiante
SAL	saline
SBSCT	contact cote a cote
SBSOP	contact cote a cote -opposé
SNC	système nerveux central
SL	semilunaire
SOM+	somatostatine positif
SON	noyau supraoptique
SP	pyramidal superficiel
TGOT	[Thr4,Gly7]-ocytocin
TO	tubercule olfactif
TrpC	potentiel récepteur transitoire canonique
TrpV	potentiel récepteur transitoire vanilloide
TTX	tetrodotoxin
VGLUT2	transporteur vésiculaire au glutamate

Sommaire

INTRODUCTION

1. Le système olfactif

a. Qu'est-ce que l'olfaction ?

L'olfaction est la modalité sensorielle dédiée à la détection de substances chimiques volatiles (Figure 1) (Ache and Young 2005). Ces substances, également appelées molécules odorantes, ne sont pas facilement définissables. En effet, contrairement aux stimuli auditifs ou visuels qui peuvent être mesurés à l'aide d'une seule propriété physique (i.e. fréquence ou longueur d'onde), les molécules odorantes sont généralement définies par des propriétés complexes et une appréciation subjective qui dépend de l'état émotionnel de l'individu et de son expérience olfactive (Agapakis and Tolaas 2012). La complexité de la définition d'une molécule odorante repose également sur le fait qu'une même odeur est composé la plupart du temps de dizaines de molécules volatiles de composition structurelle différente (aldéhyde, alcool, phénols...). Dans cette première partie de l'introduction, nous allons explorer comment le système olfactif traite des stimuli aussi complexes.

Figure 1: ***Photographie d'une volute composée de molécules odorantes.*** *L'odorant est composé d'un colorant fluorescent éclairé par un faisceau laser (Ache and Young 2005).*

b. L'importance de l'olfaction

Parmi les cinq sens (vue, ouïe, odorat, goût et toucher), l'odorat a longtemps été considéré comme une modalité sensorielle secondaire chez l'homme. En effet, le neuroanatomiste Paul Broca au XIX^{ème} siècle qualifia l'homme de "non olfactif". Même s'il est vrai que la taille relative du bulbe olfactif par rapport à la taille totale du cerveau est plus réduite chez l'homme par rapport aux autres mammifères, ses capacités olfactives fines n'ont été que récemment reconnues (McGann 2017). Dans ce contexte historique, il n'est pas surprenant que la recherche sur l'olfaction n'ait pas été très approfondie. Comparé à d'autres modalités sensorielles utilisées par l'homme, comme la vision ou l'audition, le nombre d'articles scientifiques sur l'olfaction est relativement faible (Hutmacher 2019). Cependant, l'olfaction attire de nos jours davantage l'attention, notamment depuis les travaux pionniers de Linda Buck et Richard Axel et à leur prix Nobel de physiologie de 2004 sur les protéines réceptrices des molécules odorantes. En raison de l'anatomie unique du système olfactif, notamment de ses connexions directes avec le système limbique, l'olfaction est fortement liée aux émotions et à la mémoire et joue également un rôle prépondérant dans les interactions sociales et la prise alimentaire (Sullivan et al. 2015). D'autre part, la perte d'odorat, également appelée anosmie, a été décrite comme un biomarqueur préclinique pour de nombreuses maladies neurologiques et neurodégénératives telles que la maladie de Parkinson, la maladie d'Alzheimer, la sclérose en plaques et la maladie de Huntington (Godoy et al. 2014 ; Marin et al. 2018), même si le lien direct entre l'atteinte olfactive et le début de la dégénérescence neurologique n'est pas encore élucidé. Il existe également un lien fort entre anosmie et dépression : 30% de personnes présentant des défauts d'olfaction sont considérées comme dépressives sur le plan clinique (Croy et al., 2014). Plus récemment, la pandémie de COVID-19 a remis l'olfaction au centre de l'attention en soulignant son importance dans la vie de chacun. L'un des symptômes les plus courant de la COVID-19 est une anosmie à court ou à long terme. Cette anosmie a été souvent associée par les personnes atteintes, à une diminution du plaisir de manger car elle affecte notre perception du goût des aliments (Oliveira et al., 2022). Dans certains cas, l'anosmie est liée à des risques accrus pour la santé mentale (Yom-Tov et al., 2021), démontrant encore une fois l'importance de l'olfaction chez l'homme.

Chez les rongeurs, l'olfaction joue un rôle primordial. Ils l'utilisent pour trouver de la nourriture et des partenaires potentiels, pour reconnaître leurs congénères et exprimer des comportements maternels, mais aussi pour naviguer dans leur environnement et sentir les dangers potentiels comme la présence de prédateurs (Ache and Young 2005; Sullivan et al. 2015). Dans le cadre de cette thèse, la caractérisation du système olfactif se concentrera sur la littérature des rongeurs.

c. Anatomie du système olfactif

Arrivée de l'odeur

Afin d'être perçues par les structures olfactives, les molécules odorantes sont d'abord transportées vers la cavité nasale. L'un des moyens d'y parvenir est la voie orthonasale via laquelle les molécules volatiles contenues dans l'air ambiant atteignent la cavité nasale par les narines lors de l'inhalation (Rozin 1982). La détection par cette voie est intrinsèquement liée au mode de respiration de l'animal (fréquence et amplitude) qui va contrôler le *timing* et la quantité de molécules odorantes dans la cavité (Youngentob et al. 1987) (voir Section 2. La respiration). Une autre façon d'atteindre la cavité nasale est la voie rétronasale, via laquelle les molécules odorantes contenues dans les aliments ou la boisson sont libérées dans la cavité buccale pendant la mastication et atteignent la cavité nasale pendant l'expiration (Rozin 1982). La perception de l'information olfactive peut être légèrement différente en fonction de la voie empruntée (Hannum et al. 2018), car l'épithélium olfactif reçoit des patrons de stimulations propres à chacune de ces voies (Small et al. 2005). Il est cependant possible que la voie rétronasale soit limitée chez les rongeurs du fait de l'anatomie même de leur cavité nasale (Zhao et al., 2004; Craven et al., 2010).

Épithélium olfactif principal

Une fois dans la cavité nasale, les molécules odorantes peuvent atteindre l'épithélium olfactif principal. Cet épithélium tapisse la voûte de la cavité nasale dont l'architecture complexe offre une grande surface de détection ressemblant aux circonvolutions du cortex de l'homme (Figure 2.A). L'épithélium olfactif est une structure pseudostratifiée qui contient, parmi d'autres cellules, des neurones sensoriels olfactifs (OSN) (Ennis et al. 2015). Ces OSN expriment sur leurs dendrites des récepteurs olfactifs et ont la particularité de n'exprimer qu'un seul type de

récepteur olfactif par OSN (Figure 2.B). Lorsqu'une molécule odorante se lie à un récepteur olfactif, un signal électrique est généré par l'OSN (Buck and Axel, 1991) et est transmis au bulbe olfactif pour un traitement ultérieur. Comme chaque substance odorante est reconnue par un ensemble spécifique de récepteurs olfactifs, le système olfactif code l'identité de l'odeur à l'aide d'un code combinatoire de récepteurs (Malnic et al., 1999). Il convient de noter que l'expression des récepteurs olfactifs est organisée en quatre zones au sein de l'épithélium olfactif, mais que ces récepteurs sont distribués de manière homogène à l'intérieur de ces zones (Ressler et al., 1993), ce qui contribue à une topographie partielle de la détection des odeurs dans l'épithélium olfactif.

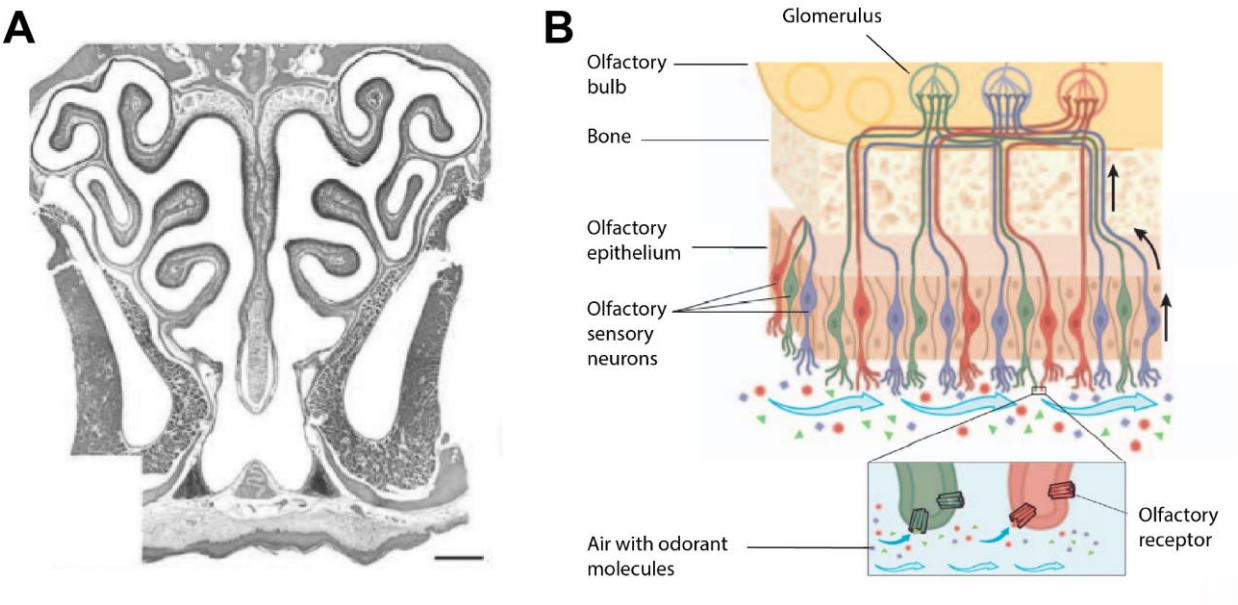

Figure 2 : ***Cavité nasale et représentation schématique de la détection des molécules odorantes dans le système olfactif. A.*** *Coloration à l'hématoxyline-éosine d'une section transversale de la cavité nasale d'une souris montrant des circonvolutions denses. Barre d'échelle = 500 µm (Modifié de (Barrios et al. 2014)).* ***B****. Représentation schématique des molécules odorantes se liant spécifiquement aux récepteurs olfactifs des neurones sensoriels olfactifs de l'épithélium olfactif. Ceux-ci envoient des projections axonales à des glomérules spécifiques d'un type de neurone sensoriel olfactif dans le bulbe olfactif (Modifié de (Rinaldi 2007)).*

Bulbe olfactif principal

Le bulbe olfactif peut être divisé en deux parties : le bulbe olfactif accessoire et le bulbe olfactif principal (BOP). Alors que le bulbe olfactif principal reçoit des projections axonales de l'épithélium olfactif principal, le bulbe olfactif accessoire reçoit

des afférences de l'épithélium olfactif de l'organe voméronasal (Rodriguez and Boehm 2008). Ces différences apparentes dans leur connectivité au niveau de l'épithélium ainsi que les résultats d'études de lésions ont permis de positionner le bulbe olfactif accessoire comme le centre de la perception des phéromones. Cependant ce dogme sur la détection des phéromones, ces puissants modulateurs des interactions intra-espèces, est remis en question par le fait qu'elles ne sont pas exclusivement détectées par l'organe voméronasal et peuvent être détectées par le système olfactif principal. De plus, le bulbe olfactif accessoire a également été impliqué dans la détection d'odeurs qui ne sont pas des phéromones (Mucignat-Caretta et al., 2012). Il apparaît donc que les rôles spécifiques de chaque structure ne soient pas aussi clairement définis qu'on ne le pensait auparavant. Dans le cadre de cette thèse, nous nous concentrerons sur la description du BOP car il est la structure d'entrée principale du cortex piriforme au cœur de mes travaux.

Le BOP est le premier relais de l'information olfactive. Comme indiqué précédemment, il reçoit des entrées des OSN de l'épithélium olfactif principal. Les OSNs exprimant le même récepteur convergent vers des modules spécifiques appelés glomérules véhiculant le même signal médié par un type de récepteur olfactif. Cette organisation en glomérules forme une carte spatiale stéréotypée et hautement organisée de l'information olfactive (Mombaerts et al., 1996; Ressler et al., 1993). Au sein des glomérules, des connexions synaptiques excitatrices sont établies entre les axones des OSNs et les dendrites des cellules *mitrales* et *tufted* (M/T) du BOP (Figure 3). Ces deux types de cellules excitatrices sont les neurones principaux de sortie du BOP : leurs axones s'assemblent pour former le tractus olfactif latéral (LOT) qui projette vers des zones de traitement supérieur de l'information. Loin d'être une simple structure de relais, le BOP façonne les informations olfactives qu'il reçoit d'abord par l'activation spécifique d'interneurones (principalement des cellules granulaires) sur les glomérules et les cellules M/T (Nagayama et al., 2014), puis par des projections *feedback* (également appelées fibres corticofugales) provenant des aires corticales sur les cellules M/T et les cellules granulaires (Strowbridge 2009).

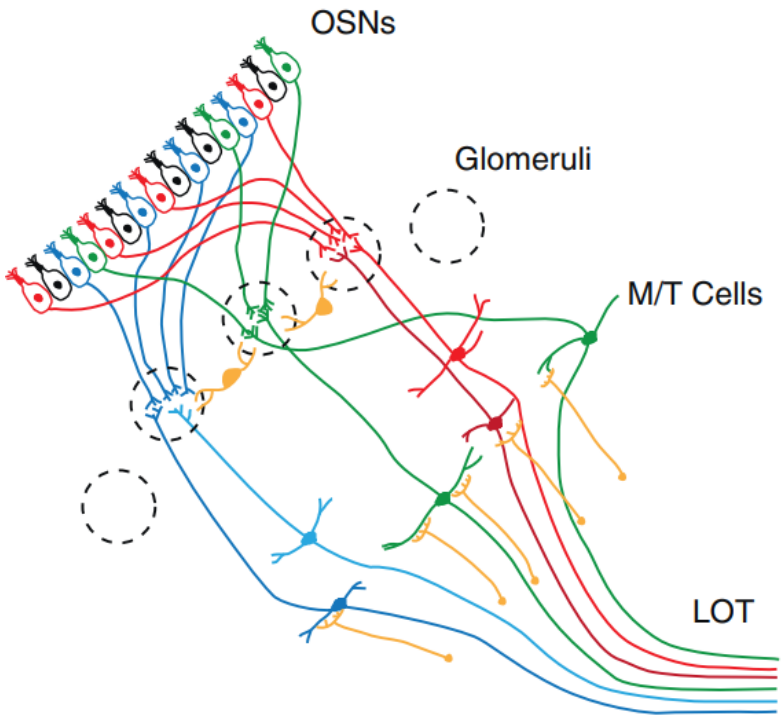

***Figure 3: Anatomie simplifiée du bulbe olfactif principal**. Les neurones sensoriels olfactifs (OSN) exprimant un seul type de récepteur envoient des axones vers des unités fonctionnelles spatiallement localisés appelées glomérules (cercles en pointillés). Les cellules mitrales et tufted (cellules M/T) du bulbe olfactif principal envoient leurs dendrites dans les glomérules et leurs axones s'assemblent pour former le tractus olfactif latéral (LOT) qui projette vers le cortex olfactif. Les interneurones (en jaune) façonnent le traitement olfactif au niveau du bulbe olfactif principal. Pour des raison de simplicité, tous les sous-types d'interneurones et les projections en feedback inhibitrices ne sont pas représentés ici (Giessel and Datta 2014).*

Le BOP envoie des projections axonales via le LOT vers les structures suivantes : noyau olfactif antérieur (NOA), tubercule olfactif (TO), partie corticale de l'amygdale, *taenia tecta*, cortex entorhinal latéral (CEL), et cortex piriforme (PIR) (Figure 4) (Haberly and Price 1977; Igarashi et al. 2012; Imai 2014). On notera l'absence de projection directe du BOP vers un relais thalamique, ce qui fait de l'olfaction un sens unique parmi les autres modalités sensorielles (Sullivan et al. 2015). Quel est l'impact de ces connections sur le traitement de l'information olfactive ?

Le rôle proposé du NOA est d'harmoniser la réponse olfactive entre les deux hémisphères grâce à ses projections feedback controlatérale vers le BOP (Brunjes et al., 2005). Le TO, avec sa dense inter connectivité avec d'autres régions cérébrales impliquées dans le traitement d'informations sensorielles, cognitives, endocrines et de

récompense, est considéré comme un centre multimodal (Wesson and Wilson 2011). L'amygdale, plus précisément son noyau cortical, est important dans les comportements innés tels que les comportements aversifs ou appétitifs (Root et al. 2014). Le CEL, avec sa connexion au gyrus denté et à la zone CA3 de l'hippocampe, est un acteur majeur pour la modulation de la mémoire liée aux odeurs (Persson et al. 2022). Enfin, le PIR formerait une représentation des « objets odorants » (Courtiol and Wilson 2017) et jouerait également un rôle clés dans la mémoire olfactive (Barnes and Wilson 2014) (Section 1.d - Rôle du cortex piriforme dans la mémoire olfactive). Il est intéressant de noter que la plupart de ces zones sont interconnectées et envoient des projections en retour au BOP. De par leur connexion directe avec le BOP, elles sont considérées comme faisant partie du "cortex olfactif".

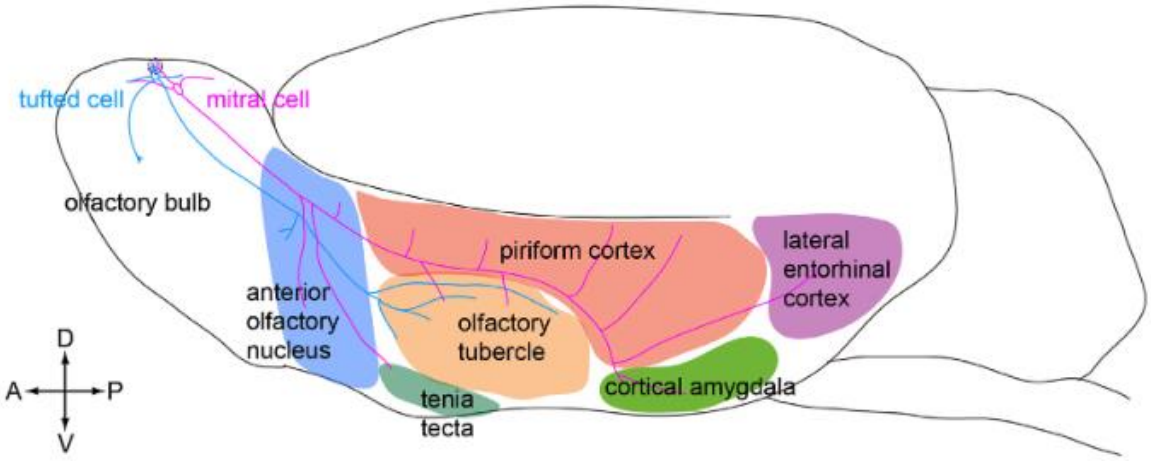

Figure 4 : ***Projections corticales des cellules mitrales et tufted du bulbe olfactif.*** *Le bulbe olfactif envoie des projections vers le noyau olfactif antérieur, le tenia tecta, le tubercule olfactif, le cortex piriforme, l'amygdale corticale, le cortex entorhinal latéral (Imai 2014).*

d. Focus sur le cortex piriforme

Anatomie du cortex piriforme

Le cortex piriforme (PIR), dont le nom provient de son anatomie en forme de poire (Gottfried 2010), représente la plus grande structure olfactive du cerveau. Il s'agit d'une structure paléocorticale à trois couches présumée être un précurseur du néocortex.

Il peut être divisé en deux parties : le PIR antérieur (aPIR) et le PIR postérieur (pPIR), divisé par l'extrémité caudale du LOT (Figure 5a) (Haberly 2001). Ces deux parties diffèrent par leurs afférences et leurs fonctions. L'aPIR est considéré comme étant plus sensible à l'information olfactive, tandis que le pPIR est plutôt considéré comme une structure associative (Calu et al. 2007). Dans le cadre de cette thèse, seul l'aPIR sera discuté par la suite.

Chaque couche (I, II, III) peut être caractérisée par une combinaison de types de cellules et d'afférences spécifiques. Certaines couches peuvent être également subdivisées en sous-couches (a,b) (Figure 5b). La couche I est la couche la plus superficielle et la plus proche de la surface ventrolatérale du cerveau. Elle est principalement caractérisée par le fait qu'elle reçoit les afférences olfactives du BOP par l'intermédiaire du LOT et qu'elle possède une population éparse de neurones (principalement des interneurones inhibiteurs). La couche II est reconnaissable grâce à la présence de ses neurones principaux densément organisés. Enfin, la couche III est caractérisée par une population éparse de neurones pyramidaux profonds (PP) et de quelques interneurones (Suzuki and Bekkers 2007).

Le PIR reçoit deux types d'entrée sensorielles. Le premier type d'entrée est constitué par les fibres sensorielles provenant du BOP qui ciblent spécifiquement la couche Ia. Le second type est constitué par les fibres associatives et commissurales provenant soit de connexions récurrentes entre les neurones du PIR, soit de connexions extrinsèques provenant d'autres zones du cerveau. Ces fibres projettent vers les couches Ib, II et III et ne se superposent pas aux fibres sensorielles du BOP (Bekkers and Suzuki 2013).

Les deux types d'entrées sensorielles sont reçus par les deux types de cellules principales du PIR : les neurones pyramidaux superficiels (SP) et les neurones semilunaires (SL). Les cellules SL ont leur soma dans la couche IIa. Elles n'ont pas de dendrites basales, mais des dendrites apicales et de grandes épines par lesquelles elles reçoivent des entrées synaptiques du BOP. En raison de leur morphologie et de leur emplacement, elles reçoivent des afférences plus fortes du BOP et sont plus sensibles aux entrées bulbaires que les cellules SP.

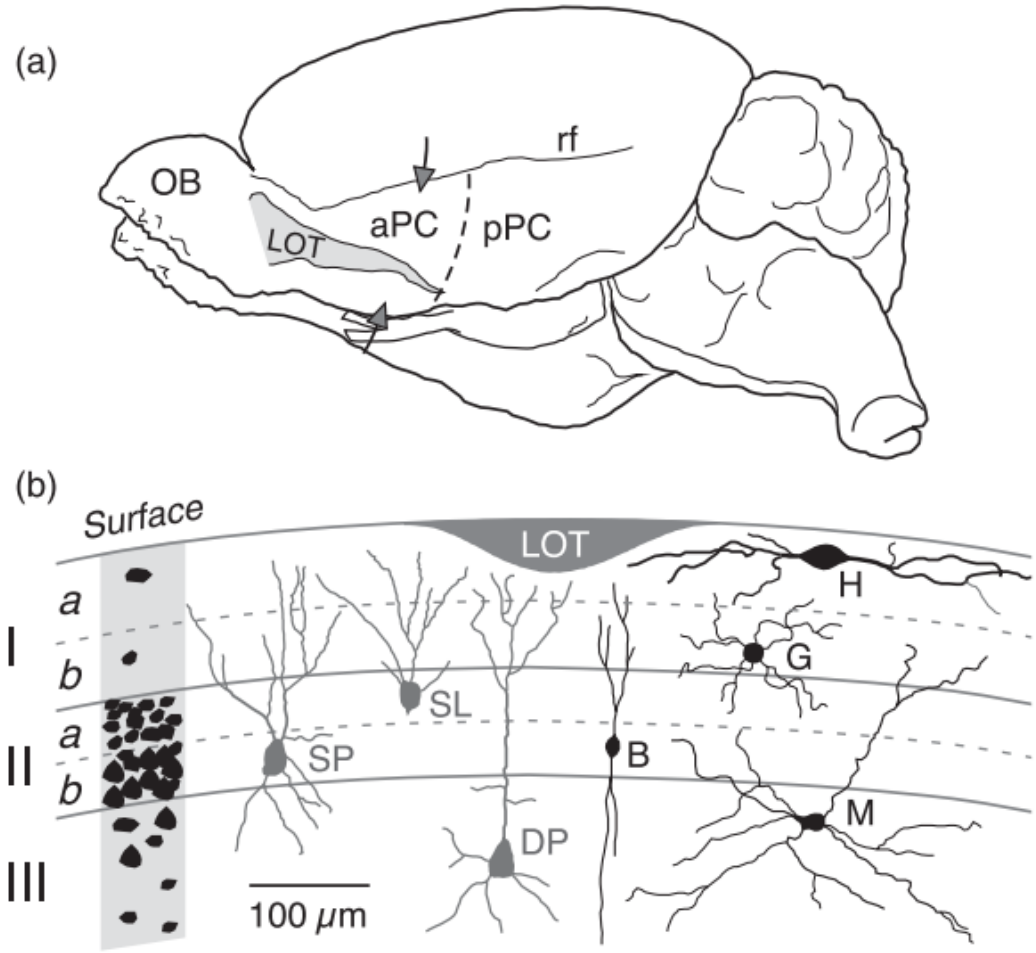

Figure 5 ***: Représentation schématique de la localisation et de l'anatomie du cortex piriforme. (a)*** *Illustration ventrolatérale du cortex piriforme dans le cerveau du rat montrant la division entre piriforme antérieur (aPC) et piriforme postérieur (pPC).* ***(b)*** *Schéma de la structure laminaire de l'aPC dans une coupe coronale à l'emplacement des flèches dans (a). L'aPC est composé de cellules glutamatergiques (SP = pyramidale superficielle, SL = semilunaire, DP = pyramidale profonde) et de cellules GABAergiques (B = bitufted, G = cellule neurogliaforme, H = cellule horizontale, M = multipolaire). OB = bulbe olfactif, LOT = tractus olfactif latéral, rf = fissure rhinale. (Suzuki and Bekkers 2007).*

En outre, les cellules SL ne sont pas facilitatrices, ne déchargent pas en *bursts* et présentent une puissante hyperpolarisation après stimulation (Suzuki and Bekkers 2006; 2011). Les cellules SP ont quant à elles leur soma dans la couche IIb. Elles ont des dendrites apicales dans la couche I et des dendrites basales s'étendant jusqu'à la couche III. Elles reçoivent à la fois des entrées du BOP, des projections récurrentes et des afférences de structures en aval (dites *top-down*). Contrairement aux cellules SL, leur activité est principalement dictée par leur connectivité locale récurrente. Ces

cellules font de la paired-pulse facilitation et émettent des *bursts* de potentiel d'action après activation (Suzuki and Bekkers 2006; 2011). Il semble donc que les cellules SL soient les principales réceptrices des entrées du BOP, tandis que les cellules SP font principalement partie de la connectivité récurrente du PIR. Des travaux récents ciblant chacun des deux types cellulaires chez des souris éveillées tête fixées en réponse à la présentation d'une odeur suggèrent que les deux types de cellules forment des canaux parallèles de traitement de l'information olfactive (Nagappan and Franks 2021), ayant des projections distinctes (Mazo et al. 2017).

L'activité du PIR est également façonnée par l'activité des interneurones. En fonction de leur profil électrophysiologique, de leur morphologie, de l'expression de marqueurs moléculaires et de leur localisation laminaire, cinq classes d'interneurones ont été décrites dans le PIR : les cellules bitufted (B), les cellules horizontales (H), les cellules neurogliales (G), les cellules multipolaires à décharge régulière (rMP) et les cellules multipolaires à décharge rapide (fMP) (Suzuki and Bekkers 2007; 2010b; 2010a). Ces interneurones couvrent toutes les couches du PIR (Figure 5b), et fournissent deux types d'inhibition : *feedforward* ou *feedback*. Les cellules H et G de la couche I, fournissent une inhibition feedforward sur les afférences provenant du BOP. Dans les couches plus profondes, les cellules G, B, rMP et fMP assurent une inhibition en feedback. Elles sont activées par les fibres associatives et inhibent les neurones principaux (Suzuki and Bekkers 2007). Franks et ses collègues ont montré que dans le PIR, l'inhibition feedback est plus forte que l'inhibition feedforward, probablement en raison de la connectivité récurrente des neurones principaux dont la force synaptique est dix fois plus élevées que les afférences du BOP (Franks et al. 2011).

Compte tenu de ce maillage complexe entre activité excitatrice et inhibitrice ainsi que de l'intégration des entrées intrinsèques et extrinsèques, comment le PIR traite-t-il les informations olfactives ?

Codage olfactif dans le cortex piriforme

Des études de traçage anatomique révèlent que les axones de glomérules individuels du BOP projettent de manière diffuse dans le PIR sans organisation spatiale apparente (Ghosh et al. 2011; Miyamichi et al. 2011; Sosulski et al. 2011) (Figure 6A). Si l'on ajoute à cela le fait que les neurones du PIR reçoivent des entrées

synaptiques convergentes de plusieurs glomérules (Apicella et al. 2010; Giessel and Datta 2014), il semble que l'organisation topographique du BOP soit complètement écartée dans le PIR. Alors comment le PIR encode-t-il les odeurs perçues ? Des expériences d'électrophysiologie et d'imagerie optique révèlent que chaque odorant active un ensemble épars de neurones distribués dans le PIR sans préférence spatiale apparente (Figure 6B) (Rennaker et al. 2007; Poo and Isaacson 2009; Stettler and Axel 2009). Ainsi, le PIR utilise un code combinatoire pour la représentation des odeurs, où chaque molécule odorante active un ensemble unique de neurones corticaux.

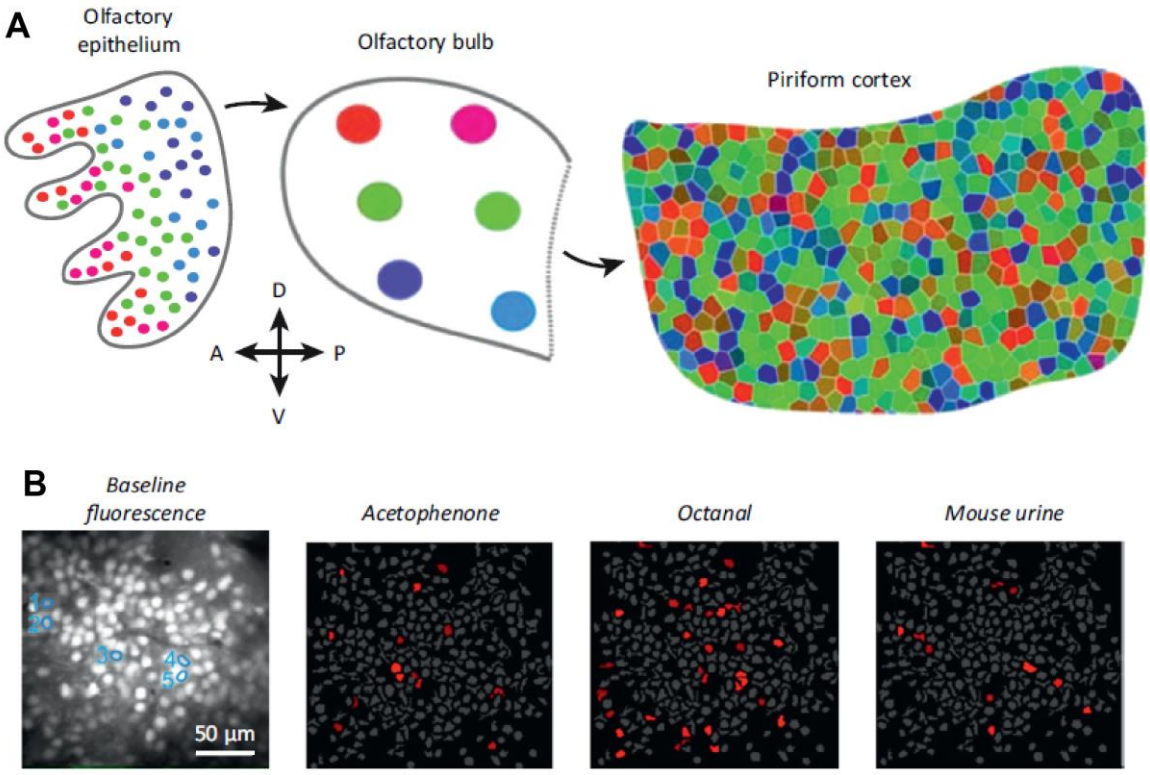

Figure 6 : ***Représentation éparse des odeurs dans le cortex piriforme. A.*** *Schéma décrivant le codage des odeurs dans le système olfactif. Les tâches de même couleur dans l'épithélium olfactif correspondent à des neurones olfactifs activés par le même récepteur olfactif. Ils projettent vers des glomérules spatialement séparés dans le bulbe olfactif qui projettent de manière diffusent dans le cortex piriforme.* ***B.*** *Réponses d'imagerie calcique fonctionnelle des neurones de la couche II du PIR à des substances odorantes chez la souris anesthésiée. La réponse à chaque odorant est éparse et ne se chevauche pas (Bekkers and Suzuki 2013). Données en B provenant de : (Stettler and Axel 2009).*

Cette capacité du PIR à coder l'identité d'une odeur repose sur l'activation et la suppression sélective de l'activité neuronale (Bolding and Franks 2017; Roland et al. 2017; Tantirigama et al. 2017). Lors de la présentation d'une odeur, le PIR présente une inhibition généralisée et une excitation éparse (Poo and Isaacson 2009). On estime qu'en réponse à une odeur, environ 15 % des cellules principales du PIR sont excitées et 15 autres pourcents sont inhibés (Tantirigama et al. 2017).

L'identité des neurones activés dans le PIR est-elle suffisante pour prédire l'identité d'une odeur ? Des études récentes se sont penchées sur cette importante question. Il semblerait que le décours temporel de l'activation des neurones du PIR ne fournisse pas d'informations supplémentaires sur l'identité de l'odeur (Miura et al. 2012; Bolding and Franks 2017). Enfin, pour que le codage de l'identité d'une odeur soit stable, la réponse du PIR aux odeurs doit être invariante à la concentration. Il se trouve que l'activité des neurones dans l'aPIR peut être inhibée par de fortes concentrations d'odeurs (Bolding and Franks 2017; Roland et al. 2017). Néanmoins, la présence d'une population invariante à la concentration dans l'aPIR (Bolding and Franks 2017; Roland et al. 2017), dépendante d'une connectivité récurrente intacte (Bolding and Franks 2019), pourrait expliquer comment l'aPIR est capable de maintenir une identité olfactive globalement stable.

Rôle du cortex piriforme dans la mémoire olfactive

Plusieurs sources indiquent que le PIR est une région du cerveau centrale pour l'apprentissage olfactif. Comme les principaux neurones du PIR reçoivent des entrées convergentes de plusieurs glomérules, on pense qu'ils encodent des "objets odorants" qui acquièrent une signification par l'expérience (Courtiol and Wilson 2017; Wilson and Sullivan 2011). Il a été démontré que l'expérience et l'apprentissage modifient la physiologie synaptique des neurones du PIR, leur excitabilité membranaire, la structure de leurs dendrites et les oscillations du réseau (Barnes and Wilson 2014; Wilson and Sullivan 2011). De plus, le PIR est impliqué dans les apprentissages associatifs avec des odeurs (Johnson et al. 2000; Roesch et al. 2006; Choi et al. 2011; Wilson and Sullivan 2011; Choe et al. 2015). L'activité du PIR est notamment nécessaire et suffisante pour l'expression de comportements guidés par la mémoire des odeurs : l'activation optogénétique d'un sous-ensemble de neurones du PIR en l'absence d'odeur est suffisante pour déclencher un comportement appris (Choi et al.

2011). En raison de son réseau dense de collatérales récurrentes, le PIR est supposé bien adapté pour réaliser de ladite « pattern completion ». Une étude élégante a montré que cette fonction est effectivement réalisée par les réseaux du PIR qui maintiennent une représentation stable d'un mélange d'odeurs y compris lorsque des composants du mélange sont omis (Barnes et al. 2008). Il est intéressant de noter que la capacité de *pattern completion* du PIR dépend de l'expérience : un entraînement comportemental visant à ignorer les différences normalement détectables entre des mélanges qui se chevauchent a permis d'améliorer la *pattern completion* dans le réseau du PIR (Chapuis and Wilson 2012). L'ensemble de ces observations suggèrent fortement que le PIR n'est pas un simple relais dans la chaîne de traitement des stimuli olfactifs mais constitue un substrat pour l'apprentissage olfactif.

Rôle du cortex piriforme dans les comportements sociaux

Des expériences utilisant l'*immediate early gene* c-Fos ont montrées que le PIR est activé pendant des interactions sociales (Ferguson et al. 2001; Kim et al. 2015) et qu'il est nécessaire pour l'apprentissage de la valence d'un stimulus social (Choi et al. 2011; Choe et al. 2015). Mis à part ces travaux, peu de choses sont connues sur le rôle du PIR pendant les comportements sociaux.

Entraînement du cortex piriforme par la respiration

De nombreux travaux ont montré que la respiration représente une importante source de modulation de l'activité neuronale dans le cerveau (Tort et al. 2018), particulièrement dans les régions olfactives dont l'arrivée sensorielle et dépendante de la respiration (Youngentob et al. 1987; Buonviso et al. 2006) (voir Section 2.a.- L'importance de la respiration pour l'activité neuronale). Plusieurs études ont investigué l'impact de la respiration sur la physiologie du PIR chez l'animal anesthésié où la respiration est lente et stéréotypée (Litaudon et al. 2003; Rennaker et al. 2007; Fontanini et al. 2003 ; Poo and Isaacson 2009). Ces études ont montré que les neurones du PIR déchargent généralement de manière couplée temporellement avec le rythme respiratoire pendant la présentation d'odeurs (Rennaker et al. 2007; Poo and Isaacson 2009) : plus de 75% de neurones du PIR répondant à une odeur sont entrainés par la respiration (Litaudon et al. 2003). De manière intéressante, les neurones du PIR spatialement proche ne déchargent pas nécessairement à la même

phase du cycle respiratoire (Rennaker et al. 2007). Il semblerait même au contraire qu'ils déchargent à des phases opposées.

Connectivité du cortex piriforme et neuromodulation

Le PIR est fortement interconnecté avec un certain nombre d'aires cérébrales dont le tubercule olfactif (TO), le bulbe olfactif principal (BOP), le cortex entorhinal lateral (CEL), le cortex orbitofrontal, le thalamus (médiodorsal) et l'amygdale (Courtiol and Wilson 2017) (Figure 7). Celles-ci peuvent moduler l'activité du PIR via leurs projections dans les couches Ib, II, III comme détaillé précédemment. Ainsi, le PIR reçoit et envoie des projections denses vers les aires olfactives, mnésiques, cognitives et limbiques. Il est intéressant de noter que certains neurones du PIR avec des marqueurs moléculaires spécifiques ciblent des zones spécifiques et prédéterminées (Diodato et al. 2016). Cela pourrait servir d'outil pour manipuler spécifiquement chaque voie de sortie dans le futur.

L'activité neuronale du PIR est également façonnée par des neuromodulateurs tels que la noradrénaline, l'acétylcholine et la sérotonine (Figure 7) (Linster 2001), produits respectivement par le locus coeruleus, la bande diagonale de Broca et le noyau du raphé. Cela est probablement lié au fait que le PIR est une structure spontanément active (Tantirigama et al. 2017). L'un des effet neuromodulateur le mieux décrit dans le PIR est celui du système noradrénergique : en modulant le réseau récurrent pendant la présentation d'une odeur, il améliore le ratio signal-bruit et augmente ainsi la réponse du PIR à la présentation d'odeurs (Bouret and Sara 2002). Récemment, le rôle d'un autre système neuromodulateur dans le PIR a été mis en évidence : le système endocannabinoïde (Terral et al. 2019). En effet, le blocage des récepteurs aux cannabinoides de type 1 (CB1) dans l'aPIR bloque spécifiquement le rappel d'une mémoire associative entre odeur et récompense. Ce blocage a été montré comme étant dépendant d'une modulation de la transmission inhibitrice.

Enfin, l'aPIR exprime des récepteurs à l'ocytocine et reçoit des afférences ocytocinergiques (Mitre et al. 2016; Choe et al. 2015). Cela soulève la question du potentiel rôle de l'ocytocine dans la modulation des circuits du PIR et son potentiel impact sur la représentation d'une odeur ou sur les souvenirs associés.

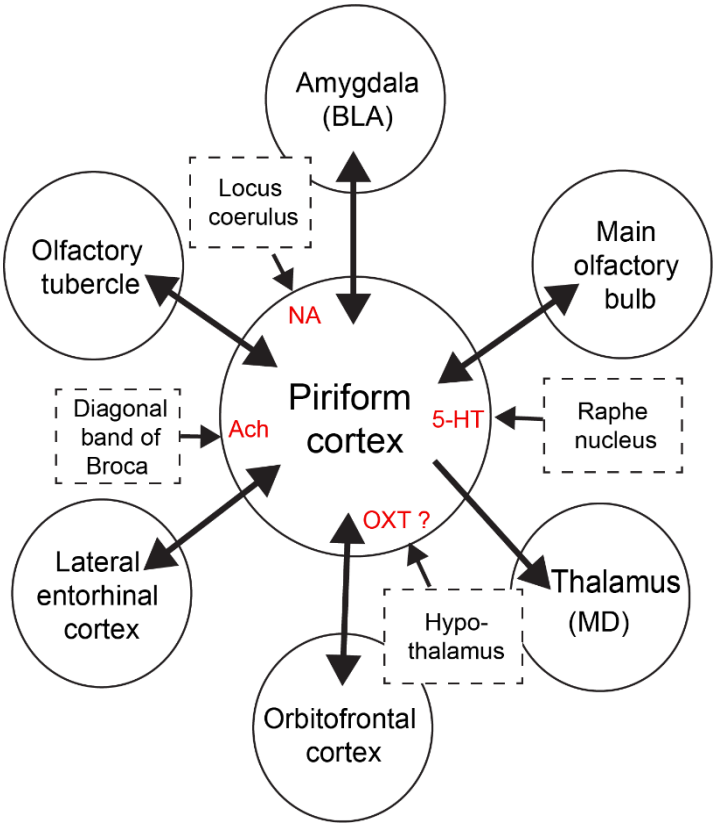

Figure 7 ***: Connectivité et neuromodulation du cortex piriforme.*** *Le cortex piriforme envoie des projections vers l'amygdale, le bulbe olfactif principal, le thalamus, le cortex orbitofrontal, le cortex entorhinal latéral, et le tubercule olfactif (cercles). La plupart de ces projections sont bidirectionnelles. Le cortex piriforme reçoit également des entrées neuromodulatrices du locus coeruleus, du noyau du raphé, de la bande diagonale de Broca (rectangles en pointillés). La présence de projections ocytocinergiques provenant de l'hypothalamus et de récepteurs à l'ocytocine dans le cortex piriforme suggère une libération d'ocytocine dans le cortex piriforme. Les doubles flèches indiquent des connexions bilatérales. Une flèche simple indique une connexion unilatérale. BLA = amygdale basolatérale, MD = médio-dorsale, Ach = acétylcholine, NA = norépinéphrine, 5-HT = sérotonine, OXT = ocytocine.*

2. La respiration

a. L'importance de la respiration …

…Pour la perception olfactive

Dans le contexte de la perception olfactive, la respiration est le mécanisme physiologique grâce auquel les molécules odorantes de l'environnement atteignent les récepteurs olfactifs dans la cavité nasale. L'augmentation de l'activité respiratoire permet que davantage de molécules odorantes atteignent le système olfactif et favorise ainsi les chances de détecter une odeur. De nombreuses études ont montré

que la respiration est un processus hautement dynamique (Welker 1964; Youngentob et al. 1987; Uchida and Mainen 2003; Kepecs et al. 2007; Verhagen et al. 2007; Wesson et al. 2008). Au repos, la respiration (également appelée *breathing*) est généralement définie par une fréquence respiratoire faible de 2 à 4 Hz. Au contraire, pendant un échantillonnage actif (la plupart du temps appelé *sniffing*), la fréquence respiratoire augmente et peut atteindre jusqu'à 12 Hz (Welker 1964; Youngentob et al. 1987; Uchida and Mainen 2003; Kepecs et al. 2007; Wesson et al. 2008). Dans ce contexte, un *sniff* (un cycle respiratoire) constitue l'unité de base de la détection active des odeurs et est analogue à un mouvement de vibrisse ou à une saccade oculaire dans les systèmes somatosensoriel et visuel, respectivement (Wachowiak 2011). Le changement respiratoire de *breathing* à *sniffing* a été décrit dans le contexte de l'exploration de nouvelles odeurs (Welker 1964; Youngentob et al. 1987; Vanderwolf 1992; Kepecs et al. 2007; Wesson et al. 2008; Shusterman et al. 2011; McAfee et al. 2016), la discrimination d'odeurs (Youngentob et al. 1987; Uchida and Mainen 2003; Verhagen et al. 2007; Courtiol et al. 2014) et les interactions sociales (Wesson 2013) qui reposent fortement sur l'olfaction chez les rongeurs.

Contrairement à ce qui a été suggéré par le passé, l'olfaction n'est pas une modalité sensorielle « lente ». En effet, un seul cycle respiratoire suffit à un rat pour réaliser une tâche de discrimination olfactive, et augmenter l'échantillonnage (le nombre de cycles) n'améliore pas substantiellement les performances (Uchida and Mainen 2003). De plus, le passage de *breathing* à *sniffing* peut se produire en un seul cycle respiratoire (Kepecs et al. 2007; Rojas-Libano et al. 2014), ce qui souligne la rapidité de la réponse motrice suite à une stimulation. Enfin, le système olfactif peut « lire » le timing des entrées olfactives au sein du cycle. En effet, des souris peuvent effectuer une tâche de type "go/no-go" en se basant uniquement sur une phase spécifique d'un cycle de *sniff* où a lieu une stimulation optogénétique de neurones OSN (Smear et al. 2011). Cela implique que le timing des entrées olfactives par rapport au début du cycle respiratoire pourrait servir d'information utile pour la perception olfactive.

Ainsi, il a été démontré que les propriétés de l'activité respiratoire modulent la perception olfactive en façonnant l'arrivée temporelle des informations olfactives dans le système olfactif.

…Pour d'autres types de comportements

De manière surprenante, des rats ayant subi une ablation du BOP continuent de renifler (Welker 1964). Cette observation implique que le *sniffing* n'est pas un mécanisme purement sensoriel. En effet, le passage de *breathing* à *sniffing* a été observé dans des contextes non olfactifs, comme lors de la présentation d'un stimulus auditif inattendu (Wesson et al. 2008) ou lors de l'attente d'une récompense (Kepecs et al. 2007). Dans cette étude, Kepecs et ses collègues rapportent que pendant l'attente d'une récompense, les rats présentent un comportement de *sniffing* à une fréquence de 9 à 12 Hz, soit une fréquence distincte de celle observée lors d'une discrimination olfactive (6 à 9 Hz). Ces résultats suggèrent que ces deux gammes de fréquences correspondent à deux processus distincts. De plus, une étude rapporte qu'une stimulation électrique des zones du cerveau impliquées dans le traitement de la récompense induit également un comportement de *sniffing* (Ikemoto and Panksepp 1994) indiquant une voie par laquelle le *sniffing* pourrait être sous contrôle cognitif.

La respiration est également modulée par l'état d'éveil et l'état émotionnel de l'animal. En effet, dans quatre états d'éveil/émotionnels différents (présentation d'une odeur, exploration de la cage, *freezing* ou sommeil), les distributions des fréquences respiratoires se sont avérées différentes (Hegoburu et al. 2011). Ces travaux ouvrent la voie à l'utilisation du mode de respiration comme un indicateur de l'état cognitif de l'animal.

Enfin, lors d'interactions sociales avec une hiérarchie établie, les individus subordonnés diminuent leur fréquence de *sniffing* lors de leur investigation par un congénère dominant et l'absence de cette diminution de fréquence de sniff entraîne des comportements agressifs (Wesson 2013) ce qui suggère que le *sniffing* peut être utilisé comme moyen de communication entre rongeurs.

En conclusion, il ressort clairement de ces études que la respiration n'est pas seulement impliquée dans les processus olfactifs mais qu'elle est également modulée dans les comportements non olfactifs tels que l'attente d'une récompense, les stimuli inattendus, l'état d'éveil et l'état émotionnel ou les interactions sociales. Cependant, hormis son rôle dans les interactions sociales, la signification comportementale de ces changements respiratoires n'est pas évidente et mériterait d'être étudiée plus profondément.

…Pour l'activité neuronale

De plus en plus d'études s'intéressent au lien entre la respiration et l'activité neuronale (Tort et al. 2018). En effet, il est désormais admis que l'activité du BO, notamment ses potentiels de champ, est entrainée par la respiration (Kay and Freeman 1998; Verhagen et al. 2007; Rojas-Libano et al. 2014; Jessberger et al. 2016; Bagur et al. 2018). Bien que l'hypothèse d'une modulation centrale (venant des centres respiratoires) ait été proposée (Ravel and Pager 1990), un grand nombre d'études indiquent que cet entraînement est dû principalement à l'activation de mécanorecepteurs présents à la surface des neurones sensoriels de l'épithélium olfactif, qui sont sensibles aux flux d'air dans la cavité nasale (Grosmaitre et al. 2007). Ce qui est de prime abord plus surprenant, c'est que d'autres régions cérébrales - olfactives et non-olfactives - sont également entrainées par la respiration (Buonviso et al. 2006; Tort et al. 2018). C'est le cas du PIR (Litaudon et al. 2003; Rennaker et al. 2007; Fontanini et al. 2003 ; Poo and Isaacson 2009), de l'hippocampe (Nguyen Chi et al. 2016), du cortex somato-sensoriel associé aux vibrisses (Ito et al. 2014) et du cortex prefrontal (Biskamp et al. 2017; Bagur et al. 2021; Karalis and Sirota 2022) notamment. Cet entrainement par la respiration peut se caractériser par la décharge de neurones à des phases spécifiques du cycle respiratoire, mais peut aussi influer sur les oscillations corticales comme les oscillations delta (Ito et al. 2014) ou les sharp wave ripples de l'hippocampe (Liu et al. 2017). Dans l'hippocampe les oscillations thêta (4-12Hz), bien que dans la même gamme de fréquence que le rythme respiratoire (2-12Hz), sont bien distinctes de la respiration (Nguyen Chi et al. 2016). Enfin, le couplage de l'activité neuronale à la respiration dans des régions distantes de l'entrée sensorielle semble fortement dépendant de la présence du BO comme l'indique le fait qu'une bulbectomie abolie l'entrainement des rythmes corticaux à la respiration (Ito et al. 2014; Liu et al. 2017; Bagur et al. 2021). Il est donc probable que l'entraînement du BO par la respiration induise une activation en chaîne des aires en aval, aboutissant à la coordination de circuits neuronaux distants (Fontanini and Bower 2006)

En conclusion, la respiration pourrait agir comme un oscillateur central, synchronisant les rythmes et ouvrant une fenêtre de dialogue entre régions corticales.

b. Comment mesurer la respiration ?

En raison de l'importance de la respiration, de multiples technologies ont été développées pour mesurer le signal respiratoire avec des degrés variables de précision, de praticité et d'invasivité. Je propose une liste non exhaustive de techniques de suivi respiratoire principalement chez les rongeurs, avec différents états de l'animal, tâches, combinées ou non à un enregistrement neuronal (Tableau 1).

Les deux principaux capteurs utilisés pour enregistrer la respiration sont les capteurs de pression et les sondes thermiques. Les sondes thermiques (thermocouples ou thermistors) ont été développées sur la base de l'observation que l'air expiré quittant le corps est plus chaud que l'air inhalé à température ambiante. Ainsi, il est possible de détecter les variations de température et d'approximer le flux respiratoire soit en implantant directement une sonde thermique dans la cavité nasale (Uchida and Mainen 2003; Kepecs et al. 2007; Wesson 2013; McAfee et al. 2016), soit en la plaçant devant les narines (Ito et al. 2014), ou en utilisant une vidéo thermique des narines (Mutlu et al. 2018). L'autre capteur principal est le capteur de pression, dont la mesure permet l'observation d'une baisse par rapport à la pression atmosphérique pendant l'inhalation, et une augmentation de la valeur de pression pendant l'expiration. Les capteurs de pression peuvent être reliés à des canules implantées dans la cavité nasale ou proche du museau des animaux en configuration tête-restreinte (Verhagen et al. 2007; Wesson et al. 2008; Shusterman et al. 2011; Smear et al. 2011) mais ils peuvent aussi être reliés à une petite chambre hermétique appelée pléthysmographe où les animaux sont introduits (Youngentob et al. 1987; Hegoburu et al. 2011; Courtiol et al. 2014). D'autres techniques ont également été utilisées pour mesurer la respiration comme l'enregistrement vidéo des mouvements des vibrisses, de la tête et du thorax (Welker 1964), l'activité oscillatoire de la muqueuse olfactive ou du bulbe olfactif (Vanderwolf 1992), ou le capteur de pression thoracique (Reisert et al. 2014).

Les mesures telles que la pléthysmographie, ou les enregistrements vidéo ont l'avantage d'être totalement non-invasives car elles ne reposent pas sur un contact physique avec l'animal (Welker 1964; Youngentob et al. 1987; Hegoburu et al. 2011; Courtiol et al. 2014; Mutlu et al. 2018). Cependant, elles manquent de précision temporelle, et ne permettent pas de détecter des changements subtils de la respiration. Au contraire, des capteurs (de température ou de pression) implantés dans la cavité nasale enregistrent la respiration à l'endroit le plus proche de l'arrivée des odeurs dans

le système olfactif (Uchida and Mainen 2003; Verhagen et al. 2007; Kepecs et al. 2007; Wesson et al. 2008; Shusterman et al. 2011; Smear et al. 2011; Wesson 2013; McAfee et al. 2016). Elles ont une détection du signal de haute-fidélité, même si par nature l'expiration est plus difficile à détecter avec les sondes thermiques en raison du réchauffement passif de la surface intranasale par le flux sanguin (Mutlu et al. 2018). Comme toute technique, elles présentent également des inconvénients. L'un des inconvénients des capteurs de pression nasale est le fait qu'ils reposent sur la perforation d'une partie de l'épithélium nasal pour l'implantation de la sonde, (bien que McAfee et al., 2016 décrivent un emplacement dans la cavité nasale sans dommage pour l'épithélium nasal), et qu'ils nécessitent le câblage des animaux. A ma connaissance, la diffusion sans fil du signal obtenu à partir d'une sonde intranasale n'a été réalisée que chez le rat pour des sondes de type thermocouples (Wesson 2013).

Le tableau ci-contre répertorie un ensemble d'études ayant eu recours à des méthodes d'enregistrement de la respiration chez le rongeur. Dans le cadre de cette thèse, les détails concernant l'état de l'animal (éveillé, tête fixée, libre de ses mouvements), les différentes tâches comportementales réalisées pendant le suivi respiratoire, les enregistrements neuronaux et les critères de respiration quantifiés ne seront pas abordés. Ce tableau permet cependant de démontrer la variété des techniques développées pour mesurer la respiration, chacune ayant ses avantages et ses inconvénients en fonction de la question scientifique que l'on souhaite aborder.

Reference	Species	Monitoring method	Animal state	Task	Neuronal recording	Criterias quantified
Welker, 1964	Rat	**Video recordings**	Freely moving	Spontaneous recording	N/A	(1) Protraction and retraction of the whiskers (2) Protraction and retraction of the tip of the snout (3) head approach and whithdrawal (4) Expiration, inspiration evaluated by thorac and abdominal mouvements
Vanderwolf 1992	Rat	**Rhythmical whisker movement and rhythmical waves in the olfactory mucosa or olfactory bulb**	Freely moving	Olfactory stimuli presentation (social- non social stimuli)	Hippocampus (DG, CA1), olfactory bulb or olfactory mucosa	Comparison of traces (hippocampus, olfactory bulb, olfactory mucosa)
Youngentob et al., 1987	Rat	**Pneumotachograph**	Freely moving	Odor detection task	N/A	Description of 52 sniff characteristics (frequency, duration of inspiratory sniff, total inspiratory volume, average total apnea duration, slope to peak for an inspiratory sniff ...)
Uchida and Mainen, 2003	Rat	**Nasal thermocouple**	Freely moving	Odor discrimination of mixture ordorants	Glomeruli activity of the olfactory bulb	1) Odor discrimination performance as a function of number of inhalation during sampling
Verhagen et al., 2007	Rat	**Nasal pressure sensor**	Awake head-fixed	Odor discrimination	Glomeruli activity of the olfactory bulb	(1) Glomeruli activity in relation to sniffing pattern (Low vs High sniff) (2) Sniffing frequency as a function of odor presentation
Kepecs et al., 2007	Rat	**Nasal thermocouple** (Chest plethysmography)	Freely moving	Odor mixture discrimination task	N/A	1) Coherence between left and right nostril and plethysmograph signals. 2) Distribution of respiration frequency during behavior 3) Duration of inhalation and exhalation 4) Timing of inhalation relative to behavior onset
Wesson et al., 2008	Mouse	**Nasal pressure sensor**	Freely moving	Exploratory behavior, odorant habituation/dishabituation, operant odor-discrimination task. Go/No-Go task	N/A	Sniffing frequency during the different behavioral trial relative to stimuli onset
Shusterman et al., 2011	Mouse	**Nasal pressure sensor**	Awake head-fixed	Spontaneous respiration during odor delivery and odor discrimination task	Olfactory bulb Mitral/Tufted cells	Mitral/Tufted cells in regard to respiration (1) Locking to inhale onset (2) Excitatory or inhibitory activity throughout sniff cycle
Smear et al., 2011	Mouse	**Nasal pressure sensor**	Awake head-fixed	Go/NoGo task during OSN optogenetic stimulation at specific sniff phase	Olfactory bulb Mitral/Tufted cells	Specific timing in the sniff cycle are used as a locking signal for optogenetic stimulation.
Hegoburu et al., 2011	Rat	**Plethysmograph** as part of the Respiration-USV-Behavior cage.	Freely moving	Spontaneous respiration during odor delivery, exploration or sleep or during fear conditioning	N/A	(a) Respiration frequency during 4 types of behaviors
ito et al., 2014	Mouse	**Thermistor** in front of nostril & chest movement	Awake head-fixed	Spontaneous recording	Whisker barrel cortex	Correlation of respiratory signal and barrel cortex (1) LFP (2) Single and multi-unit activity (3) Delta and gamma oscillation
Wesson et al., 2013	Rat	**Nasal thermocouple** fused to chronic headplug for wireless transmission	Freely moving	Social interaction in open arena	N/A	Pourcentage of sniff rate change relative to type of social interactions behavior
Courtiol et al., 2014	Rat	Whole body **plethysmograph**	Freely moving	Two-alternative choice discrimination task of odorants with similar sorption properties.	N/A	1) Inspiration and expiration duration 2) Inspiration peak flow rate
Reisert et al., 2014	Mouse	Wireless thoracic **pressure sensor** (Nasal pressure sensor)	Freely moving	Go/No-Go odorant-driven behavioral task	N/A	Comparison between the two signals of 1) Breathing frequencies 2) Timing of inhalation onset 3) Magnitude of inhalation and exhalation
McAfee et al., 2016	Mouse	**Thermistor** implanted without penetrating epithelial tissue (chest movement & plethysmography & therminstor in front of nares)	Awake head-fixed & freely moving	Spontaneous respiration pattern and during odor presentation	N/A	Comparison with the 3 signals of (1) Detection of inhalation onset (2) Phase of respiration
Mutlu et al., 2018	Mouse & Human	Infrared **thermography** (Nasal pressure sensor)	Awake head-fixed	No task. Spontaneous respiration	N/A	(1) Comparison of delay in inhalation onset detection (2)Distribution of respiration rate

Tableau 1 : ***Exemples de méthodes d'enregistrement de la respiration dans la littérature****. Ce tableau se concentre principalement sur les données relatives aux rongeurs. Dans la colonne « Monitoring method », les méthodes écrites entre parenthèse ont été utilisées comme méthodes de référence. DG = gyrus denté, CA1 = cornu ammonis 1, LFP = potentiel de champ local, OSN = neurone sensoriel olfactif, USV = vocalisation ultrasonique.*

3. Le système ocytocinergique

Historiquement, la recherche sur le système ocytocinergique a commencé par l'étude de l'hypophyse. En effet, en 1895 G. Oliver et E.A. Schafer ont découvert que des extraits hypophysaires avaient des effets vaso-constricteurs. Sir Henry H.Dale, en 1906, a ensuite rapporté que ces extraits, appliqués sur des utérus de chattes en début de gestation, entraînaient une contraction utérine. De ce fait, ce phénomène physiologique a été nommé "ocytocine", ce qui signifie "naissance rapide" en grec. Des recherches ultérieures ont conduit à l'identification de deux molécules distinctes : d'une part la vasopressine (AVP) aux effets antidiurétiques, et d'autre part l'ocytocine (OCT), responsable des contractions utérines et de l'éjection du lait. Il est désormais largement admis que les effets attribués à l'hypophyse sont liés aux neurones magnocellulaires du noyau paraventriculaire (NPV) et du noyau supraoptique (NSO) de l'hypothalamus, qui envoient des projections axonales dans la partie postérieure de l'hypophyse où ils libèrent l'OCT et l'AVP dans la circulation sanguine.

Outre les effets de l'OCT sur les organes périphériques, des études récentes ont mis en évidence un large nombre d'autres effets comportementaux et physiologiques de l'OCT engendrés par son action directe dans le cerveau. Il s'agit notamment d'effets sur les comportements sociaux tels que les comportements maternels, les comportements sexuels, et la mémoire sociale (Section 3.c Modulation par l'ocytocine des comportements sociaux et de l'olfaction), mais aussi d'effets « non-sociaux » tels que des effets anxiolytiques, analgésiques ou de modulation de la sensation de satiété (Gimpl and Fahrenholz 2001; Jurek and Neumann 2018).

a. L'ocytocine

Synthèse de l'ocytocine

L'ocytocine est un petit neuropeptide composé de seulement 9 acides aminés (Cys-Tyr-Ile-Gln-Asn-Cys-Pro-Leu-Gly) formant une structure simple composé d'un anneau associé à une queue (Figure 8). Il a été synthétisé pour la première fois par Vincent du Vigneaud en 1954 (du Vigneaud et al. 1954).

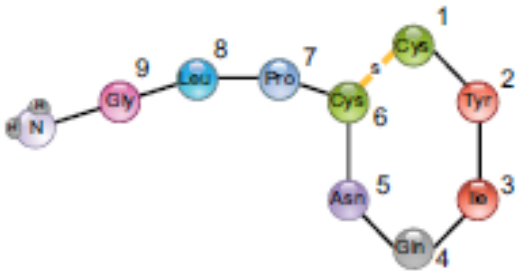

Figure 8 : ***Représentation schématique de la structure de l'ocytocine.*** *(Jurek and Neumann 2018)*

Dans le système nerveux central (SNC), l'OCT est principalement produite par le NPV, le NSO et, dans une moindre mesure, par les noyaux accessoires (NA) de l'hypothalamus (Sofroniew 1983; Swanson and Sawchenko 1983). Des zones de synthèse de l'OCT en périphérie ont également été détectées dans l'utérus, l'amnios, le placenta, les glandes surrénales, le cœur et le thymus par exemple (Jurek and Neumann 2018), mais elles ne seront pas détaillés dans le cadre de cette thèse.

Dans l'hypothalamus, l'OCT peut être produite par deux types de cellules clairement distinctes situées dans le NPV et le NSO (Figure 9) : les neurones magnocellulaires et les neurones parvocellulaires. Les neurones magnocellulaires, qui ont été les premiers à être décrits, envoient d'importantes projections axonales vers l'hypophyse postérieure (aussi appelée neurohypophyse) et des axones collatéraux vers le cerveau antérieur (Grinevich and Ludwig 2021). En revanche, les neurones parvocellulaires, plus petits, ne projettent pas vers la neurohypophyse, mais connectent le mésencéphale, le tronc cérébral et la moelle épinière (Grinevich and Ludwig 2021; Sofroniew 1983; Swanson and Sawchenko 1983) (Figure 9). Ainsi, de par leurs connexions anatomiques, les neurones magnocellulaires ont été impliqués dans des comportements tels que la lactation, les comportements maternels, le transfert émotionnel entre congénères ou les réactions de peur sociale, tandis que les neurones parvocellulaires ont été principalement associés à des réactions cardiovasculaires, à la perception de la douleur ou à la prise alimentaire (Grinevich and Ludwig 2021). Il a été démontré que les neurones parvocellulaires du NPV ciblent aussi les neurones magnocellulaires du NPV et du NSO, ce qui en fait des régulateurs potentiels de la libération d'ocytocine (Grinevich and Ludwig 2021).

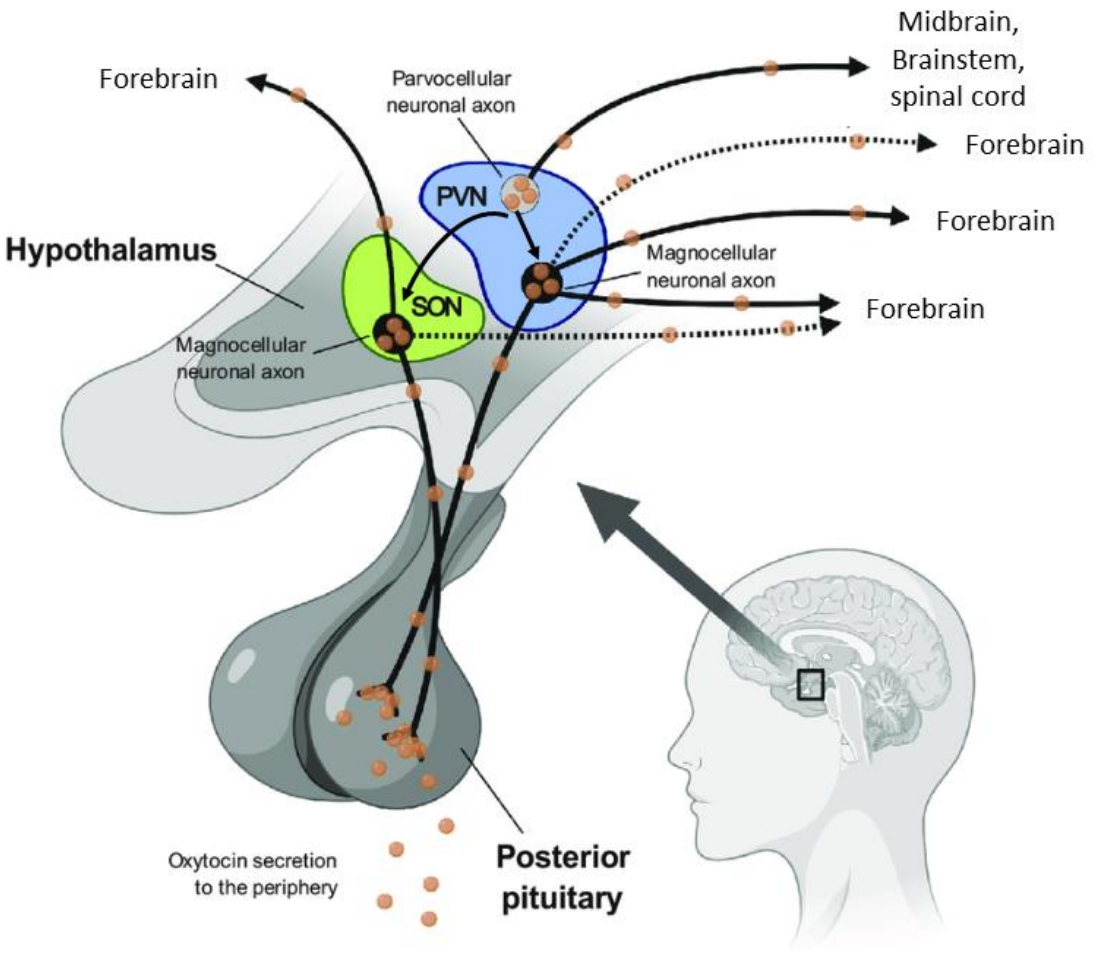

Figure 9 : ***Production d'ocytocine dans le cerveau****. Dans le NPV, l'OCT peut être produite par les neurones parvocellulaires qui projettent vers le mésencéphale, le tronc cérébral ou la moelle épinière, ou par les neurones magnocellulaires qui ciblent la neurohypophyse pour une sécrétion périphérique et envoient des axones collatéraux vers le cerveau antérieur. L'OCT peut aussi être produite par des neurones magnocellulaires du NSO qui ciblent la neurohypophyse et envoient des axones collatéraux vers le cerveau antérieur. Les neurones parvocellulaires peuvent envoyer des projections vers les neurones magnocellulaires du NPV et du NSO. Modifié à partir (Quintana and Guastella 2020). PVN = noyau paraventriculaire de l'hypothalamus. SON = noyau supraoptique.*

Au niveau cellulaire, les travaux de H. Gainer et de ses collègues ont montré que l'OCT est synthétisée sous la forme d'un précurseur protéique contenant à la fois le futur peptide OCT et la protéine neurophysine-1 qui semble être importante pour le transport et le stockage de l'OCT. Après leurs paquetages dans de grandes vésicules à noyau dense, la neurophysine-1 est clivée, et l'OCT ainsi que son précurseur peuvent être libérées dans le cerveau (Ben-Barak et al., 1985).

Libération de l'ocytocine

Les modes de libération de l'OCT dans le cerveau font encore débat (Busnelli and Chini 2017). Cependant, la voie de libération la plus reconnue est celle médiée par les neurones magnocellulaires via leurs projections axonales au niveau de la neurohypophyse qui y libèrent l'OCT dans le sang (Figure 10). Une fois dans le sang, l'OCT a une demi-vie courte, puisqu'elle est de seulement 3 à 6 minutes (Rydén and Sjöholm 1969).

Bien que les axones collatéraux des neurones magnocellulaires contenant l'OCT couvrent de longues distances et que l'OCT se retrouve dans plus de 50 régions du cerveau antérieur (Sofroniew 1983; Busnelli and Chini 2017), il existe peu de preuves que les neurones ocytocinergiques forment des synapses fonctionnelles avec d'autres neurones (Grinevich and Ludwig 2021).

Il est cependant admis que l'OCT peut être libérée par des synapses *en passant* ainsi que de manière somato-dendritique. L'ocytocine pourrait donc agir de manière paracrine, en diffusant dans l'espace extracellulaire et en activant les récepteurs ocytocinergiques (OCTR) à la fois localement dans le NPV et le NSO, ainsi que dans les zones cibles (Landgraf and Neumann 2004; Froemke and Carcea 2017; Grinevich and Ludwig 2021). Il est intéressant de noter que l'OCT elle-même, peut agir comme activateur de sa propre libération dendritique (Froemke and Carcea 2017; Grinevich and Ludwig 2021).

Un autre aspect marquant du système ocytocinergique est le fait que les dendrites et/ou les axones des neurones ocytocinergiques se trouvent en proximité immédiate du troisième ventricule (Jurek and Neumann 2018). Ajouté au fait que l'OCT a une demi-vie relativement longue dans le liquide céphalo-rachidien (LCR) (environ 20 minutes (Mens et al, 1983)), la libération dans le troisième ventricule et la diffusion dans le LCR pourraient être un autre mécanisme de transmission de l'OCT dans le cerveau.

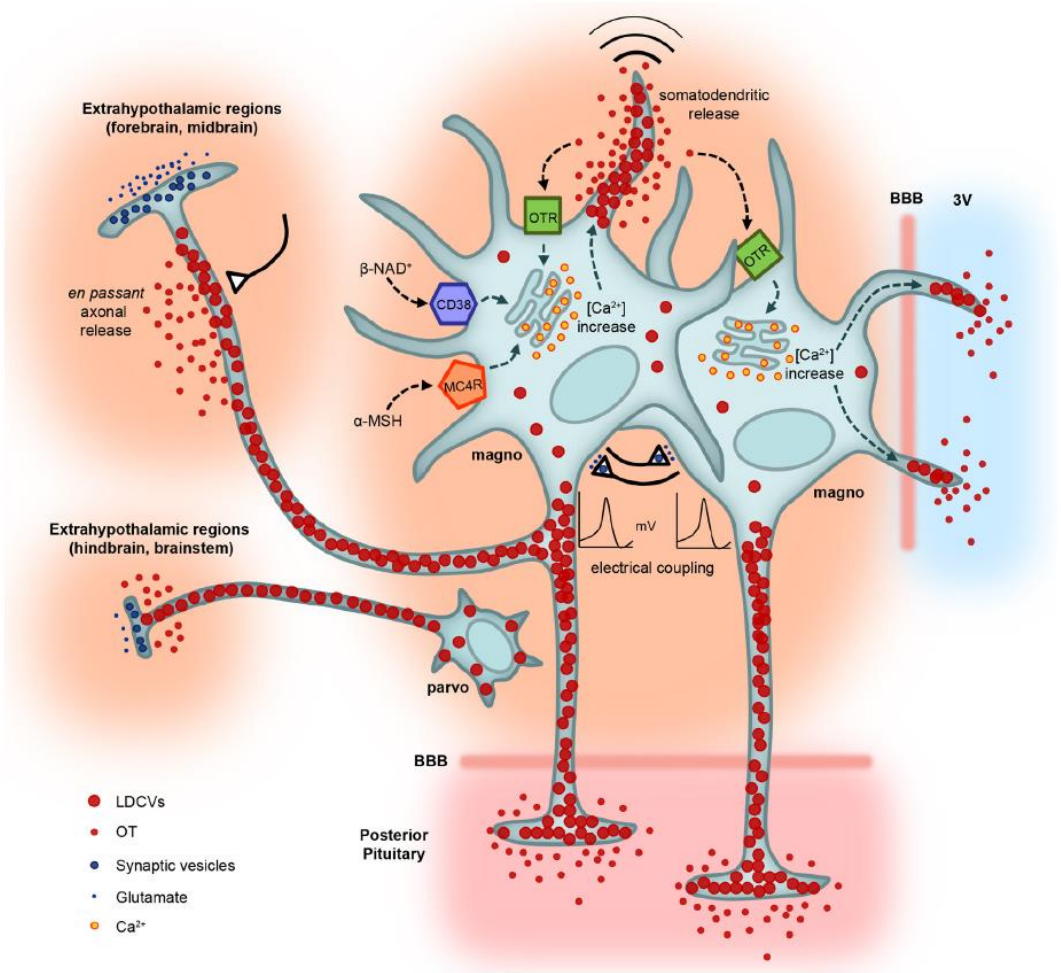

Figure 10 : ***Morphologie des neurones ocytocinergiques, leurs projections et modes de libération.*** *Les neurones magnocellulaires projettent vers l'hypophyse postérieure et vers des régions extra-hypothalamiques. Ils peuvent libérer l'OCT dans la circulation sanguine au niveau de l'hypophyse postérieure, mais aussi via une libération axonale « en passant », via une libération somato-dendritique ou par relargage dans le troisième ventricule. Les neurones parvocellulaires de plus petite taille ciblent principalement les régions extra-hypothalamiques (Johnson and Young 2017). BBB = barrière hémato-encéphalique, 3V = troisième ventricule*

L'ocytocine est-elle co-libérée avec d'autres neuromodulateurs ou neurotransmetteurs ? Il est en effet probable que l'OCT soit co-libérée avec du glutamate, comme le montre la présence de l'ARNm du transporteur vésiculaire au glutamate (VGLUT2) dans les neurones ocytocinergiques et la co-localisation observée entre VGLUT2, et des marquages d'OCT et de synaptophysine (Kawasaki et al. 2005; Knobloch et al. 2012; Grinevich and Ludwig 2021). Ces données suggèrent que l'OCT et le glutamate pourraient avoir des effets coordonnés.

Régulation des niveaux d'ocytocine

La concentration d'OCT dans le cerveau dépend de trois facteurs principaux : sa production, sa libération mais aussi sa dégradation. L'OCT est dégradée par une enzyme, l'ocytocinase placentaire amino peptidase (P-LAP). La P-LAP peut être exprimée par les neurones qui expriment les OCTR, vraisemblablement pour réguler les effets auto excitateurs potentiels de l'OCT. Ce phénomène a été mis en évidence pendant l'éjection du lait (Tobin et al. 2014) mais il semble que cette voie de dégradation enzymatique soit généralisable, car l'ocytocinase est largement exprimée dans le cerveau, du moins dans toutes les régions cérébrales exprimant le récepteur (Grinevich et al. 2016).

b. Le récepteur de l'ocytocine

Structure du récepteur de l'ocytocine

Composé d'un seul sous-type, l'OCTR est codé par un seul gène et est hautement conservé au cours de l'évolution (Gimpl and Fahrenholz 2001). Ce récepteur, dont la structure a été identifiée pour la première fois chez l'homme en 1992 (Kimura et al. 1992), appartient à la famille des récepteurs couplés aux protéines G (RCPG). Il est composé de sept hélices transmembranaires, trois boucles extracellulaires et trois boucles intracellulaires (Inoue et al. 1994) (Figure 11). Il est à noter que l'OCTR partage un ancêtre commun et une forte homologie structurelle et de séquence avec les récepteurs de la vasopressine (AVPR) (3 sous-types : V1A, V1B, V2) (Jurek and Neumann 2018).

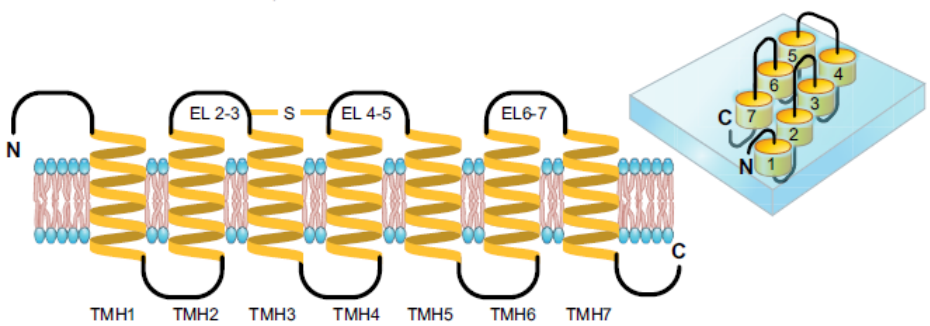

Figure 11 : ***Représentation schématique de la structure de l'ocytocine récepteur*** *(Jurek and Neumann 2018)*

La proximité structurelle entre OCTR et AVPRs a été un obstacle majeur à l'étude des OCTRs dans le cerveau. En effet, des outils très spécifiques sont nécessaires pour étudier l'OCTR sans risquer d'avoir des effets confondants sur les AVPRs. Ce n'est que depuis 2016 et les travaux du laboratoire de Robert Froemke, qu'un anticorps OCTR fonctionnel et spécifique a été produit (OCTR-2) (Mitre et al. 2016). Leur travail a montré pour la première fois des preuves convaincantes de la spécificité de leurs anticorps, notamment l'absence de marquage chez une souris OCTR KO. Avant cette étude, les anticorps disponibles dans le commerce se sont révélés largement non spécifiques (Yoshida et al. 2009). Les études antérieures avaient donc été réalisées soit sur l'ARNm de l'OCTR en utilisant des techniques d'hybridation *in situ* et d'autoradiographie (Tribollet et al. 1989; Young et al. 1997), soit en utilisant des souris rapportrices pour l'expression des OCTR combinées à des injections virales (Knobloch et al. 2012) ou à des rapporteurs fluorescents (Yoshida et al. 2009; Nakajima et al. 2014). Bien que très informatifs, ces outils n'indiquent pas nécessairement la présence de la protéine fonctionnelle.

Liaison avec le récepteur de l'ocytocine

Comme les autres RCPG, l'OCTR peut être couplé à différentes protéines G (Gq, Gi/Go), activant ainsi différentes cascades de signalisation. La nature de ce couplage est complexe : il dépend de la concentration du ligand, de l'état d'affinité du récepteur (faible ou élevé) et du type de ligand (agoniste, antagoniste, agoniste dit « biaisé »).

Busnelli et al. ont montré qu'à faible dose (correspondant aux niveaux endogènes d'OCT soit 0,59 nM), l'OCTR est préférentiellement couplé à Gq (Busnelli et al. 2013), alors qu'à forte dose, il est préférentiellement couplé à Gi/Go. Ces deux types de couplage ont des effets différentiels et la plupart du temps opposés tant sur la cellule que sur le comportement (Busnelli et al. 2012; Busnelli and Chini 2017). Ceci est particulièrement clair si l'on prend l'exemple des cellules du myomètre de rat où l'OCTR est couplé à Gq/11 chez les rates non gestantes et à Gi chez les rates gestantes, ce qui induit soit une contraction (pour Gq/11) soit une absence de contraction (pour Gi), protégeant ainsi les rates gestantes d'un travail prématuré (Zhou et al. 2007).

Il a aussi été démontré que l'état d'affinité de l'OCTR dépendait de la présence de cations divalents (zinc, magnésium, nickel, manganèse, cobalt) et de cholestérol (Busnelli and Chini 2017; Jurek and Neumann 2018). La présence de ces cations, et le regroupement du récepteur à l'intérieur de clusters de cholestérol augmentent l'affinité des OCTR pour l'OCT.

À ce jour, il n'existe qu'un seul agoniste de l'OCTR hautement sélectif et puissant chez le rat et la souris : le [Thr4,Gly7]-ocytocin ou « TGOT » (Chini and Manning 2007; Busnelli et al. 2013; Jurek and Neumann 2018). En effet, il a une affinité de plus de 10.000 fois supérieure pour l'OCTR en comparaison à l'AVPR (Busnelli et al. 2013) et a été largement utilisé dans des études *in vitro* et *in vivo.* (Zaninetti and Raggenbass 2000; Owen et al. 2013; Oettl et al. 2016; Hung et al. 2017; Tirko et al. 2018; Tan et al. 2019). Il convient de noter que deux agonistes biaisés pour l'OCTR ont été créés depuis : l'Atosiban et la Carbetocin. Bien que leur spécificité pour l'OCTR soit réduite par rapport au TGOT, ils présentent l'avantage d'activer spécifiquement les voies Gi ou Gq respectivement, ce qui permet d'étudier l'impact de chaque voie individuellement (Jurek and Neumann 2018).

Concernant les antagonistes de l'OCTR, il existe deux composés principalement utilisés : le Des-Gly-NH_2-D$(CH_2)_5$(Tyr(Me)^{2}Thr^4)-Ovt également appelé « composé d'Inga » et le L-368.899. Il a été démontré que le Des-Gly-NH_2-D$(CH_2)_5$(Tyr(Me)^{2}Thr^4)-Ovt bloque sélectivement les effets endogènes de l'OCT dans le NPV et le NSO (Neumann et al. 1994; Huber et al. 2005; Lukas et al. 2011; Knobloch et al. 2012; Marlin et al. 2015). Le L-368.899 est un antagoniste non peptidique sélectif qui présente l'avantage de traverser la barrière hémato-encéphalique (Nakajima et al. 2014; Marlin et al. 2015; Choe et al. 2015; Hung et al. 2017; Tan et al. 2019).

Cascade de signalisation du récepteur de l'ocytocine

Dans le cadre de cette thèse, le détail des nombreuses cascades de signalisation activées suite à la fixation de l'OCT sur son récepteur ne seront pas développées. Cependant l'exemple de l'activation de la voie Gq dans les neurones est présenté succinctement ci-dessous. Lors de la liaison de l'OCT sur l'OCTR, les sous-unité β/γ sont dissociées et activent la sous-unité Gαq. À son tour, la phospholipase C

est activée et l'inositol-3-phosphate (IP3) est généré à partir du phosphatidylinositol 4,5-biphosphate (PIP_2). L'IP3 induit la libération de Ca^{2+} à partir des réserves intracellulaires. Trois types de canaux sont également responsables de l'augmentation du Ca^{2+} suite à la liaison de l'OCT : les canaux canoniques TrpC (de type 1-3-4-5-6), les canaux TrpV (de type 2-4) et les canaux Ca^{2+} voltage dépendant. Cette augmentation du Ca^{2+} intracellulaire active les cascades de signalisation de la protéine kinase C et de CamKII. D'autre part, la dissociation des sous-unités de la protéine G induit l'activation de l'EGFR et la cascade des MAP kinases qui s'ensuit (Figure 12). L'activation de l'OCTR peut également moduler les canaux potassiques inward rectifying (Jurek and Neumann 2018; Busnelli and Chini 2017). En conclusion, il est largement admis que l'activation de l'OCTR induit une augmentation du calcium intracellulaire.

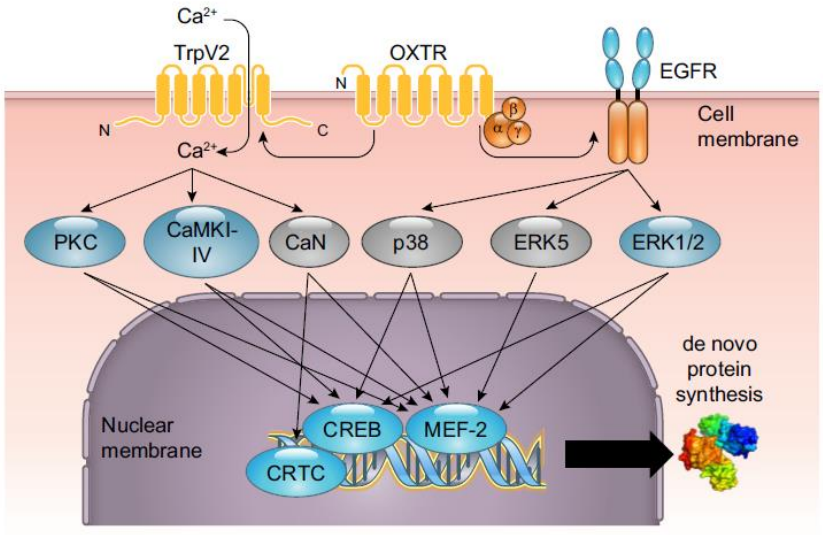

Figure 12 ***: Exemple de cascade de signalisation de l'OCTR.*** *Ca2+ = calcium, TrpV2 = transient receptor potential vanilloid type 2, EGFR = epidermal growth factor receptor, PKC = protein kinase C, CaMK = calcium/calmodulin-dependent kinase, CaN = calcineurin, ERK = extracellular signal regulated kinase, CRTC = cyclic-AMP-regulated transcriptional coactivator, CREB = cyclic AMP responsive element binding protein, MEF = myocyte enhancer factor (Jurek and Neumann 2018)*

Modulation de l'expression du récepteur de l'ocytocine

De multiples observations suggèrent une régulation de la quantité d'OCTR, notamment pendant la gestation. En utilisant la liaison d'OCT radiomarquée ([^{3}H]-OCT) sur son récepteur comme un indicateur de la concentration d'OCTR, il a été montré la présence d'un pic de liaison d'OCT dans l'utérus de rates gestantes pendant l'accouchement, et un pic dans les glandes mammaires pendant la lactation (Soloff et al. 1979). Cela va de pair avec le fait que l'utérus des souris présente une augmentation drastique de l'expression de l'ARNm de l'OCTR pendant la gestation (Kawamata et al. 2004). Dans cette même étude, aucune différence dans l'ARNm de l'OCTR n'a été observée entre les phases d'œstrus et de dioestrus du cycle ovarien, bien que la contraction utérine induite par l'OCT n'ait été observée qu'en dioestrus. Cette observation suggère que les niveaux d'ARNm de l'OCTR ne sont pas toujours corrélés avec l'impact physiologique de l'OCT. Qu'en est-il de la modulation des niveaux d'OCTR dans le cerveau pendant la gestation ? En utilisant l'anticorps OCTR-2 ou des méthodes de détection de l'ARNm de l'OCTR, des spécificités en fonction des régions cérébrales ont été observées (Young et al. 1997; Mitre et al. 2016), certaines régions présentent une augmentation, une diminution ou aucun changement de l'expression des OCTR pendant la gestation. Il est intéressant de noter que Mitre et ses collègues n'ont observé aucune différence dans les niveaux d'expression de l'OCTR dans le NPV ou dans le cortex auditif au cours du cycle ovarien.

Le niveau d'expression de l'OCTR est également régulé par la quantité d'OCT qui se fixe sur celui-ci. En effet, dans les cas où des niveaux élevés d'OCT sont induits, que ce soit lors d'une administration ponctuelle ou dans le cas d'administrations quotidiennes, le récepteur peut se désensibiliser et ensuite être internalisé (Busnelli and Chini 2017).

En conclusion, l'expression de l'OCTR est régulée et dépendante de la présence de stimuli externes et internes.

Type de cellule et localisation subcellulaire de l'ocytocine récepteur

Jusqu'à présent, l'expression de l'OCTR a été localisé dans les interneurones GABAergiques du medial prefrontal cortex (mPFC) (Nakajima et al. 2014), du cortex auditif (Marlin et al. 2015), du septum latéral (Menon et al. 2018) et de la région CA2 de l'hippocampe (Tirko et al. 2018; Young and Song 2020). Dans d'autres cas, même si une co-localisation de l'OCTR avec des marquages d'interneurones n'a pas été mise en évidence, il a été démontré que les interneurones sont modulés par l'OCT. C'est par exemple le cas dans la région CA1 de l'hippocampe (Owen et al. 2013) et le noyau central de l'amygdale (Huber et al. 2005, Knobloch et al. 2012). En comparaison, l'expression du récepteur dans des cellules pyramidales excitatrices a été plus rarement décrite, excepté dans la région CA2 de l'hippocampe (Tirko et al. 2018; Liu et al. 2022) et dans le noyau olfactif antérieur (Oettl et al. 2016). Bien que l'ensemble de ces observations suggèrent que l'OCT agit principalement sur la transmission inhibitrice, ceci-reste donc fortement dépendant de la région du cerveau considérée. Cependant, une résolution subcellulaire est nécessaire pour disséquer plus en détail les mécanismes d'action de l'OCT.

Grâce à l'anticorps spécifique OCTR-2, l'expression des protéines au niveau subcellulaire a récemment été identifiée pour la première fois (Mitre et al. 2016). En utilisant la microscopie électronique chez des souris femelles vierges dans le cortex auditif, le marquage OCTR-2 a été observé dans des synapses supposées excitatrices à la fois à la pré-synapse et à la post-synapse, dans les segments dendritiques ainsi qu'en périsomatique dans les synapses inhibitrices. Ces observations impliqueraient que l'OCT peut agir à la fois sur la transmission excitatrice et inhibitrice dans le cortex auditif, mais il reste à confirmer si ces observations sont généralisables à d'autres régions du cerveau.

Il est intéressant de noter que l'OCTR n'est pas seulement présent dans les neurones, mais est aussi exprimé dans les cellules gliales (Yoshida et al. 2009; Mitre et al. 2016) où il pourrait jouer un rôle beaucoup plus important que ce qui a été établi précédemment. En effet, Wahis et al., ont récemment démontré que l'OCT agit sur l'OCTR dans une sous-population spécifique d'astrocytes dans l'amygdale centrale et médie ainsi les effets anxiolytiques du neuropeptide dans cette zone (Wahis et al. 2021). Cela ouvre la porte à une vision plus complexe de la modulation de la

transmission neuronale par l'OCT, où les cellules gliales joueraient également un facteur déterminant.

Impact physiologique de la modulation de l'ocytocine récepteur

Quel est l'impact de l'OCT sur la physiologie neuronale ? En utilisant une combinaison d'études en électrophysiologie *in vitro* et *in vivo*, il a été démontré que l'OCT module la transmission inhibitrice dans plusieurs régions du cerveau (Zaninetti and Raggenbass 2000; Huber et al, 2005; Owen et al. 2013; Marlin et al. 2015; Mitre et al. 2016; Tirko et al. 2018). Ceci est en accord avec l'observation mentionnée ci-dessus selon laquelle l'OCTR est principalement exprimée dans les interneurones GABAergiques. De plus, il a été démontré que l'application de TGOT (agoniste de l'OCTR) sur des tranches de cerveau dépolarise des interneurones à décharge rapide (de type parvalbumine positifs – PV+) dans CA1 et CA2 (Zaninetti and Raggenbass 2000; Owen et al. 2013; Tirko et al. 2018) ainsi que des interneurones à décharge régulière (positifs pour la somatostatine - SOM+) dans le mPFC (Nakajima et al. 2014). Enfin, la libération d'OCT via des stimulations optogénétique dépolarise les neurones du noyau centro-latéral de l'amygdale, qui est principalement composé de cellules GABAergiques (Knobloch et al. 2012). Comment ces effets sur l'activité neuronale influent-ils sur la transmission synaptique ?

L'application de TGOT dans l'hippocampe CA1 (Owen et al. 2013) ou la libération endogène d'OCT dans le cortex piriforme (PIR), le NPV et le cortex auditif. (Mitre et al. 2016) diminue rapidement l'activité inhibitrice évoquée. Cette activité réduite, est également observée en présence des antagonistes des récepteurs au glutamate, AMPA et NMDA, dans le cortex auditif et le NPV, suggérant que l'impact de l'OCT est indépendant de la transmission excitatrice dans ces régions : il s'agirait donc d'un effet direct sur les interneurones GABAergiques. Ce n'est cependant pas le cas dans le PIR, ce qui implique que la modulation de la transmission inhibitrice évoquée dans le PIR par l'OCT pourrait fonctionner différemment, de manière indirecte, en reposant sur une modulation des cellules excitatrices.

Il semblerait que cette modulation de l'activité évoquée par l'OCT soit différente de sa modulation de l'activité spontanée. En effet, l'activité spontanée est réduite dans les

cellules pyramidales de CA1 en présence de TGOT (Owen et al. 2013) et les courants post-synaptique inhibiteurs spontanés sont augmentés dans le NPV, le cortex auditif et le PIR (Mitre et al. 2016). Cet effet combiné de l'OCT à diminuer l'inhibition évoquée, mais à augmenter l'inhibition spontanée, implique que l'OCT améliore le rapport signal/bruit de la transmission synaptique. L'OCT favoriserait donc une inhibition tonique à l'état basal mais induirait une désinhibition rapide en présence de stimuli, ce qui améliorerait le transfert d'informations (Owen et al. 2013; Mitre et al. 2016). Parce que l'OCT est un modulateur des comportements sociaux, cette modulation de la transmission synaptique en présence d'un stimuli, serait spécifique aux stimuli sociaux et améliorerait la *salience* de ceux-ci (Shamay-Tsoory and Abu-Akel 2016).

Un excellent exemple de l'impact *in vivo* de l'OCT, à la fois sur la neurophysiologie et sur le comportement, a été mis en évidence dans le cortex auditif de souris femelles, au cours/suite aux vocalisations des souriceaux (Marlin et al. 2015). Chez les mères, ou les femelles vierges qui sont devenues expertes dans la récupération des petits dites « expérimentées », l'activité de décharge des neurones augmente de manière très robuste en réponse aux appels des petits. Dans le cas des vierges naïves (qui n'ont pas encore appris à récupérer les petits), l'activité dans le cortex auditif est réduite et plus variable. Cela va de pair avec une coordination précise de l'inhibition et de l'excitation chez les mères et les femelles expérimentées, que l'on ne retrouve pas chez les vierges naïves. En jouant sur l'équilibre inhibition/excitation dans le cortex auditif, l'OCT modulerait la transmission de l'information, ceci étant peut-être à l'origine de l'augmentation des performances au regard des comportements maternels.

Un autre exemple pertinent a été décrit dans le noyau olfactif antérieur (NOA) (Oettl et al. 2016). L'activation de l'OCTR dans le NOA augmente les afférences excitatrices reçues par les cellules granulaires du bulbe olfactif (BO) qui inhibent ensuite les cellules mitrales (cellules principales du bulbe). Cette activation des OCTR du NOA *in vivo* augmente le rapport signal/bruit de la réponse olfactive dans le bulbe en abaissant l'activité basale (en absence de stimuli) et en augmentant le pic des réponses. Via ce mécanisme, l'OCT dans le NOA pourrait agir sur la modulation *top/down* précoce du traitement des signaux olfactifs au niveau du BO.

Enfin, il est intéressant de noter l'exemple à part de la région CA2 de l'hippocampe, une région connue pour son rôle dans la mémoire sociale (Hitti and Siegelbaum, 2014). En effet, les travaux récents de Tirko et ses collègues ont montré que les cellules pyramidales deviennent *bursty* en présence de TGOT. L'impact comportemental de ce profil de décharge en *burst* dans CA2 n'est cependant pas encore connu (Tirko et al. 2018).

Projections des fibres ocytocinergiques et expression de son récepteur dans le cerveau

En raison du nombre croissant d'études montrant que l'OCT module de nombreuses régions cérébrales, des efforts importants ont été déployés pour caractériser l'expression des OCTR et/ou des fibres ocytocinergiques dans l'ensemble du cerveau (Yoshida et al. 2009; Knobloch et al. 2012; Mitre et al. 2016; Inoue et al. 2022; Son et al. 2022). La première observation issue de ces études est que l'OCTR est largement exprimé dans le cerveau des rongeurs, ce qui démontre une fois de plus que le système ocytocinergique peut avoir un impact considérable sur l'activité du SNC. Une autre observation intéressante, est **qu'il peut y avoir une absence de correspondance entre l'expression des OCTR et la présence de fibres ocytocinergiques,** avec certaines régions qui expriment des OCTR mais qui ne semblent pas recevoir de fibres ocytocinergiques, comme c'est le cas dans le bulbe olfactif (Figure 13) (Mitre et al. 2016; Grinevich et al. 2016; Busnelli and Chini 2017; Son et al. 2022). Cette inadéquation est cohérente avec l'hypothèse selon laquelle l'OCT serait libérée au niveau somatodendritique et diffuserait ensuite dans le parenchyme cérébral. Cependant, Knobloch et ses collègues ont montré que chez des rates allaitantes, chez lesquelles le marqueur fluorescent Venus était exprimé sous le contrôle du promoteur de l'OCT, des axones ocytocinergiques pouvaient être détectés dans toutes les principales régions du cerveau antérieur, y compris dans des structures dont on pensait auparavant qu'elles étaient dépourvues de fibres ocytocinergiques (Knobloch et al. 2012; Grinevich et al. 2016). Il est donc possible qu'en raison de la dépendance du système ocytocinergique au regard de l'état physiologique de l'animal, certaines fibres soient passées inaperçues parce qu'elles ne contenaient pas une quantité suffisante d'OCT pour être détectées (Grinevich et al. 2016).

La libération axonale d'OCT pourrait alors avoir une place plus importante que précédemment décrite.

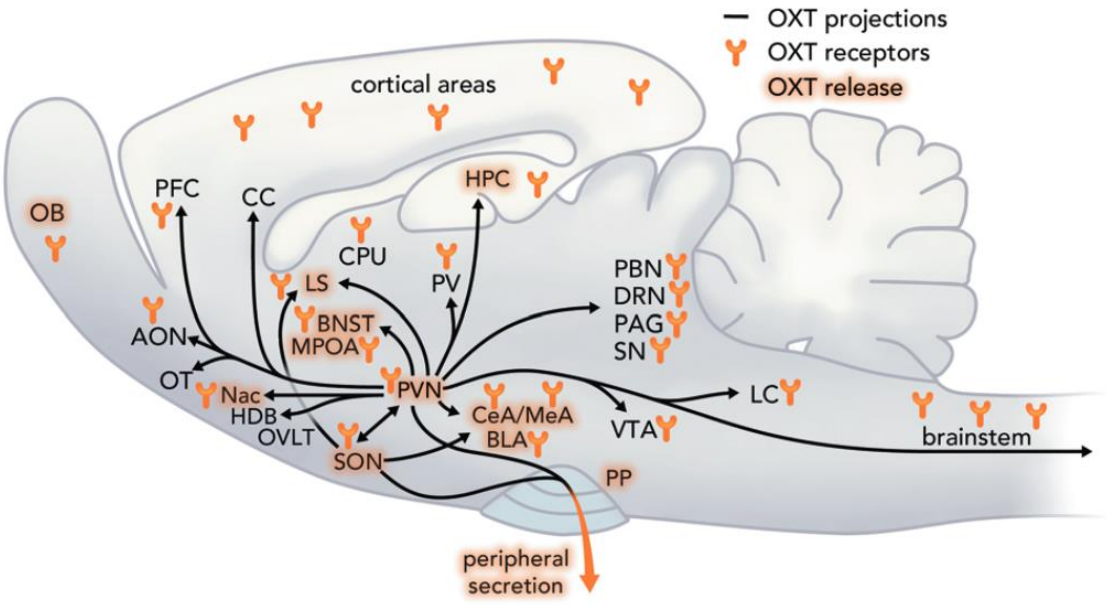

Figure 13 : ***Vue sagittale d'un cerveau de rat montrant les projections, les récepteurs et la libération de l'ocytocine****. AON noyau olfactif antérieur, OB bulbe olfactif, OT tubercule olfactif, Nac noyau accumbens, OVLT organum vasculosum laminae terminalis, SON noyau supraoptique, PVN noyau paraventriculaire, PP hypophyse postérieure, PFC cortex préfrontal, CC cortex cingulaire, MPOA aire préoptique médiane, BNST noyau du lit de la stria terminalis, LS septum latéral, CPu caudate putamen, PV noyau périventriculaire du thalamus, CeA amygdale centrale, MeA amygdale médiale, BLA amygdale basolatérale, VTA aire tegmentale ventrale, LC locus coeruleus, PBN noyau parabrachial, DRN noyau du raphé dorsal, PAG gris périaqueducal, SN substantia nigra, HPC hippocampe, HDB noyau de la branche horizontale de la bande diagonale (Grinevich and Neumann 2021).*

Ocytocine récepteur dans les systèmes sensoriels

Le patron d'expression des OCTR dans le cerveau peut donner des informations quant au rôle de l'OCT sur plan comportemental. En effet, loin d'être aléatoires, les variations inter-espèces dans les comportements sociaux semblent être liées à des différences dans l'expression du récepteur dans les systèmes sensoriels (Grinevich et al. 2016). Les primates utilisent la vision comme un sens primordial, et les OCTR sont densément exprimés dans les zones de traitement de l'information

visuelle et de l'attention, comme le noyau basal de Meynert et le colliculus supérieur (Freeman and Young 2016). Chez les oiseaux chanteurs, qui communiquent des informations essentielles via des signaux vocaux, les OCTR sont exprimés dans la plupart des noyaux moteurs des nerfs crâniens, ce qui suggère qu'ils jouent un rôle dans la commande motrice de la génération du chant (Grinevich et al. 2016). Chez les rongeurs, chez qui l'olfaction est au centre des interactions sociales, les OCTR sont enrichis dans l'ensemble du circuit olfactif (c'est-à-dire dans l'épithélium olfactif, les cellules granulaires du BO, dans le NOA, le PIR et le tubercule olfactif (Figure 14) (Choe et al. 2015; Grinevich et al. 2016; Oettl and Kelsch 2017). La distribution spécifique de l'OCTR dans les régions du cerveau cruciales pour la principale modalité sensorielle engagée dans les comportements sociaux, suggère que l'OCT est un modulateur du traitement des stimuli sensoriels provenant d'autres congénères.

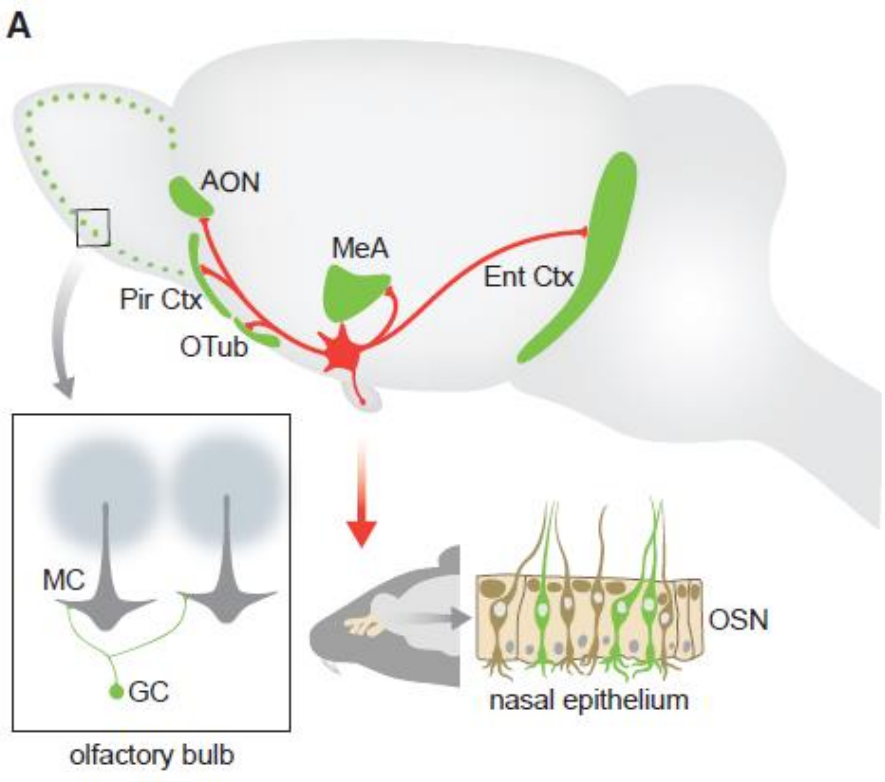

Figure 14 : ***L'ocytocine dans le système olfactif du rongeur****. L'expression des récepteurs de l'OCT (en vert) et les fibres ocytocinergiques (en rouge) couvrent les aires du système olfactif. AON, noyau olfactif antérieur ; GC, cellules granulaires ; Ent Ctx, cortex entorhinal ; MC, cellules mitrales ; MeA, amygdale médiane ; OSN, neurones sensoriels olfactifs ; OTub, tubercule olfactif ; Pir Ctx, cortex piriforme (Grinevich and Stoop 2018).*

c. Modulation par l'ocytocine des comportements sociaux et de l'olfaction

On ne peut aborder la question de l'impact de l'OCT sur la sociabilité des rongeurs sans prendre en compte le système olfactif (Section 1. Le système olfactif, pour des informations détaillées sur le traitement des odeurs). Les individus libèrent dans leur environnement un ensemble de molécules odorantes (sécrétions corporelles, urine etc…) qui leur sont propres (certaines de ces molécules dépendent notamment du patrimoine génétique) et représentent de véritables outils de communication (Stopka et al. 2007; Natynczuk and Macdonald 1994). Cette communication chimique informe les individus sur le statut hiérarchique, l'état de santé ou encore l'identité de leurs semblables (Hurst et al. 2001; Roberts et al. 2018).

Il est donc important de garder à l'esprit que les informations recueillies par les souris lors des interactions sociales sont pour la plupart de nature olfactive, bien que les vocalisations ultrasoniques restent aussi un moyen par lequel les souris peuvent communiquer (Premoli et al. 2021). **Les rongeurs reposent d'ailleurs principalement sur la détection de signaux olfactifs sociaux pour former leur mémoire sociale**, comme le montre les altérations de la mémoire de reconnaissance sociale lorsque le BO est inactivé par lésion (Dantzer et al. 1990) ou chimiquement (Popik et al. 1991).

Quels sont les comportements ayant été montré comme étant modulé par l'OCT ? Il est admis que l'OCT est libérée pendant les comportements sociaux impliqués dans la reproduction tels que l'activité sexuelle, la parturition et la lactation (Jurek and Neumann 2018) et que cette libération est également cruciale pour l'initiation des comportements maternels (Insel 1992; Keverne and Kendrick 1992). Cependant, l'OCT n'est pas seulement libérée dans le contexte de la reproduction. **Il a été démontré que l'activité ocytocinergique du NPV *in vivo*, est augmentée spécifiquement pendant les interactions sociales** (Hung et al. 2017; Tang et al. 2020) et que la stimulation de ces neurones augmente la durée des interactions entre congénères (Oettl et al. 2016). Cela va de pair avec le fait que les souris dépourvues d'OCTR (OCTR knock out - KO) présentent des troubles de la sociabilité : elles sont

plus agressives et passent moins de temps dans des situations de contact « nez-nez » (Takayanagi et al. 2005; Sala et al. 2011). Elles passent moins de temps à renifler le nez et les parties anogénitales d'une souris nouvellement rencontrée (Pobbe et al. 2012) et moins de temps aussi en interaction sociale lorsqu'elles ont le choix entre une souris et une cage vide (Sala et al. 2011). Dans l'ensemble, ces souris OCTR KO présentent des déficits sociaux typiques des souris autistes, et leurs déficits sociaux peuvent être corrigés par une injection intra-cérébroventriculaire d'OCT (Sala et al. 2011).

L'OCT est également d'une importance critique pour la mémoire sociale. En effet, les souris OCT KO ne parviennent pas à développer une mémoire sociale bien que leur détection olfactive pour les stimuli non sociaux reste intacte. En outre, le traitement de ces souris avec de l'OCT rétablit la mémoire sociale (Ferguson et al. 2000), soulignant la nécessité du peptide pour ce type de mémoire. D'autres déficiences de la mémoire sociale chez les souris OCT ou OCTR KO ont également été rapportées dans d'autres études (Takayanagi et al. 2005; Pobbe et al. 2012; Raam et al. 2017; Sala et al. 2011). Ces délétions à l'échelle du cerveau ne permettent cependant pas de savoir quelles zones du cerveau sont cruciales pour la mémoire sociale. Certains éléments de réponses proviennent d'une étude sur le NOA. L'OCT module le traitement des odeurs dans le BO par des projections descendantes provenant du NOA. Chez les souris dépourvues d'OCTR spécifiquement dans le NOA, la mémoire sociale est altérée (Oettl et al. 2016). De plus, il a été démontré que l'OCT dans le BO facilite la libération de norépinephrine et favorise la mémoire sociale (Dluzen et al. 2000). Ce résultat contraste, avec l'observation que l'infusion local d'un OCTR antagoniste (OTA) dans le BO n'impact pas la mémoire sociale (Ferguson et al. 2001). Dans cette même étude par ailleurs, l'infusion locale d'OTA entraine un déficit de mémoire sociale dans l'amygdale médial (Ferguson et al. 2001). Ce qui a aussi été remarqué dans le cas d'une infusion d'OTA dans le septum latéral (Lukas et al. 2013).

L'OCT est également nécessaire pour d'autres comportements sociaux tels que l'apprentissage social (Choe et al. 2015), la reconnaissance des émotions (Ferretti et al. 2019), pour assurer l'aspect gratifiant du comportement social (Dölen et al. 2013), le comportement de consolation (Burkett et al. 2016), ou encore le lien entre partenaires chez des espèces monogames comme le campagnol des prairies

(Williams et al. 1994). Le travail pionnier de Larry Young sur les campagnols a notamment beaucoup contribué à mettre l'OCT sur le devant de la scène depuis ces 20 dernières années, promouvant l'idée que l'OCT serait un peptide « pro-social ». En effet, il existe deux types de campagnols. Les campagnols des prairies qui forment des liens monogames et qui sont parentaux, et les campagnols des montagnes qui ne forment pas de lien long terme, et présentent peu de comportement parentaux. Entre ces deux types de campagnols, une expression différentielle des régions cérébrales exprimant l'OCTR est évidente. De plus un traitement intracerebroventiculaire avec de l'OCT chez le campagnol des prairies induit la formation d'un lien entre partenaire, alors que la présence d'un OCTR antagoniste, le bloque (Williams et al. 1994; Young et al 1998).

Cependant, cette vision d'un neuropeptide pro-social a récemment été remise en question par le fait que l'infusion répétitive d'OCT peut avoir des effets sociaux opposés (Huang et al. 2014). **Ceci suggère que l'OCT n'est pro-sociale que pour une gamme spécifique de concentrations.**

Enfin, le rôle de l'OCT dans le cerveau ne se limite pas à son impact sur les comportements sociaux. Ainsi, l'OCT a été reporté comme ayant des impacts anxiolytiques et analgésiques (Yoshida et al. 2009; van den Burg et al. 2015) ainsi qu'induisant la réduction du comportement alimentaire (Gimpl and Fahrenholz 2001; Jurek and Neumann 2018). Les rôles de l'OCT dans les comportements non-sociaux n'étant pas au cœur de mon travail de thèse, ils ne seront pas développés davantage dans cette introduction.

d. Ocytocine dans le cortex piriforme

Comme souligné précédemment, l'OCT est un neuromodulateur crucial des comportements sociaux. Les comportements sociaux chez les rongeurs reposent en grande partie sur l'olfaction. Il semble donc pertinent de se demander si et comment l'OCT impacte le cortex olfactif piriforme (PIR), où elle pourrait potentiellement moduler le traitement des informations olfactives sociales, comme c'est le cas dans le BO suite à la modulation du NOA (Oettl et al. 2016).

On ne sait pas grand-chose de l'impact de l'OCT dans le PIR. Cependant, il a été montré que **l'OCTR est exprimé de manière importante dans le PIR** (Gimpl and

Fahrenholz 2001; Yoshida et al. 2009; Mitre et al. 2016) **et qu'il reçoit des projections ocytocinergiques du PVN** (Choe et al. 2015) (Figure 15). La quantité de fibres ocytocinergiques dans le PIR semble faible, cependant, il est possible que ces fibres ne soient visibles que suite à des interactions sociales spécifiques qui augmenteraient le contenu en OCT des fibres (Section 3.b - Modulation de l'expression du récepteur de l'ocytocine). L'expression des OCTR dans le PIR est particulièrement élevée chez les souris femelles par rapport aux souris mâles (Mitre et al. 2016) ce qui suggère que des différences spécifiques au sexe pourraient être observées dans cette zone. Cependant à ce jour, **l'expression de l'OCTR dans les cellules excitatrices ou inhibitrices du PIR n'a pas été investigué**.

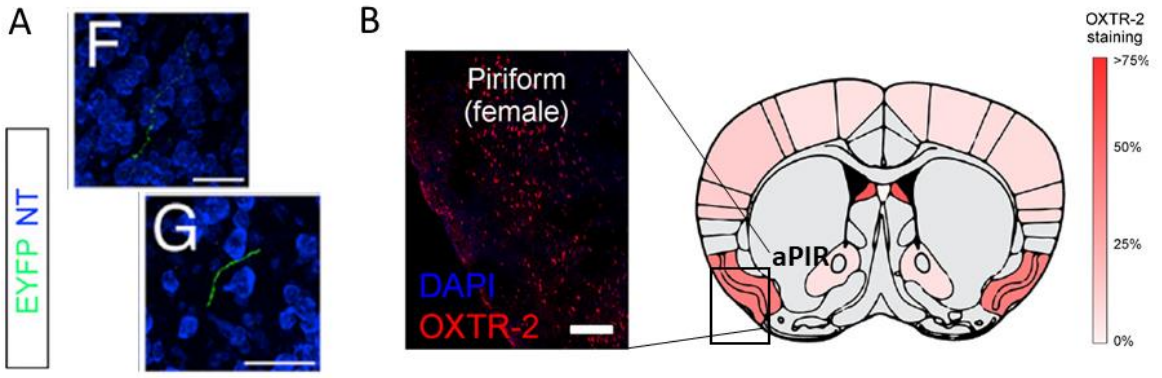

Figure 15 : ***Le cortex piriforme reçoit des fibres ocytocinergiques et exprime des récepteurs de l'OCT****. A. Les fibres ocytocinergiques des souris OCT-cre injectées avec un virus cre-dépendant ChR2:eYFP sont visibles dans le PIR (Choe et al. 2015). B. Marquage OCTR-2 dans le PIR d'une souris femelle vierge (Mitre et al. 2016). NT = NeuroTrace, aPIR = piriforme antérieur*

Sur le plan comportemental, il a été démontré que le **PIR est activé par une rencontre sociale**, comme en témoigne le marquage de l'*immediate early gene* c-FOS (Ferguson et al. 2001; Kim et al. 2015). De plus, il semble que l'activation de l'OCTR dans le PIR soit nécessaire pour l'apprentissage social (Choe et al. 2015). En effet elle permet le conditionnement d'un stimulus odorant initialement neutre a un stimulus ayant une valence (positive ou négative). Cependant, **l'investigation de la modulation de l'OCT dans le PIR pendant les comportements sociaux reste largement inexploré.**

Enfin, seul le travail de (Mitre et al. 2016), apporte des indications sur l'impact électrophysiologique de l'OCT sur le PIR. Comme précédemment cité, l'OCT dans le PIR réduit les courants post synaptique inhibiteurs évoqué, et semble pour cela dépendant de la présence d'une transmission synaptique excitatrice intact. De plus, l'OCT induit une augmentation de la fréquence des courants post synaptique excitateurs et une augmentation nettement supérieure des courants inhibiteurs. En conclusion, **l'ocytocine semble moduler la transmission synaptique dans le cortex piriforme de manière sélective, en diminuant l'inhibition évoquée et en augmentant l'inhibition spontanée**.

OBJECTIFS DE LA THESE

Partie 1

Le traitement des odeurs par le cerveau est fortement lié à l'activité respiratoire de l'animal qui médie l'apport des stimuli odorants dans la cavité nasale. La première partie de ma thèse s'est focalisée sur ce phénomène physiologique fondamental. La respiration est un processus hautement dynamique dont les variations sont liées à l'état cognitif et à l'activité de l'animal. En effet, à l'état basal la respiration est de faible fréquence (1-3Hz), alors que quand l'animal est dans un mode actif (exploration d'odeur, exploration d'un congénère, tâche de discrimination olfactive, …), il rentre dans un mode de respiration active appelé *sniffing* (8-12Hz). L'objectif de ce projet était donc de mettre au point une technique d'enregistrement de la respiration qui soit précise et compatible avec des enregistrement électrophysiologiques chez l'animal libre de ses mouvements pour pouvoir caractériser les propriétés fines de l'activité respiratoire des souris en conditions naturelles et notamment au cours des trois états de vigilance (éveil – sommeil lent – sommeil paradoxal). Ce travail a été effectué en collaboration avec d'autres membres du laboratoire, notamment une ingénieure de recherche (Tiphaine Dolique) et deux post-doctorants (Giulio Casali et Nicolas Chenouard). L'exploration du lien entre activité respiratoire et activité neuronale dans le cortex piriforme a eu lieu dans la dernière partie de mon travail de doctorat en se basant sur ce développement technologique.

<u>Manuscrit:</u> Nasal pressure dynamics reveal state-specific features of respiratory cycles in freely moving mice

Camille Miermon*, Giulio Casali*, Tiphaine Dolique, Geoffrey Terral, Pascal Ravassard, Edith Lesburguères, David Jarriault, Frederic Gambino, Nicolas Chenouard, Lisa Roux

*Co-premier auteurs

Manuscrit en cours de soumission.

Partie 2

L'ocytocine est un neuropeptide qui est très largement accepté comme étant un modulateur majeur des comportements sociaux. Il favorise notamment les interactions sociales, la mémoire sociale et la formation de lien sociaux. Chez le rongeur, les récepteurs à l'ocytocine sont très largement exprimés dans les régions du système olfactif, notamment dans la plus grande région du cortex olfactif : le piriforme cortex. Le cortex piriforme reçoit également des afférences ocytocinergiques provenant de l'hypothalamus (observation que nous avons confirmée au sein de notre équipe lors de mon doctorat). L'olfaction étant la modalité principalement utilisée par les rongeurs au cours des interactions sociales, nous avons émis l'hypothèse que l'ocytocine module l'activité du piriforme cortex pour promouvoir la sociabilité et/ou la mémoire sociale. L'objectif de ce projet a été d'investiguer d'un point de vue comportemental les effets d'un blocage pharmacologique local de l'activité des récepteurs à l'ocytocine dans le cortex piriforme pendant des tâches de sociabilité et de mémoire sociale. Des expériences complémentaires seront nécessaires pour consolider les observations réalisées lors de ce travail.

Ebauche de manuscrit: Blocking oxytocin receptors in the piriform cortex unexpectedly promotes specific social behaviors

Camille Miermon, Alena Spitsyn, Tiphaine Dolique, Fabrice De Chaumont, Lisa Roux

Partie 3

Pour les mêmes raisons que précédemment évoquées, nous nous sommes intéressés au rôle de l'ocytocine dans le cortex piriforme, avec cette-fois l'objectif d'en comprendre la modulation physiologique *in vitro* et *in vivo* et son lien avec la respiration. Les expériences *in vitro* ont été réalisées en partenariat avec une étudiante en Master 2 (Julian Pi Macedo) que j'ai supervisée au cours de ma thèse. Les expériences *in vivo* ont pu être réalisées grâce aux souris implantées par un post-doctorant de l'équipe (Geoffrey Terral) que j'ai pu enregistrer et analyser pour mon propre projet.

Ebauche de manuscrit: Oxytocin in the piriform cortex affects neuronal burstiness and coupling to respiration

Camille Miermon, Juliana Pi Macedo, Giulio Casali, Geoffrey Terral, Lisa Roux

RESULTATS

Nasal pressure dynamics reveal state-specific features of respiratory cycles in freely moving mice

Authors: Camille Miermon*, Giulio Casali*, Tiphaine Dolique, Geoffrey Terral, Pascal Ravassard, Edith Lesburguères, David Jarriault, Frédéric Gambino, Nicolas Chenouard, Lisa Roux (*shared authorship)

Abstract

While respiration is crucial for survival by its peripheral action, it also shares strong functional links with the brain. On the one hand, respiratory patterns are modulated by sensory stimuli, attention, emotions, and can be affected in the case of cognitive disorders. On the other hand, respiration shapes brain function, influencing perception, emotions and cognition. Despite the importance of this intricate brain-body relationship, monitoring respiration in freely moving animals has remained challenging: acquisitions in awake moving subjects usually lack the precision reached in head-fixed protocols and have rarely been combined with neuronal recordings. Here we propose a new method to monitor nasal pressure in freely moving mice that can be coupled to in vivo electrophysiological recordings. Thanks to the precision of the respiratory signal obtained, we found that inhalation and exhalation amplitudes vary according to the respiratory rate. However, their durations were overall invariant regardless of the respiration frequency except during high-frequency sniffing. When mice are awake and exploring their environment, respiration is made of a combination of elementary units interspersed among respiratory pauses, the durations of which dictate the ongoing respiratory rate. Combining nasal pressure monitoring with *in vivo* recordings in the CA1 region of the hippocampus, we then extracted the precise features of the identified respiratory cycles specific for each brain state (wake, non-REM and REM sleep). We also trained an artificial network based on these state-specific features, and show that it can reliably predict the state of the animal based on nasal pressure recordings. Overall, we are convinced that having access to the precise features of respiratory waveforms will open a window on the brain internal states and yield a deeper understanding of brain function in olfaction and cognition.

INTRODUCTION

Respiration is a fundamental phenomenon that maintains blood pH, O2 and CO2 levels within a range compatible with survival (Feldman et al 2013). While we cannot live without breathing, respiration also influences our brain and often reflects our cognitive states (Buonviso et al 2016, Heck et al 2016, Kleinfeld et al 2014, Wachowiak 2011). In rodents, respiration is known as a rhythmic and highly dynamic process with cycles occurring between 2 Hz (at rest) and 12 Hz. *Sniffing* (8-12Hz) is related to selective attention in olfactory-guided behaviors (Adrian 1942, Courtiol et al 2014, Welker 1964, Wesson et al 2009, Youngentob et al 1987) and response to odorants (Johnson et al 2003, Rozenkrantz et al 2015, Wesson et al 2008b). But sniffing is also observed in absence of olfactory stimuli (Clarke & Trowill 1971, Kepecs et al 2007, Wesson 2013, Wesson et al 2008b). For instance, respiration frequency increases in response to unexpected stimuli (Welker 1964, Wesson et al 2008b) (Macrides 1975), or in anticipation of an outcome (Kepecs et al 2007, Wesson et al 2008b, Wesson et al 2009, Zelano et al 2005). Respiratory frequencies are also modulated by vigilance states (Girin et al 2021, Jessberger et al 2016, Schreck et al 2022), emotions (Bagur et al 2021, Bloch et al 1991, Boiten et al 1994, Hegoburu et al 2011, Yackle et al 2017), social interactions (Butler et al 2006, Frumin et al 2015, Wesson 2013) and can be affected in some pathologies (Matarazzo et al 2017, Peupelmann et al 2009, Sobel et al 2001) including Parkinson's disease (Hardie et al 1986, Rice et al 2002, Sobel et al 2001) and autism spectrum disorders (Ming et al 2016, Rozenkrantz et al 2015). Overall, because of the intimate link they share with brain functions, respiratory patterns open a window on brain internal states.

While cognitive states can influence breathing, respiration can in turn modulate perception, emotions, cognition and learning, as shown in human subjects (Arshamian et al 2018, Bensafi et al 2003, Brown & Gerbarg 2009, Heck et al 2016, Herrero et al 2018, Perciavalle et al 2017, Zelano et al 2016) or in animal models (Wachowiak 2011). For instance, humans show better performance when solving complex cognitive tasks during nasal inhalation (Zelano et al 2016). During memory consolidation, breathing through the nose - but not with the mouth - enhances recognition memory (Arshamian et al 2018). Explanation for these behavioral results likely resides in the fact that nasal airflow, even in absence of odorants, influences ongoing brain activity. Indeed, growing evidence indicates that respiratory rhythm impact neuronal activity in multiple brain

regions (Bagur et al 2018, Ito et al 2014, Karalis & Sirota 2022, Yanovsky et al 2014), in addition to the olfactory system (Fontanini et al 2003, Macrides & Chorover 1972, Sobel et al 1998). The respiratory rhythm could play a central role for the brain-wide coordination of neuronal circuits (Buonviso et al 2016, Fontanini & Bower 2006, Girin et al 2021, Heck et al 2016, Moore et al 2013, Tort et al 2018).

Besides these global effects on the brain which can have important impacts on cognition, respiration is of course central to olfactory processing. In olfaction, odor sampling is controlled by sniffing, which determines the time course of odor stimulation (Wachowiak 2011). Indeed, odorant molecules are carried by the air entering the nasal cavity at inhalation, before they are captured by the mucosa of the olfactory epithelium that contains the cilia of the sensory neurons with olfactory receptors. Depending on their volatility, sorptiveness, and water solubility, odorants elicit different responses in the olfactory nerve when flowed across the nasal mucosa at different rates (Mozell et al 1992). Moreover, the activation of olfactory sensory neurons and mitral cells in the main olfactory bulb is altered by changes in olfactory sampling frequency (Courtiol et al 2011, Oka et al 2009, Shusterman et al 2011, Spors et al 2006) and magnitude (Bathellier et al 2008, Carey & Wachowiak 2011). Increasing evidence also indicates that the olfactory system uses a precise temporal code which requires the detection of sniff onsets with millisecond-precision (Bolding & Franks 2017, Smear et al 2011, Wilson et al 2017). Besides these observations highlighting the importance of monitoring sniff rate, amplitude and onset, it remains unclear whether other characteristics of the sniff waveforms (such as airflow direction and respiratory pauses) can impact olfactory coding and - more generally - cognitive processes.

Because of the central role of respiration for sensation and cognition, several methods have been developed over the years to monitor respiration in animal models (Bolding & Franks 2017, Grimaud & Murthy 2018, Liu & Han 2022, McAfee et al 2016) and in humans (Noto et al 2018, Oudiette et al 2018) in parallel with brain function. These methods rely on neuronal recordings in olfactory areas, air movement to/from the nostril, body movement, temperature or pressure changes. The choice of a given method usually reflects a tradeoff between precision and practicality, notably in freely moving conditions where body movements become an important constraint (Grimaud & Murthy 2018). As a consequence, the precise features composing the respiration cycles in naturalistic conditions and across different brain states are largely unknown.

These considerations prompted us to develop a new method which allows monitoring nasal pressure in freely moving mice for long (>2h) periods of time in combination with neuronal activity. The precision of the respiratory signal obtained is similar to the precision reached in head-fixed preparations and we show that it provides additional information as compared to thermocouple or whole-chamber plethysmography recordings. Using this technology, we found that respiration is made of a combination of elementary units interspersed among respiratory pauses, the durations of which dictate the overall respiratory rate. Combining nasal pressure monitoring with *in vivo* recordings in the CA1 region of the hippocampus, we extracted the precise features of the identified respiratory cycles specific for each brain state (Wake, Non-REM and REM sleep). We trained a supervised artificial neuronal network based on these state-specific features, and showed that we can reliably predict the state of the animal based on nasal pressure recordings, even when training was based on recordings from other animals. This pipeline provides therefore key information on natural respiratory behaviors and can be a valuable asset for future studies focusing on the impact of respiration on brain network activity, in the context of olfaction and beyond.

RESULTS

Monitoring nasal pressure in freely moving rodents

Among the several approaches used for respiration monitoring in rodents (Grimaud & Murthy 2018), pressure sensors connected to intranasal cannula allowed studying respiration-driven neuronal activity with an unprecedented precision level (Shusterman et al 2011, Smear et al 2011, Verhagen et al 2007, Wilson et al 2017). Yet, measuring nasal pressure has so far proven difficult in freely moving mice although it has been occasionally achieved (Reisert et al 2014, Schreck et al 2022, Wesson et al 2008b). Combining such nasal pressure monitoring methods with *in vivo* neuronal recordings represents an even bigger challenge that has so far never been accomplished in freely moving rodents. In these conditions, a commonly used method consists in measuring variations of intranasal temperature using thermocouples or thermistors (Kepecs et al 2007, McAfee et al 2016, Uchida & Mainen 2003, Wesson 2013). Alternatively, respiration is monitored *via* whole-body plethysmographs which measure pressure changes in small hermetic enclosures where rodents are placed (Courtiol et al 2014, Hegoburu et al 2011, Merle et al 2019). Our goal was to develop a method for

respiration monitoring in freely moving mice that would provide a detailed picture of the respiratory waveforms comparable to recordings performed in head-fixed preparations (Shusterman et al 2011, Smear et al 2011, Verhagen et al 2007) and that would be compatible with *in vivo* neuronal recordings. To do so, we adopted the method that consists in measuring intranasal air pressure and adapted it to freely moving mice by using light-weight pressure sensors (<1g; Honeywell part # SSC S RN N 004ND AA5) that can be easily carried by small rodents on their head caps during recording sessions (**Supplementary Fig.1A**). As described earlier (Reisert et al 2014, Shusterman et al 2011), surgery consists in inserting a stainless steel cannula at a defined location into the nasal bone and cementing it in place (see **Supplementary Fig.1** and Methods for surgery details). During recording sessions, the pressure sensor is temporarily attached on the mouse cap and coupled to the nasal cannula *via* a small piece of tubing (**Supplementary Fig.1**). Since the insertion of the cannula through the olfactory epithelium could potentially impair olfactory performance, we conducted a behavioral assay to assess whether implanted mice have higher odor detection thresholds compared to sham mice (same surgery procedure but cannula is cemented directly onto the nasal bone without craniotomy). When presenting mice with odorant of increasing concentrations during the course of 4 trials (Soria-Gomez et al 2014), we did not detect any difference in the detection thresholds for the two mouse groups (**Supplementary Fig.3C**; Mann-Whitney rank sum test: $P > 0.999$; $n = 5$ cannula-implanted and 7 sham mice). In both groups, the majority of mice (5 out of 5 cannula-implanted mice and 5 out of 7 sham mice) detected odor at a concentration of 0.01%. The exploratory behavior of the two groups of mice was comparable (**Supplementary Fig.3B**). This result suggests that the nasal cannula insertion through the olfactory epithelium does not dramatically impact olfactory function and overall exploration, as least in our detection task.

Portable pressure sensors connected to nasal cannula in freely moving mice provided low signal-to-noise signals comparable to recordings collected in head-fixed preparations (Shusterman et al 2011, Smear et al 2011, Verhagen et al 2007, Wilson et al 2017) (**Fig.1B and D**). We extracted the features of the pressure signal waveforms using a signal processing MATLAB toolbox named *BreathMetrics* developed in the Zelano lab (Northwestern University) (Noto et al 2018). We modified the script to fit rodent data collected in different brain states (**Methods** and **Supplementary Fig.4**).

This automatized analysis pipeline allows detecting the components of individual respiratory cycles (inhalation, exhalation and pauses) and extracting numerous of their features (e.g. time to peak, amplitude, volume, pause duration). To validate our approach, we first compared the signals obtained with nasal pressure sensors with methods commonly used to monitor respiration in freely moving rodents. We simultaneously recorded nasal pressure from one nasal cavity and temperature variations from the other cavity where a thermocouple had been implanted in the same mouse (**Fig.1A**). We compared these two signals and observed striking differences in the distributions of the data obtained (**Fig.1C**): while the pressure sensor signal showed a prominent peak centered around the mean, the thermocouple signal showed a broader Gaussian-like distribution. These distributions reflect primarily the fact that pressure sensor allows the detection of pauses in the respiratory behavior (when the signal goes back to atmospheric pressure) while the thermocouple signal was more continuous and sinusoid-like, at least during the wake state (**Fig.1D, left**). Importantly, when the animal fell asleep, the thermocouple signal became nearly flat preventing any possible extraction of cycle features, which was not the case with the pressure sensor signal (**Fig.1D, right**). We then compared the temporal relationships between the two signals. Precisely, we examined the temporal shift between the detected cycle onsets in the pressure signal and the peaks in the temperature signal, we found that the temperature peaks were on average preceding the pressure-defined cycle onset by 8.3 ± 0.02 msec (n = 27493 cycles). Yet, judging from the dispersion of the delays around this mean value, it was clear that the delay was not fixed preventing any possible extrapolation of precise cycle onset from the thermocouple signal. Comparison of intranasal pressure recordings with whole-body plethysmograph signal showed a strong similitude when recorded simultaneously (**Supplementary Fig.2**) but plethysmography is not compatible with complex behavioral tasks due to the small size of the chamber. Based on these comparisons, we were convinced that the tool that we propose presents all the characteristics required to acquire high-precision respiration signal from freely moving mice with minimal interference on olfactory behaviors. The next step was to test its compatibility with *in vivo* electrophysiological recordings in order to provide a detailed characterization of the respiratory behavior of mice as they explore their environment and fall asleep.

Respiration in awake freely moving mice

During awake exploratory behavior, rodents show a considerably large range of respiration rates characterized by the baseline breathing (2-4 Hz) with transient peaks up to 12 Hz during epochs of high sniffing rate (Kurnikova et al 2017, Uchida & Mainen 2003, Welker 1964, Wesson et al 2008b, Youngentob et al 1987). We aimed to investigate the principles of the temporal structure governing respiration pattern and the variability in the respiratory rate observed in this context. To address this question we recorded 60 sessions from 10 cannula-implanted mice. In these mice, we combined pressure sensor monitoring with neuronal recordings in the CA1 region of the hippocampus by chronically implanting silicon probes in this region (**Methods**). As in previous studies (Mizuseki et al 2009), the spectral features of the local field potential in CA1 was used to assess brain states. To detect the different components the respiratory cycles (inhalation/exhalation/pauses) and extract their precise characteristics (such as duration, amplitude, volume) in different brain states, we modified the freely available BreathMetrics toolbox (Noto et al 2018)(https://github.com/zelanolab/breathmetrics) (see **Methods**). We focused first on the wake state (Wake).

The fundamental question we aimed to ask concerned whether the duration of the respiratory cycles follows isometric deformation (i.e. they follow an inverse relationship with long duration during low sniff rate and short duration during high sniff rate) or whether instead the structure of the respiration cycles is rather frequency-invariant and so composed of temporally-fixed units with intermingled pauses of variable duration between cycles (**Fig. 2A**).

To test these hypotheses, we first examined the average inhalation/exhalation features of cycles across respiration rates and we found a marginal, yet significant, decrease in the mean duration of both inhalation/exhalation across respiration cycles of different rates (**Fig 2B**: 15-20 ms difference in mean inhalation duration across rate 1-10 Hz, $F_{(9,59)} = 121.1$, $P < 0.0001$; 5-10 ms difference in mean exhalation duration across respiration rate 1-10 Hz, $F_{(9,59)} = 123.4$, $P < 0.0001$). Together with the reduction in the overall duration, we also found for both inhalation/exhalation significant differences in the time to reach the peak (10-15 ms difference in mean inhalation peak time across rate 1-10 Hz, $F_{(9,59)} = 158.1$, $P < 0.0001$; 0-5 ms in mean exhalation peak time across rate 1-10 Hz, $F_{(9,59)} = 177.7$, $P < 0.0001$), the amplitude (-6×10^6 a.u. difference in

mean inhalation peak amplitude across rate 1-10 Hz, $F_{(9,59)}$ = 755.1, P < 0.0001; -8 x 10^6 a.u. difference mean exhalation peak amplitude across rate 1-10 Hz, $F_{(9,59)}$ = 991.1, P < 0.0001). Together, these results indicate that respiration cycles show temporal modulation by the respiration rate (**Fig 2B**) theoretically consistent with the hypothesis that cycles can be temporally compressed to allow higher respiration rate. It should be noted however that between 1 and 10Hz, the total cycle duration is theoretically reduced by 900 ms (from 1000 ms to 100 ms) and this value vastly exceeds the 20-30 ms gain obtained by combining the compression of both inhalation and exhalation across the two considered rates. These observations suggest that the degree of compression of inhalation and exhalation plays a negligible role in modulating the overall respiration rate.

Therefore, we next focused on the role of the intermingled pauses to investigate their putative role for the respiration rate. Consistent with the hypothesis that pauses after inhalation modulate the respiration rate, we observed that drops in the respiration rate mostly coincided with long pauses occurring between inhalation and exhalation within respiratory cycles (**Fig 2D**). In contrast, during bouts of high respiratory rate, respiratory cycles occurred with no intermingled pauses between inhalation and exhalation.

In light of the observation that in Wake the mean fraction of time spent during pauses after inhalation is significantly greater than pauses after exhalation (pauses after inhalation = 19.6 ± 0.5 %, pauses after exhalation = 1.3 ± 0.1 %, t_{59} = 33.3, P < 0.0001) we proposed that the duration of pauses occurring after inhalation are the key factor to rule out between the two scenarios we conceived. Indeed, visual examination of the respiratory cycles sorted by their total duration (inverse of the respiration rate) – revealed a clear gradient in the duration of the pauses after inhalation (**Fig. 2C**) – suggesting an inverse relationship between respiration rate and pause duration.

To answer whether the reduced duration of inhalation/exhalation or rather the decrease in pauses duration correlated the most with the full cycle duration, within each experimental session we scored a “respiration rate predictor” obtained as the Pearson (r) correlation value between the duration of each component of the respiratory cycle against the full cycle duration (**Fig 2E*i-iv***). Across sessions we found that the respiration rate predictor was significantly different across components (**Fig 2E*v***, $F_{(3,59)}$ = 300.2, P < 0.0001) and the pauses after inhalation were highest and significantly increased compared to any other component (inhalation duration = 0.64 ±

0.01 r, pause after inhalation duration = 0.75 ± 0.01 r , exhalation duration = 0.48 ± 0.01 r, pause after exhalation duration = 0.34 ± 0.01 r; *post hoc* comparison with Bonferroni correction between inhalation duration and pause after inhalation duration: t_{59} = 6.71, P < 0.0001; *post hoc* comparison with Bonferroni correction between exhalation duration and pause after inhalation duration: t_{59} = 16.0, P < 0.0001; *post hoc* comparison with Bonferroni correction between pause after exhalation duration and pause after inhalation duration: t_{59} = 22.5, P < 0.0001). Together, these results speak in favor of the latter hypothesis that the duration of the pauses after inhalation is the primary factor for predicting the respiration rate.

Overall, the interpretation of these results is twofold. Firstly, although the duration of inhalation/exhalation slightly decreases as respiration rate increases, this fails to fully predict the instantaneous rate. Instead, our data suggest that during Wake the inhalation and exhalations act like “units” of roughly fixed duration intermingled by variable pauses occurring mostly after inhalation. Secondly, the onset and duration of such pauses dictate the respiration rate, pointing at these events as key modulators of respiration rate-dependent mechanisms involved in olfactory processing.

Respiration across brain states

Besides these observations about the composition of the respiration cycles in awake freely moving mice, nasal cannula-coupled pressure sensors allowed us to monitor mice throughout long (>2h) periods of time as they explore their environment and rest in their home cages. In these long recordings, animals typically alternated between wakefulness (Wake), to Non-Rapid-Eye-Movement (NREM) sleep and to REM sleep episodes (**Fig. 3A-B**). As neuronal activity in the olfactory bulb has been shown to be a good predictor of animals’ brain states (Bagur et al 2018), and because respiration has been shown to vary considerably depending on the degree of vigilance (Girin et al 2021, Jessberger et al 2016, Schreck et al 2022), we hypothesized that nasal pressure dynamics would also reflect mouse internal brain states. Hippocampal CA1 LFP signals allowed us to detect the three main brain states - Wake, Non-Rapid-Eye-Movement (NREM) and Rapid-Eye-Movement (REM) sleep - which overall differed in averaged duration across mice (mean ± SEM: wake = 7126 ± 345 seconds, REM = 583 ± 47 seconds, NREM = 7740 ± 431 seconds). Next, we examined the respiratory pattern and observed that it substantially differed between states (**Fig 3B*i-iii***).

Having identified respiration cycles in each session, we next determined the smoothed respiratory rate by calculating the number of detected respiratory cycles with a time-bin of 200 ms for the entire session (with a Gaussian smoothing of sigma 400 ms). Similarly, for each respiratory feature, we averaged the results obtained by BreathMetrics with the same time-bin of 200 ms. We calculated the mean as representative example of each respiratory feature during each behavioral state so that we could then pool results across sessions. Similar trends between states were obtained when the averaged features across cycles were compared.

Firstly, we compared the respiration rate: during NREM and REM we found unimodal distribution in the 2-4 Hz range whilst during Wake it was increased and spanned a significantly greater range of frequencies (**Fig 3C**; respiration rate mean ± SEM: wake = 4.6 ± 0.1 Hz, NREM = 2.6 ± 0.5 Hz, REM = 3.2 ± 0.5 Hz, $F_{(2,51)} = 408$, $P < 0.0001$). *Post-hoc* comparison with Bonferroni correction showed that the mean respiration rate during Wake was greater than NREM ($t_{51} = 24.6$, $P < 0.0001$) and REM ($t_{51} = 17.9$, $P < 0.0001$), but also that rate during REM was increased compared to NREM ($t_{51} = 11.6$, $P < 0.0001$). Having previously shown that during Wake the total cycle duration is strongly correlated to the duration of pauses after inhalation but less to inhalation/exhalation duration (**Fig 2**), we compared respiratory components across states. We quantified the fraction of time assigned to each of the respiratory cycle components and found remarkable differences across states, in particular with respect to the pause behavior.

Firstly, we observed that fraction of time spent in inhalation was reduced during Wake but did not differ between REM and NREM (**Fig 3D*i***; inhalation time (%) ± SEM: wake = 36.3 ± 0.3 %, NREM = 43.3 ± 0.3 %., REM = 43.7 ± 0.3 %, $F_{(2,51)} = 138$, $P < 0.0001$; *post-hoc* comparison with Bonferroni correction: between Wake and NREM: $t_{51} = 12.6$, $P < 0.0001$; between Wake and REM: $t_{51} = 15.1$, $P < 0.0001$; between NREM and REM: $t_{51} = 0.56$, $P > 0.05$).

An opposite trend was found for the fraction of time spent during pauses after inhalation which was greater in Wake compare to both NREM and REM but also differed between NREM and REM (**Fig 3D*ii***; pause after inhalation time (%) ± SEM: wake = 20.0 ± 0.5 %, NREM = 5.1 ± 0.4 %., REM = 0.7 ± 0.2 %, $F_{(2,51)} = 735$, $P < 0.0001$; *post-hoc* comparison with Bonferroni correction: between wake and NREM: $t_{51} = 29.2$, $P <$

0.0001; between wake and REM: t_{51} = 32.7, P < 0.0001; between NREM and REM: t_{51} = 9.45, P < 0.0001).

Similar to that of inhalation, the time spent during exhalation in Wake was reduced compared to both NREM and REM with REM being also significantly greater than NREM (**Fig 3D*iii***; exhalation time (%) ± SEM: wake = 42.3 ± 0.3 %, NREM = 45.0 ± 0.6 %., REM = 52.2 ± 0.6 %, $F_{(2,51)}$ = 131.4, P < 0.0001; *post-hoc* comparison with Bonferroni correction: between Wake and NREM: t_{51} = 5.15, P < 0.0001; between Wake and REM: t_{51} = 16.2, P < 0.0001; between NREM and REM: t_{51} = 9.7, P < 0.0001).

Importantly, the fraction of time spent during pauses after exhalation was also remarkably different between states and showed different trend compared to the pauses after inhalation, as during wake it was nearly absent while it was increased during NREM compared to REM (**Fig 3D*iv***; pause after exhalation time (%) ± SEM: wake = 1.5 ± 0.1 %, NREM = 6.4 ± 0.5 %., REM = 3.4 ± 0.4 %, $F_{(2,51)}$ = 55.4, P < 0.0001; *post-hoc* comparison with Bonferroni correction: between wake and NREM: t_{51} = 11.0, P < 0.0001; between Wake and REM: t_{51} = 5.0, P < 0.0001; between NREM and REM: t_{51} = 5.3, P < 0.0001). These results thus suggest that the duration of pauses after inhalation is a key modulator of respiration rate during Wake but represents a small fraction of time during sleep. In contrast, pauses after exhalation represent a significantly greater fraction during sleep compared to Wake especially during NREM.

Next, we focused on the characteristics of inhalation/exhalation components across states: visual examination of averaged cycle waveform across states revealed substantial differences for both inhalation (**Fig 3E*i***) and exhalation (**Fig 3E*ii***): indeed, consistent with the overall greater frequency during wake, we found that the mean duration of inhalation and exhalation was substantially reduced during wake compared to both NREM and REM (**Fig 3E*iii*;** inhalation duration mean ± SEM: wake = 72.7 ± 1.6 ms, NREM = 164.8 ± 4.4 ms, REM = 132.8 ± 2.5 ms, $F_{(2,51)}$ = 346, P < 0.0001; *post-hoc* comparison with Bonferroni correction: between Wake and NREM: t_{51} = 20.4, P < 0.0001; between Wake and REM: t_{51} = 20.7, P < 0.0001; between NREM and REM: t_{51} = 10.7, P < 0.0001; Fig 3E*iv* exhalation duration mean ± SEM: Wake = 78.2 ± 1.4 ms, NREM = 166.7 ± 2.6 ms, REM = 157.6 ± 3.2 ms, $F_{(2,51)}$ = 380, P < 0.0001; *post-hoc* comparison with Bonferroni correction: between Wake and NREM: t_{51} = 30.1, P < 0.0001; between Wake and REM: t_{51} = 23.0, P < 0.0001; between NREM and REM: t_{51}

= 2.21, $P > 0.03$). Similar decrease in wake was also found when we examined the mean duration to reach the trough/peak for inhalation and exhalation (**Fig 3E*iv***; trough inhalation duration mean ± SEM: wake = 25.1 ± 0.6 ms, NREM = 54.3 ± 0.9 ms, REM = 54.5 ± 0.7 ms, $F_{(2,51)} = 598$, $P < 0.0001$; *post-hoc* comparison with Bonferroni correction: between Wake and NREM: $t_{51} = 31.2$, $P < 0.0001$; between Wake and REM: $t_{51} = 29.4$, $P < 0.0001$; between NREM and REM: $t_{51} = 0.25$, $P > 0.05$; 3E*vi* peak exhalation duration mean ± SEM: Wake = 27.6 ± 0.3 ms, NREM = 29.1 ± 0.6 ms, REM = 19.8 ± 0.4 ms, $F_{(2,51)} = 174$, $P < 0.0001$; *post-hoc* comparison with Bonferroni correction: between Wake and NREM: $t_{51} = 2.59$, $P < 0.012$; between Wake and REM: $t_{51} = 18.4$, $P < 0.0001$; between NREM and REM: $t_{51} = 15.3$, $P < 0.0001$).

Moreover, we also found that the amplitude of the trough/peak of inhalation and exhalation were increased in Wake compared to both REM and NREM (**Fig 3E*vii***; inhalation trough mean ± SEM: wake = 4215 ± 146 a.u., NREM = 1701 ± 101 a.u., REM = 1892 ± 99 a.u., $F_{(2,51)} = 384$, $P < 0.0001$; *post-hoc* comparison with Bonferroni correction: between wake and NREM: $t_{51} = 21.2$, $P < 0.0001$; between wake and REM: $t_{51} = 19.0$, $P < 0.0001$; between NREM and REM: $t_{51} = 4.5$, $P < 0.0001$; Fig 3E*viii* exhalation peak mean ± SEM: Wake = 3900 ± 123 a.u., NREM = 1419 ± 85 a.u., REM = 1854 ± 84 a.u., $F_{(2,51)} = 364$, $P < 0.0001$; *post-hoc* comparison with Bonferroni correction: between Wake and NREM: $t_{51} = 20.7$, $P < 0.0001$; between Wake and REM: $t_{51} = 18.1$, $P < 0.0001$; between NREM and REM: $t_{51} = 10.5$, $P < 0.0001$).

In contrast, the volumes of air did not differ between states during inhalation (**Fig 3E*ix***; inhalation volume mean ± SEM: wake = 153757 ± 5356 a.u. x ms, NREM = 152656 ± 8341 a.u. x ms , REM = 162149 ± 8801 a.u. x ms, $F_{(2,51)} = 1.57$, $P > 0.05$), while they changed during exhalation (**Fig 3C*x***; exhalation volume mean ± SEM: wake = 153203 ± 5106 a.u. x ms, NREM = 127947 ± 7586 a.u. x ms, REM = 154670 ± 8626 a.u. x ms, $F_{(2,49)} = 14.2$, $P < 0.0001$; *post-hoc* comparison with Bonferroni correction: between Wake and NREM: $t_{51} = 4.22$, $P < 0.002$; between wake and REM: $t_{51} = 0.21$, $P > 0.05$; between NREM and REM: $t_{51} = 7.76$, $P < 0.0001$). Altogether these findings suggest that not only the respiration rate, but also the overall structure of the respiratory cycles differs across states.

In summary, here we reported striking differences both in the respiration pattern between Wake and sleep but also between NREM and REM. Importantly such differences not only reflect crucial features of the respiratory cycle (duration, amplitude

etc), but also to the general structure of the cycle as revealed by opposite trends in the pause behavior across states. Spurred by these results, we aimed employ the fine characterization of the respiration pattern shown here to demonstrate that the respiratory signal can be used to detect Wake and but also NREM and REM during sleep.

Nasal pressure dynamics predict brain state

If the features embedded in the nasal pressure signal are brain-state-specific, we reasoned that a machine learning algorithm should be able to predict brain-state based on respiratory cycles features extracted from pressure sensor signals. To test this hypothesis, we built an artificial neuronal network and trained it under supervision with data collected from 26 sessions recorded in 7 different mice. In this case, we used BreathMetrics without *a priori* knowledge of the brain-states since our ultimate goal was to use the network to infer this information (**Methods**). The training set was composed of 10 features extracted from BreathMetrics for all the respiratory cycles detected in each session. Each cycle was annotated with its corresponding state (Wake, NREM or REM) thanks the CA1 LFP signals that had been simultaneously recorded. The architecture of the network is illustrated in (**Fig.4A**). As its output, the network provides the estimated probability value (Pr) for each of the 3 brain states for a given respiratory cycle. The predicted state corresponds to the one with greater probability and the degree of confidence associated with this prediction was this maximal probability (**Methods**).

To test how efficiently our network could decode brain-states, but also how the respiration-brain states links can be generalized in between animals, we trained it on all mice but one and used this last mouse for validation. As shown in **Fig.4B**, the network learned to predict brain states for mice 3C030 and 7C012, even though data from these animals was not in the training set, hence highlighting the inference of generalized rules for prediction. Long periods of wake and NREM sleep were correctly predicted with confidence close to 1. Lower confidence was observed at the transition between brain states, periods which are challenging to accurately annotate from LFP signals for human experts as well. Lower confidence was prominent for REM sleep periods which are much shorter, even though many were correctly predicted. Some extra, short, REM periods were also predicted for mouse 7C012 (between 4-5 10^4

breathing cycles) opening the possibility of discovering REM periods that were neglected by the expert who annotated the data.

We repeated the training procedure for all the 7 mice as validation animal and assessed the prediction quality (**Fig.4C**). Overall, we found that 94% of annotated Wake cycles were correctly predicted as Wake cycles; 92% of annotated NREM cycles were correctly predicted as NREM cycles and 80% of REM cycles were correctly predicted as REM cycles. The largest confusion was observed between NREM and REM: 18% of annotated REM cycles were predicted as NREM. However, only 2% were wrongly assigned to Wake. Interestingly, the confidence of the predictor across the different pairs of annotated and predicted states reveals that confusions (annotated Wake labeled as NREM for instance) occur when confidence is low. In comparison, when annotated states match the prediction (annotated Wake labeled as Wake for instance), the confidence is high and show little dispersion. This highlights that the predicted confidence is a good indicator of the trust one can put into the prediction of the method (a feature not traditionally available for possibly faulty manual annotations and automated state prediction from LFP (Bagur et al 2018, Stephenson et al 2009)): low-confidence cycles should be under increased scrutiny as compared to high-confidence ones.

Overall, this experiments highlights the existence of general, cross-animal, rules linking breathing features to brain states. We also think that the already-trained networks can be applied to other datasets and become a valuable asset for state scoring based on respiratory pressure signals solely, without requirement for electrophysiological recordings.

DISCUSSION

In this study, we first provide detailed methodological indications onto how to conduct precise respiration monitoring in freely moving mice based on portable pressure-sensors compatible with *in vivo* neuronal recordings. Thanks to this approach we dissected the precise dynamics of respiratory waveforms during awake exploratory behavior as well as during the two major sleep phases: NREM and REM- sleep. We highlighted the importance of respiratory pauses in dictating the overall respiratory rate as we found that inhalation and exhalation remain roughly time-invariant in wake

except during sniffing when inhalation and exhalation shorten with increasing sniffing frequency. Finally, based on the unique properties of respiratory cycles recorded in each brain state, we trained an artificial neuronal network able to predict brain states solely based on nasal pressure signal and across animals.

The method we present gives access to the fine architecture of individual respiratory cycles thanks to the variations of the air pressure within the nasal cavity. The main benefit of this approach, as compared to commonly used methods for in freely moving rodents is the dynamic range and the precise detection of inhale onsets and pauses in the respiratory behavior. Both the amplitude changes and the presence of pauses can have important implications for olfactory processing, especially in rodents which are obligatory nose-breathers. The increased dynamic range is particularly relevant during epochs of active sampling, when the amplitude of the signal increases dramatically together with the respiration rate (Reisert et al 2014).

Past work indicated that changes in respiration intensity and rate affect the responses to odorants in the olfactory system (Courtiol et al 2011, Oka et al 2009, Spors et al 2006, Wachowiak 2011) thus we investigated the amplitude and the duration of each cycle component during Wake state. When considering both inhalation/exhalation, the peak amplitude was strongly modulated by the respiration rate. On the other hand, we found that the duration of inhalation/exhalation shows rather negligible cycle compression (5-15 ms) as rate increases, suggesting a marginal contribution to the respiration rate (total cycle duration spanned over a range of 50 to >1000 ms in this state). In contrast, the duration of pauses was a strong predictor of the overall respiratory rate: while inhalation and exhalation durations remain relatively constant regardless of the total cycle duration, pause durations strongly correlate with it. This observation is in line with previous studies which indicate that respiration frequency does not affect behavioral performance in olfactory tasks (Wesson et al 2009). It has been proposed that neurons in the olfactory system encode odor identity within a ~100 ms time window after inhalation onset (Bolding & Franks 2017, Shusterman et al 2011, Wilson et al 2017) and that the precise timing of neuronal activation relative to inhalation onset underlies odor identification (Smear et al 2011). The stability of inhalation durations across respiratory rates would therefore contribute to the preservation of this temporal code in conditions where animals freely explore their environment and dramatically modulate their respiratory behavior. This could

potentially explain why rats perform similarly in a simple olfactory discrimination task regardless of whether they sniff or breath and why odorant-evoked inputs to the olfactory bulb remain comparable between these two respiratory behaviors (Wesson et al 2009).

Yet, the role of cycle amplitude variations and pauses in olfactory processing remains to be addressed. It appears that during wake state, mice *hold their breath* or at least they pause before exhaling. It is possible that during these epochs, a more refined extractions of odor properties (such as concentration, valence, identity…), processing of retronasal olfactory information (Gautam & Verhagen 2012) or memory-related processes are at play, with a possible involvement of top-down mechanisms onto the sensory areas (Manabe & Mori 2013). The gradual recruitment of olfactory sensory neurons after inhalation onset (Carey et al 2009, Cury & Uchida 2010, Shusterman et al 2011, Wesson et al 2008a) could possibly contribute to this additional level of olfactory information processing. Future studies combining precise respiration monitoring with in vivo neuronal recordings will allow disentangling these exciting questions.

Besides these considerations on olfactory information processing, this work also highlights the fundamental differences of respiratory waveform features across three brain states: wake, NREM and REM sleep. These differences confirm previous work (Girin et al 2021, Jessberger et al 2016, Schreck et al 2022) and are expected from the neurophysiological mechanisms underlying breathing in these different states (Feldman et al 2013). Yet, the description of the precise features of individual respiratory cycles that we uncovered thanks to dual respiration and electrophysiological recordings is fulfilling a gap of knowledge regarding respiratory behavior in naturalistic conditions. Using the state-specific features of respiratory cycles, we have built an artificial neuronal network that can predict brain state solely based on nasal pressure signal. The ability to accurately predict brain states for animals which were not part of the training set highlights that the relationships between states and respiratory features are conserved across animals. Moreover, we provide a freely-available pipeline that can be used by other labs interested in state scoring in head-fixed or freely moving rodents. The advantage of this approach is its independence electrophysiological and body motion recordings. Since the network has already been trained with our annotated dataset, users can automatically obtain

predictions on behavioral states based on their own respiration data, with the related confidence levels. This method can allow automatic detection of brain states or, at least, refinement of state detections when integrated in existing state-scoring pipelines (Bagur et al 2018, Stephenson et al 2009).

Respiration both reflects our internal cognitive states and is a strong modulator of brain activity (Bagur et al 2021, Buonviso et al 2016, Heck et al 2016, Moore et al 2013, Tort et al 2018). It has been proposed that the respiratory drive, which likely originates from mechanoreceptors located in the olfactory epithelium (Grosmaitre et al 2007), could govern long-range coordination among neuronal networks (Buonviso et al 2016, Fontanini & Bower 2006, Girin et al 2021, Heck et al 2016, Karalis et al 2016, Moore et al 2013) and even entrain sharp wave ripples in the CA1 region of the hippocampus (Liu et al 2017). Based on these observations, we argue that understanding brain function can no longer be achieved without information about body physiological rhythms such as respiration. Pressure sensor monitoring in freely moving mice combined with neuronal recordings is a key for the interpretation of neuronal activity in vivo and opens a window on the brain internal states.

FIGURES

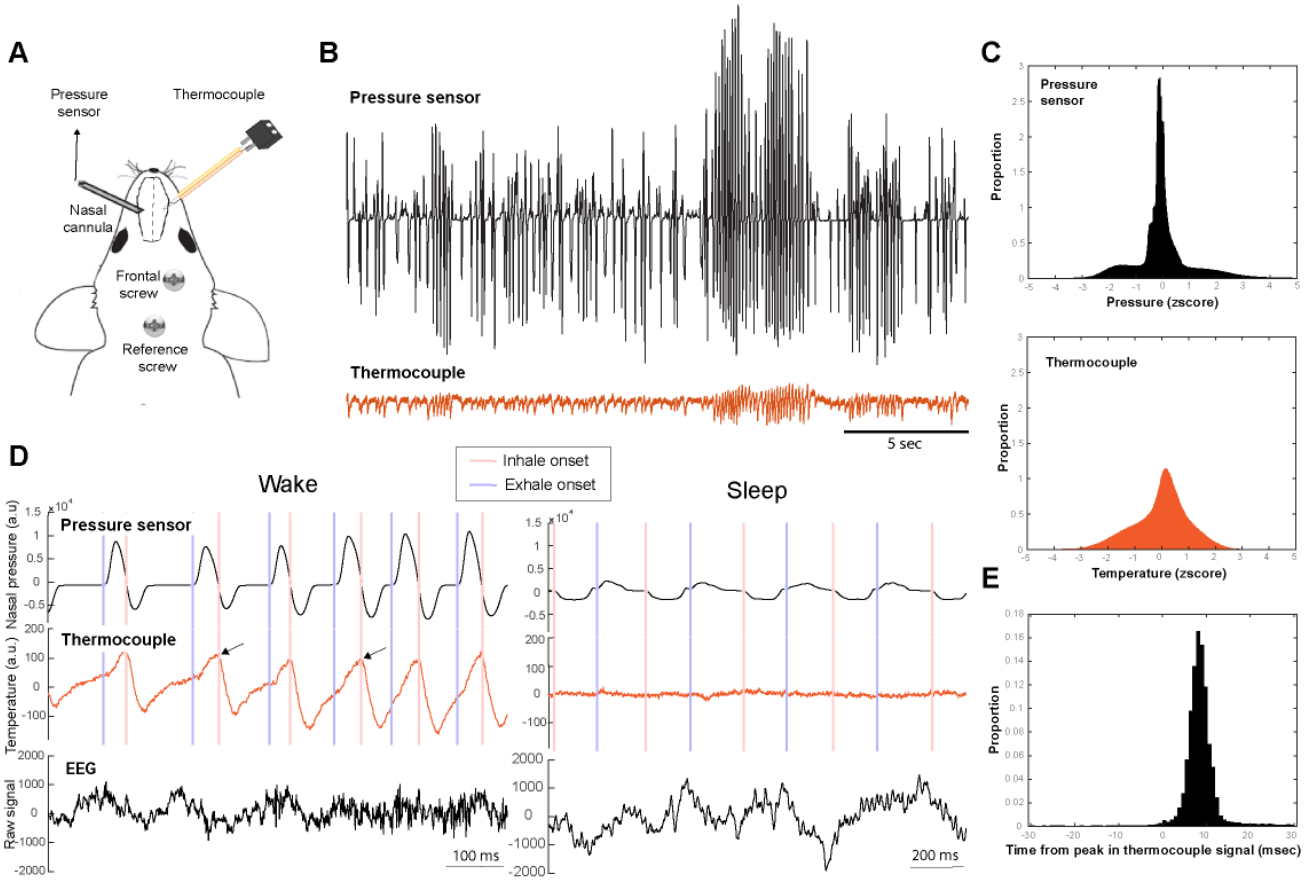

Figure 1: Comparison between pressure sensor and thermocouple signals based on simultaneous recordings. **A.** Schematic of the experimental procedure. The nasal cannula connected to the pressure sensor is chronically implanted into the left nasal cavity while the thermocouple is implanted into the right one. A screw above the frontal cortex is used for EEG recording. A screw is placed above the cerebellum and serves as the reference for the EEG recordings. All signals are simultaneously acquired in a freely moving mouse. **B.** Examples of raw recordings collected in parallel during wake state with the two sensors showing variations in nasal pressure (top) or intranasal temperature (bottom) in arbitrary units. **C.** Distributions of pressure sensor (top) or thermocouple (bottom) data. **D.** Examples of raw recordings during wake and sleep state. Inhale and exhale onsets are detected using the pressure signal (see Methods). Arrows indicate peaks in the thermocouple signal. **E.** Distribution of the time delays of the inhale onsets as compared to the peaks of the thermocouple signal. Both are considered as respiratory cycle onsets in previous studies.

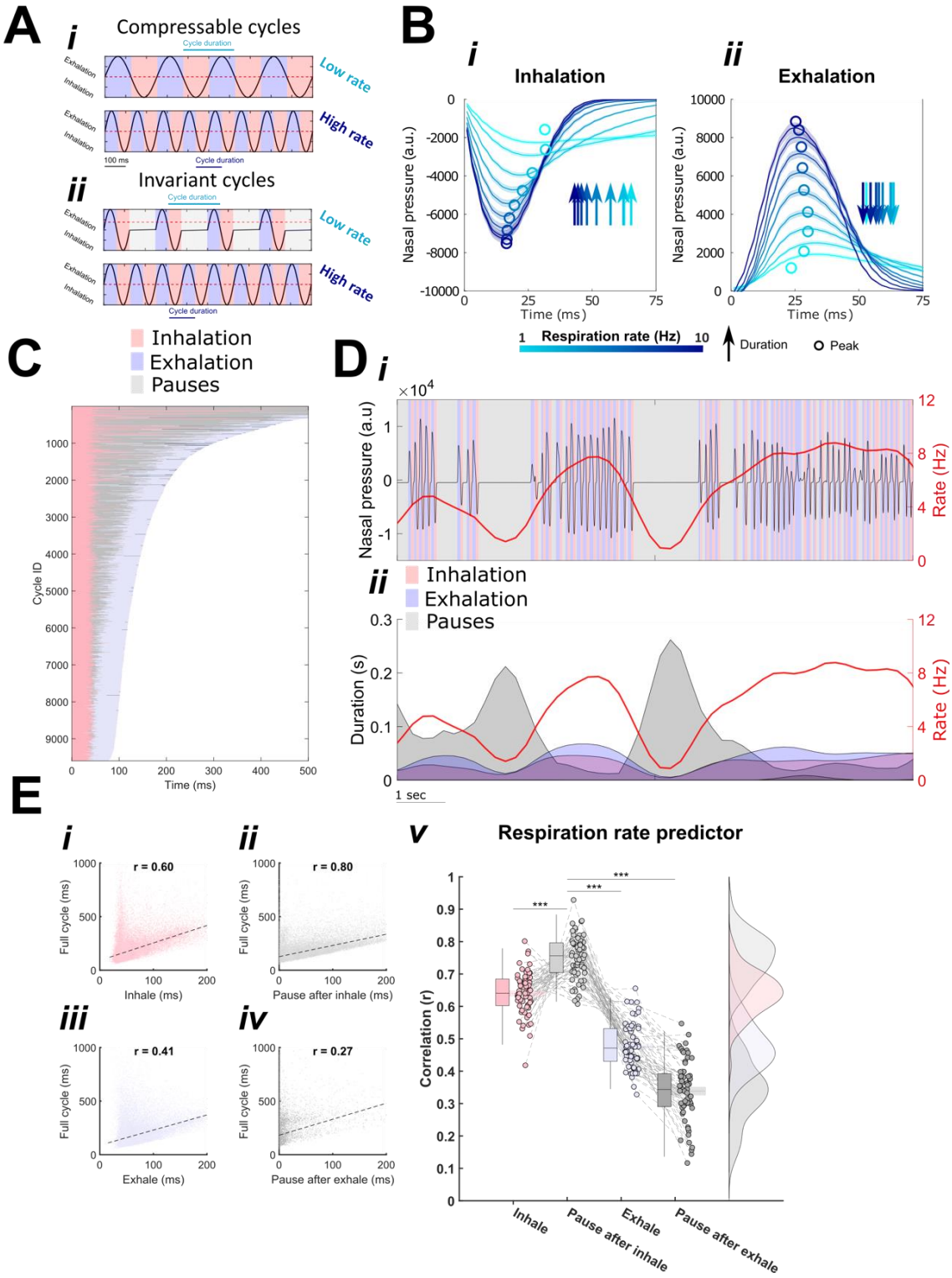

Figure 2: Temporal structure of respiratory patterns across rate during wake. **A.** Schematic representation of the hypothesized respiration patterns across respiration rate: ***i*** respiration cycles are “expandable/compressable” with the duration of cycles being inversely proportional to the respiration rate (overall cycle duration is equivalent

to the sum of inhalation (pink area) and exhalation (lavender area) duration); ***ii*** respiration cycles consists of inhalation/exhalation epochs of fixed duration intermingled by pauses (grey area) of variable duration ultimately dictating respiration rate. **B.** Mean ± S.E.M. waveform during inhalation (***i***) and exhalation (***ii***) across respiration rate (color-coded turquoise-blue corresponds to 1-10 Hz). Arrows indicate the mean duration and circle the waveform peak. Note the anticipation for duration and peaks together with higher amplitude for both inhalation and exhalation with increasing rate. **C.** Cycle components (inhalation = pink, exhalation = lavender, pauses = grey) across respiratory cycles sorted by duration during one representative session. Note the increasing duration of pauses after inhalation as the overall cycle duration increases (i.e. respiration rate decreases). **D.** Representative example of respiration signal monitored during wake. ***i*** Instantaneous nasal pressure (black line, left y-axis) relative to instantaneous respiration rate (red-line, right y-axis) during 10 seconds. The instantaneous rate was obtained by calculating the number of detected respiratory cycles with a time-bin of 200 ms (with a Gaussian smoothing of sigma 400 ms). Note the relationship between the rate and the duration of each respiration cycle component within each time bins (inhalation = pink area, exhalation = lavender area, pauses = grey area). ***ii*** Mean duration of respiration components (inhalation, exhalation, pauses) within each time bin revealing inverse relationship between pause duration and respiration rate in contrast to both inhale/exhale which are only marginally affected by fluctuations in respiration rate. **E.** Scatter plots showing duration of respiration components (***i*** inhalation, ***ii*** pause after inhalation, ***iii*** exhalation, ***iv*** pause after exhalation) against full respiration cycle during a representative session. Note the weaker relationship between full cycle duration and inhalation, exhalation and pause after exhalation duration as quantified by the corresponding Pearson coefficient (r) obtained in contrast to the pause after inhalation. ***v*** Comparisons of mean r obtained for each respiration component across sessions revealed a significantly greater predictive strength for the pause after inhalation compared to any other respiration component. N = 60 sessions in 10 mice. See Results for statistics.

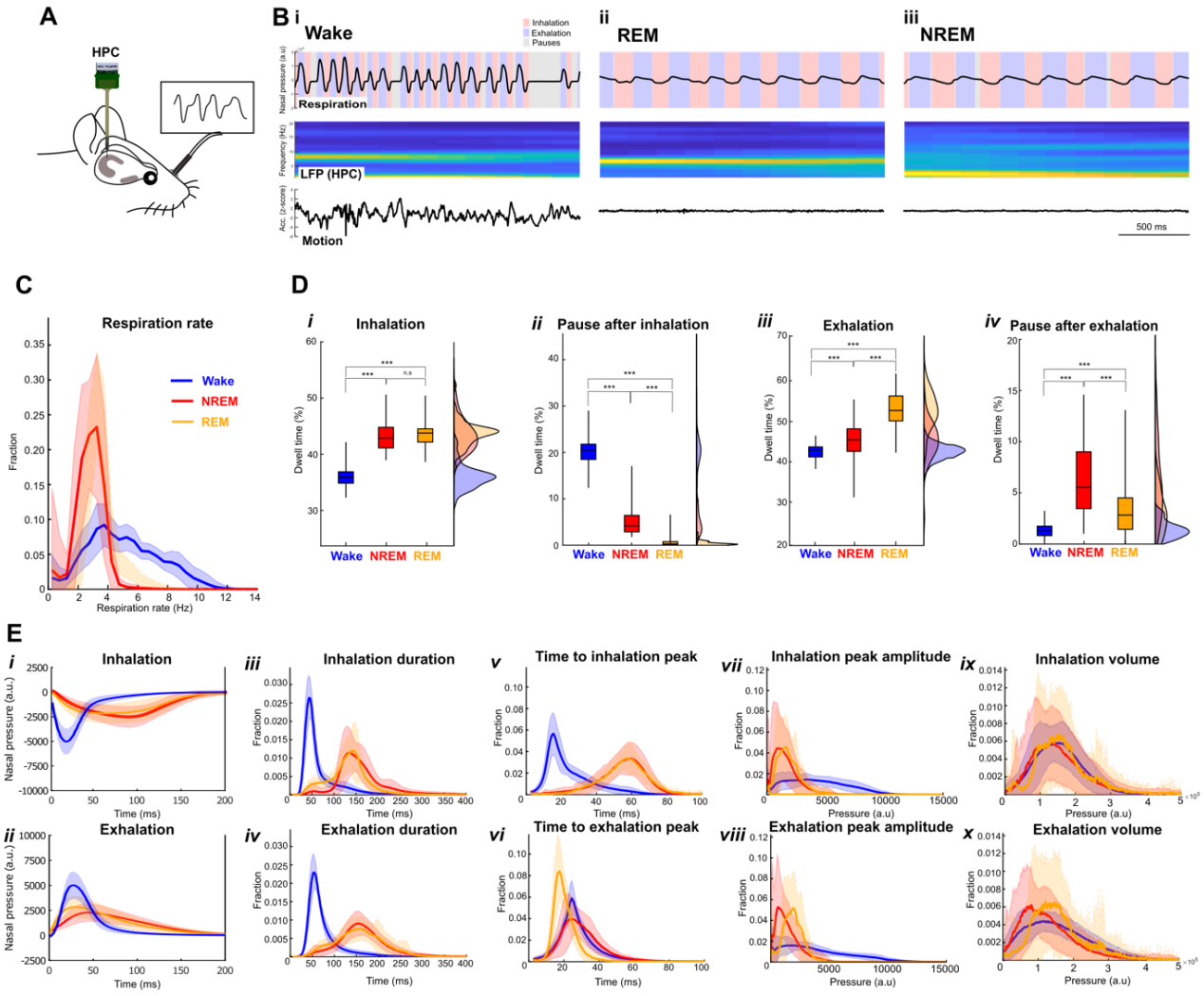

Figure 3: Respiratory cycle features across brain states.

A. Schematic representation of nasal cannula implantation used to monitor instantaneous respiration. **B.** Representative traces of respiration co-recorded with silicon probes implanted in the dorsal hippocampus states and accelerometer. (*Top*) Instantaneous intra-nasal pressure (black line) monitored during inhalation (pink area), exhalation (lavender area), and pauses (grey area), during Wake (***i***), REM (***ii***) and NREM (***iii***). Note the higher rate and amplitude of respiration cycles during Wake compared to REM and NREM. (*Middle*) Spectrogram of co-recorded CA1 LFP during respiration across states. Note the similarity between Wake and REM state in contrast to NREM. (*Bottom*) Instantaneous acceleration co-recorded with neural traces. Note the similarly flat acceleration during REM and NREM despite changes in the power spectrum (middle) and respiration pattern. **C.** Mean ± S.E.M histogram of respiration rate across sessions between brain states. Note the peak in the 2-4 Hz range for respiration rate during REM and NREM compared to Wake where the rate spanned

substantially larger range. **D.** Box plots representing percentage of time across brain states during inhalation (***i***), pauses after inhalation (***ii***), exhalation (***iii***) and pauses after exhalation (***iv***). **E.** Comparisons for respiration features revealed key differences across brain states. Mean ± S.E.M. respiration waveform during inhalation (***i***) and exhalation (***ii***) across brain states. There was a significant reduction in the duration of inhalation (***iii***) and exhalation (***iv***) during Wake compared to REM and NREM. Similarly, there was a significant reduction in the time required to reach peak in inhalation (***v***) and exhalation (***vi***) during Wake compared to both REM and NREM. There was a significant increase in the amplitude in inhalation (***vii***) and exhalation (***viii***) during Wake compared to both REM and NREM. No significant changes were found in the mean inhalation volume across states (***ix***) unlike in the exhalation volume (***x***) which was weakly yet significantly different across brain states. See Results for statistics.

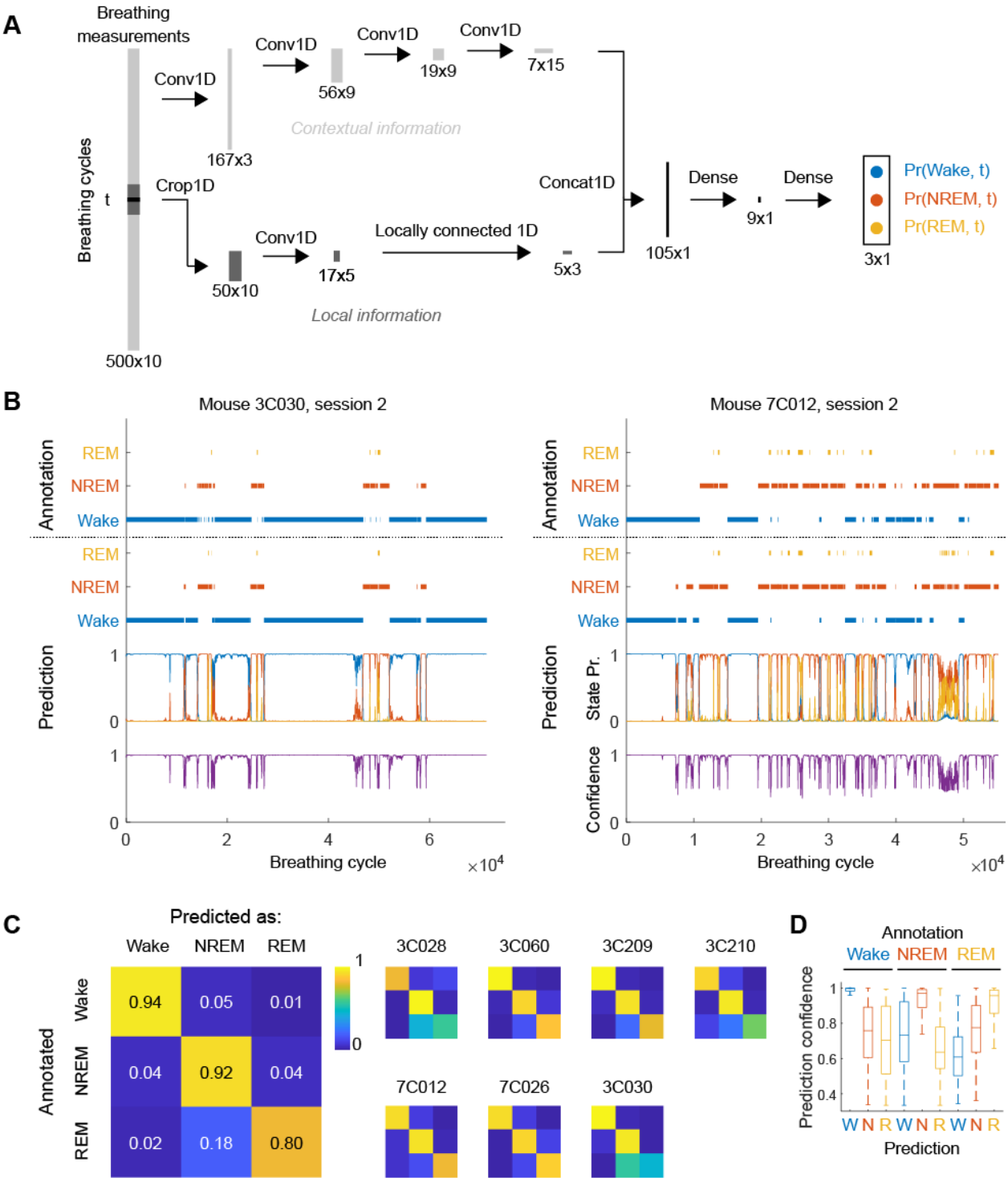

Figure 4: Respiration cycle properties predict brain states

A. Architecture of the artificial neuronal network used to predict the three main brain states from respiratory cycles characteristics. A total of 10 normalized features over 500 cycles around (both before and after) the breathing cycle at index *t* are analyzed to predict the probability of each of the brain states at *t*. The network relies on two branches analyzing the broad contextual (upper branch) and local information (lower

branch) for cycle *t* in parallel, before converging for probability computation (right). Network parameters optimization was supervised: parameters minimized the categorical cross-entropy between the predicted states probabilities and manual annotations of brain states by several experts based on electrophysiological recordings of local-field potentials in freely-moving animals (7 animals). **B.** Prediction of brain states with the predictor in (a) for exemplar sessions from two animals which were alternatively left out of the training process (for validation). Predicted states were chosen as the ones with highest predicted probability. Confidence in the prediction at cycle *t* (=max(Pr(*Wake*, *t*), Pr(*NREM, t*), Pr(*REM*, *t*)))) was computed as the maximal predicted state probability. **C.** Left: Confusion matrix of prediction for all cycles, from all sessions, when each animal was alternatively used for validation (*ie* left out of the parameter optimization process). Values correspond to fractions of annotations (lines sum to 1). Total number of annotated Wake cycles=871387, NREM cycles = 407501, REM cycles=42976. Right: confusion matrices for each individual validation animal. **D.** Confidence for each of the correct predictions (*Wake* as *Wake, NREM* as *NREM* and *REM* as *REM*) compare to all the six types of predictions errors for the validation data as in (c).

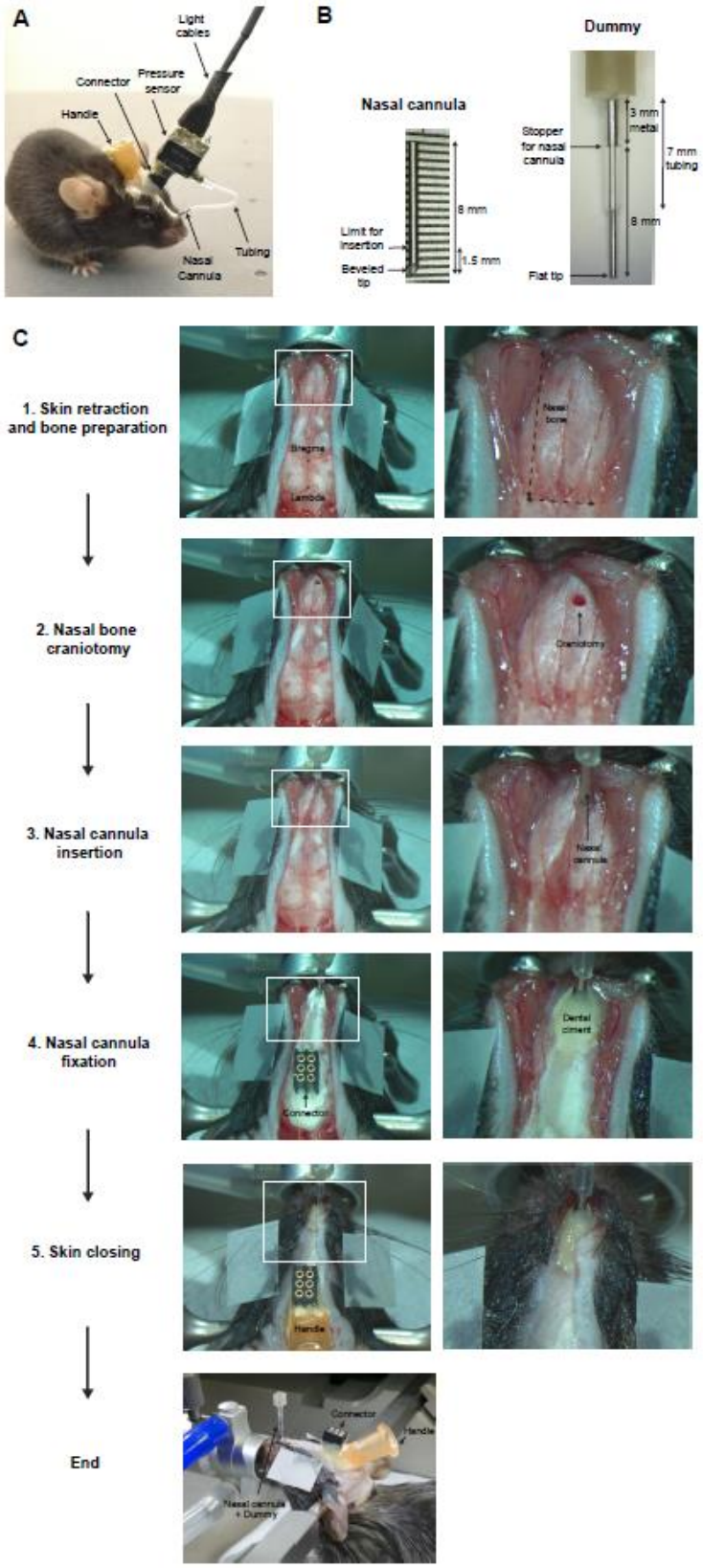

Supplementary Figure 1: Implantation procedure of a nasal cannula for nasal pressure recording in freely moving mice.

A. Photograph of a mouse implanted with a nasal cannula. Nasal airflow from the nasal cavity flows through the nasal cannula and a piece of tubing, and can be detected as variations in pressure by a pressure sensor plugged on a connector cemented on the head of the animal. Pressure signal is then sent to the acquisition board through light cables. A handle can be used for easy manipulation of the mouse by the experimenter. **B.** Photograph of a home-made nasal cannula (left), and its dummy (right). The nasal cannula is 8 mm long, has a beveled tip for optimal signal detection and has a mark at 1.5 mm from the tip to label the limit of insertion during surgery. The dummy is made to be inserted in the nasal cannula until its tip to avoid blockade of the cannula. It holds in the cannula via a piece of tubing which allows stable dummy placement. **C.** Photographs of the 5 steps surgical procedure for nasal cannula implantation. The white rectangle from the left column of

images indicate the position of the zoomed-in photographs from the right column of images.

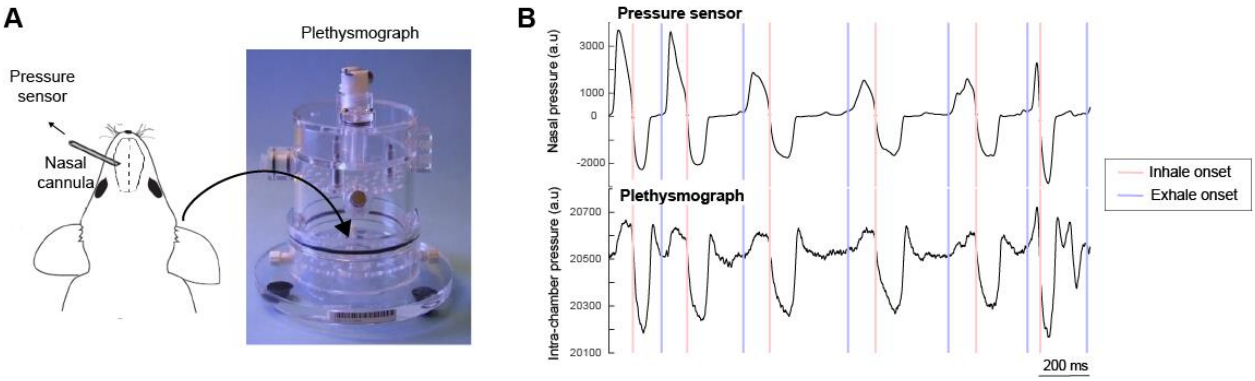

Supplementary Figure 2: Comparison between pressure sensor and plethysmograph signals based on simultaneous recordings.

A. Schematic of the experimental procedure. The nasal cannula connected to the pressure sensor is chronically implanted into the left nasal cavity. The mouse was placed in the chamber of a plethysmograph while nasal pressure was simultaneously monitored. **B.** Examples of raw recordings collected in parallel during wake state showing variations in nasal pressure (top) or plethysmograph pressure (bottom) in arbitrary units.

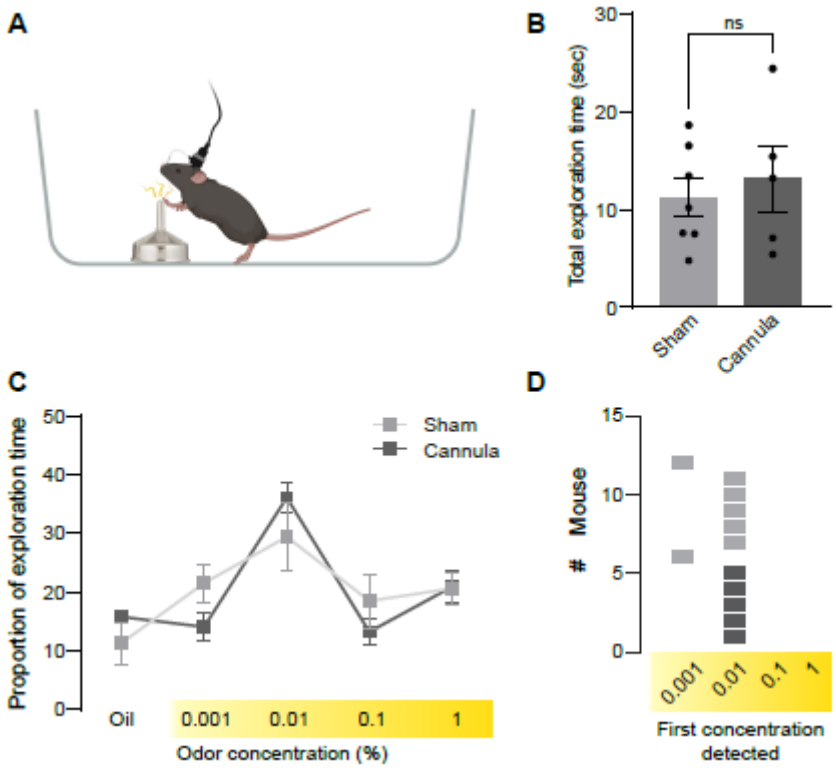

Supplementary Figure 3: Performance of mice implanted with intranasal cannula in an odor detection task.

A. Illustration of the explorative odor detection task (see Methods). **B.** Total exploration time within the 5 trials comparing Sham (gray, n=7) and Cannula (dark gray, n=5) mice. Sham mean 11.23 ± 1.93 sec vs. Cannula mean 13.10 ± 3.38 sec. Mann-Whitney rank sum test: P > 0.999. **C.** Proportion of exploration time spent sniffing mineral oil and increasing concentrations of odor for Sham (gray, n=7) and Cannula (dark gray, n=5) mice. Two-way repeated measures ANOVA interaction: P = 0.395. Data in (**B** and **C**) are expressed as Mean ± SEM. **D.** Distribution of individual mice (Sham, gray, n=7 and Cannula, dark gray, n=5) according to the concentration they detected first.

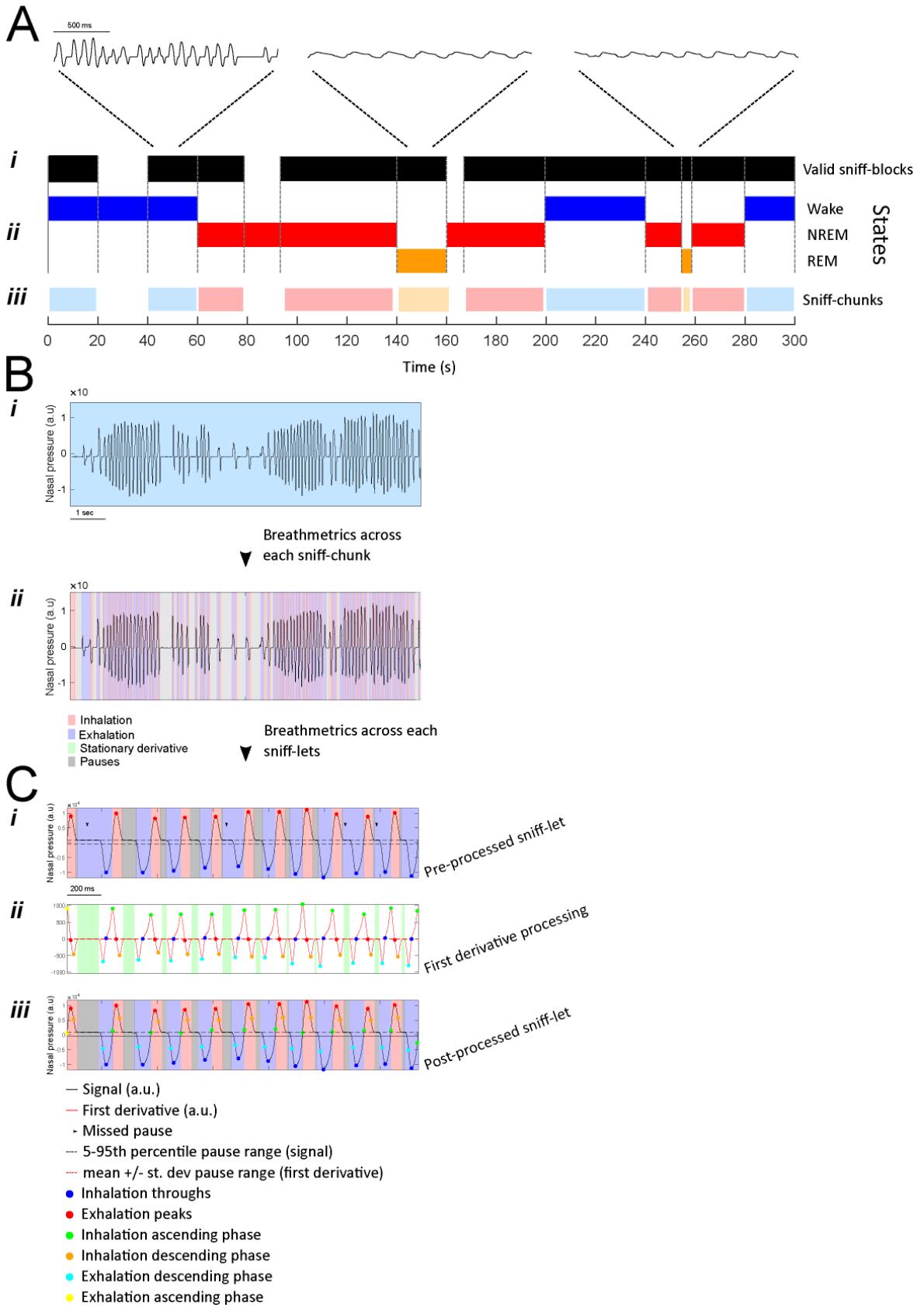
A
500 ms
i
ii
iii
Valid sniff-blocks
Wake
NREM
REM
States
Sniff-chunks
0 20 40 60 80 100 120 140 160 180 200 220 240 260 280 300
Time (s)
B
i
×10
Nasal pressure (a.u)
1 sec
Breathmetrics across each sniff-chunk
ii
Inhalation
Exhalation
Stationary derivative
Pauses
Breathmetrics across each sniff-lets
C
i
200 ms
Pre-processed sniff-let
ii
First derivative processing
iii
Post-processed sniff-let
Signal (a.u.)
First derivative (a.u.)
Missed pause
5-95th percentile pause range (signal)
mean +/- st. dev pause range (first derivative)
Inhalation throughs
Exhalation peaks
Inhalation ascending phase
Inhalation descending phase
Exhalation descending phase
Exhalation ascending phase

Supplementary Figure 4: Pressure sensor analysis pipeline. **A** Schematic representation of a putative respiratory session recorded across time. (***i***) Valid sniff-blocks (black area) represent intervals during which respiration was considered as real. (***ii***) Color-coded intervals representing states (wake = blue, REM = orange, NREM = red) were intercepted with valid sniff-blocks to produce sniff-chunks (***iii***) – consecutive intervals units of valid respiration assigned to an individual state. **B** Representative example of a single sniff-chunk assigned to wake state (***i***) individually analyzed with BreathMetrics (***ii***) returning per-cycle information (inhalation, exhalation, pause intervals, peaks, through etc) across the whole sniff-chunk. **C** Schematic representation of the analytical pipeline used for each individual sniff-let. (***i***) Representative example of an individual sniff-let comprising 11 respiration cycles prior to re-iterative BreathMetrics analysis. ***ii***) First derivative of the respiration signal of the corresponding sniff-let shown in (***i***) highlight minima/maxima (representing inhalation ascending phase, inhalation descending phase, exhalation descending phase and exhalation ascending phase) alternated to stationary epochs (green area). (***iii***) Same sniff-let shown in (***i***) after re-iterative BreathMetrics analysis showed refined inhalation, exhalation and pause intervals.

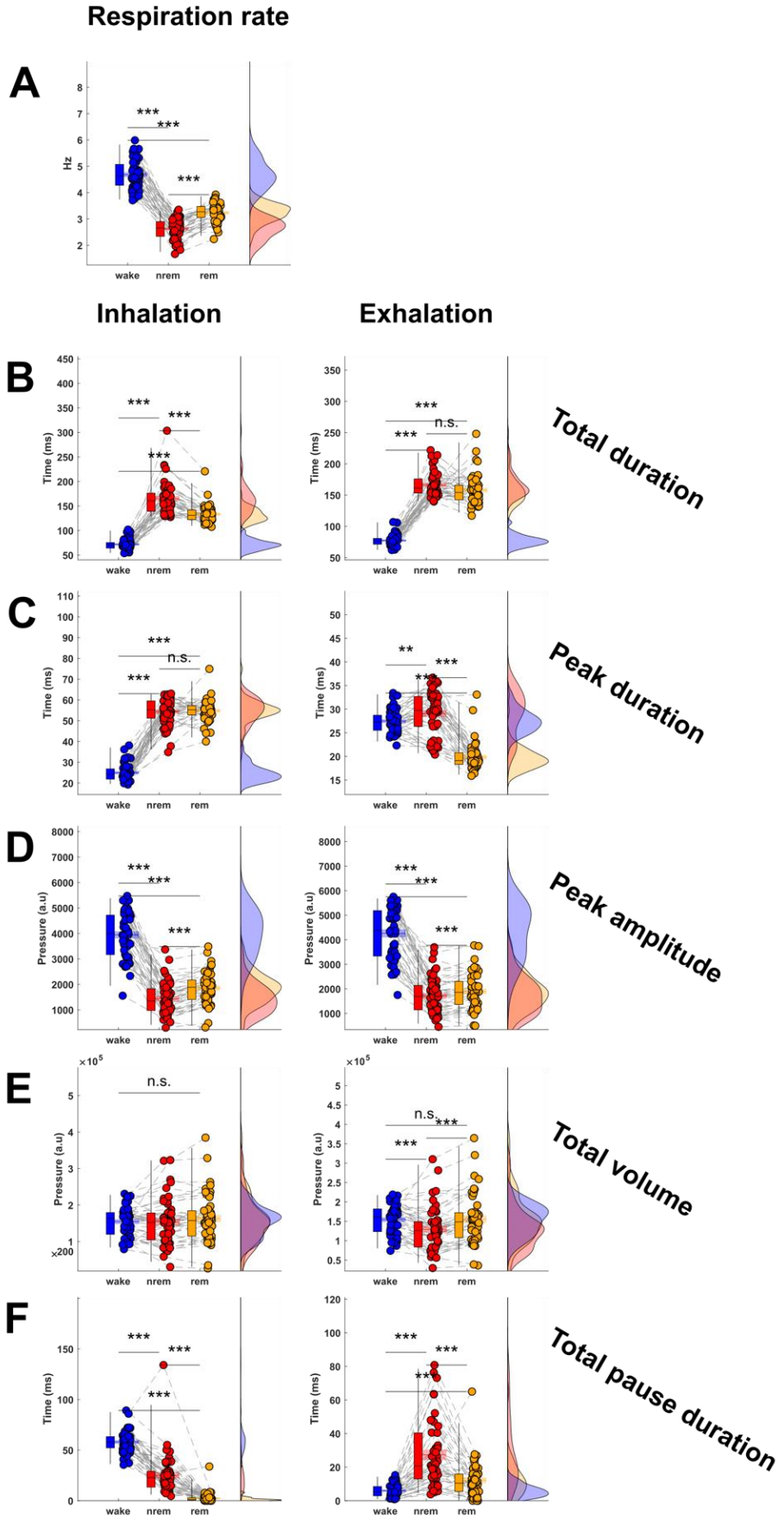
Respiration rate
A
Hz
wake
nrem
rem
Inhalation
Exhalation
B
Time (ms)
Total duration
C
Peak duration
D
Pressure (a.u)
Peak amplitude
E
Total volume
F
Total pause duration
n.s.

Supplementary Figure 5: Comparisons of respiratory cycle features across brain states.

A Comparisons between the respiration rate of each individual session revealed significant increase in wake compared to both REM and NREM which was also significantly reduced compared to REM. **B-F.** Comparisons between mean respiration features of each individual session extracted for inhalation (left column) and exhalation (right column). **B.** Total inhalation duration was significantly reduced during wake compared to both REM and NREM which was also significantly increased compared to REM. Total exhalation duration was significantly reduced during wake compared to both REM and NREM which was instead not significantly different from REM. **C** Inhalation peak duration was significantly reduced during wake compared to both REM and NREM which was instead not significantly different from REM. Exhalation peak duration was significantly reduced during REM compared to both wake and NREM which was also increased compared to wake. **D** Inhalation peak amplitude was significantly increased during wake compared to both REM and NREM which was also reduced compared to REM. Exhalation peak amplitude was significantly increased during wake compared to both REM and NREM which was also reduced compared to REM. **E** Total inhalation volume was not significantly different across brain states, in contrast to the exhalation volume during NREM which was significantly reduced compared to both wake and REM. **F** Total pause after inhalation duration was significantly increased during wake compared to both REM and NREM which was also significantly increased compared to REM. Total pause after exhalation duration was significantly reduced during wake compared to both REM and NREM which was also significantly increased compared to REM.

REFERENCES

Adrian ED. 1942. Olfactory reactions in the brain of the hedgehog. *The Journal of physiology* 100: 459-73

Arshamian A, Iravani B, Majid A, Lundstrom JN. 2018. Respiration Modulates Olfactory Memory Consolidation in Humans. *J Neurosci* 38: 10286-94

Bagur S, Lacroix MM, de Lavilleon G, Lefort JM, Geoffroy H, Benchenane K. 2018. Harnessing olfactory bulb oscillations to perform fully brain-based sleep-scoring and real-time monitoring of anaesthesia depth. *PLoS Biol* 16: e2005458

Bagur S, Lefort JM, Lacroix MM, de Lavilleon G, Herry C, et al. 2021. Breathing-driven prefrontal oscillations regulate maintenance of conditioned-fear evoked freezing independently of initiation. *Nat Commun* 12: 2605

Bathellier B, Buhl DL, Accolla R, Carleton A. 2008. Dynamic Ensemble Odor Coding in the Mammalian Olfactory Bulb: Sensory Information at Different Timescales. *Neuron* 57: 586-98

Bensafi M, Rouby C, Farget V, Bertrand B, Vigouroux M, Holley A. 2003. Perceptual, affective, and cognitive judgments of odors: pleasantness and handedness effects. *Brain Cogn* 51: 270-5

Bloch S, Lemeignan M, Aguilera N. 1991. Specific respiratory patterns distinguish among human basic emotions. *International journal of psychophysiology : official journal of the International Organization of Psychophysiology* 11: 141-54

Boiten FA, Frijda NH, Wientjes CJ. 1994. Emotions and respiratory patterns: review and critical analysis. *International journal of psychophysiology : official journal of the International Organization of Psychophysiology* 17: 103-28

Bolding KA, Franks KM. 2017. Complementary codes for odor identity and intensity in olfactory cortex. *Elife* 6

Brown RP, Gerbarg PL. 2009. Yoga breathing, meditation, and longevity. *Annals of the New York Academy of Sciences* 1172: 54-62

Buonviso N, Dutschmann M, Mouly AM, Wesson DW. 2016. Adaptation and Plasticity of Breathing during Behavioral and Cognitive Tasks. *Neural plasticity* 2016: 2804205

Butler EA, Wilhelm FH, Gross JJ. 2006. Respiratory sinus arrhythmia, emotion, and emotion regulation during social interaction. *Psychophysiology* 43: 612-22

Carey RM, Verhagen JV, Wesson DW, Pirez N, Wachowiak M. 2009. Temporal structure of receptor neuron input to the olfactory bulb imaged in behaving rats. *J Neurophysiol* 101: 1073-88

Carey RM, Wachowiak M. 2011. Effect of sniffing on the temporal structure of mitral/tufted cell output from the olfactory bulb. *J Neurosci* 31: 10615-26

Clarke S, Trowill JA. 1971. Sniffing and motivated behavior in the rat. *Physiol Behav* 6: 49-52

Courtiol E, Hegoburu C, Litaudon P, Garcia S, Fourcaud-Trocme N, Buonviso N. 2011. Individual and synergistic effects of sniffing frequency and flow rate on olfactory bulb activity. *J Neurophysiol* 106: 2813-24

Courtiol E, Lefevre L, Garcia S, Thevenet M, Messaoudi B, Buonviso N. 2014. Sniff adjustment in an odor discrimination task in the rat: analytical or synthetic strategy? *Frontiers in behavioral neuroscience* 8: 145

Cury KM, Uchida N. 2010. Robust odor coding via inhalation-coupled transient activity in the mammalian olfactory bulb. *Neuron* 68: 570-85

Feldman JL, Del Negro CA, Gray PA. 2013. Understanding the rhythm of breathing: so near, yet so far. *Annual review of physiology* 75: 423-52

Fontanini A, Bower JM. 2006. Slow-waves in the olfactory system: an olfactory perspective on cortical rhythms. *Trends Neurosci* 29: 429-37

Fontanini A, Spano P, Bower JM. 2003. Ketamine-xylazine-induced slow (< 1.5 Hz) oscillations in the rat piriform (olfactory) cortex are functionally correlated with respiration. *J Neurosci* 23: 7993-8001

Frumin I, Perl O, Endevelt-Shapira Y, Eisen A, Eshel N, et al. 2015. A social chemosignaling function for human handshaking. *Elife* 4

Gautam SH, Verhagen JV. 2012. Retronasal odor representations in the dorsal olfactory bulb of rats. *J Neurosci* 32: 7949-59
Girin B, Juventin M, Garcia S, Lefevre L, Amat C, et al. 2021. The deep and slow breathing characterizing rest favors brain respiratory-drive. *Scientific reports* 11: 7044
Grimaud J, Murthy VN. 2018. How to monitor breathing in laboratory rodents: a review of the current methods. *J Neurophysiol* 120: 624-32
Grosmaitre X, Santarelli LC, Tan J, Luo M, Ma M. 2007. Dual functions of mammalian olfactory sensory neurons as odor detectors and mechanical sensors. *Nat Neurosci* 10: 348-54
Grosmark AD, Mizuseki K, Pastalkova E, Diba K, Buzsaki G. 2012. REM sleep reorganizes hippocampal excitability. *Neuron* 75: 1001-7
Hardie RJ, Efthimiou J, Stern GM. 1986. Respiration and sleep in Parkinson's disease. *Journal of neurology, neurosurgery, and psychiatry* 49: 1326
Heck DH, McAfee SS, Liu Y, Babajani-Feremi A, Rezaie R, et al. 2016. Breathing as a Fundamental Rhythm of Brain Function. *Front Neural Circuits* 10: 115
Hegoburu C, Shionoya K, Garcia S, Messaoudi B, Thevenet M, Mouly AM. 2011. The RUB Cage: Respiration-Ultrasonic Vocalizations-Behavior Acquisition Setup for Assessing Emotional Memory in Rats. *Frontiers in behavioral neuroscience* 5: 25
Herrero JL, Khuvis S, Yeagle E, Cerf M, Mehta AD. 2018. Breathing above the brain stem: volitional control and attentional modulation in humans. *J Neurophysiol* 119: 145-59
Ito J, Roy S, Liu Y, Cao Y, Fletcher M, et al. 2014. Whisker barrel cortex delta oscillations and gamma power in the awake mouse are linked to respiration. *Nat Commun* 5: 3572
Jessberger J, Zhong W, Brankack J, Draguhn A. 2016. Olfactory Bulb Field Potentials and Respiration in Sleep-Wake States of Mice. *Neural plasticity* 2016: 4570831
Johnson BN, Mainland JD, Sobel N. 2003. Rapid olfactory processing implicates subcortical control of an olfactomotor system. *J Neurophysiol* 90: 1084-94
Karalis N, Dejean C, Chaudun F, Khoder S, Rozeske RR, et al. 2016. 4-Hz oscillations synchronize prefrontal-amygdala circuits during fear behavior. *Nat Neurosci* 19: 605-12
Karalis N, Sirota A. 2022. Breathing coordinates cortico-hippocampal dynamics in mice during offline states. *Nat Commun* 13: 467
Kepecs A, Uchida N, Mainen ZF. 2007. Rapid and precise control of sniffing during olfactory discrimination in rats. *J Neurophysiol* 98: 205-13
Kleinfeld D, Deschenes M, Wang F, Moore JD. 2014. More than a rhythm of life: breathing as a binder of orofacial sensation. *Nat Neurosci* 17: 647-51
Kurnikova A, Moore JD, Liao SM, Deschenes M, Kleinfeld D. 2017. Coordination of Orofacial Motor Actions into Exploratory Behavior by Rat. *Curr Biol* 27: 688-96
Liu S, Han S. 2022. Simultaneous recording of breathing and neural activity in awake behaving mice. *STAR Protoc* 3: 101412
Liu Y, McAfee SS, Heck DH. 2017. Hippocampal sharp-wave ripples in awake mice are entrained by respiration. *Scientific reports* 7: 8950
Macrides F. 1975. Temporal relationships between hippocampal slow waves and exploratory sniffing in hamsters. *Behavioral biology* 14: 295-308
Macrides F, Chorover SL. 1972. Olfactory bulb units: activity correlated with inhalation cycles and odor quality. *Science* 175: 84-7
Manabe H, Mori K. 2013. Sniff rhythm-paced fast and slow gamma-oscillations in the olfactory bulb: relation to tufted and mitral cells and behavioral states. *J Neurophysiol* 110: 1593-9
Matarazzo V, Caccialupi L, Schaller F, Shvarev Y, Kourdougli N, et al. 2017. Necdin shapes serotonergic development and SERT activity modulating breathing in a mouse model for Prader-Willi syndrome. *Elife* 6
McAfee SS, Ogg MC, Ross JM, Liu Y, Fletcher ML, Heck DH. 2016. Minimally invasive highly precise monitoring of respiratory rhythm in the mouse using an epithelial temperature probe. *Journal of neuroscience methods* 263: 89-94

Merle L, Person O, Bonnet P, Gregoire S, Soubeyre V, et al. 2019. Maternal high fat high sugar diet disrupts olfactory behavior but not mucosa sensitivity in the offspring. *Psychoneuroendocrinology* 104: 249-58
Ming X, Patel R, Kang V, Chokroverty S, Julu PO. 2016. Respiratory and autonomic dysfunction in children with autism spectrum disorders. *Brain Dev* 38: 225-32
Mizuseki K, Sirota A, Pastalkova E, Buzsaki G. 2009. Theta oscillations provide temporal windows for local circuit computation in the entorhinal-hippocampal loop. *Neuron* 64: 267-80
Moore JD, Deschenes M, Furuta T, Huber D, Smear MC, et al. 2013. Hierarchy of orofacial rhythms revealed through whisking and breathing. *Nature* 497: 205-10
Mozell MM, Kent PF, Murphy SJ. 1992. The effect of flow rate upon the magnitude of the olfactory response differs for different odorants. *Chemical Senses* 17: 361-61
Noto T, Zhou G, Schuele S, Templer J, Zelano C. 2018. Automated analysis of breathing waveforms using BreathMetrics: a respiratory signal processing toolbox. *Chem Senses* 43: 583-97
Oka Y, Takai Y, Touhara K. 2009. Nasal airflow rate affects the sensitivity and pattern of glomerular odorant responses in the mouse olfactory bulb. *J Neurosci* 29: 12070-8
Oudiette D, Dodet P, Ledard N, Artru E, Rachidi I, et al. 2018. REM sleep respiratory behaviours mental content in narcoleptic lucid dreamers. *Scientific reports* 8: 2636
Perciavalle V, Blandini M, Fecarotta P, Buscemi A, Di Corrado D, et al. 2017. The role of deep breathing on stress. *Neurol Sci* 38: 451-58
Peupelmann J, Boettger MK, Ruhland C, Berger S, Ramachandraiah CT, et al. 2009. Cardio-respiratory coupling indicates suppression of vagal activity in acute schizophrenia. *Schizophr Res* 112: 153-7
Reisert J, Golden GJ, Matsumura K, Smear M, Rinberg D, Gelperin A. 2014. Comparing thoracic and intra-nasal pressure transients to monitor active odor sampling during odor-guided decision making in the mouse. *Journal of neuroscience methods* 221: 8-14
Rice JE, Antic R, Thompson PD. 2002. Disordered respiration as a levodopa-induced dyskinesia in Parkinson's disease. *Mov Disord* 17: 524-7
Rozenkrantz L, Zachor D, Heller I, Plotkin A, Weissbrod A, et al. 2015. A Mechanistic Link between Olfaction and Autism Spectrum Disorder. *Curr Biol* 25: 1904-10
Schreck MR, Zhuang L, Janke E, Moberly AH, Bhattarai JP, et al. 2022. State-dependent olfactory processing in freely behaving mice. *Cell Rep* 38: 110450
Shusterman R, Smear MC, Koulakov AA, Rinberg D. 2011. Precise olfactory responses tile the sniff cycle. *Nat Neurosci* 14: 1039-44
Smear M, Shusterman R, O'Connor R, Bozza T, Rinberg D. 2011. Perception of sniff phase in mouse olfaction. *Nature* 479: 397-400
Sobel N, Prabhakaran V, Desmond JE, Glover GH, Goode RL, et al. 1998. Sniffing and smelling: separate subsystems in the human olfactory cortex. *Nature* 392: 282-6
Sobel N, Thomason ME, Stappen I, Tanner CM, Tetrud JW, et al. 2001. An impairment in sniffing contributes to the olfactory impairment in Parkinson's disease. *Proc Natl Acad Sci U S A* 98: 4154-9
Soria-Gomez E, Bellocchio L, Reguero L, Lepousez G, Martin C, et al. 2014. The endocannabinoid system controls food intake via olfactory processes. *Nat Neurosci* 17: 407-15
Spors H, Wachowiak M, Cohen LB, Friedrich RW. 2006. Temporal dynamics and latency patterns of receptor neuron input to the olfactory bulb. *J Neurosci* 26: 1247-59
Stephenson R, Caron AM, Cassel DB, Kostela JC. 2009. Automated analysis of sleep-wake state in rats. *Journal of neuroscience methods* 184: 263-74
Tort ABL, Brankack J, Draguhn A. 2018. Respiration-Entrained Brain Rhythms Are Global but Often Overlooked. *Trends Neurosci* 41: 186-97
Uchida N, Mainen ZF. 2003. Speed and accuracy of olfactory discrimination in the rat. *Nat Neurosci* 6: 1224-9
Verhagen JV, Wesson DW, Netoff TI, White JA, Wachowiak M. 2007. Sniffing controls an adaptive filter of sensory input to the olfactory bulb. *Nat Neurosci* 10: 631-9

Wachowiak M. 2011. All in a sniff: olfaction as a model for active sensing. *Neuron* 71: 962-73
Welker WI. 1964. Analysis of sniffing of the albino rat. *Behaviour* 22: 223-44
Wesson DW. 2013. Sniffing behavior communicates social hierarchy. *Curr Biol* 23: 575-80
Wesson DW, Carey RM, Verhagen JV, Wachowiak M. 2008a. Rapid encoding and perception of novel odors in the rat. *PLoS Biol* 6: e82
Wesson DW, Donahou TN, Johnson MO, Wachowiak M. 2008b. Sniffing behavior of mice during performance in odor-guided tasks. *Chem Senses* 33: 581-96
Wesson DW, Verhagen JV, Wachowiak M. 2009. Why sniff fast? The relationship between sniff frequency, odor discrimination, and receptor neuron activation in the rat. *J Neurophysiol* 101: 1089-102
Wilson CD, Serrano GO, Koulakov AA, Rinberg D. 2017. A primacy code for odor identity. *Nat Commun* 8: 1477
Yackle K, Schwarz LA, Kam K, Sorokin JM, Huguenard JR, et al. 2017. Breathing control center neurons that promote arousal in mice. *Science* 355: 1411-15
Yanovsky Y, Ciatipis M, Draguhn A, Tort AB, Brankack J. 2014. Slow oscillations in the mouse hippocampus entrained by nasal respiration. *J Neurosci* 34: 5949-64
Youngentob SL, Mozell MM, Sheehe PR, Hornung DE. 1987. A quantitative analysis of sniffing strategies in rats performing odor detection tasks. *Physiol Behav* 41: 59-69
Zelano C, Bensafi M, Porter J, Mainland J, Johnson B, et al. 2005. Attentional modulation in human primary olfactory cortex. *Nat Neurosci* 8: 114-20
Zelano C, Jiang H, Zhou G, Arora N, Schuele S, et al. 2016. Nasal Respiration Entrains Human Limbic Oscillations and Modulates Cognitive Function. *J Neurosci* 36: 12448-67

METHODS

Animals

All experimental procedures were performed in accordance with standard ethical guidelines (European Communities Directive 86/60-EEC) and approved by the local committee on animal health and care of Bordeaux and the French ministry of agriculture and forestry (authorization numbers 18625, 19746, 23974 / facility agreements A33063940 and A33 063 943). All mice were maintained in pathogen free facilities in a diurnal 12h light/dark cycle with food and water ad libitum. A total of 11 mice were used in this study: 9 C57bl6/J male, and 2 OXT-IRES-cre female mice.

Pressure sensor

Pressure sensors (PS) were purchased from Honeywell (part #: SSC S RN N 004ND AA5) (**Supplementary Fig. 1A**). Our protocol is based on a previous approach (Shusterman et al 2011) that we adapted to recordings in freely moving mice in two ways. First we added a 6 pin male connector below the PS to fit a 6 pin female connector cemented on the head of the animal. This ensured a stable fixation of the PS during recordings in freely moving mice. Second, we soldered the input and output electric connections of the PS to thin Litz wires which were themselves held by a pulley system ensuring very low weight on the head of the animal. A piece of polyethylene tubing (801000, A-M Sys-tems, ID 0.015in, OD 0.043 in) of adjustable length allowed to connect the PS port to the nasal cannula. During inhalations, the inward flow of air into the nose causes a decrease in the measured pressure. During exhalations, the outward flow of air from the nose results in an increase in the measured pressure. Besides these inhalation- or exhalations-induced deflections, flat pressure signal corresponds to atmospheric pressure and respiratory pauses.

Nasal cannula

Nasal cannulas were home made from 23G hypodermic stainless steel tube (A-M Systems). Briefly, the tube was cut to an 8mm length and the tip was beveled with a 45 degrees' angle (**Supplementary Fig. 1B**). A mark at 1.5 mm from the beveled tip symbolizes the limit for insertion during surgery. To ensure that cannulas do not get blocked by dust or litter between recording sessions, they are capped with dummy plugs when animals are not being recorded. Dummies consist in 11mm long 27Gx1/2''

industrial dispensing tip (CML supply) (**Supplementary Fig. 1B**). Only 2mm of plastic is kept from the top of the dispensing tip to allow for an easy removal by the experimenter. On this dummy a 3mm piece of 23G stainless steel tube and an 8mm of polyethylene tubing (801000, A-M Sys-tems, ID 0.015in, OD 0.043 in) are glued to the base. The 3mm tube acts as a stopper to ensure that the dummy does not exceed the length of the cannula, and the polyethylene tubing holds the dummy onto the cannula.

Thermocouples

Thermocouple-based measurements of respiratory behaviors rely on the fact that the body temperature of mice (38℃) is warmer than external temperature in our recording conditions (20-24℃). During inhalations, the inward flow of external air into the nose causes a decrease in the measured temperature. During exhalations, the outward flow of air from the nose results in an increase in the measured temperature. Here we used K-type thermocouples (Omega) inserted in the nasal cavity of mice and cemented in place on the skull (see below).

Surgery

Surgeries for local cannula implantation were performed as previously (Smear et al 2011). For local cannula implantation, mice were anesthetized using isoflurane (induction 3 minutes at 4%, then at 1.5% during the surgery). They received an intraperitoneal injection of an analgesic (Metacam, 5mg/kg) and hair above the skull was removed using a hair removing cream (Veet). Mice were then placed on a stereotaxic frame (RWD) where vitals (body temperature, heart rate, blood oxygenation level) were tracked using PhysioSuite (Kent Scientific). The eyes were protected against dryness with Vaseline. A midline incision was performed above the skull and the nasal bone following a local subcutaneous injection of 0.1ml of lurocaine (5mg/kg) (**Supplementary Fig. 1 C1**). The skull was cleaned of any conjunctive tissue using a micro-curette (Fine Scientific Tools). A dental drill (small size) was used to perform a craniotomy in the nasal bone (**Supplementary Fig.1 C2**). We advise to perform the craniotomy with a single and franc movement of the drill ensuring effective opening of the nasal epithelium membrane located right below the nasal bone. During this delicate step, it is important not to touch the turbinates located below the hole with the drill tip to prevent any subsequent clogging of the cannula. Coordinates for optimal respiratory recordings (AP = 3.5-4, ML = 0.5, DV = 1.5mm) were defined from the

junction between the midline and the fronto-nasale sutures (but these can potentially vary depending on the mouse strain and age). During insertion, the beveled tip of the cannula was oriented towards the midline to increase successful signal collection (**Supplementary Figure 1 C3**). We also advise to implant the cannula with its dummy to avoid any blood or tissue to enter the cannula during insertion. Nasal cannula is then fixed to the bone via Superbond (C&B) (**Supplementary Figure 1 C4**), and a 6 pin connector is cemented on the back of the skull to allow attachment of the pressure sensor in subsequent recordings (see Pressure sensor section). Finally, a handle is cemented on the skull to facilitate the immobilization of the mouse during pressure sensor attachment and the skin is closed with Vetbond (3M) (**Supplementary Figure 1 C5-6**). Sham animals used in the odor detection task (**Supplementary Fig.3**) underwent the same surgical procedure except that no craniotomy was performed and the cannula was cemented at the surface of the skull, above the nasal bone.

For 7 mice, high density silicon probes (Buzsaki 32, NeuroNexus) were implanted in the CA1 region of the hippocampus (AP = -1.8, ML=1.4, DV = -1.2). The local field potentials recorded in this region combined with the accelerometer signal obtained from the Intan headstages (RHD 32ch, Intan), allowed brain-state annotations.

For the comparison of the signals obtained from PS and thermocouple (K-type TC, Omega), two symmetrical craniotomies were performed above the nasal bone at the same AP coordinates as for PS implants. PS was implanted as described above. For TC, removal of the nasal bone was performed by progressively thinning the skull with gentle drilling until the highly irrigated nasal epithelium membrane was revealed. The membrane was pierced with a fine cotton tip, creating the hole required to insert the TC 1.5mm deep into the cavity. The craniotomy was then protected with Kwik-Sil (WPI), and the implant was stabilized with Superbond (C&B). For brain state detection, electroencephalogram (EEG) signals were collected using a miniature screw implanted in the cortical bone and referenced to a ground screw above the cerebellum.

Plethysmograph

Whole-body plethysmography (Hegoburu et al 2011, Merle et al 2019) provides a non-invasive biomechanical measure of respiration. Here, a whole-body plethysmograph chamber (Emka Technologies, France) was used to record mouse respiratory activity in parallel with intranasal pressure monitoring. Mouse breathing induces pressure

changes in the plethysmograph chamber. These were captured by a differential pressure sensor that compares pressure in the animal chamber with the reference chamber. Constant airflow (2.2 L/min) was provided through the apparatus. The respiratory signal collected from the plethysmograph was interfaced to a computer equipped an Intan acquisition board (see Data acquisition section).

Data acquisition

Pressure sensor, thermocouple and plethysmograph signals were acquired continuously at 20 kHz on an Intan RHD2000 interface board analog input channels (Intan Technologies). A voltage divider was placed between the pressure sensor and the acquisition board to insure that the voltage range was not exceeding 3.3V. Thermocouple signal was amplified before acquisition (amplification factor: 192). Electrophysiological signals were simultaneously acquired at 20 kHz after being amplified by 32 and 64-channel digital headstages (Intan Technologies).

Pressure sensor data analysis

All analyses were performed using MATLAB (The MathWorks) built-in functions, the FMAToolbox (http://fmatoolbox.sourceforge.net/), Buzsaki lab toolbox – *buzcode* (https://github.com/buzsakilab/buzcode), the freely available MATLAB toolbox from the Zelano lab *BreathMetrics* (https://github.com/zelanolab/breathmetrics) and custom-written scripts.

Respiration was analyzed *post-hoc* using a modified version of *BreathMetrics*, a toolbox designed to automatically describe respiratory features from pressure sensor signals acquired from human or rodent subjects (Noto et al 2018). Here, we used *BreathMetrics* with a redundant re-iterative approach aimed at maximizing the number of respiratory cycles. This was done in order to both account for signal instability of our recordings (baseline drift, electrical noise, transient loss of signal) and to prevent potential artefacts due to radical changes in the respiration pattern across behavioral states. All the documentation and MATLAB functions used in this study can be downloaded from here (https://github.com/RouxLaboratory/BreathMetrics2.0 – *upload pending*). Briefly, the steps followed to analyze respiratory signal of each session are summarized here and can be visualized in **Supplementary Figure 4**. Examples of detections in different brain states can also be inspected in Supplementary Movie 1.

Firstly, the respiratory signal was examined by the experimenter to ensure that only intervals with valid data, “valid sniff-blocks”, were taken into account (ex 0-20s, 40-80s, 95-160 etc in **Supplementary Fig. 4** Ai). This step was necessary for sessions with transient nasal cannula clogging that results in pressure signal loss.

Secondly, valid sniff-blocks were intercepted with brain states (see **Supplementary Fig. 4** Aii wake: 0-60 seconds, 200-240 seconds, 280-300 seconds; sws: 60-140 seconds, 160-200 seconds, 140-260 seconds, 240-255 seconds, 260-280 seconds; rem: 140-160 seconds, 255-260 seconds) previously detected using hippocampal LFP spectral features (theta/delta ratio) and accelerometer (movement) as previously described (Grosmark et al 2012, Mizuseki et al 2009) with the help of a GUI - *TheStateEditor* – available from the buzcode for manual inspection. The resulting “sniff-chunks” contained homogeneous signal belonging to only one behavioral brain state (see **Supplementary Fig. 4** Aiii; wake chunk: 0-20 seconds, 40-60 seconds ecc; sws chunk: 60-80 seconds, 95- 140 seconds; rem chunk: 140-160 seconds, 255-260 seconds).

Thirdly, each sniff-chunk was individually analyzed using *BreathMetrics (***Supplementary Fig. 4** Bi), so that a preliminary characterization of the respiratory cycles could be obtained (**Supplementary Fig. 4** Bii). However, we noticed that errors in the detection of the onset/offset of the respiratory components were frequently encountered mostly due to the inaccurate pause detection. More rarely, respiratory cycles were found to be “skipped” due to short epochs of baseline-drift in the raw signal, heavily altering the quality of the results during those short windows. To account for this, we used *BreathMetrics* with a redundant re-iterative approach to maximize the number of respiratory cycles in each sniff-chunk. We further split each sniff-chunk in “sniff-lets”, short time intervals containing the signal of 10+1 pre-detected respiration cycles (see **Supplementary Fig. 4** Ci). Theoretically each sniff-let contained 11 cycles but this was ensured by iteratively altering its signal with a moving-average window correction of increasing size (20 iterations, window size 1-3 seconds). In each iteration, the altered signal was run with *findExtrema* from *BreathMetrics* toolbox yielding each time the number of detected respiratory cycles. At the end of 20 iterations, the altered signal with highest number of sniff cycles was chosen for the next steps – otherwise the raw signal was maintained. Once ensured each sniff-let contained the highest

number of cycles, the signal was re-examined using the following functions from *BreathMetrics* toolbox:

Breathmetrics
correctRespirationToBaseline
findExtrema
findOnsetsAndPauses
findInhaleAndExhaleOffsets
findBreathAndPauseDurations
findInhaleAndExhaleVolumes

In order to obtain a finer detection of respiratory components (in particular pauses during wake state), we took into account minima and maxima of the sniff-let raw signal first derivative reflecting troughs and peaks in the rate of instantaneous pressure (see **Supplementary Fig. 4** Cii).
In each sniff-let, inhalation and exhalation were re-calculated after pause detection which were assigned if the following criteria were simultaneously met (see **Supplementary Fig. 4** Ciii):

a) pressure signal in the 5-95th percentile range during previously assigned pauses epochs of the entire sniff-chunk;
b) first derivative in the mean + standard deviation of the first derivative signal during previously assigned pauses epochs of the entire sniff-chunk;
c) outside of the window between ascending peak and descending through of the first derivative of the sniff-let (putative inhalation);
d) outside of the window between descending through and ascending peak of the first derivative of the sniff-let.

<u>Pressure sensor data analysis prior to brain state predictor</u>

The brain state predictor requires to process the nasal pressure signal with *BreathMetrics* as it uses the respiratory cycle features for state detection. However, in this case, knowledge about the brain state the animal is in is obviously absent since this is precisely the information the predictor is supposed to retrieve. In this case, we ran breathmetrics on each valid sniff-block, without breaking out the signal into state-specific chunks. The same analysis pipeline as the one described above was conducted.

Thermocouple data analysis

Raw thermocouple and PS signals were downsampled to 1250 Hz for analyses. The signal was then smoothened using a Gaussian kernel (SD = 32 msec) in order to avoid spurious peak detection in noisy TC signals. Detection of peaks was performed using *findpeak* function in MATLAB. Inhale onsets detected in the PS signals with our modifier version of *BreathMetrics* were then aligned on each TC peak to examine the time delays between the two.

Automated brain state prediction with artificial neural networks

Training data

We set out to train a predictor for brain states (*Wake, REM* and *NREM* sleep) with a supervised strategy in which annotated data from experts served as exemplars for non-annotated data. Brain state annotation was based on electrophysiological recordings acquired in the hippocampus during freely-moving recording sessions with varying *Wake*/*REM*/*NREM* fractions. The same animals were equipped with nasal pressure sensors for simultaneous characterization of breathing. Recordings from 7 animals (males and females) were analyzed and annotated by different experts for training: animal 3C028 (3 sessions), 3C060 (4 sessions), 3C209 (3 sessions), 3C210 (3 sessions), 7C012 (4 sessions), 7C026 (3 sessions), 3C030 (4 sessions).

Data normalization

Respiratory features extracted by *BreathMetrics* and used for prediction were the following: ‘peakInspiratoryFlows','troughExpiratoryFlows', 'inhaleTimeToPeak', 'timeToTroughs', 'inhaleVolumes', 'exhaleVolumes', 'inhaleDurations', 'exhaleDurations', 'inhalePauseDurations', 'exhalePauseDurations'. Values obtained for each individual cycle feature were first normalized to approximately distribute over the range [-1, 1] with a Gaussian-like shape to facilitate the training of artificial neuronal networks. We applied the normalization function $f(x) = sign(x) \log (1 + |(x - a)/b|)$ with parameters *a* and *b*, after thresholding outlier values (0.1% and 99.9% quantiles). Parameters were fixed *a priori* and were used unchanged for all sessions from all animals.

Artificial neuronal network

We designed an artificial network specialized for brain state prediction as shown in **Fig.4A**. It takes as inputs 500 breathing cycles described by 10 normalized features. The network is composed of two sets of layers: 1) a set of convolutive layers which can extract broad contextual information, 2) locally connected layers processing data around the breathing cycle of interest. Outputs of both branches are then concatenated and combined with densely connected layers to predict the probabilities of each three states. Activation functions are all rectified linear units (ReLU), except for the output layer which uses the softmax function. A total of 3772 parameters are required.

Implementation detail

The algorithm was implemented using Python Jupyter notebook. Numpy and Scipy libraries are mainly used for mathematical computation. The proposed artifcial NN structures are implemented thanks to the TensorFlow (2.0.0) dedicated library with GPU support.

Parameter training and validation

Network parameter optimization was carried out using sessions from 6 animals, leaving one out for validating the ability of the network to infer generalized properties of breathing features and brain states to other animals, while avoiding overfitting of the training data. Training was therefore repeated 7 times, cycling through different animals for validation. Parameter optimization was performed by minimizing the categorical cross-entropy between the discrete manual annotations of states and the continuous prediction of their probabilities by the networks. To cope for the imbalance between the frequency of each state (REM being the rarest), different weights were used for the prediction of sates: 0.1 for *Wake* cycles, 0.25 for *NREM*, and 1 for *REM*. A gradient-descent-type algorithm (Nadam) was used with learning rate 10^{-5}. 150 iterations were performed, in which only 2.5K random cycles were analyzed from each training sessions to limit memory usage. For training only, ‘dropout’ (with a rate of 10%) layers were inserted between the layers in **Fig. 4A** to regularize the optimization problem and thus limit training data overfitting.

Explorative odor detection task

The explorative odor detection task was adapted from previous studies (Soria-Gomez et al 2014). Briefly, the materials used consisted of a test cage similar to the home

cage but with an odor holder that was made from a stainless-steel lid of an unused mouse water bottle. The bottle lid fit flush in a hole which prevented it from being displaced by the mice during the test. The tip of the lid's nozzle extended 5cm and contained a 3mm hole from which odors could emanate. Cameras were installed above the test cage and on each side of the odor holder to allow easier visualization**.** The cage was placed on a table in a dedicated testing room (separate to the housing room).

The behavioral protocol consisted of 2 days of habituation to the test cage before the test day. Each mouse was placed in the test cage for 3 minutes each of 5 separate trials for the odor detection experiment with a 3-minutes inter-trial interval. Before each trial, 10 µL of mineral oil was placed on a 2cm strip of filter paper and placed in the odor holder. All mice were water deprived after the 2nd day of habituation for 24 hours before the test to increase their motivation to explore.

Based on a serial dilution method with mineral oil, increasing concentrations of the odor (Isoamyl acetate [banana-like (Sigma-Aldrich)]) was tested as follow: mineral oil, 0.001%, 0.01%, 0.1% and 1%. 10µL of these solutions were placed on a strip of filter paper immediately before each trial and then introduced inside the nozzle of the odor holders. The odor holders were cleaned with 4% sodium bicarbonate and water between trials and experiments.

The time mice spent investigating the presented odor was counted manually using a customized program (BehavScor v3.0 beta): considered epochs corresponded to the time intervals when mice directed their nose <1cm from the tip of the holder. Mice exploring less than a total of 5 seconds within the 5 trials were excluded from the analysis and each animal was tested only once with a single odor. The odor threshold was defined as the odor concentration the most explored or the lower odor concentration for which the mice spent less than 10% to investigate it as compared to the most explored concentration.

Statistical Analyses

Statistical analyses were performed using MATLAB scripts. Most comparisons were performed using repeated measure ANOVA tests. For *post-hoc* tests, Bonferroni corrections were applied to account for multiple comparisons. Additional nonparametric tests (Mann-Whitney U tests or Wilcoxon signed rank tests in the two-tailed configuration) were conducted. Linear regressions were conducted using

Pearson's linear correlations and tested using a Student's t distribution (MATLAB *corr* function). Significance was set with alpha = 0.05 and was represented on graphs as the following: * = P < 0.05, ** = P < 0.01, ***= P < 0.001, **** = P < 0.0001. As mentioned in the figure legends, individual data-points are plotted above bars indicating mean ± SEM next to box plots (representing 25th, 50th, 75th percentile of distribution).

Method references

Grosmark AD, Mizuseki K, Pastalkova E, Diba K, Buzsaki G. 2012. REM sleep reorganizes hippocampal excitability. Neuron 75: 1001-7

Hegoburu C, Shionoya K, Garcia S, Messaoudi B, Thevenet M, Mouly AM. 2011. The RUB Cage: Respiration-Ultrasonic Vocalizations-Behavior Acquisition Setup for Assessing Emotional Memory in Rats. Frontiers in behavioral neuroscience 5: 25

Merle L, Person O, Bonnet P, Gregoire S, Soubeyre V, et al. 2019. Maternal high fat high sugar diet disrupts olfactory behavior but not mucosa sensitivity in the offspring. Psychoneuroendocrinology 104: 249-58

Mizuseki K, Sirota A, Pastalkova E, Buzsaki G. 2009. Theta oscillations provide temporal windows for local circuit computation in the entorhinal-hippocampal loop. Neuron 64: 267-80

Noto T, Zhou G, Schuele S, Templer J, Zelano C. 2018. Automated analysis of breathing waveforms using BreathMetrics: a respiratory signal processing toolbox. Chem Senses 43: 583-97

Shusterman R, Smear MC, Koulakov AA, Rinberg D. 2011. Precise olfactory responses tile the sniff cycle. Nat Neurosci 14: 1039-44

Smear M, Shusterman R, O'Connor R, Bozza T, Rinberg D. 2011. Perception of sniff phase in mouse olfaction. Nature 479: 397-400

Soria-Gomez E, Bellocchio L, Reguero L, Lepousez G, Martin C, et al. 2014. The endocannabinoid system controls food intake via olfactory processes. Nat Neurosci 17: 407-15

PART 2

Title: Blocking oxytocin receptors in the piriform cortex unexpectedly promotes specific social behaviors

Authors: Camille Miermon, Alena Spitsyn, Tiphaine Dolique, Fabrice de Chaumont, Lisa Roux

Abstract:

The neuropeptide oxytocin has been widely described as having pro-social effects. Indeed, the stimulation of its release increases social interactions and social memory. In rodents, olfaction is crucial for social behaviors. It allows for the detection and recognition of an individual thanks to the unique combination of odorants it produces. Those odorants, after binding onto specific receptors in the olfactory epithelium, activate the olfactory bulb and higher order cortical areas such as the piriform cortex. This cortex has been described to encode odor identity and to be involved in the formation of olfactory memory. Because, recent evidence indicates that the piriform cortex receives oxytocinergic fibers and express a high density of oxytocin receptors in female mice, we made the hypothesis that oxytocin could modulate the perception and/or memory of conspecifics in females. To test this, we pharmacologically blocked oxytocin receptors in the piriform cortex of female mice performing social tasks. We found that this local piriform cortex blockade unexpectedly promoted specific types of social interactions, and tended to induce a higher level of olfactory driven social interest. No pharmacological effects were found on social memory however. Thus, our results are controversial with regards to the literature, and could imply that endogenous oxytocin in the piriform cortex does not have a pro-social effect.

Introduction:

Oxytocin (OXT) is a 9 amino acids neuropeptide mainly produced by the paraventricular nucleus of the hypothalamus, the supraoptic nucleus, and the accessory nuclei of the hypothalamus (Sofroniew 1983; Swanson and Sawchenko 1983). Plethora of evidence have demonstrated the role of OXT as a powerful modulator of social behaviors. Historically, OXT has been best described in the context of parturition, lactation (Jurek and Neumann 2018), and maternal behaviors (Insel, 1992; Kendrick and Keverne 1992; Marlin et al. 2015). Yet, maternal behaviors are far from being the only social behaviors in which OXT has been involved. Indeed, OXT

has also been described to promote sexual behavior (Caldwell 1992; Argiolas 1992; Nakajima et al., 2014), to increase the duration of social interactions and social memory (Oettl et al. 2016), to facilitate pair-bonding (Williams et al. 1994; Young et al., 1998) and to increase trust (Kosfeld et al. 2005). These effects have led to the designation of OXT has a “pro-social” neuropeptide. It is not surprising then, that individuals impaired in the production of OXT or the oxytocin receptor (OXTR) display impaired social behaviors. OXT and OXTR KO mice are aggressive, spend less time interacting and fail to develop social memory (Ferguson et al. 2000; Takayanagi et al. 2005; Sala et al. 2011; Pobbe et al. 2012). Of note, rats with OXTR specific deletion in a part of the olfactory cortex, the anterior olfactory nucleus (AON), are also impaired in social memory (Oettl et al. 2016) suggesting that OXT is important in the olfactory system for social behaviors.

Olfaction is one of the most important sensory modality for rodents. They use it to navigate in the environment, detect danger from predators, find mates but also to recognize and form memories of conspecifics (Ache and Young 2005; Sullivan et al. 2015). Indeed, to recognize conspecifics, rodents can use the unique olfactory signature (composed of volatiles and non-volatiles molecules) that defines an individual (Natynczuk and Macdonald 1994; Stopka, Janotova, and Heyrovsky 2007). In the olfactory system, volatile odorants are processed by the main olfactory system. After their detection by olfactory sensory neurons of the olfactory epithelium, volatile odorants induce the activation of the main olfactory bulb which in turn project to higher order processing areas (Imai 2014). The piriform cortex (PIR) is one of these structures. It is the largest olfactory area in the brain and receives convergent inputs from the amygdala, lateral entorhinal cortex, olfactory tubercle, the orbitofrontal cortex and the main olfactory bulb (Hagiwara et al. 2012; Courtiol and Wilson 2017). The PIR has been described for its role in olfactory memory as it is associated with odor-association learning (Roesch et al., 2006; Choi et al. 2011; Wilson and Sullivan 2011).

c-FOS staining reveals that the PIR is activated during social interactions (Kim et al. 2015), and that it both receives OXTergic fibers (Choe et al. 2015), and expresses a particularly high density of OXTRs as compared to other cortical regions (Mitre et al. 2016). Interestingly, levels of OXTR expression in the PIR are higher in female mice compared to males (Mitre et al. 2016), suggesting that the PIR of female mice is more sensitive to OXT modulation. Finally, OXTR signaling in the PIR is required for social

learning (Choe et al. 2015). Because OXT modulates social behaviors, and since social behaviors rely on the olfactory system in which the PIR is a central player sensitive to OXT, we wondered: what is the endogenous role of OXT in the PIR of female mice? Does OXT in the PIR of female mice facilitate social behaviors and social memory? To address these questions, we used pharmacology and selectively blocked OXTR signaling in the PIR during social interactions and social memory tasks.

Methods:

Animals

All experimental procedures were performed in accordance with standard ethical guidelines (European Communities Directive 86/60-EEC) and approved by the local committee on animal health and care of Bordeaux and the French ministry of agriculture and forestry (project authorization numbers #18625 and 19746 / facility agreement #A33063940). All mice were maintained in a pathogen free facility in a diurnal 12h light/dark cycle with food and water ad libitum. Experimental mice used in this study were 14-22 week-old heterozygous OXT-IRES-cre (Oxt-cre) female mice (Jackson Laboratory stock #024234). The colony was maintained on the original C57bl/6x129s background. In this mouse line, the cre-recombinase is expressed under the control of the endogenous oxytocin promoter. In this study, we did not take advantage of the cre expression in the OXT neurons, but it allowed us to validate behavior on this mouse line for later optogenetic manipulation. Unless otherwise specified, stimulus mice used in this study were 5-12 week-old outbreed NMRI females.

Pharmacology - Drug preparation and administration.

For local blockade of OXTRs within the aPC, we used intracerebral infusions of the OXTR antagonist (d(CH_2)$_5^1$,Tyr(Me)^2,Thr^4,Orn^8,des-Gly-NH_2^9)-Vasotocin (OTA) (Bachem). Single infusion cannulas (Bilaney) were glued together with 5mm spacing to form bilateral implants customized to target the aPIR in both hemispheres (aPIR ML = +/-2.5). To minimize potential tissue damage around the infusion sites, our injectors projected 1.5mm below the tip of the cannulas. This enabled us to implant the cannulas above the aPIR and reach it *via* the injector for the infusions. During experiments we injected 1µL of 1µM OTA at 0.5µL/min using an infusion system (Legato 101) with 1µL

syringes (Hamilton 7000). To insure proper drug diffusion, we maintained the injector in place two minutes after the infusion stopped.

For systemic OXTR blockade, we used the high affinity non-peptide OXTR antagonist L-368.899 (OTA-L) (Tocris Bioscience) which crosses the blood-brain barrier (Boccia et al. 2007). After being solved in DMSO and saline (1.25% and 98.75%, respectively), OTA-L was administered intraperitoneally at 10mg/kg. As in a previous study (Pisansky et al. 2017), we waited 30 minutes post-injection before behavioral testing. A vehicle solution containing a mixture of 1.25% DMSO and 98.75% saline was used as control.

Surgery

For local cannula implantation, mice were anesthetized using isoflurane (induction 3 minutes at 4%, then at 1.5% during the surgery). They received an intraperitoneal injection of an analgesic (Meloxicam, 5mg/kg) and hair above the skull was removed using a trimmer. Mice were then placed on a stereotaxic frame (RWD) where vitals (body temperature, heart rate, blood oxygenation level) were tracked using PhysioSuite (Kent Scientific). The eyes were protected against dryness with Vaseline. A midline incision was performed above the skull following a local subcutaneous injection of 0.1ml of lurocaine (5mg/kg). The skull was cleaned of any conjunctive tissue using a micro-curette (Fine Scientific Tools). A dental drill was then used to perform the craniotomies above the aPIR (AP = +1.6mm, ML = +/- 2.5mm). The bilateral cannula implant was then inserted 1.5mm deep and cemented to the bone with SuperBond (C&B). A holder was cemented at the back of the skull to facilitate head maintenance during the insertion of the injector in the experiments that followed. A 6 pin connector was also cemented to attach the reflector cues that allow tracking the mice during the experiments. Finally, the skin was closed with Vetbond (3M). Mice were allowed a minimum of two days to recover before the beginning of the behavioral experiments.

Behavior

Habituation-Dishabituation task

The habituation dishabituation task is a social memory paradigm where an individual is free to explore another individual – a “stimulus” mouse for four consecutive trials. On the last trial, the contained individual is replaced by a new one. Because mice are

innately attracted by novelty, mice typically show a decrease of interest throughout the four trials and a rebound of interest towards the new individual is typically observed (Ferguson et al. 2000). Our custom-made set up consisted of a 36x36cm arena connected to a start box. The enclosure containing the stimulus mice was placed in the middle of the arena. This enclosure (Aquineuro) consisted in a transparent cylinder (12 cm diameter) made of evenly spaced vertical bars (to allow mutual interactions between mice) and a circular top. Care was made to limit the maximum light intensity to 14Lux. Between each session, the arena and the cylinder were cleaned with an odor-free solution of sodium bicarbonate 4%. During the task, an initial 5-minute exploration of the arena was performed to establish the general locomotion of our experimental mouse. This exploration was followed by the aPIR infusion of either saline or OTA, and a 10-minute rest period in an isolated neutral cage. After that, five trials of 3 minutes separated by 10-minute inter-trial intervals were performed. The beginning of a trial was defined as the first time the experimental mice entered the sniffing zone (4cm radius around the cylinder). To reduce stress, experimental mice were habituated for three days prior to testing: the first 2 days they were allowed to explore the arena, the 3rd day a mouse was place in the cylinder (different than the mouse used for testing). They also received intracerebral infusion on the last day of habituation. Stimulus mice were also habituated to the cylinder during those 3 days (10 minutes / day inside the cylinder). On the day of testing, mice arrived in the experimental room 10 minutes before the task. Care was always taken to place experimental and stimuli mice at opposite sides of the room to limit odor contamination. Mice were used for up to four sessions and received injections of both saline and OTA with a minimum of 1 day between the two conditions. In the case of 4 mice, the loss of the pharmacological cannula's dummy induced the clogging of the cannula and reduced the total number of sessions.

Three chamber test – classic and olfactory versions

The three-chamber test can be used as a sociability and/or a social memory task (Yang, et al., 2016). In the sociability test, an experimental mouse is free to explore one of three compartments (or chambers) each containing (1) an object, (2) a mouse, or (3) nothing (middle chamber). If mice are "social", they spend more time in the social chamber (containing the mouse). The second part of the test is intended to assess social memory performance. Mice can again explore the three compartments which

now contain (1) the mouse they previously met (familiar mouse), (2) a new mouse or (3) nothing. Because of their innate “novelty-seeking” behavior, if mice remember having explored the familiar mouse, they spend more time with the novel one. The particularity of our paradigm, is that before this test, experimental mice were allowed a 5-minute free exploration of the arena which enabled us to estimate general locomotion and possible intrinsic place preference. This was followed by the aPIR infusion of either SAL or OTA, and a subsequent 10-minute rest period. Then the test consisted of two times 10-minute free exploration of the three compartments (sociability test followed by memory test) separated by a 10-minute inter-trial interval. To avoid a possible confound due to the fact that mice can show displaced object recognition memory, we chose to leave the familiar mouse in the same chamber during sociability and social memory tasks. In our experiments, the test arena consisted of three 36*26cm chambers, with two 12cm diameter cylinders placed in the center of the left and right chambers. Mice were habituated to the arena for two days and for four days to intracerebral injections prior to testing. Stimulus mice were habituated for three days to be inside the cylinder (10min / day). Experimental mice were randomly assigned on either saline or OTA group and received only one injection. Between each session, the arena and the cylinders were cleaned with an odor-free solution of sodium bicarbonate 4%. In a separate set of experiments, we wanted to isolate the importance of the stimulus mouse’s odor in the performance of the task. A subset of mice moved on to an olfactory version of the three-chamber test. In this version, the social stimulus was replaced by soiled NMRI bedding distributed over the whole compartment. Control stimuli consisted of clean bedding.

Live Mouse Tracker

The Live Mouse Tracker (LMT) is a technology used for live automated tracking and behavioral labelling of multiple animals for long periods of time in a 50x50cm arena (Chaumont et al. 2018). Briefly, both tracking and behavioral labelling rely on an infrared (Kinekt) camera placed above the arena and processing of the acquired images through machine learning approaches. Reliable mouse identification is based on the Radio Frequency Identification (RFID) technology: mice are implanted with RFID tags placed under the skin on the side of their body and a floor containing RFID antennas is positioned below the arena. Antennas are transiently turned on based on the animals’ position to detect the RFID numbers. Thanks to fine detection of mice

body parts such as the nose, a wide variety of behavioral motives can be extracted (Chaumont et al. 2018).This technology allowed us to analyze in an unbiased an automatized manner the specific profiles of social interactions displayed by two freely moving mice the first time they meet in a naturalistic setup. Experimental and stimulus mice were independently habituated to the arena with their home cage partner for 10 min over 2 days. Experimental mice were also habituated to injections (either intracerebral (for Fig 3) or intraperitoneal (for Fig 1) for 2 days prior to testing, with NaCl (0.9%). Mice were randomly assigned to either the vehicle or the drug condition. Some mice from the Fig 3 experiment were also used in the classical and olfactory three chamber test, and thus had already received pharmacological infusions.

Data analysis

Habituation-Dishabituation task

To measure the amount of time experimental mice spent around the cylinder, 3D localization was tracked using an Optitrack system. This technology is based on the detection of reflective markers by multiple infrared cameras. In our conditions, six infrared cameras were tracking an ensemble of five markers - a “Mouse Tree” – attached on the head of the experimental animal, as well as four markers for the extremities of the arena and five markers on top of the cylinder. Thanks to the high number of Mouse Tree markers and cameras, 3D position of the mouse was followed at all times during the task. The center of mass for the Mouse Tree markers was used as a proxy for head position. Using custom-made Matlab codes (the MathWorks), position data of the Mouse Tree barycenter was analyzed to count the amount of time, and number of instances mice were detected in a 4cm radius around the cylinder (green trajectory – inside sniffing zone Fig 5.B). The time spent in the rest of the arena was deduced by taking the time the animal was not detected in this radius (orange trajectory – outside sniffing zone Fig 5.B). Because mice could be in the sniffing zone but not actually be sniffing each other, we also manually scored sniffing events using the video recordings which were simultaneously acquired during the experiments with a webcam (Logitech) placed next to the arena. A sniffing event was defined as an epoch when the experimental mouse is immobile in the sniffing zone and showing interest for the stimulus mouse’s nose, body or tail. We used this slightly different measure than the classical nose-nose measure, to reflect the experimental mouse’s

interest independently from the interest of the stimulus mouse. However, the time of the first nose-nose event of each trial was also detected, as this likely reflect the initial interest of the two mice for each other. To be able to compare the social memory performance of the two pharmacological groups, an index was defined as the following:

$$\text{Index} = (\text{Retention}-T4)/(\text{Retention}+T4)$$

Three chamber test – classic and olfactory

These experiments were performed using webcam video recordings as mice were not carrying any reflective markers. To measure the amount of time spent in the three compartments, we made use of the bonsai software (https://bonsai-rx.org/). Bonsai is an open source software based on visual reactive programming which makes it easy to build complex workflows working with different type of data (video, audio, Arduino, TTL …) and to analyze them online or offline. In our case, we used it to detect mouse localization offline. After loading the video in the software, we manually defined three regions of interest (ROIs) corresponding to the three compartments but leaving out the cylinder areas (to exclude times where the mouse was climbing on the cylinder). Briefly, we converted the color of the video to hue saturation value (HSV) color space in which each HSV color is defined by the combination of color, brightness and saturation value hereby making the mouse's color unique. After applying an HSV threshold, we obtained x/y position of the centroid of the biggest shape corresponding to the mouse's body. Information of the mouse's position in each compartment was then combined and exported in an excel file. Using custom-made Matlab (the MathWorks) codes, we then calculated the time spent in each compartment across time. We also manually scored the number of sniffing events (cf "Data analysis, Habituation-Dishabituation task" for definition*).* For the olfactory version of the three-chamber test, the same approach was applied except that no area had to be left out as no cylinders were used in this case. To be able to compare the sociability and social memory performance of the two pharmacological groups, an index was defined as the following:

$$\text{Sociability index} = (\text{Social}-\text{Non-social})/(\text{Social}+\text{Non-social})$$

$$\text{Social memory index} = (\text{New}-\text{Familiar})/(\text{New}+\text{Familiar})$$

Live Mouse Tracker

A Python-based pipeline for behavioral data extraction is available online (https://github.com/fdechaumont/lmt-analysis) (Chaumont et al. 2018).Based on these data, we developed a Matlab code to analyze duration and number of events for the behaviors of interest.

Histology for cannula placement validation

Mice were deeply anaesthetized using a mix of Ketamine (100mg/ml) and Xylazine (20mg/ml) (i.p injection) and transcardially perfused with PBS followed by 4% paraformaldehyde in PBS. Brains were fixed overnight in 4% paraformaldehyde then sliced at 50-80 micron thickness using a vibratome (Leica VT 1000 or VT1200). Slides were washed and counter-stained for 5 min with 4′,6-diamidino-2-phenylindole (DAPI) (1:10000, Fisher Scientific), and mounted with Fluoromont mountain medium (Invitrogen). Fluorescent images were imaged with an epifluorescence microscope (Eclipse Ni-U, Nikon) and collected with an Zyla SCMOS camera (Andor Technology).

Immunohistochemistry

Brain preparation: Mice were deeply anaesthetized using a mixture of Ketamine (100mg/ml) and Xylazine (20mg/ml) (IP injection) and transcardially perfused with phosphate-buffered saline (PBS) followed by 4% paraformaldehyde. Brains were fixed overnight in 4% paraformaldehyde then sliced at 50-70 µm thickness using a vibratome (Leica VT 1200).

Immunostaining procedures and imaging: For OXT fibers identification, endogenous eYFP genetic labeling was used. Coronal sections containing the paraventricular nucleus (PVN), the supraoptic nucleus (SON) and the piriform cortex (PIR) were washed and counter-stained with 4′,6-diamidino-2-phenylindole (DAPI) (1:10000, D1306, Invitogen), and mounted with Fluoromount mountain medium (Invitrogen). Both z-stack fluorescent images and tiled images were acquired on a Leica SP8 confocal microscope and maximum projection was performed using Fiji-ImageJ Wiki software (National Institutes of Health, USA

Results:

Systemic blockade of OXTR increases specific social interactions between unfamiliar female mice

Before addressing the specific role of OXTR modulation in the PIR, we started by testing whether an acute blockade of OXTR has an impact on social interactions between female mice. Indeed, past works have focused on KO mice for the OXTR, and not on acute manipulations. To answer this question, we combined a pharmacological approach with the Live Mouse Tracker (LMT) (Chaumont et al. 2018). This technology allows for automated tracking of the position of multiple individual mice as they interact freely in an open arena (Fig 1.A). Importantly, it can also automatically detect a large panel of behavioral motives that mice display alone or in groups. Here, we focused on nose-nose events (NOSE), orogenital events from the experimental mouse towards the stimulus mouse (OGEXP), side by side contacts (SBSCT), and side by side opposite events (SBSOP) (Fig 1.A), which stand among the most frequent types of social interactions between mice.

In order to block OXTR in the tested mice, we performed intraperitoneal injections of an OXTR antagonist which crosses the blood brain barrier, L-368,899 (OTA-L), and used injections of a vehicle solution as controls (Fig 1.B). After a 30min wait-time to allow for drug diffusion in the brain, the injected mice were allowed 90 minutes of free interactions in the LMT arena with another female mouse they had never met before. Because 90 minutes of free social interaction encompasses multiple type of behaviors (i.e initial encounter of the unknown individual vs established grouped interactions), we first focused our analysis on the initial 10 minutes of interactions. We controlled that the OTA-L did not impact the mobility of mice which reflects their overall activity level. As there was no difference in the total travelled distance between the mice injected with OTA-L and those injected with Vehicle, we concluded that a systemic blockade of OXTR does not affect general mobility levels (Fig 1.C). However, OXTR blockade surprisingly induced an increase in the time spent in three types of social behaviors: “nose-nose” contacts, “side by side contacts”, and “side by side opposite” (Fig 1.D and Suppl 1.A for individual data). Because the time spent in a given type of interaction does not necessarily correlate with the number of interactions we also calculated mean number of events for each behavioral motif (Fig 1.E and Suppl 1.B for individual data). An increase in the number of nose-nose, side by side, and side by side opposite events

following OXTR blockade was detected which is in line with the increased time spent in these interaction types.

OXTR blockade did not affect orogenital contacts (neither their duration nor their number of events), suggesting that the observed effects of OTA-L are specific for a subtype of social behaviors (Fig 1.D,E). Interestingly, we observed the same effects of OXTR blockade on duration of events over the 90-minute total exploration (Fig Suppl 2). In conclusion, contrary to the classical view of OXT as a pro-social neuropeptide, we observe that blocking endogenous OXT increases specific social interactions. As the antagonist-induced increase in specific social behaviors was observed during the initial 10-minute encounter, the endogenous function of OXT may play a role during social memory formation and/or modulating the motivation of a mouse to explore a novel individual. We then wondered whether OXTR blockade specifically in the PIR would yield similar results.

The piriform cortex does receive sparse oxytocinergic projections

We first confirmed previous reports that the PIR receives oxytocinergic axonal projections (Choe et al. 2015). To do this, we used a transgenic mouse line where eYFP was under the control of the cre recombinase in oxytocinergic neurons. eYFP fluorescence revealed that this mouse line efficiently labelled the dense oxytocinergic fibers of the PVN and SON (Fig 2, upper panels). After this initial validation step, we investigated for the presence of oxytocinergic fibers in the anterior and posterior portions of the PIR (Fig 2, lower panels). We observed the presence of sparse oxytocinergic projections in the aPIR and pPIR. These fibers seemed to be spread through the layers of the PIR (both aPIR and pPIR).

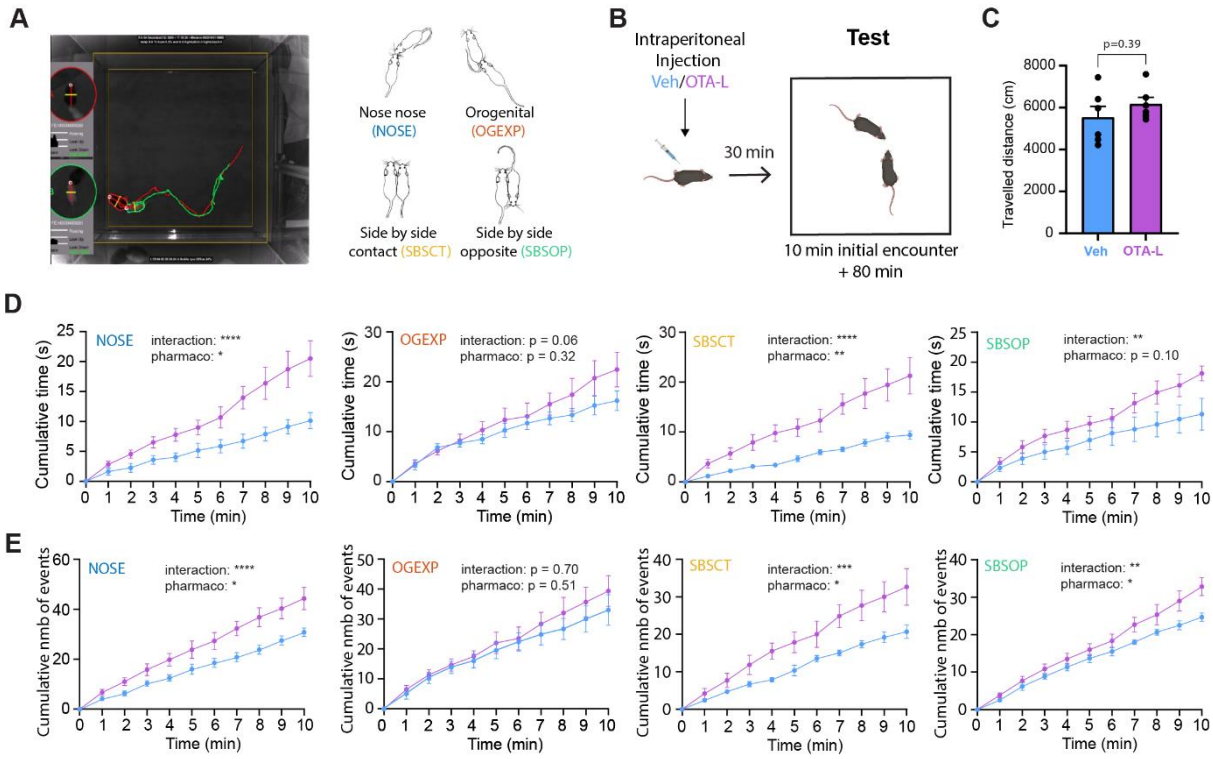

Figure 1 : Systemic OXTR blockade increases specific types of social interactions during freely moving exploration. **A.** Left. Example trajectories and detection of 2 female mice (red and green) in the Live Mouse Tracker. Right. Illustration of 4 types of automatically detected social interaction motives (adapted from (Chaumont et al. 2018). **B.** Experimental protocol consisting of an intraperitoneal injection of the OXTR antagonist (OTA-L) or its vehicle in female mice, followed by a 30 min rest period, and 90 min of free interactions with a previously unseen female conspecific (10 min initial encounter + 80 minutes). **C.** Travelled distance over the 10 initial min is not different between the two groups (Mann-Whitney test, p = 0.39). **D.** Mean cumulative time spent in NOSE, OGEXP, SBSCT, SBSOP contacts for the two groups (mean +/- SEM) (2-way ANOVAs, NOSE: Time*pharmaco < 0.0001, Pharmaco = 0.01; SBSCT: Time*pharmaco < 0.0001, Pharmaco = 0.003; SBSOP: Time*pharmaco = 0.002, Pharmaco = 0.10). No significant difference was observed for OGEXP events (2-way ANOVA, OGEXP: Time*pharmaco = 0.06, Pharmaco = 0.32). **E.** Mean cumulative number of events in NOSE, OGEXP, SBSCT, SBSOP contacts for the two groups (mean +/- SEM) (2-way ANOVAs, NOSE: Time*pharmaco < 0.0001, Pharmaco = 0.01; SBSCT: Time*pharmaco = 0.0003, Pharmaco = 0.02; SBSOP: Time*pharmaco = 0.005, Pharmaco =0.04). No significant differences were observed on OGEXP number of events (2-way ANOVA, OGEXP: Time*pharmaco < 0.70, Pharmaco = 0.51). Vehicle = 6 mice, OTA-L = 6 mice. NOSE = nose-nose, OGEXP = orogenital from experimental mouse, SBSCT = side by side contact, SBSOP = side by side opposite. *p<0.05, **p<0.005, ***p<0.001, ****p<0.0001.

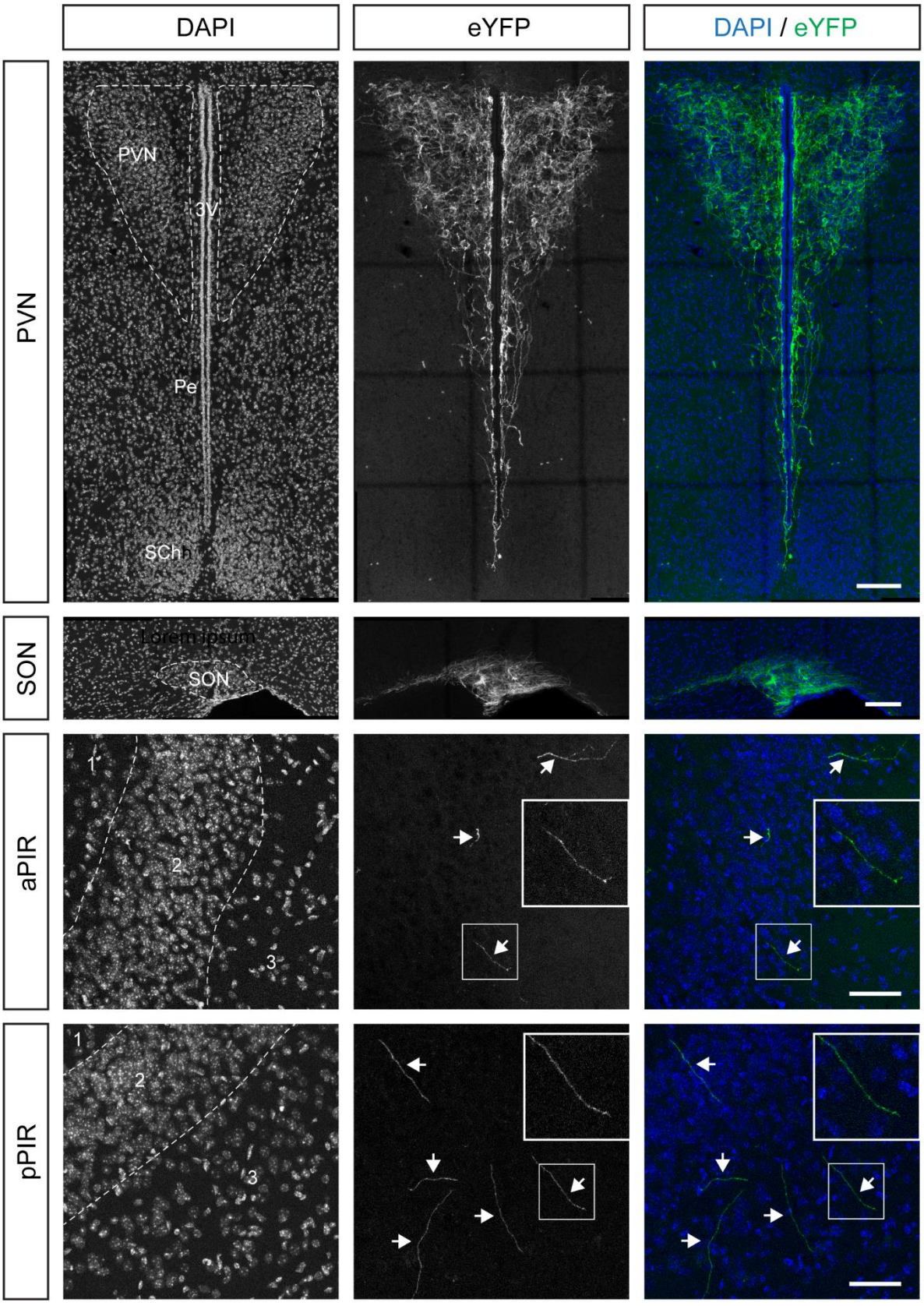
DAPI
eYFP
DAPI / eYFP
PVN
SON
aPIR
pPIR
PVN
3V
Pe
SCh
Lorem ipsum
SON
1
2
3
1
2
3

Figure 2 : Anterior and posterior piriform cortex receive oxytocinergic projections. Confocal images in a female mouse. Oxytocinergic fibers are visualized by the fluorescent reporter eYFP under the control of the cre-recombinase in oxytocinergic neurons. They can be visualized in the PVN, SON, aPIR, pPIR. Numbers in aPIR and pPIR indicate cell layer number. Arrows indicate the presence of sparse oxytocinergic fibers in the aPIR and the inserts (larger square) correspond to the zoomed image of an oxytocinergic fiber (smaller square). Scale bar = 100µm for PVN and SON and 50 µm for aPIR. PVN = paraventricular nucleus. SON = supraoptic nucleus. aPIR = anterior piriform. pPIR = posterior piriform. 3V = third ventricle. Pe = periventricular nucleus. Sch = suprachiasmatic nucleus.

Piriform cortex local blockade of OXTR subtly increases specific social interactions between unfamiliar female mice

In order to assess whether OXTR blockade specifically in the piriform cortex perturbs social behaviors in female mice, we used bilateral infusions of either SAL or OTA locally in the PIR, and placed the injected mice in the LMT for 10 min where they could freely interact with a female mouse they had never encountered (Fig 3.A). No difference in the total travelled distance was observed between the two groups (Fig 3.B) suggesting that local OXTR blockade does not impact the overall activity level of mice. The behavioral effects of the local OTA injections were subtler than with systemic injections but we observed a similar trend towards an increase in social behaviors. Specifically, we found a trend for an initial increase in the duration of side by side opposite contacts (Fig 3.C.i,ii), and an overall increase in the number of side by side events across time (Fig 3.D) (Suppl 3 for individual data). These observations are in line with the enhanced occurrence of side by side behaviors with the systemic injection of OTA-L. However, no effects were observed for nose-nose and orogenital contacts (Fig 3.C,D). Taken together, these observations suggest an unexpected role of endogenous OXTR activity in the PIR which would prevent some of the key social interactions between mice as they first encounter. Olfaction is central for social interactions between rodents but other sensory modalities can also contribute to their attitude towards conspecifics (de la Zerda et al. 2022). Because the effect of local PIR-targeted OXTR blockade were subtle as compared to systemic blockade, we hypothesized that OXTR activity outside of the PIR was also contributing to the overall positive impact of OXTR blockade on social behaviors. To more specifically study the role of OXTR activity in the PIR when mice are exposed to social olfactory cues, we carried on a new set of experiments with an olfactory selective social task.

OXTR blockade in the PIR increases attraction to social odors

The three chamber test (3chTest) is a widely-used social test aimed at assessing sociability (phase 1) and social memory (phase 2) in rodents. During phase 1, sociability is estimated by comparing the time spent in the chamber containing a mouse (social stimulus) with the chamber containing an object (non-social stimulus) (Yang et al., 2016). We adapted this sociability test to our needs by creating an olfactory-based version of the task: in our protocol, the social stimulus consisted in soiled bedding spread over the floor of the social chamber, and the non-social stimulus was clean bedding. The central chamber did not contain any bedding (Fig 4.A). After an initial exploration of the empty apparatus, mice were infused bilaterally with SAL or OTA in the PIR. After 10 min recovery from the injection, they were allowed to explore the three chambers for 10 min (Fig 4.A). Mice spent on average more time in the compartment containing social odors, both in the SAL and the OTA conditions (Fig 4.B,C) (see Suppl 4 for example trajectories of a mouse during the task). The difference in sociability index across time between the two groups showed a trend for increased attraction for social bedding in the OTA group compared to the SAL group (Fig 4.D). Data for individual mice also seemed to point to a more consistent preference for the social chamber in the OTA group (Suppl 5). We therefore identified, within the tested mice, those who spent more than 2 minutes longer in the social chamber as compared to the non-social chamber and defined them as “social”. When we compared the proportions of “social” mice in each group we found that the OTA-infused group contained more “social” animals than the SAL-infused group (Fig 4.E).

Of note, mice exhibited social behavior in the classical version of the 3chTest (where the social stimulus was a mouse) when infused in the PIR with SAL or OTA (Suppl 6). In this version of the test, no differences between the two groups were observed in terms of time spent in the different compartments, number of sniffing events, time spent in sniffing events, first nose-nose duration or single sniff duration. These effects are contrasting with the LMT observations which have a better precision in describing the subtleties of social behaviors. We therefore assumed that the classical version of the 3chTest was not precise enough for detecting the effects of our selective manipulation.

Overall, we show that blocking the OXTR in the PIR before an olfactory-based version of the 3chTest tends to increase the levels of olfactory driven social interest.

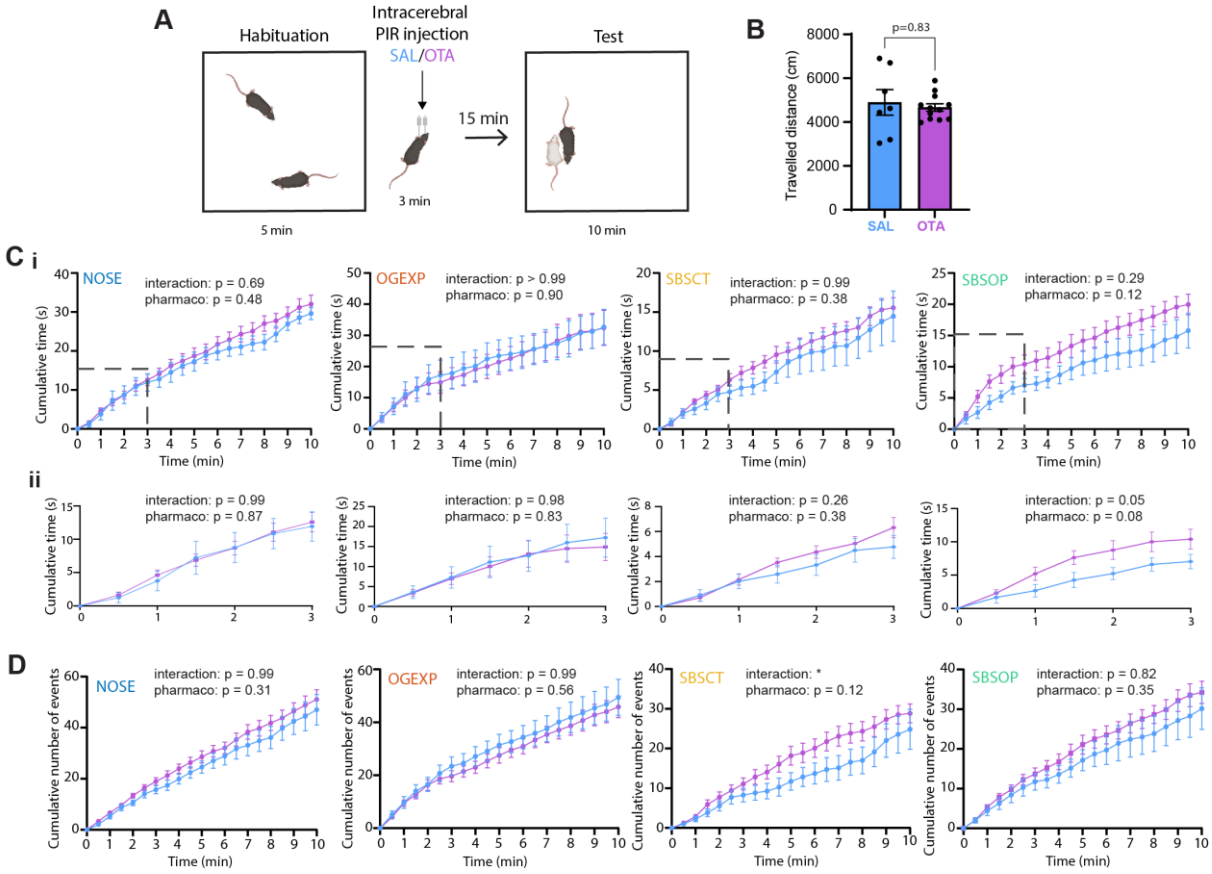

Figure 3 : OXTR blockade in the piriform cortex induces subtle changes in social interactions. **A.** Experimental protocol: after being habituated for 5 min in the arena with their cage partner, female mice were bilaterally infused in the piriform cortex (PIR) with either saline (SAL) or an oxytocin receptor antagonist (OTA) for 3 min. After 15 min post-infusion recovery, they were allowed to interact for 10 min with an unfamiliar female mouse in the LMT arena**.** **B**. Total travelled distance shows no differences between the 2 groups (Mann Whitney, p = 0.83). **C. Top** Mean cumulative time spent in NOSE, OGEXP, SBSCT, SBSOP contacts for the two groups (mean +/- SEM (2-way ANOVAs: NOSE: Time*pharmaco = 0.69, Pharmaco = 0.48; OGEXP: Time*pharmaco > 0.99, Pharmaco = 0.90; SBSCT: Time*pharmaco = 0.99, Pharmaco = 0.38; SBSOP Time*pharmaco = 0.29, Pharmaco =0.12). Dashed box shows data presented in the plot bellow. **Bottom**. 3 min zoom of data presented above. (2-way ANOVAs, NOSE: Time*pharmaco = 0.99, Pharmaco = 0.87; OGEXP: Time*pharmaco = 0.98, Pharmaco = 0.83; SBSCT: Time*pharmaco = 0.26, Pharmaco = 0.38; SBSOP: Time*pharmaco = 0.05, Pharmaco = 0.08). **D.** Mean cumulative number of NOSE, OGEXP, SBSCT, SBSOP events for the two groups (mean +/- SEM) (2-way ANOVAs: NOSE: Time*pharmaco = 0.99, Pharmaco =0.31; OGEXP: Time*pharmaco = 0.99, Pharmaco = 0.56; SBSCT: Time*pharmaco = 0.03, Pharmaco = 0.12; SBSOP: Time*pharmaco = 0.82, Pharmaco = 0.35). SAL = 7 mice, OTA = 12 mice. NOSE = nose-nose, OGEXP = orogenital from experimental mouse, SBSCT = side by side contact, SBSOP = side by side opposite, LMT = Live Mouse Tracker, *p<0.05.

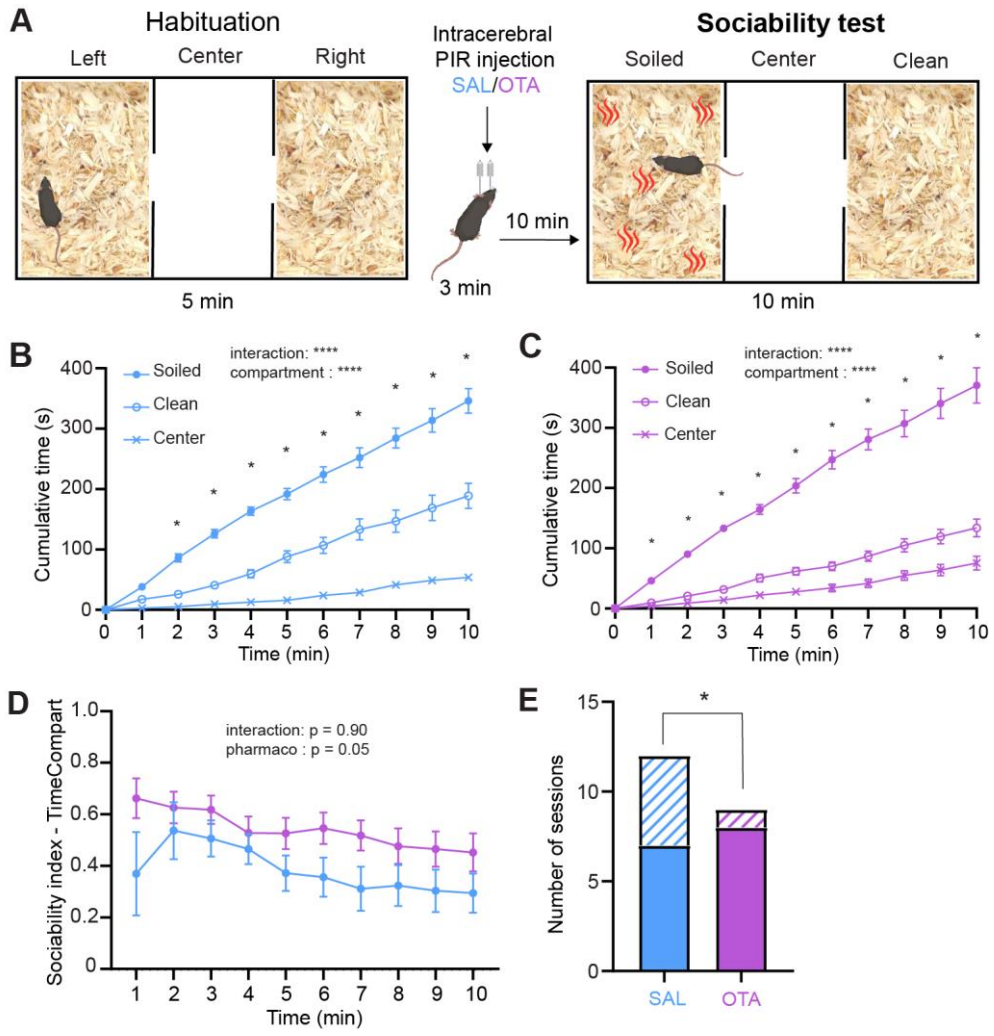

Figure 4 : OXTR blockade in the piriform cortex tends to increase sociability in the olfactory 3-chamber test. **A.** Experimental design. Female mice were allowed to explore the 3-chamber apparatus containing clean bedding for 5 minutes. Following infusion of either SAL or OTA bilaterally in the PIR, and a 10-min post-infusion recovery time, mice were allowed to freely explore the 3 chambers containing either social odors (soiled female bedding), non-social odor (clean bedding), or nothing (central compartment). A sociability index was defined based on the time spent in the social chamber against the time spent in the non-social chamber. **B.** Mice in the SAL group displayed attraction to social odors – i.e as a population, they spent more time in the chamber containing the social odor. Mean cumulative time spent in each compartments +/- SEM (2-way ANOVA: Time*Compartment < 0.0001, Compartment < 0.0001)**. C.** Mice in the OTA group displayed attraction to social odors. Mean cumulative time spent in each compartments +/- SEM (2-way ANOVA: Time*Compartment < 0.0001, compartment < 0.0001. **D.** SAL and OTA mice have positive sociability indices meaning they spent more time in the social chamber compared to the non-social chamber, and OTA mice tend to have higher sociability indices compared to SAL mice (2-way ANOVA: Time*Pharmaco = 0.90, Time = 0.10, Pharmaco = 0.05). **E.** SAL and OTA groups are different in their proportion of "social" (filled color) compared to "non-social" (dashed lines) sessions, based on a threshold of the sociability index, Chi-square p = 0.04, (SAL n = 12 mice, OTA, n= 10 mice). ****p<0.0001.

OXTR blockade in the piriform cortex does not impair social memory and memory for social odors

With systemic injections of OXTR antagonist, we found increased social interactions when mice encounter for the first time. This could be explained by two distinct phenomena: an increased level of sociability or a defective social memory. We observed that mice are more
attracted by social odors when PIR OXTR are blocked which points towards an increased sociability. Yet, we wondered whether social memory performance could also be affected as OXTR KO mice have been shown to have impaired social memory (Takayanagi et al. 2005). We therefore first conducted a habituation-dishabituation task on mice with bilateral infusion of either SAL or OTA in the PIR. In this test, mice could interact with the same mouse contained in a cylinder during the course of 4 trials (Fig 5.A = blue asterisk), and then with a new mouse in the last trial (Fig 5.A = red asterisk, - retention trial). Normally, mice with intact social memory spend a decreasing amount of time exploring the familiar mouse across trials and display a rebound of exploration for the new mouse because of their innate attraction to novelty (Ferguson et al. 2000). To estimate this social interest, we tracked the position of the mouse and defined two zones in the arena: the ‘’inside sniffing zone” (a circle around the cylinder of the mouse’s head size), and the “outside sniffing zone‘’ which corresponds to the rest of the arena (Fig 5.B).

As it is the case from the example trajectories (Fig 5.B), mice decreased their presence in the sniffing zone throughout the 4 trials and increased the time spent in this zone during the retention phase (Fig 5.B.C). No differences in the time spent in the sniffing zone across trials was observed between SAL and OTA-infused mice (Fig 5.C). Yet, we observed that the rebound of interest in the OTA group (i.e the difference between Ret and T4) seemed more consistent across mice than in the SAL group (Fig 5.D.E). In fact, only one session out of 19 in the OTA group did not show any rebound (time in Ret > T4) whereas in the SAL group, 5 out of 19 did so (FIG 5.F.G). This trend, although not significant, is opposite to the idea that social memory would be affected when OXTR are blocked in the PIR. Because mice could be in the sniffing zone but not actually be interested in the social stimulus, we also quantified the number of sniffing

events towards the stimulus mouse in each trials. We found a similar habituation-dishabituation pattern with no clear differences between OTA and SAL groups (Fig 5. H.I.J.K.L).

Finally, we looked at other measures such as the duration of the first nose-nose events which, based on our observations, was increased in the first and last trials, indicating that probably they are highly informative for the mice (Suppl 7.A). We looked at the time it took the mice to start the trials which is a measure of interest and motivation (Suppl 7.B), and the number of sniffing zone entries which could be a measure of both interest and hyperactivity (Suppl 7.C). In none of these last three tests we observed a significant difference between the SAL- and OTA-infused mice.

To confirm that OTA-infusion in the PIR does not impair social memory, we conducted an additional set of experiments using the classical version of the 3chTest (Suppl 8). No differences between the SAL- and OTA-infused mice were observed when comparing the time spent in each chambers, the number of sniffing events, the time spent in sniffing events, the first nose-nose duration or the single sniff duration. Similar observations were made when we used an olfactory-based version of the 3chTest (Fig 6, Suppl 9): both SAL and OTA-infused mice spent more time in the chamber containing new social bedding as compared to familiar social bedding (Fig 6 B.C) and their performances across time were not significantly different (Fig 6.D). No differences in the proportion of mice belonging to the memory and no memory groups was observed (Fig 6.E).

In conclusion, mice in which OXTR were blocked in the PIR showed no signs of impairment in social memory. Instead, the overall trend was quite the opposite with robust memory performance in OTA-infused mice in the habituation-dishabituation task. Based on these observations, we ruled out the possibility that the OTA-induced increase in social interactions is due to impaired social memory. The enhanced attraction towards social odors when OXTR activity in the PIR is blocked is instead likely contributing to this unexpected effect.

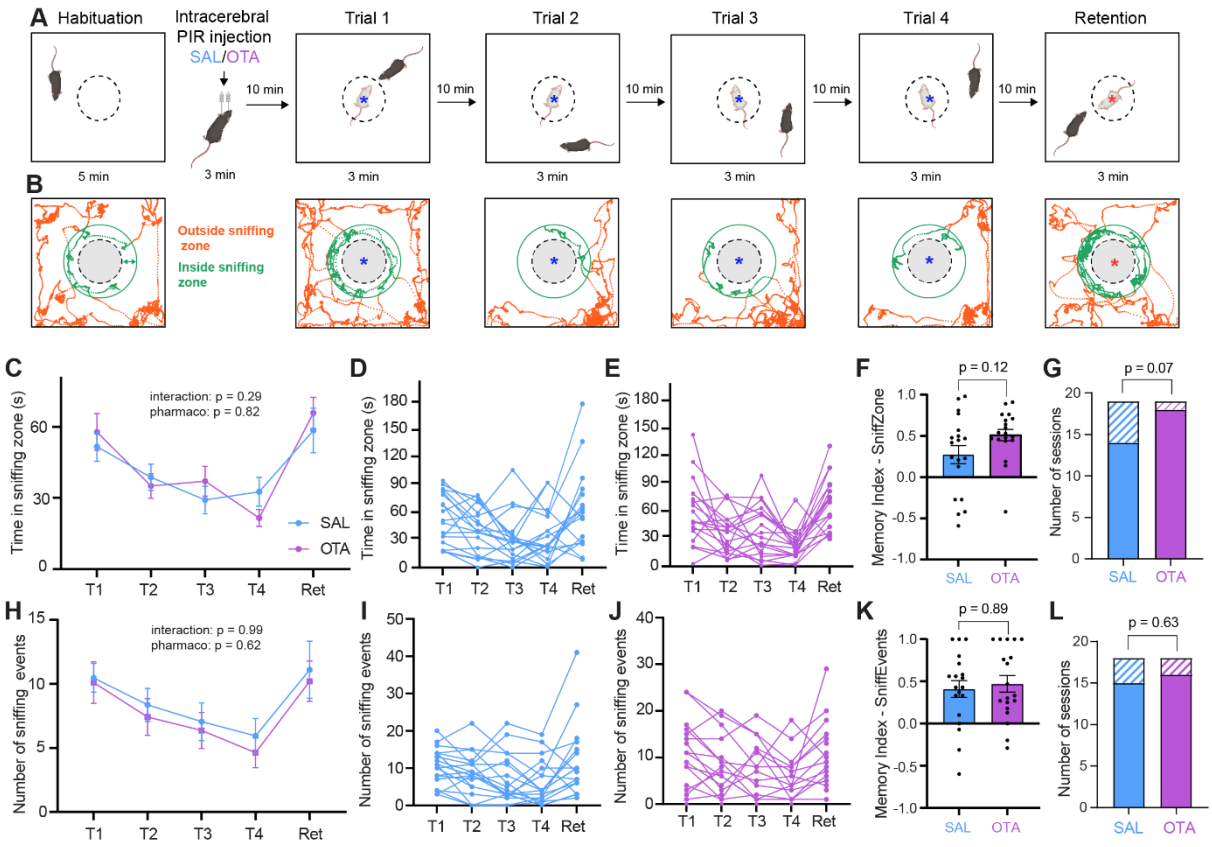

Figure 5 : OXTR blockage in the piriform cortex does not impact social memory in the habituation dishabituation task. A. Experimental paradigm. Female mice could explore the empty arena containing the cylinder (dashed circle) for 5 min of habituation. They were then infused bilaterally in the PIR with either SAL or OTA and had a 10-min post-infusion recovery time. After that, they could interact with the same female mice (blue asterisk), for four 3-min trials separated by 10-min inter-trials in a neutral cage. On the fifth trial they could explore a novel female mouse (red asterisk – retention trial). **B.** Color traces show example positions of the mouse's head detected by the Optitrack technology. The green circle represents the limit for the position of the mouse to be considered in the sniffing zone (2.5cm from the cylinder edge). Position could be detected inside the sniffing zone (green), or outside the sniffing zone (orange). Blue asterisk corresponds to familiar mouse; red asterisk corresponds to new mouse. **C.** Mean time in sniffing zone +/- SEM (2-way ANOVA: Trial*Pharmaco = 0.29, Trial = <0.0001, Pharmaco= 0.82). **D.E.** Time in sniffing zone for individual mice in the SAL and OTA groups, respectively. **F.** Memory indices based on the time in zones shows not significant difference between groups (Mann Whitney test, p = 0.12). **G.** Mice were either showing social memory (filled color, time in sniffing zone for Ret>T4), or no social memory (dashed lines, Ret<T4) groups. The distribution of these two categories of mice in the two groups were not statistically different (Chi-square test: p = 0.07). **H.I.J.K.L** Same has in C.D.E.F.G but for the number of sniffing events. No pharmaco group effect was observed across trials (2-way ANOVA: Trial*Pharmaco = 0.99, Trial < 0.0001, Pharmaco= 0.62) or by comparing memory indices (Mann Whitney test: p = 0.89), and belonging to the memory or no memory group (Chi-square test: p = 0.63).

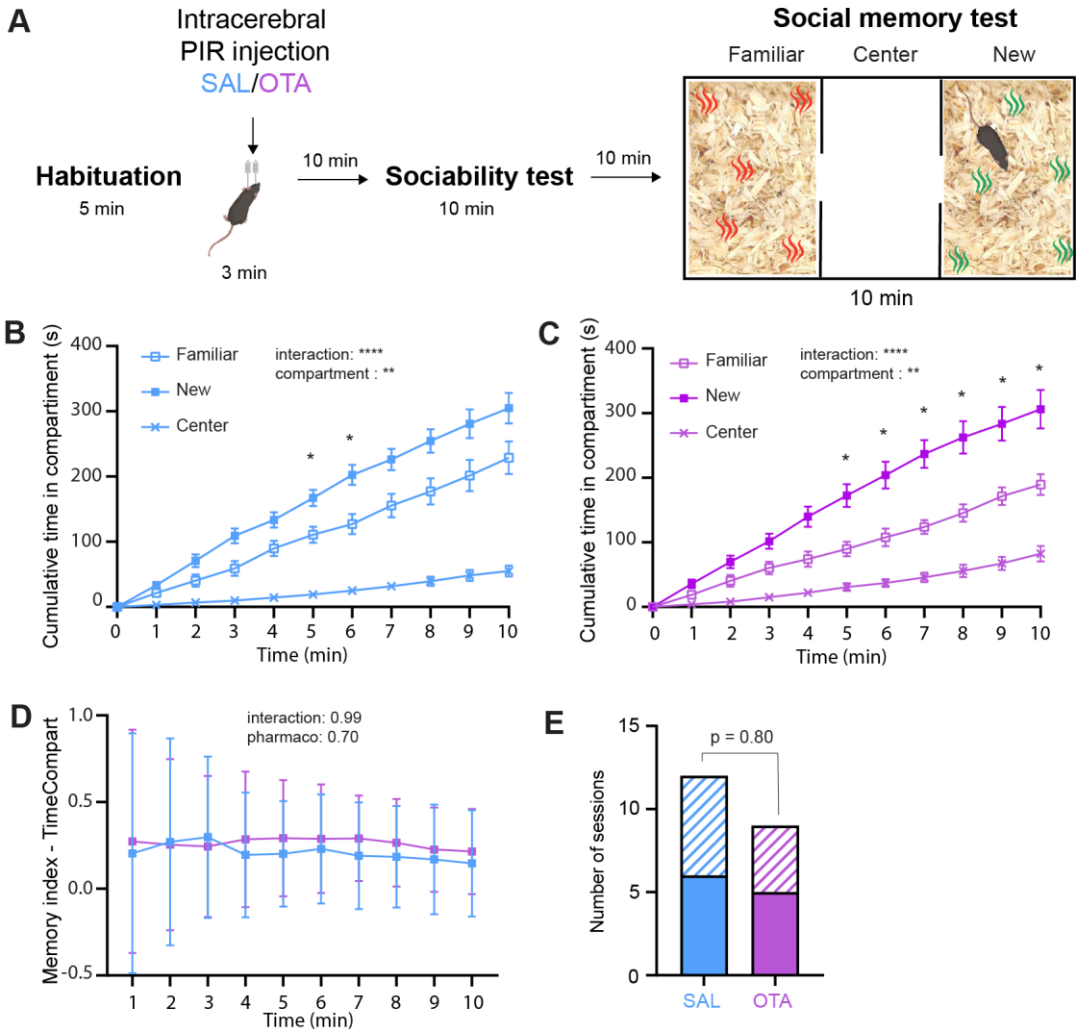

Figure 6 : OXTR blockade in the piriform cortex does not impact social memory in the olfactory 3-chamber test. A. Experimental design. After a 5 min habituation followed by a SAL or OTA infusion in the PIR, female mice performed the olfactory 3-chamber sociability test described before (soiled bedding vs clean bedding). Subsequently, they could perform an olfactory social memory test, in which they were allowed to freely explore a compartment containing the now-familiar female bedding (odor 1 – red symbol), a compartment containing new female bedding (odor 2 – green symbol) or the central compartment devoid of bedding. **B.** Mice in the SAL group displayed social memory – i.e they spent more time in the compartment containing the new odor. Mean cumulative time spent in each compartment +/- SEM (2-way ANOVA: Time*Compartment < 0.0001, Compartment = 0.006). **C.** Mean cumulative time spent in each compartment for the OTA group showed that mice displayed social memory +/- SEM (2-way ANOVA: Time*Compartment < 0.0001, Compartment < 0.003). **D** SAL and OTA mice have positive social memory indices across time, but do not show differences (2-way ANOVA: Time*Pharmaco = 0.99, Time = 0.72, Pharmaco= 0.70). **E.** The proportion of mice belonging to the memory or no memory group is not different between the two groups (Chi-square: p = 0.80) (SAL: n = 12 mice, OTA: p = 9), *p<0.05, **p<0.005, ****p<0.0001.

Discussion:

In this study we have found previously undescribed effects of OXTR blockade on sociability and social memory. Systemic OXTR antagonist injections induced an increase of specific types of social interactions in freely interacting female mice. This observation goes against data from the literature, showing that OXT and OXTR KO mice spend less time interacting and are more aggressive (Takayanagi et al. 2005; Sala et al. 2011; Pobbe et al. 2012). In particular OXTR KO mice show decreased nose-nose and orogenital exploration (Pobbe et al. 2012). We found that systemic injections of OXTR antagonist had the opposite effect: it increased nose-nose interactions and orogenital interactions were not affected. OXTR antagonist infused locally in the PIR had no effect on nose-nose and orogenital contacts. However, we found that local injection of OXTR-antagonist in the PIR increased – although only in a subtle way – the number of side by side contacts. These types of events, which commonly emerge during extended body contact, rely on strong and positive mutual interactions between the two mice. As such, out of the four behavioral motives investigated here, the two that correspond to side-by-side contacts are the most representative of pro-social interactions (i.e. positive interactions). Our findings that OXTR antagonist injections induced an increase of those contacts further points towards a pro-social effect of OXTR blockade in the PIR, which is consistent with the data obtained with systemic blockade. It is worth noticing that the observed pro-social effects do not specifically affect investigatory sampling behavior (e.g. nose-nose events) but rather the attitudes mice adopt after the initial sampling phase (e.g. side-by-side events) which better reflect the valence associated with social interactions. Overall, our results could imply that endogenous OXT in naïve female mice is not pro-social. If replicated, this observation would be – to our knowledge – the first observation that blockade of endogenous OXT in female mice does not induce an impaired sociability but an increased sociability. In the literature, findings of anti-social effects of OXT have only been reported in the case of high levels of OXT (Huang et al. 2014). It is thus possible that OXT levels are higher in the female mice we tested, resulting in anti-social effects that are blocked by our manipulation. Dosage of OXT levels and experiments in male mice could allow addressing this possibility.

We wondered why the effects of OXTR blockade in the PIR were subtle? A first hypothesis would be that the PIR is not a crucial structure for sociability. Indeed, even

if the PIR is activated following a social interaction (Ferguson et al. 2001; Kim et al. 2015), and seems necessary for social learning (Choi et al. 2011; Choe et al. 2015), no direct evidence links the PIR with sociability levels. Another hypothesis would be that because the PIR is a wide structure, our pharmacological inactivation of OXTR only impacts a small portion of the PIR, and thus only induces small effects. This could be tested by infusing the OXTR antagonist at multiple locations along the antero-posterior axis. A third hypothesis, would be that because social interactions are complex multisensory events, OXTR modulation in the PIR would only impact the olfactory component of theses interactions leading to subtle modulation of social behaviors. We decided to focused on the olfactory component of social interactions by blocking OXTR in the PIR using the olfactory three chamber test and social bedding. We observed that in this version of the three chamber test, local PIR OXTR blockade induced a strong trend towards an increased attraction towards the social olfactory stimulus. This effect was consistent with the freely moving experiments, and points to an unexpected role of endogenous OXT in the PIR of female mice. A future manipulation could investigate if we would observe the opposite effects (i.e. anti-social) with the infusion of the OXTR agonist.

Finally, we show that OXTR blockade in the PIR does not impair social memory as it could have been hypothesized from OXTR KO studies in which animals exhibit social memory deficits (Ferguson et al. 2000). Thus, even if the PIR is a structure of choice for olfactory learning in the brain (Barkai and Saar 2001), oxytocinergic transmission in the PIR does not impact social memory in our condition. One hypothesis could be that OXTR blockade does not impact the formation of social memory but rather impact its consolidation or recall. This could be tested in the future by injecting the antagonist immediately after the acquisition or before the retrieval test instead of before the acquisition phase. Along these lines, it has been shown that in the lateral septum of male rats, intracerebroventricular injection of OTA impaired the maintenance of social memory if injected immediately after acquisition, but not 20 min prior to retrieval (Lukas et al. 2013). The timing of OTA infusion relative to the different phases of the learning task could thus be a critical factor. Knowing the dynamic of OXT release in the PIR would be extremely relevant in order to better estimate the most appropriate timing for OTA infusion. To this end, the use of newly developed OXT sensors, could shine light

onto the dynamics of OXT release in the PIR during social interaction and social memory tasks (Ino et al. 2022).

References

Ache, Barry W., and Janet M. Young. 2005. “Olfaction: Diverse Species, Conserved Principles.” *Neuron* 48 (3): 417–30. https://doi.org/10.1016/j.neuron.2005.10.022.

Argiolas, Antonio. 1992. “Oxytocin Stimulation of Penile Erection: Pharmacology, Site, and Mechanism of Actiona.” *Annals of the New York Academy of Sciences* 652 (1): 194–203. https://doi.org/10.1111/j.1749-6632.1992.tb34355.x.

Barkai, Edi, and Drorit Saar. 2001. “Cellular Correlates of Olfactory Learning in the Rat Piriform Cortex.” *Reviews in the Neurosciences* 12 (2). https://doi.org/10.1515/REVNEURO.2001.12.2.111.

Boccia, Maria L., Anne-Pierre S. Goursaud, Jocelyne Bachevalier, Kenneth D. Anderson, and Cort A. Pedersen. 2007. “Peripherally Administered Non-Peptide Oxytocin Antagonist, L368,899®, Accumulates in Limbic Brain Areas: A New Pharmacological Tool for the Study of Social Motivation in Non-Human Primates.” *Hormones and Behavior* 52 (3): 344–51. https://doi.org/10.1016/j.yhbeh.2007.05.009.

Caldwell, Jack D. 1992. “Central Oxytocin and Female Sexual Behaviora.” *Annals of the New York Academy of Sciences* 652 (1): 166–79. https://doi.org/10.1111/j.1749-6632.1992.tb34353.x.

Chaumont, Fabrice de, Elodie Ey, Nicolas Torquet, Thibault Lagache, Stéphane Dallongeville, Albane Imbert, Thierry Legou, et al. 2018. “Live Mouse Tracker: Real-Time Behavioral Analysis of Groups of Mice.” Preprint. Animal Behavior and Cognition. https://doi.org/10.1101/345132.

Choe, Han Kyoung, Michael Douglas Reed, Nora Benavidez, Daniel Montgomery, Natalie Soares, Yeong Shin Yim, and Gloria B. Choi. 2015. “Oxytocin Mediates Entrainment of Sensory Stimuli to Social Cues of Opposing Valence.” *Neuron* 87 (1): 152–63. https://doi.org/10.1016/j.neuron.2015.06.022.

Choi, Gloria B., Dan D. Stettler, Benjamin R. Kallman, Shakthi T. Bhaskar, Alexander Fleischmann, and Richard Axel. 2011. “Driving Opposing Behaviors with Ensembles of Piriform Neurons.” *Cell* 146 (6): 1004–15. https://doi.org/10.1016/j.cell.2011.07.041.

Courtiol, Emmanuelle, and Donald A. Wilson. 2017. “The Olfactory Mosaic: Bringing an Olfactory Network Together for Odor Perception.” *Perception* 46 (3–4): 320–32. https://doi.org/10.1177/0301006616663216.

Ferguson, Jennifer N., J. Matthew Aldag, Thomas R. Insel, and Larry J. Young. 2001. “Oxytocin in the Medial Amygdala Is Essential for Social Recognition in the Mouse.” *The Journal of Neuroscience* 21 (20): 8278–85. https://doi.org/10.1523/JNEUROSCI.21-20-08278.2001.

Ferguson, Jennifer N., Larry J. Young, Elizabeth F. Hearn, Martin M. Matzuk, Thomas R. Insel, and James T. Winslow. 2000. “Social Amnesia in Mice Lacking the Oxytocin Gene.” *Nature Genetics* 25 (3): 284–88. https://doi.org/10.1038/77040.

Hagiwara, Akari, Sumon K. Pal, Tomokazu F. Sato, Martin Wienisch, and Venkatesh N. Murthy. 2012. “Optophysiological Analysis of Associational Circuits in the Olfactory Cortex.” *Frontiers in Neural Circuits* 6. https://doi.org/10.3389/fncir.2012.00018.

Huang, Huiping, Caterina Michetti, Marta Busnelli, Francesca Managò, Sara Sannino, Diego Scheggia, Luca Giancardo, et al. 2014. “Chronic and Acute Intranasal Oxytocin Produce Divergent Social Effects in Mice.” *Neuropsychopharmacology* 39 (5): 1102–14. https://doi.org/10.1038/npp.2013.310.

Imai, Takeshi. 2014. “Construction of Functional Neuronal Circuitry in the Olfactory Bulb.” *Seminars in Cell & Developmental Biology* 35 (November): 180–88. https://doi.org/10.1016/j.semcdb.2014.07.012.

Ino, Daisuke, Yudai Tanaka, Hiroshi Hibino, and Masaaki Nishiyama. 2022. “A Fluorescent Sensor for Real-Time Measurement of Extracellular Oxytocin Dynamics in the Brain.” *Nature Methods*, September. https://doi.org/10.1038/s41592-022-01597-x.

Insel, Thomas R. n.d. “OXYTOCIN - A NEUROPEM’IDE FOR AFFILIATION: EVIDENCE FROM BEHAVIORAL, RECEPTOR AUTORADIOGRAPHIC, AND COMPARATIVE STUDIES,” 33.

Jurek, Benjamin, and Inga D. Neumann. 2018. “The Oxytocin Receptor: From Intracellular Signaling to Behavior.” *Physiological Reviews* 98 (3): 1805–1908. https://doi.org/10.1152/physrev.00031.2017.

Kendrick, K. M., and E. B. Keverne. 1992. “Control of Synthesis and Release of Oxytocin in the Sheep Braina.” *Annals of the New York Academy of Sciences* 652 (1): 102–21. https://doi.org/10.1111/j.1749-6632.1992.tb34349.x.

Kim, Yongsoo, Kannan Umadevi Venkataraju, Kith Pradhan, Carolin Mende, Julian Taranda, Srinivas C. Turaga, Ignacio Arganda-Carreras, et al. 2015. “Mapping Social Behavior-Induced Brain Activation at Cellular Resolution in the Mouse.” *Cell Reports* 10 (2): 292–305. https://doi.org/10.1016/j.celrep.2014.12.014.

Kosfeld, Michael, Markus Heinrichs, Paul J. Zak, Urs Fischbacher, and Ernst Fehr. 2005. “Oxytocin Increases Trust in Humans.” *Nature* 435 (7042): 673–76. https://doi.org/10.1038/nature03701.

Lukas, Michael, Iulia Toth, Alexa H. Veenema, and Inga D. Neumann. 2013. “Oxytocin Mediates Rodent Social Memory within the Lateral Septum and the Medial Amygdala Depending on the Relevance of the Social Stimulus: Male Juvenile versus Female Adult Conspecifics.” *Psychoneuroendocrinology* 38 (6): 916–26. https://doi.org/10.1016/j.psyneuen.2012.09.018.

Marlin, Bianca J., Mariela Mitre, James A. D’amour, Moses V. Chao, and Robert C. Froemke. 2015. “Oxytocin Enables Maternal Behaviour by Balancing Cortical Inhibition.” *Nature* 520 (7548): 499–504. https://doi.org/10.1038/nature14402.

Mitre, Mariela, Bianca J. Marlin, Jennifer K. Schiavo, Egzona Morina, Samantha E. Norden, Troy A. Hackett, Chiye J. Aoki, Moses V. Chao, and Robert C. Froemke. 2016. “A Distributed Network for Social Cognition Enriched for Oxytocin Receptors.” *The Journal of Neuroscience* 36 (8): 2517–35. https://doi.org/10.1523/JNEUROSCI.2409-15.2016.

Nakajima, Miho, Andreas Görlich, and Nathaniel Heintz. 2014. “Oxytocin Modulates Female Sociosexual Behavior through a Specific Class of Prefrontal Cortical Interneurons.” *Cell* 159 (2): 295–305. https://doi.org/10.1016/j.cell.2014.09.020.

Natynczuk, Stephan E., and David W. Macdonald. 1994. “Scent, Sex, and the Self-Calibrating Rat.” *Journal of Chemical Ecology* 20 (8): 1843–57. https://doi.org/10.1007/BF02066226.

Oettl, Lars-Lennart, Namasivayam Ravi, Miriam Schneider, Max F. Scheller, Peggy Schneider, Mariela Mitre, Miriam da Silva Gouveia, et al. 2016. “Oxytocin Enhances Social Recognition by Modulating Cortical Control of Early Olfactory Processing.” *Neuron* 90 (3): 609–21. https://doi.org/10.1016/j.neuron.2016.03.033.

Pisansky, Marc T., Leah R. Hanson, Irving I. Gottesman, and Jonathan C. Gewirtz. 2017. “Oxytocin Enhances Observational Fear in Mice.” *Nature Communications* 8 (1): 2102. https://doi.org/10.1038/s41467-017-02279-5.

Pobbe, Roger L.H., Brandon L. Pearson, Erwin B. Defensor, Valerie J. Bolivar, W. Scott Young, Heon-Jin Lee, D. Caroline Blanchard, and Robert J. Blanchard. 2012. “Oxytocin Receptor Knockout Mice Display Deficits in the Expression of Autism-Related Behaviors.” *Hormones and Behavior* 61 (3): 436–44. https://doi.org/10.1016/j.yhbeh.2011.10.010.

Roesch, M. R., T. A. Stalnaker, and G. Schoenbaum. 2006. “Associative Encoding in Anterior Piriform Cortex versus Orbitofrontal Cortex during Odor Discrimination and Reversal Learning.” *Cerebral Cortex* 17 (3): 643–52. https://doi.org/10.1093/cercor/bhk009.

Sala, Mariaelvina, Daniela Braida, Daniela Lentini, Marta Busnelli, Elisabetta Bulgheroni, Valeria Capurro, Annamaria Finardi, et al. 2011. “Pharmacologic Rescue of Impaired Cognitive Flexibility, Social Deficits, Increased Aggression, and Seizure Susceptibility in Oxytocin Receptor Null Mice: A Neurobehavioral Model of Autism.” *Biological Psychiatry* 69 (9): 875–82. https://doi.org/10.1016/j.biopsych.2010.12.022.

Sofroniew, M.V. 1983. “Morphology of Vasopressin and Oxytocin Neurones and Their Central and Vascular Projections.” In *Progress in Brain Research*, 60:101–14. Elsevier. https://doi.org/10.1016/S0079-6123(08)64378-2.

Stopka, Pavel, Katerina Janotova, and David Heyrovsky. 2007. “The Advertisement Role of Major Urinary Proteins in Mice.” *Physiology & Behavior* 91 (5): 667–70. https://doi.org/10.1016/j.physbeh.2007.03.030.

Sullivan, Regina M., Donald A. Wilson, Nadine Ravel, and Anne-Marie Mouly. 2015. “Olfactory Memory Networks: From Emotional Learning to Social Behaviors.” *Frontiers in Behavioral Neuroscience* 9 (February). https://doi.org/10.3389/fnbeh.2015.00036.

Swanson, L W, and P E Sawchenko. 1983. “Hypothalamic Integration: Organization of the Paraventricular and Supraoptic Nuclei.” *Annual Review of Neuroscience* 6 (1): 269–324. https://doi.org/10.1146/annurev.ne.06.030183.001413.

Takayanagi, Yuki, Masahide Yoshida, Isadora F. Bielsky, Heather E. Ross, Masaki Kawamata, Tatsushi Onaka, Teruyuki Yanagisawa, et al. 2005. “Pervasive Social Deficits, but Normal Parturition, in Oxytocin Receptor-Deficient Mice.” *Proceedings of the National Academy of Sciences* 102 (44): 16096–101. https://doi.org/10.1073/pnas.0505312102.

Williams, Jessie R., Thomas R. Insel, Carroll R. Harbaugh, and C. Sue Carter. 1994. “Oxytocin Administered Centrally Facilitates Formation of a Partner Preference in Female Prairie Voles (Microtus Ochrogaster).” *Journal of Neuroendocrinology* 6 (3): 247–50. https://doi.org/10.1111/j.1365-2826.1994.tb00579.x.

Wilson, Donald A., and Regina M. Sullivan. 2011. “Cortical Processing of Odor Objects.” *Neuron* 72 (4): 506–19. https://doi.org/10.1016/j.neuron.2011.10.027.

Yang, Mu, Jill L Silverman, and Jacqueline N Crawley. 2016. “Automated Three-Chambered Social Approach Task for Mice,” 24.

Young, Larry J, Zuoxin Wang, and Thomas R Insel. n.d. “Neuroendocrine Bases of Monogamy,” 5.

Zerda, Shani Haskal de la, Shai Netser, Hen Magalnik, Mayan Briller, Dan Marzan, Sigal Glatt, Yasmin Abergel, and Shlomo Wagner. 2022. “Social Recognition in Laboratory Mice Requires Integration of Behaviorally-Induced Somatosensory, Auditory and Olfactory Cues.” *Psychoneuroendocrinology* 143 (September): 105859. https://doi.org/10.1016/j.psyneuen.2022.105859.

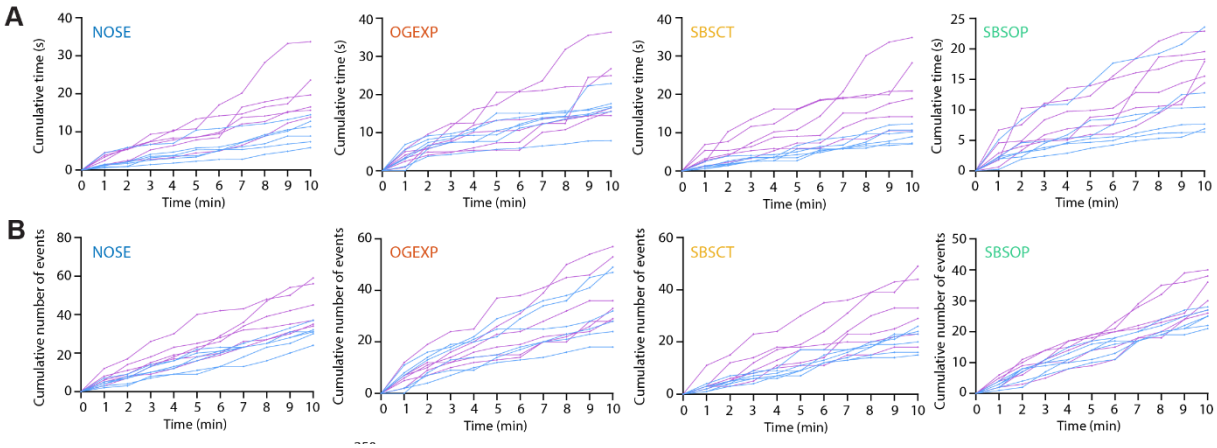

Supplementary 1 : Impact of systemic OXTR blockade on initial social interactions between two freely moving female mice. A. Individual data of cumulative time spent in the 4 types of social interactions used for Fig 1.D. **B.** Individual data of cumulative number of events used for Fig 1.E. blue = vehicle (n=6), magenta = OTA-L (n=6). NOSE = nose-nose, OGEXP = orogenital from experimental mouse, SBSCT = side by side contact, SBSOP = side by side opposite.

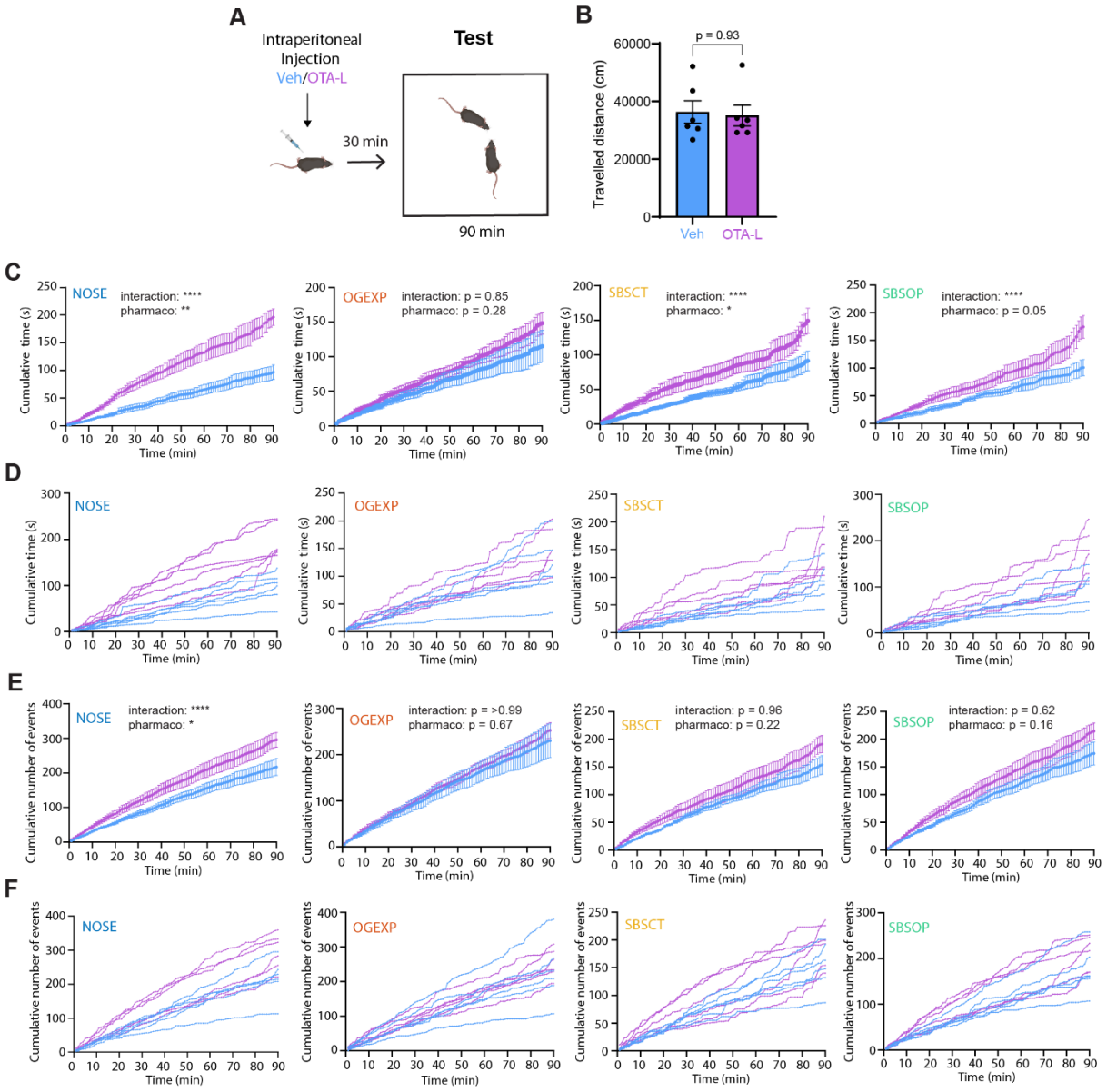

Supplementary 2 : Impact of systemic OXTR blockade on social interactions between two freely moving female mice A. Experimental protocol consisting of an intraperitoneal injection of the OXTR antagonist (OTA-L) or its vehicle in female mice, followed by a 30 min rest period, and 90 min of free interactions with a previously unseen female conspecific. **B.** Total travelled distance is not different between the two groups (Mann-Whitney test, p = 0.93). **C.** Mean cumulative time spent in NOSE, OGEXP, SBSCT, SBSOP contacts for the two groups (mean +/- SEM) (2-way ANOVAs, NOSE: Time*pharmaco <0.0001, Pharmaco = 0.003; OGEXP: Time*pharmaco = 0.85, Pharmaco = 0.28; SBSCT: Time*pharmaco <0.0001, Pharmaco = 0.04; SBSOP: Time*pharmaco <0.0001, Pharmaco = 0.05). **D.** Same data as in C, showing individual data. **E.** Mean cumulative number of events in NOSE, OGEXP, SBSCT, SBSOP contacts for the two groups (mean +/- SEM) (2-way ANOVAs, NOSE: Time*pharmaco <0.0001, Pharmaco = 0.04; OGEXP: Time*pharmaco > 0.99, Pharmaco = 0.67; SBSCT: Time*pharmaco = 0.96, Pharmaco =0.22; SBSOP: Time*pharmaco = 0.62, Pharmaco = 0.16. **F.** Same data as in E, showing individual data. (Vehicle n=6, OTA-L n=6), *p<0.05, **p<0.005, ***p<0.001, ****p<0.0001.

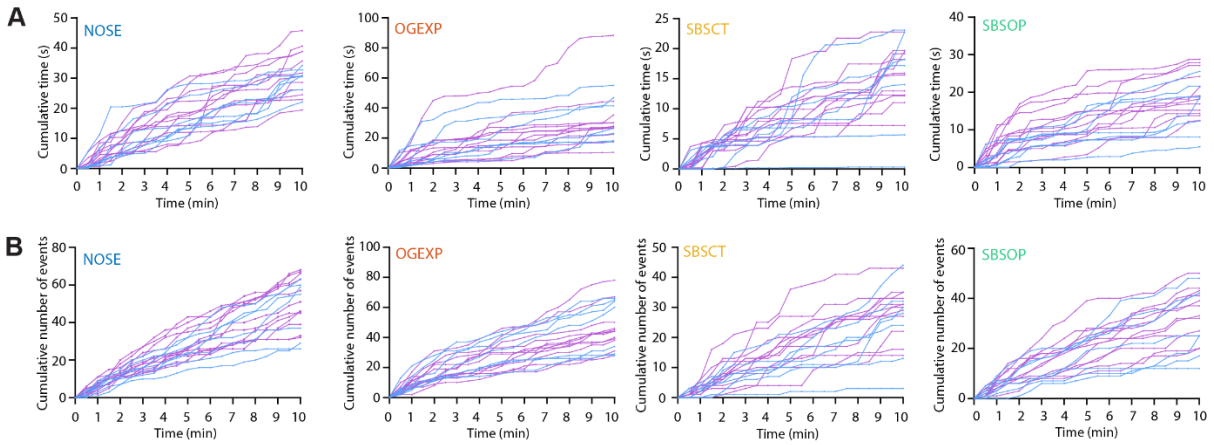

Supplementary 3 : Impact of piriform cortex local OXTR blockade on social interactions between two freely moving female mice A. Individual data of cumulative time spent in the 4 types of social interactions used for Fig 3.C.i. **B.** Individual data of cumulative number of events used for Fig 3.D. blue = SAL (n=7), magenta = OTA (n=12). NOSE = nose-nose, OGEXP = orogenital from experimental mouse, SBSCT = side by side contact, SBSOP = side by side opposite.

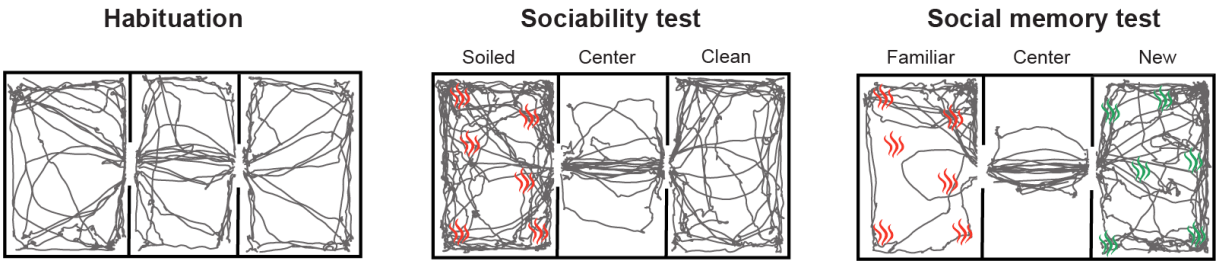

Supplementary 4 : Example trajectories of mice in the 3-chamber test. Black lines represent position of the center of mass of a mouse detected using the Bonsai software during habituation, sociability test or social memory test in an olfactory version of the 3chTest (Fig 4). Red symbols represent social stimuli in the sociability test (social bedding odor). In the social memory test, they represent the familiar stimuli (familiar social bedding odor). Green symbols represent new stimuli in the social memory test (new social bedding odor). Trajectories show that mice explored equally the three compartments during habituation, but had a clear preference for the social chamber during the sociability test, and a clear preference for the compartment containing the new social stimulus in the social memory test.

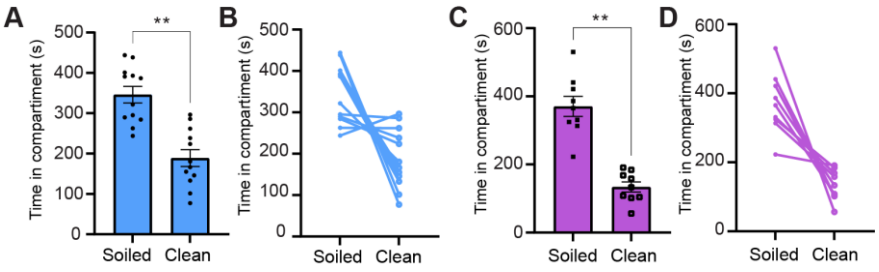

Supplementary 5: OXTR blockade in the piriform cortex doesn't impair sociability in the olfactory 3-chamber test. **A**. Total time of SAL injected mice in the social chamber (soiled bedding) and the non-social chamber (clean bedding) (Wilcoxon matched-pairs signed rank test, p=0.003). **B.** Distribution of the time spent in the chambers for SAL mice**. C.** Total time of OTA injected mice in the social chamber and the non-social chamber (Wilcoxon matched-pairs signed rank test, p=0.003). **D.** Distribution of the time spent in the chambers for all mice. (SAL: n= 12 mice, OTA: n= 9), **p<0.005,

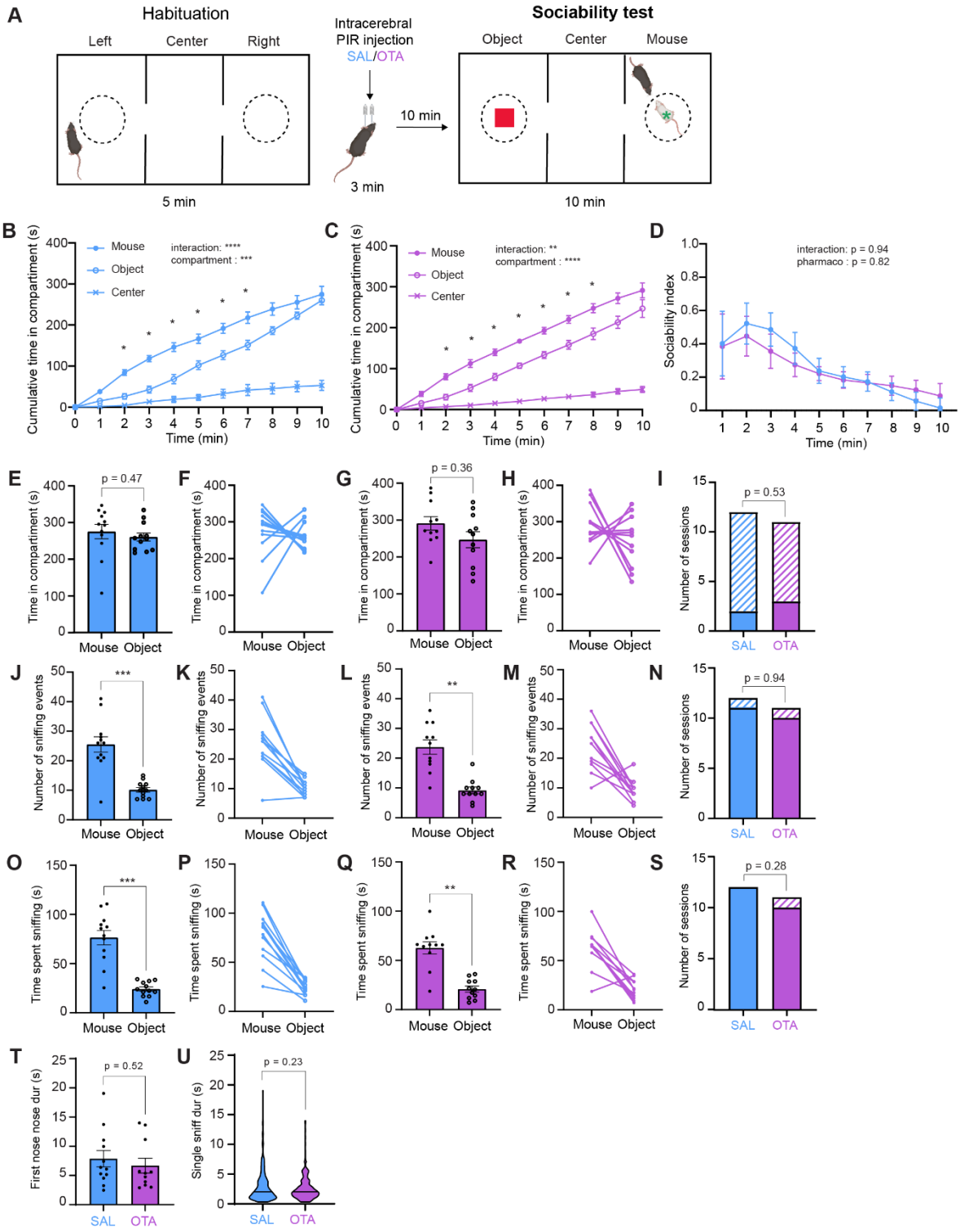
A
Habituation
Left
Center
Right
5 min
Intracerebral
PIR injection
SAL/OTA
3 min
10 min
Sociability test
Object
Center
Mouse
10 min
B
Cumulative time in compartment (s)
Mouse
Object
Center
interaction: ****
compartment : ***
Time (min)
C
Cumulative time in compartment (s)
Mouse
Object
Center
interaction: **
compartment : ****
Time (min)
D
Sociability index
interaction: p = 0.94
pharmaco : p = 0.82
Time (min)
E
Time in compartment (s)
p = 0.47
Mouse Object
F
Time in compartment (s)
Mouse Object
G
Time in compartment (s)
p = 0.36
Mouse Object
H
Time in compartment (s)
Mouse Object
I
Number of sessions
p = 0.53
SAL
OTA
J
Number of sniffing events
***
Mouse Object
K
Number of sniffing events
Mouse Object
L
Number of sniffing events
**
Mouse Object
M
Number of sniffing events
Mouse Object
N
Number of sessions
p = 0.94
SAL
OTA
O
Time spent sniffing (s)
***
Mouse Object
P
Time spent sniffing (s)
Mouse Object
Q
Time spent sniffing (s)
**
Mouse Object
R
Time spent sniffing (s)
Mouse Object
S
Number of sessions
p = 0.28
SAL
OTA
T
First nose nose dur (s)
p = 0.52
SAL
OTA
U
Single sniff dur (s)
p = 0.23
SAL
OTA

Supplementary 6 : OXTR blockade in the piriform cortex does not impact sociability in the classical 3-chamber test. A. Experimental protocol. Female mice first explored freely the apparatus with the cylinders (dashed circles) but without stimulus mice for 5 min. This was followed by bilateral PIR infusion of either SAL or OTA. After 10 min of post-infusion recovery, mice could explore a social chamber containing an unfamiliar female mouse, a non-social compartment containing an object, or an empty central compartment. A sociability index was calculated for each mouse from the time spent in each of the two external chambers. **B.** Mean cumulative time spent in each compartments shows that SAL-infused mice have a preference for the social compartment (2-way ANOVA: Time*Compartment < 0.0001, Compartment = 0.0004). **C**. Mean cumulative time spent in each compartment shows that OTA-infused mice also have a preference for the social compartment (2-way ANOVA: Time*Compartment = 0.001, Compartment < 0.0001). **D**. SAL and OTA mice have positive sociability indices meaning they spent more time in the social chamber compared to the non-social chamber. Sociability indices decrease across the 10-min trial but do not show any differences between the 2 groups (2way ANOVA: Time*Pharmaco = 0.94, Time = 0.002, Pharmaco = 0.82). **E.F.G.H.** The total time spent in social and non-social chambers was not significantly different for both the SAL and OTA groups (Wilcoxon matched-pairs signed rank tests: SAL, p = 0.47, OTA p= 0.36). **I.** SAL and OTA groups are not different in their proportion of “social” (filled color) compared to “non-social” (dashed lines) sessions, based on a threshold of the sociability index, Chi-square p = 0.53. **J.K.L.M.N.** Same has in E.F.G.H.I, but for the number of sniffing events. The number of sniffing events was higher towards the stimulus mouse compared to the object both in the SAL and OTA groups (Wilcoxon matched-pairs signed rank tests: SAL, p = 0.001, OTA, p = 0.003). No difference in the proportion of social (filled color) compared to non-social (dashed lines), between groups, Chi-square p = 0.94. **O.P.Q.R.S** Same has in E.F.G.H.I but for the time spent sniffing. The total time spent sniffing the stimulus mouse was higher compared to the time spent sniffing the object both in the SAL and OTA groups (Wilcoxon matched-pairs signed rank test (SAL, p = 0.0005, OTA, p = 0.002). No difference in the proportion of social (filled color) compared to non-social (dashed lines), between groups, Chi-square p = 0.28. **T.** Comparison of the first nose-nose duration showed no differences between groups (Mann Whitney test: p = 0.52). **U.** Violin plot showing the distributions of the durations for individual events of sniffing interest of the experimental mouse. These were not different between groups (Kolmogorov-Smirnov test: p= 0.23) (line = median, dashed line = quartile). Except otherwise specified data are represented as mean +/- SEM. (SAL = 12 mice, OTA = 11 mice) **p<0.005, ***p<0.001, ****p<0.0001.

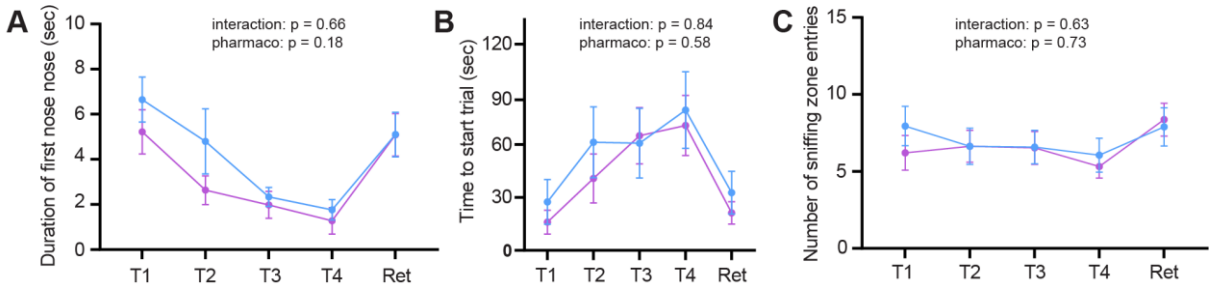

Supplementary 7 : OXTR blocked in the piriform cortex does not impact the interest or motivation of mice for social interactions. Duration of first nose-nose (**A**), time to start a trial (**B**) or number of sniffing zone entry (**C**) were not different between SAL (blue) and OTA (magenta) injected mice (2-way ANOVAs: A. Trial*Pharmaco = 0.66, Trial < 0.0001, Pharmaco= 0.18; B. Trial*Pharmaco = 0.84, Trial < 0.0001, Pharmaco= 0.58; C. Trial*Pharmaco = 0.64, Trial = 0.03, Pharmaco= 0.73) (SAL: n = 11 mice, 19 sessions, OTA = 11 mice, 19 sessions)

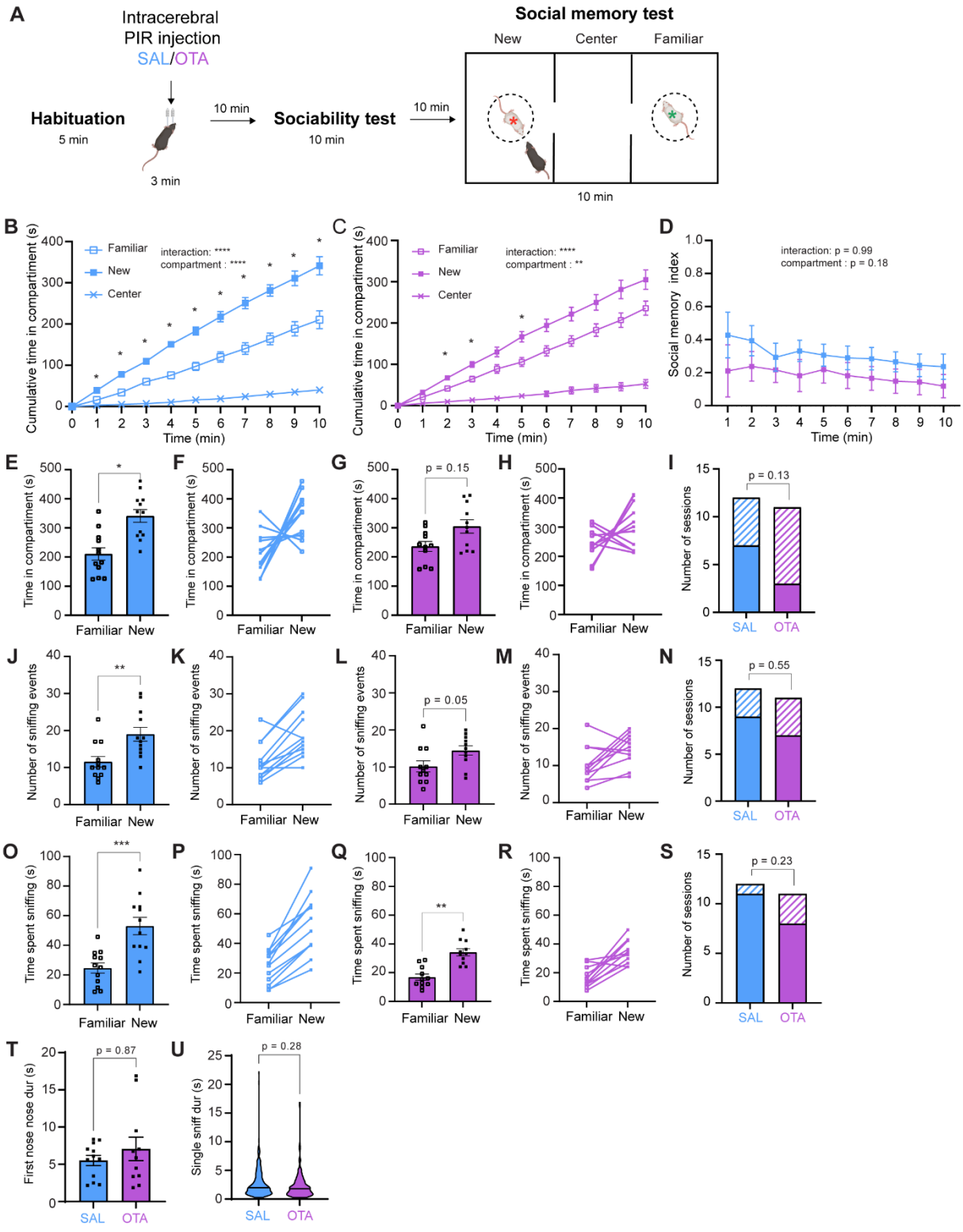
A
Intracerebral
PIR injection
SAL/OTA
Habituation
5 min
3 min
10 min
Sociability test
10 min
10 min
Social memory test
New
Center
Familiar
10 min
B
Cumulative time in compartment (s)
Familiar
New
Center
interaction: ****
compartment : ****
Time (min)
C
Cumulative time in compartment (s)
Familiar
New
Center
interaction: ****
compartment : **
Time (min)
D
Social memory index
interaction: p = 0.99
compartment : p = 0.18
Time (min)
E
Time in compartment (s)
Familiar New
F
Time in compartment (s)
Familiar New
G
Time in compartment (s)
p = 0.15
Familiar New
H
Time in compartment (s)
Familiar New
I
Number of sessions
p = 0.13
SAL OTA
J
Number of sniffing events
Familiar New
K
Number of sniffing events
Familiar New
L
Number of sniffing events
p = 0.05
Familiar New
M
Number of sniffing events
Familiar New
N
Number of sessions
p = 0.55
SAL OTA
O
Time spent sniffing (s)
Familiar New
P
Time spent sniffing (s)
Familiar New
Q
Time spent sniffing (s)
Familiar New
R
Time spent sniffing (s)
Familiar New
S
Number of sessions
p = 0.23
SAL OTA
T
First nose nose dur (s)
p = 0.87
SAL OTA
U
Single sniff dur (s)
p = 0.28
SAL OTA

Supplementary 8 : OXTR blockade in the piriform cortex does not impact social memory in the classical 3 chamber test. **A.** Experimental protocol. After a 5 min habituation followed by a SAL or OTA infusion in the PIR, female mice performed the 3 chamber sociability test described before (mouse vs object). Subsequently, they could perform the social memory test, in which they were allowed to freely explore a compartment containing the now-familiar female mouse (red asterisk), a compartment containing a new female mouse (green asterisk), or the empty central compartment. **B.** Mean cumulative time spent in each compartment shows that SAL-infused mice have a preference for the new compartment (2-way ANOVA: Time*Compartment = <0.0001, Compartment = <0.0001). **C.** Mean cumulative time spent in each compartments shows that OTA-infused mice also have a preference for the new compartment (2-way ANOVA: Time*Compartment = <0.0001, Compartment = 0.003). D. Social memory indices have a positive value for both groups, but do not show any differences between the 2 groups (2-way ANOVA: Time*Pharmaco = 0.99, Time = 0.30, Pharmaco= 0.18). **E.F.G.H.** The total time spent in the new and familiar chambers was significantly different for the SAL group (Wilcoxon matched-pairs signed rank test (p = 0.01), but not for the OTA group (Wilcoxon matched-pairs signed rank test: p = 0.15). **I.** No differences in the proportion of mice belonging to the memory group or no memory group was observed (Chi-square: p = 0.13). **J.K.L.M.N.** Same is E.F.G.H.I but for the number of sniffing events. The number of sniffing events was higher towards the new mouse compared to the familiar mouse in the SAL group (Wilcoxon matched-pairs signed rank test: p = 0.002), but not significantly different in the OTA group (Wilcoxon matched-pairs signed rank test: p = 0.05). No differences in the proportion of mice belonging to the memory or no memory group was observed (Chi-square: p = 0.55). **O.P.G.R.S** same as in E.F.G.H.I, but for the time spent sniffing. The total time spent sniffing the new mouse was higher compared to the time spent sniffing the familiar mouse both in the SAL and OTA groups (Wilcoxon matched-pairs signed rank test: SAL, p = 0.0005, OTA, p = 0.002). No differences in the proportion of mice belonging to the memory or no memory group was observed (Chi-square: p = 0.23). **T.** Comparison of the first nose-nose duration showed no differences between groups (Mann Whitney test: p = 0.87). **U.** Violin plot showing the distributions of the durations for single events of sniffing interest of the experimental mouse. These were not different between groups (Kolmogorov-Smirnov test: p = 0.28). (line = median, dashed line = quartile). (SAL = 12 mice, OTA = 11 mice). Except otherwise specified data are represented as mean +/- SEM. *p<0.05, **p<0.005, ***p<0.001, ****p<0.0001.

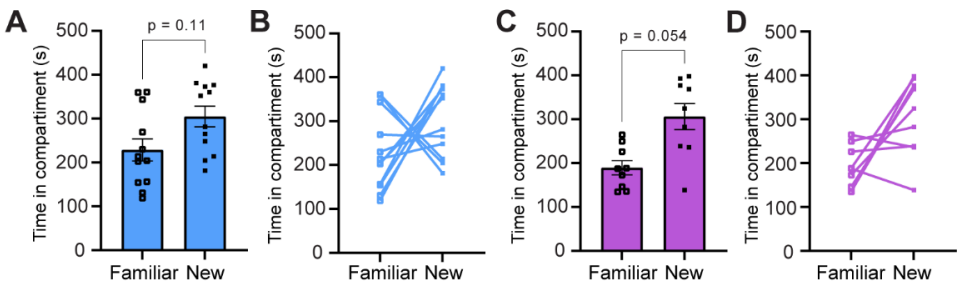

Supplementary 9 : OXTR blockade in the piriform cortex does not impair social memory in the olfactory 3-chamber test. A. Total time spent in the familiar and new compartment was not significantly different in the SAL group (Wilcoxon matched-pairs signed rank test: p = 0.11). **B.** Distribution of the data for individual SAL-infused mice. **C.** Total time in the familiar and new compartments was not significantly different in the OTA group (Wilcoxon matched-pairs signed rank test: p = 0.05). **D.** Distribution of the data for individual OTA-infused mice. (SAL: n=12, OTA: n = 9).

RESULTS

PART 3

Title: Oxytocin in the piriform cortex affects neuronal burstiness and coupling to respiration

Authors: Camille Miermon, Juliana Pi Macedo, Giulio Casali, Geoffrey Terral, Lisa Roux

Abstract:

In most Mammals, olfaction plays a central role in shaping social behaviors, as olfactory cues emitted by individuals can convey information such as health, reproductive and hierarchical status, but also identity. Oxytocin also has an important influence on interactions between conspecifics but how this pro-social neuropeptide impacts piriform circuit function remains largely unknown. In this study, we applied an agonist of OXT receptors in acute slices from the anterior piriform cortex to assess its impact on the intrinsic properties of the two main types of excitatory cells located in layer II: the semilunar (SL) and the superficial pyramidal cells (SP). While SL cell properties were unaffected by the agonist, we found that OXT receptor activation abolishes the ability of SP cells to generate burst of action potentials upon depolarization. To test whether this effect was also observed *in vivo*, we recorded piriform neurons using chronically implanted silicon probes in freely moving mice and performed systemic injections of the OXT receptor agonist. In these conditions, we found that the burstiness of the putative excitatory cells was reduced, in line with the results obtained *in vitro*. Interestingly, the agonist also disrupted the coupling of piriform units with the respiratory rhythm. Altogether, these results indicate that OXT in the piriform can directly affect the intrinsic properties of pyramidal cells, possibly modulating their response to incoming sensory inputs. Further work will allow deciphering whether synaptic properties are also affected by OXT.

Introduction:

The neuropeptide oxytocin is known for its powerful impact on social behaviors (Jurek and Neumann 2018) but the mechanisms underlying its physiological impact on neuronal circuits only start to be uncovered (Knobloch et al. 2012; Owen et al. 2013;

Marlin et al. 2015; Tirko et al. 2018). In the CA1 region of the hippocampus, OXT enhances spike transmission by modulating interneurons and therefore improved the signal-to-noise ratio (Owen et al. 2013). The impact of OXT in the auditory cortex, amygdala, the PVN, and prefrontal cortex is also primarily mediated by a modulation of interneuron activity (Huber et al., 2005; Nakajima et al., 2014; Marlin et al. 2015; Mitre et al. 2016). Yet, the existence of a generic mode of action of OXT that would be conserved across brain regions is unlikely because OXT receptors (OXTR) are expressed at different levels depending on the brain region considered (Mitre et al. 2016) and oxytocinergic axonal projections show an equal level of heterogeneity (Grinevich et al. 2016). The complexity also derives from the fact that OXTR are expressed in a variety of neuronal subtypes, as well as in glial cells (Baudon et al. 2022). The proportions of OXTR-expressing cells among each cell types can also substantially vary across brain areas.

In this context, the piriform cortex is unique in numerous aspects:

(1) the density of OXTR-expressing cells is extremely high as compared to other cortical areas, especially in female mice (Mitre et al. 2016);

(2) the targets of OXT in the piriform may not be restricted to interneurons: indeed, our histological data show that OXTR expression is enriched in layer II where the cell bodies of the two types of excitatory neurons (the superficial pyramidal (SP) cells and semilunar (SL) cells are mainly located;

(3) *in vitro* recordings suggested that OXT may indirectly affect inhibitory transmission through a direct impact on excitatory cells, unlike the mechanism found in auditory cortex and PVN slices where presynaptic inhibition is directly reduced by OXT (Mitre et al. 2016).

Altogether, these observations suggest that OXT has a mode of action specific to piriform circuits that have not been uncovered yet. Given the central role of both olfaction and OXT in social behaviors (Oettl and Kelsch 2017), our objective was to determine how OXT modulated neuronal intrinsic properties in the piriform cortex in vitro and whether *in vivo*, activation of OXTR modulates piriform neuronal circuits.

Methods:

Animals

All experimental procedures were performed in accordance with standard ethical guidelines (European Communities Directive 86/60-EEC) and approved by the local committee on animal health and care of Bordeaux and the French ministry of agriculture and forestry (authorization number APAFIS # 23974 / agreement #A33063940. All mice were maintained in a pathogen free facility in a diurnal 12h light/dark cycle with food and water ad libitum. For *in vivo* experiments, 5 adult (4-6 months old) C57bl/6 male mice were recorded.

The *ex vivo* electrophysiology experiments were divided into two parts. In the characterization of PIR neuronal intrinsic properties, OXTR-cre::Ai9Tomato female mice (C57bl/6 background) aged 7 to 9 week-old were used. OXTR-cre::Ai9Tomato mice were used in the intend to record selectively from OXTR positive cells but we found – using immunostainings with the OXTR antibody - that this strain was not specific for targeting OXTR expression. The fluorescence was therefore ignored in these experiments.

Silicon probes and nasal cannula

32 recording channels silicon probes were used for hippocampal recordings (Buzsaki 32, 4 shanks, NeuroNexus). For aPIR recordings, 64 recording channels silicon probes of either 6 shanks (Buzsaki 64, NeuroNexus) or 2 shanks (H6 Cambridge, Neurotech) were chosen. Each probe was mounted on custom-made 3D printed micro-drives allowing precise and flexible movement of the probes on the vertical axis after implantation. Nasal cannulas were custom made from 23G hypodermic stainless steel tube (detailed fabrication: Miermon et al., 2022, in prep).

Surgery for silicon probe and nasal cannula implantation

A total of 5 mice were implanted with a combination of two silicon probes (one in the aPIR and one in the CA1 region of the hippocampus - HPC) as well as one nasal cannula to provide respiratory monitoring. In 4 out of 5 mice we obtained simultaneous electrophysiological recordings from aPIR and HPC. In 4 out of 5 mice we obtained simultaneous recordings of aPIR and respiration. For surgery, mice were anesthetized using isoflurane (induced 3 min at 4% - maintenance at 1.5% for the duration of

surgery) and received an intraperitoneal (i.p.) injection of metacam (5 mg/kg). After being placed on a stereotaxic apparatus (RWD), local anesthesia (lurocaine 5mg/kg) above the skull was performed, followed by a midline skin incision. Vitals and body temperature were tracked at all times using PhysioSuite (Kent Scientific), and i.p injections of NaCl 0.9% was given if necessary to avoid dehydration. Nasal cannula implantation was performed as previously described (Miermon et al., 2022, in prep). Briefly, a nasal cannula was inserted and cemented 1.5mm deep in a craniotomy of the nasal plaque. This was followed by two ipsilateral craniotomies above the aPIR (AP = +2mm, ML = +/- 2.2mm, DV = 2.5mm from brain surface), and HPC (AP = -1.8mm, ML = +/- 1.4mm, DV = 0.7 from brain surface). Craniotomies were protected with silicon (3-4680, Dow corning). One stainless steel screw above the cerebellum was used as reference for the electrodes. Finally, a faraday cage was built from copper mesh and attached to the skull with dental cement and connected to the ground screw. Animals recovered for at least one week and were placed in individual cages before the start of experiments. During post-surgery recovery, probes were gradually lowered to reach the target position. Electrophysiological signatures of the two regions were used to estimate arrival to cellular layers. The presence of sharp wave ripple oscillations during sleep was used as a landmark for HPC (Buzsáki 2015). The absence of up/down states together with population burst activity and strong gamma oscillations was the signature for PIR (Manabe et al. 2011).

Drug preparation and protocol for administration

During the light phase (8am – 2pm), freely moving mice were recorded for a five-hour recording session. After 1h of baseline activity recording, mice received an i.p injection of either vehicle or saline (NaCl 0.9%). This was followed by 2h of rest at the end of which they received a second i.p injection of either an OXTR agonist or antagonist. Mice were then allowed two more hours of rest. To reduce stress and thus promote the probability to record mice in different brain states (i.e wake, non-REM, REM) before and after drug injections, mice were habituated to i.p injections and were recorded in their home cage.

For activation of OXTR, the high affinity OXTR agonist TGOT ([Thr4, Gly7]-oxytocin) was given at 10mg/kg (dissolved in NaCl 0.9%,(Tan et al. 2019)) for a total of 6

sessions in 5 mice. I.p injections of saline were used as control. For systemic OXTR blockade, we used the high affinity non-peptide OXTR antagonist L-368.899 (prepared in 1.25% DMSO, 98.75% NaCl 0.9%, Tocris Bioscience) which was shown to cross the blood-brain barrier. In order to maximize the number of sessions and the use of mice, 2 sessions at 5 mg/kg and 2 sessions at 10mg/kg (Tan et al. 2019) were analyzed together in 3 different mice. A vehicle solution (1.25% DMSO, 98.75% NaCl 0.9%) was used as control. To maximize the use of implanted mice, 3 out of 5 mice received first an injection of OXTR agonist and then an injection of the antagonist with a minimum of four days between the two sessions.

Histology

At the end of experiments, mice underwent electrolytic lesioning under isoflurane anesthesia (1.5%) of 1 site per shank (10µA for 10s, A365RC Stimulus isolator from World Precision Instruments) to facilitate electrode placement validation. After a minimum of 24h following the lesions, mice were sacrified by intracardiac perfusion of 4% PFA after having received a lethal dose of ketamine/xylazine (100mg/kg and 20mg/kg, respectively). After 24h in 4% PFA, brains were sliced in coronal sections using a vibratome (Leica, VT 1200S) at 50µM. After donkey anti-mouse Cy5 (1:200) and DAPI staining (1:10 000, Fisher scientifique), floating slices were washed, and mounted under coverslips for visualization under the epifluorescence microscope (Eclipse Ni-U, Nikon). Electrode positions were then confirmed by the combination of electrolytic lesions visualization and/or probe tracks visualization.

Data analysis

Preprocessing – spike sorting and unit classification – respiratory signal

All analyses were performed using Matlab (The MathWorks), the FMAToolbox (http://fmatoolbox.sourceforge.net/), Buzsaki lab toolbox – Buzcode (https://github.com/buzsakilab/buzcode), and custom-written scripts.

Electrophysiological signals were acquired continuously at 20 kHz on an Intan RHD2000 interface board and amplified by 32 and 64-channel digital headstages (Intan Technologies). Respiratory signals were detected by a pressure sensor (Honeywell) and simultaneously acquired on the Intan board analog input channels

after the voltage was reduced below 3.3V using a custom-made voltage-divider. Data were then visualized with Neuroscope (Neurosuite, http://neurosuite.sourceforge.net, (Hazan et al., 2006). Spike sorting was performed semi-automatically with KiloSort (Pachitariu et al., 2016), https://github.com/cortex-lab/KiloSort) followed by manual clustering with Phy (Phy 2.0 beta, https://github.com/cortex-lab/phy) with the help of custom-designed plugins (https://github.com/petersenpeter/phy-plugins). Brain states were scored based on hippocampal spectrograms as well as accelerometer signal using TheStateEditor (Grosmark et al. 2012). Respiratory signals were analyzed using the Breathmetrics toolbox (https://github.com/zelanolab/breathmetrics) optimized for intra-brain state accuracy (see Miermon et al., 2022).

Putative excitatory and inhibitory aPIR neurons were separated on the basis of a Gaussian-mixture model using two waveform features: trough-to-peak and spike width (Stark et al. 2013) Only units showing a high classification confidence (P<= 0.01) were used for the study. Due to the low number of recorded inhibitory neurons, only putative excitatory neurons were presented in this study (see SUPPL 3 for the number of recorded neuron in function of the pharmacological condition).

The effect of control and drug injections were done by analyzing aPIR activity and respiration on a 30-min interval before and after injection. To remove possible confounding effects due to i.p injection stress, the first 10 minutes after injection were excluded from the analysis. Brain state intervals shorter than 1 minute were excluded from the analysis.

Firing rates – Burstiness

For firing rate analyses, only data where there was wake in the condition before and after drug were analyzed. Burstiness was defined as a minimum spike interval bellow 6ms. We displayed data as the ratio of how many spikes are in burst compared to total spike number.

Modulation of neuronal activity by respiration

First, we defined the instantaneous respiratory phase by assigning each inhalation onset to phase zero and assigning the remaining cycle phases by interpolation. To determine whether a unit was significantly entrained by respiration, we used the Rayleigh test which compares actual neuronal spike train distribution across all the

phases of the reference oscillation (here, the respiration phases) to a homogeneous distribution.

Ex vivo slice preparation

All mice were sacrified by dislocation under isoflurane anesthesia (5% - 3min), during the light phase (8am – 2pm). Brains were quickly removed and immerged in ice-cold oxygenated cutting solution (in mM: 180 Sucrose, 26 NaHCO3, 12 MgCl2, 11 Glucose, 2.5 KCl, 1.25 NaH2PO4, 0.2 CaCl2, oxygenated with 95% 02/5% CO2 ≈ 300mOsm). Coronal aPIR slices (300 µM thick) were obtained using a vibratome (VT1200 S, Leica) in ice-cold oxygenated cutting solution. Slices were then transferred for 30min into a 34°C bath of oxygenated aCSF (in mM: 123 NaCl, 26 NaHCO3, 11 Glucose, 2.5 KCl, 2.5 CaCl2, 1.3 MgCl2, 1.25 NaH2PO4 ≈ 305 mOsm). After a minimum of 30min recovery at RT (22-25°C), slices were transferred to a recording chamber on aCSF 32°C.

Patch-clamp recordings

Recordings were performed using a Multiclamp 700B amplifier (Molecular devices) and Digidata 1550 series digitizer in principal glutamatergic neurons with glass pipettes (4.5-9 MΩ). Using the clampex 11.2 software, cells were recorded in voltage-clamp at -70mV for access (Ra), and input (Ri) resistance measurements. Excitatory cells were identified based on their morphology and somatic localization (using a contrast microscope – Olympus BV51WI) – and through their electrical properties by measuring their excitability in current-clamp mode. Neurons with large apical dendrites, soma located in the upper half of layer II and displaying regular spiking were considered as semilunar cells (SL). Instead, neurons with large basal dendrites, soma located in the lower half of layer II and upper part of layer III and showing initial burst firing were classified as superficial pyramidal neurons (SP), based on prior work (Suzuki and Bekkers 2006)

Intrinsic properties and modulation by an OXTR-agonist

For the characterization of the intrinsic properties of SL and SP cells of the aPIR, we used a potassium gluconate based intracellular solution (in mM: 135 K-Gluconate, 10 KCl, 10 HEPES, 1 EGTA, 2 MgCl2, 0.3 CaCl, 7 Phosphocreatin, 3 Mg-ATP, 0.3 Na-GTP). Few seconds following the opening of the cells, resting membrane potential

was measured in the current-clamp configuration in gap free mode (= continuous recording). For frequency*Injected curves (F-I curves) and action potential characterization, cells received 500ms steps of current injections (-150 to 440 pA, delta = 10pA). Finally, a second measurement of Ra was performed. In another group of neurons, we determined the effects of an OXTR-agonist on piriform excitatory neurons, by bath applying the selective OXTR agonist, TGOT (5 µM) for at least 10 min before recording.

Analysis

Intrinsic properties

Clampfit 11 was used to export recorded data and perform measurements. Access resistance (Ra) and membrane resistance (Rm) were measured using "Membrane Test" function. For that, a 10-mV square voltage pulse was applied at 50 Hz, and the current response was used to calculate membrane parameters. Results were exported with Clampfit 11 for the whole recording time after stabilization, then mean Ra and mean Rm were calculated. Input resistance (Ri) was calculated as the sum of Ra and Rm. Resting membrane potential was measured as the mean value over the first 60 seconds of recording. All the other parameters, except the burstiness index, were measured using the Matlab FFFPA application for the first spike of each sweep (see (Nagaeva et al., 2021)**,** 'Data analysis'for the application, and (Nagaeva et al. 2020)**,** 'Appendix Table 1' for detailed definitions). Burstiness was calculated for the first sweep containing a train of 8 action potentials (or 9 if the cell did not present 8) as the inverse of the adaptation ratio (which is Fmax SS/Fmax init, with Fmax SS being the steady state maximum frequency, that is the inverse of the average mean of the last three intervals inter-spike (ISI); and Fmax init being the initial maximum frequency, there is the inverse of the shortest ISI among the first three spikes). Recordings were excluded from analysis if Ra changed more than 30% (5 out of 31 recorded cells).

Immunohistochemistry

Brain preparation: Mice were deeply anaesthetized using a mixture of Ketamine (100mg/ml) and Xylazine (20mg/ml) (i.p injection) and transcardially perfused with phosphate-buffered saline (PBS) followed by 4% paraformaldehyde. Brains were fixed

overnight in 4% paraformaldehyde then sliced at 50-70 µm thickness using a vibratome (Leica VT 1200).

Immunostaining procedures and imaging: For OXTR staining, coronal sections containing the PIR were incubated for 1h in blocking solution containing 5% Normal Goat Serum and 0.3% Triton-X100 in PBS. Sections were then incubated overnight with a rabbit anti-OXTR antibody (gift from Robert C. Froemke, 1:250) at 4°C, washed three times with PBS-Triton 0,1%, and then incubated 1-2h with a goat anti rabbit Alexa fluor 488 secondary antibody (1:1000, A11008, ThermoFischer Scientific). Slides were washed and counter-stained for 5 min with DAPI (1:10000, D1306, Invitogen), and mounted with Fluoromount mountain medium (Invitrogen). Fluorescent images were acquired on a Leica SP8 confocal microscope and analysis were performed using Fiji-ImageJ Wiki software (National Institutes of Health, USA). To measure OXTR Mean Fluorescence Intensity (MFI) in the different PIR layers, specific region of interest (ROI) was manually defined for each layer using the DAPI staining. After background subtraction, the ratio OXTR / DAPI MFI was calculated for each layer. Eight sections per animal was analyzed.

Results:

Principal neurons of the piriform cortex of female mice can be distinguished based on their firing profiles and action potential shapes

To characterize the intrinsic properties of piriform (PIR) principal neurons – the superficial pyramidal (SP) cells and semilunar (SL) cells – we performed patch-clamp recordings in acute slices from adult female mouse brains. Cells were recorded in whole-cell configuration, in the current-clamp mode. We first investigated the differences between the two cell types on their resting membrane potential and input resistance. Unlike what has been described in younger animals and adult male mice (Suzuki and Bekkers 2006; Terral et al. 2019), resting membrane potential was not significantly different between SP cells (-71.82 ± 1.6 mV; n = 6 cells) and SL cells (-68.92 ± 1.48 mV; n = 11 cells) (Mann-Whitney test, p = 0.30). The input resistance (Ri) was also not significantly different between the two groups (Ri = 150 ± 26.62 MOhm and 212.6 ± 15.59 MOhm in SP and SL cells, respectively; Mann Whitney test, p =

0.09). Thus in our conditions, female PIR SP and SL cells could not be distinguished based on their membrane potential and input resistance. How about based on their firing profiles?

As previously described by other groups, we found that SP and SL cells presented different firing profiles (Fig 1). Indeed, SP cells during depolarization-induced spike trains, had their first pair of action potentials occurring in a burst (Fig 1.A) contrary to SL cells. This was reflected by a higher burstiness index of SP cells compared to SL cells (Fig 1.B). SP cells fired earlier during a single current step (Fig 1.C), but started to fire for higher current step values – i.e they had a higher rheobase than SL cells (Fig 1.D.E). Overall SP cells had a reduced firing frequency throughout the increased current steps compared to SL cells (Fig 1.D) but the two cell types had no differences in saturating current value (Fig 1.F). In summary, SP cells are characterized by their initial burst profile, whereas SL cells fire for smaller current steps but at higher frequencies.

Do SP and SL cells also differ regarding the shape of their action potentials? To answer this question, we analyzed the first spike they produce at rheobase (Fig 2.A). We observed no difference in the first spike threshold between the two cell-types (Fig 2.B), but we did observe that SP cells had higher first spike amplitude (Fig 2.C), lower first spike decay time (Fig 2.D) and lower after-hyperpolarization amplitude (Fig 2.E) compared to SL cells. This is consistent with observations from the work of Suzuki and Bekkers 2006, who reported differences in action potentials shapes between the two cell-types.

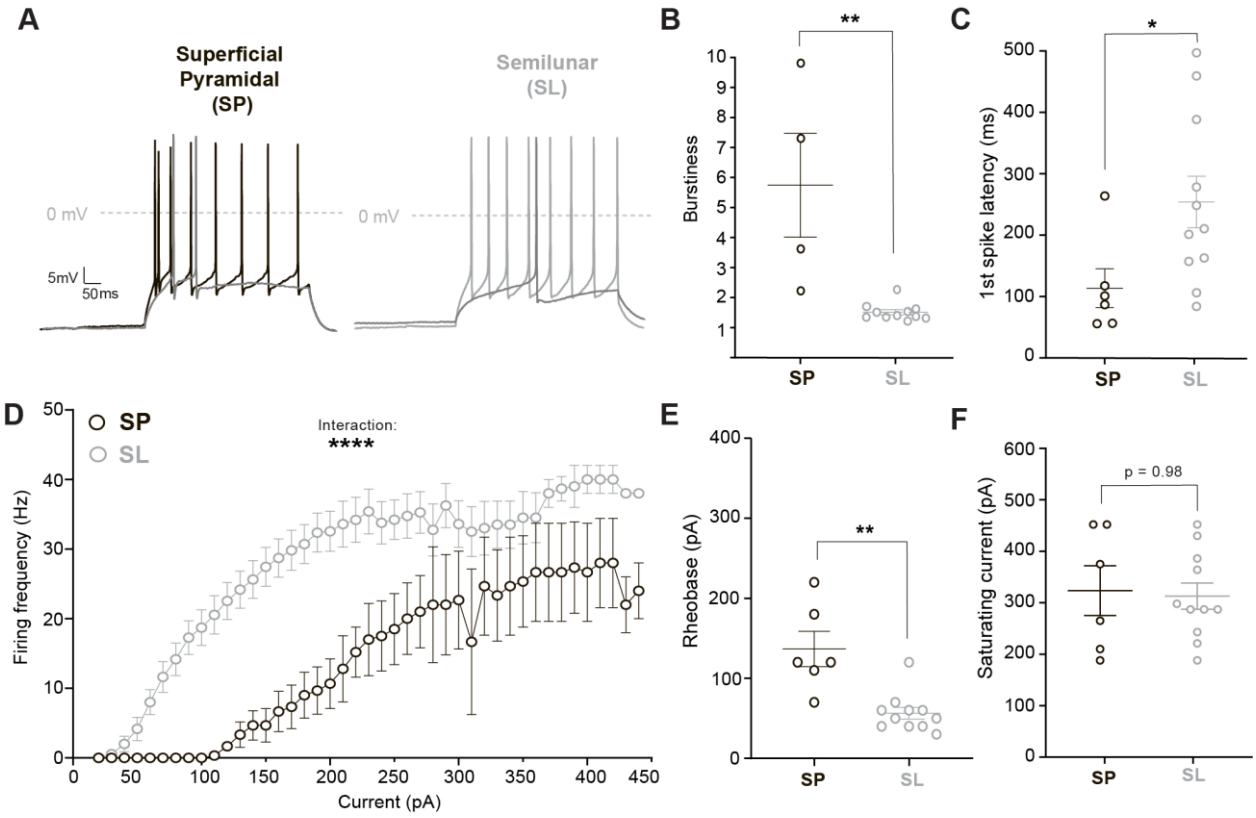

Figure 1 : Superficial pyramidal and semilunar piriform neurons exhibit different firing profiles. **A.** Illustrative recordings at rheobase (medium gray), or at the current step with 8 action potentials (black or light gray) for a piriform superficial pyramidal (SP) neuron (left), and a semilunar (SL) neuron (right). **B.** Mean burstiness index is significantly higher for SP cells (n = 4 cells) than for SL cells (n = 11 cells) (Mann-Whitney test: p = 0.0015). **C.** First spike latency is significantly shorter for SP cells compared to SL cells (Mann-Whitney test: p = 0.02). **D.** Mean frequency x Injected current curve for SP and SL cells from the rheobase until they reach saturation. Current x cell interaction is significant (Mixed-effects analysis: Cell-type effect, p = 0.0005, Current effect, p < 0.0001, Interaction, p < 0.0001). **E.** Mean rheobase current of SP cells is significantly higher than for SL cells (Mann-Whitney test: p = 0.0013). **F.** Mean saturating current is not different between the two cell types (Mann-Whitney test: p = 0.98). Except in panel B, SP (n = 6 cells), SL (n= 11 cells). Rb = rheobase. Error bars represent SEM. *p<0.05, **p<0.005, ****p<0.0001

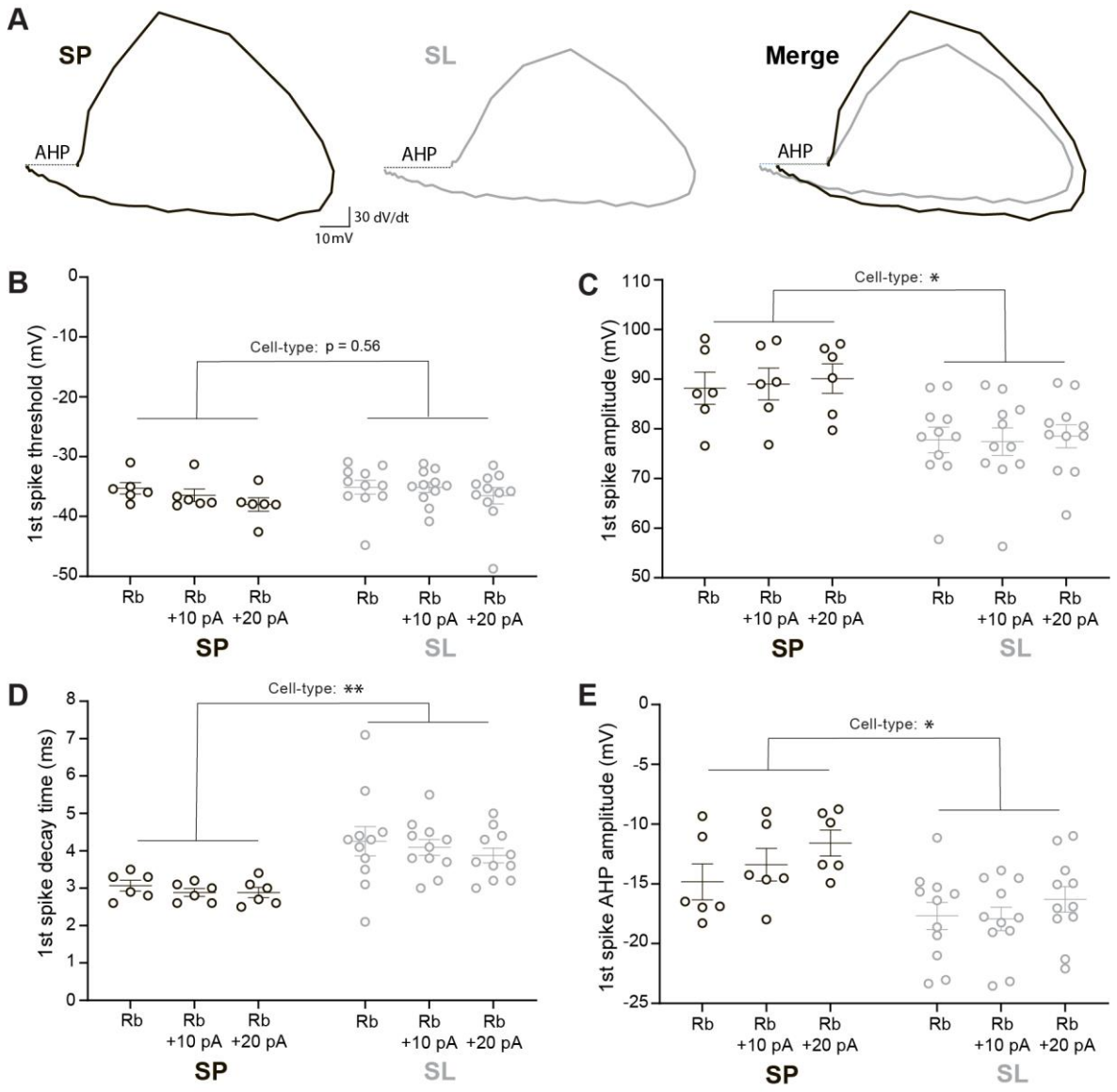

Figure *2* : Superficial pyramidal and semilunar piriform neurons present different action potential shapes. A. Curves represent the derivative of the voltage over time (dV/dt), as a function of the voltage (mV) for the first action potential (AP) at the rheobase. Illustrative dV/dt x mV curves for a representative SP cell (left) and a SL cell (center). Merge (right) illustrates differences on AP shape. Curves are aligned on AP threshold. AHP represents after-hyperpolarization amplitude. **B.** Mean first spike threshold is not significantly different between SL and SP cells (2-way ANOVA: Cell type effect, p = 0.56, Current effect, p = *0.002, Interaction, p = 0.34*). **C.** Mean first spike amplitude is significantly bigger for SP cells compared to SL cells (2-way ANOVA: Cell type effect, p = 0.016, Current effect, p = 0.08, Interaction, p = 0.52). **D.** Mean first spike decay time is significantly higher for SL cells compared to SP cells (2-way ANOVA: Cell type effect, p = 0.0074, Current effect, p = 0.15, Interaction, p = 0.67). **E.** Mean first spike after-hyperpolarization amplitude (AHP) is significantly larger for SL cells compared to SP cells (2-way ANOVA: Cell type effect, p = 0.025, Current effect, p = 0.0013, Interaction p = 0.19). SP (n = 6 cells), SL (n = 11 cells). Rb = rheobase, Rb+10pA: sweep following the Rb; Rb+20pA: two sweeps following the rheobase. Error bars represent SEM. *p<0.05

OXTR activation in the piriform cortex blocks bursting activity in superficial pyramidal cells without affecting semilunar cells

To test whether the activation of the oxytocin receptor (OXTR) in the PIR impacts the intrinsic properties previously described, we repeated the previous experiments with the oxytocin receptor agonist (TGOT) bath applied. *Please note that these are preliminary experiments, that will need to be replicated in order to be confirmed.*

TGOT application did not significantly change resting membrane potential in SP and SL cells (Mann-Whitney tests: SP: $p = 0.79$; SL: $p = 0.10$) nor did it change the input resistance (Mann-Whitney tests: SP: $p = 0.93$, SL: $p > 0.99$) compared to the control condition (aCSF).

The firing profile of SP cells in the presence of TGOT was then analyzed (Fig 3). We found that all the five SP cells that we recorded failed to present an initial burst (Fig 3.A), and consequently had a significantly decreased burstiness index in the presence of TGOT compared to the control condition (Fig 3.B). No significant differences due to TGOT application were observed on the other parameters – i.e first spike latency (Fig 3.C), firing frequency (Fig 3.D), rheobase (Fig 3.E), and saturating current (Fig 3.F). We also did not observe any impact of TGOT on SP action potential shape (Suppl 1). Preliminary observations from immunohistochemistry shows enrichment of the OXTR in layer II and III (Suppl 4) which could be consisted with an expression of OXTR on SP cells which are known to have their soma in layer IIb (Suzuki and Bekkers 2006).

We also tested whether SL cells intrinsic properties are modulated by TGOT-mediated OXTR activation. We could not find a significant difference between aCSF and TGOT conditions regarding firing profiles or action potential shapes (Suppl 2).

Based on these in vitro experiments, we concluded that OXTR activation in the PIR blocks burstiness of SP cells. Can this effect be observed *in vivo*?

Systemic OXTR activation induces a reduction of bursting in putative excitatory piriform cortex cells *in vivo*

To access the impact of OXTR activation in the PIR *in vivo*, we implanted a high density silicon probes in the anterior PIR, and another one in the CA1 region of the hippocampus (HPC) (Fig 4.A). Hippocampal recordings were used to define the brain states of the animal (Wake, Non-Rapid-Eye-Movement – NREM – or REM sleep).

Because *in vivo* electrophysiological recordings are not compatible with local pharmacology, we started these experiments with systemic injections of TGOT (OXTR-ago) and its control (saline - SAL). Our protocol consisted in 2 successive injections (SAL then OXTR-ago) separated by a minimum of two hours. Mice were left in their home cage during the whole recording duration when they alternated between spontaneous exploration and sleep (Fig 4.B). Here we focused on the wake state and first controlled that the recording durations in this state was similar across the different conditions pre and post injections (Suppl 3). The total number of neurons recorded was also comparable (Suppl 3). These controls insured that our level of confidence was similar across conditions. After this verification step, we classified the unit we recorded into two categories: putative excitatory and putative inhibitory units (see Methods). We found that putative excitatory neurons have an increased firing rate after TGOT injection compared to before (Mean +/- SEM: Before = 2.22+/- 0.1; After = 2.62 +/- 0.13) (Fig 4.C). However, SAL injection also induced an increase in firing rate (Mean +/- SEM: Before = 2.44+/- 0.16; After = 2.69 +/- 0.14) (Fig 4.E). As a consequence, we could not conclude on the impact of OXTR activation on firing rate. However, we found that TGOT systemic injections significantly decreased the ratio of spikes in burst of putative excitatory PIR neurons (Mean +/- SEM: Before = 7.38 +/- 0.46, After = 6.8 +/- 0.41) (Fig 4.D) and it was not the case during SAL injections neurons (Mean +/- SEM: Before = 7.0 +/- 0.49, After = 7.1 +/- 0.53) (Fig 4.F). Based on these results, we concluded that systemic OXTR activation decreases the burstiness of putative excitatory neurons which is consistent with our findings *in vitro*.

Past studies have shown that the PIR is modulated by the respiration (Fontanini et al., 2003 ; Poo and Isaacson 2009; Rennaker et al. 2007), potentially impacting the way it processes olfactory signals. In this last analysis we wondered whether OXTR activation modulates the entrainment of excitatory PIR cells to the respiration signal.

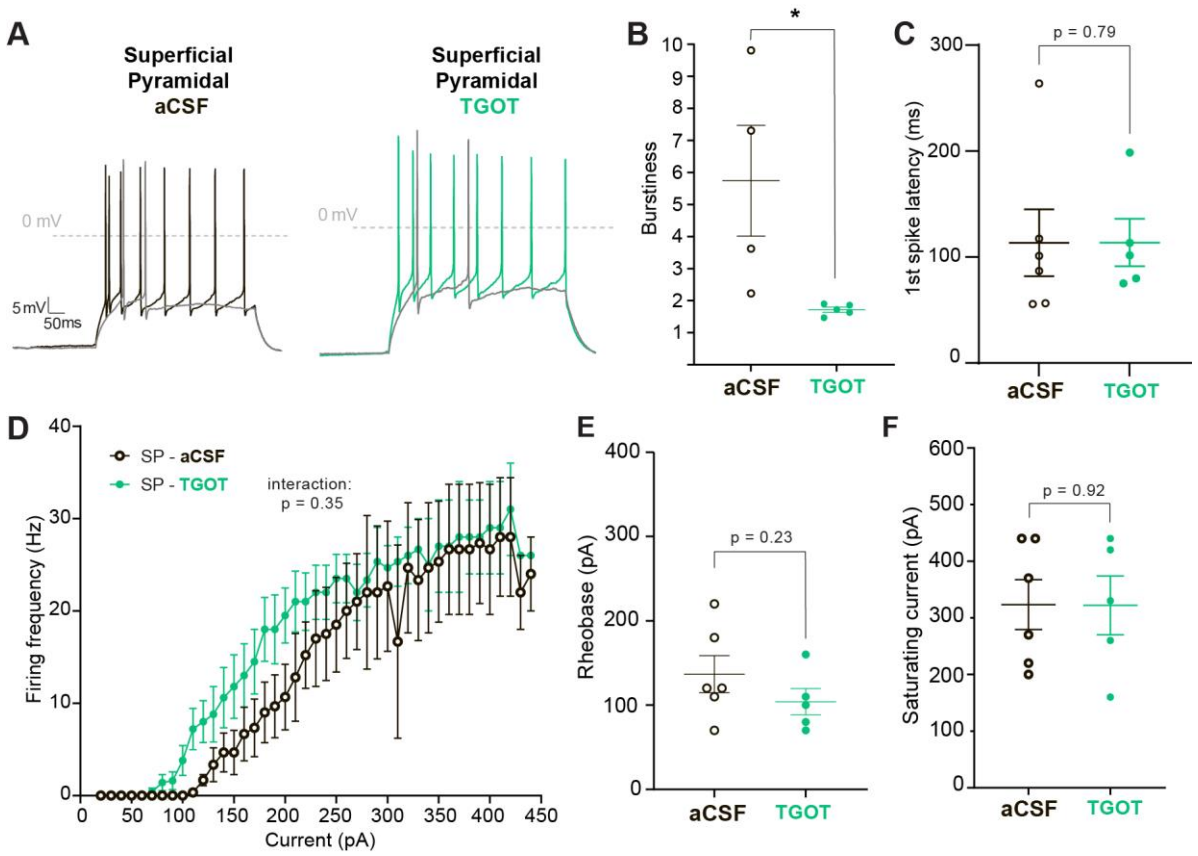

Figure 3 : Oxytocin receptor agonist TGOT reduced the burstiness of superficial pyramidal cells. **A.** Illustrative recordings at rheobase (gray) or at current step with 8 action potentials (black or green) for SP cells in aCSF (left) or TGOT (right) condition. In this and all the following panels, data for SP-aCSF group is the same as shown in Figures 1 and 2. **B.** Mean burstiness index is significantly decreased for SP cells in the presence of TGOT compared to aCSF (Mann-Whitney test: p = 0.016) (aCSF: n = 4 cells, TGOT: n = 5 cells). **C.** Mean first spike latency is not significantly different between both conditions (Mann-Whitney test: p = 0.79. **D.** Mean frequency x injected current curves for SP cells in aCSF or TGOT conditions. No significant effect of the drug (Mixed-model analysis: Group effect, p = 0.17, Current effect, p = 0.001, Interaction, p = 0.35). **E.** Mean rheobase is not significantly different for SP cells in the two conditions (Mann-Whitney: p = 0.23). **F.** Mean saturating current is not significantly different for SP cells in the two conditions (Mann-Whitney: p = 0.92). Error bars represent SEM. Except for panel B, SP-aCSF (n = 6 cells), SP-TGOT (n = 5 cells). *p<0.05

Systemic OXTR activation induces a reduction of the strength of entrainment of putative excitatory piriform cortex cells to respiration

To answer this question, we used mice implanted with HPC, PIR silicon probes and nasal cannula implanted to record respiration (Fig 5.A). We recorded nasal pressure and PIR local field potential (LFP), before and after systemic injections of SAL and OXTR-ago (Fig 5.B,C). From PIR LFP we extracted spiking activity and quantified

whether a specific cell was modulated or not by respiration. A modulated cell displayed an increased probability of firing during a specific phase of the respiratory cycle (with one cycle being described as starting at inhalation onset and finishing at the next inhalation onset) (Fig 5.D.i), whereas a non-modulated cell fired regardless of the cycle phase (Fig 5.D.ii). The strength of this modulation was reflected by the resultant length, and the preferred phase by the circular angle mean. OXTR systemic activation induced a reduction in the number of respiratory modulated cells (Fig 5.E) as well as a significant decrease in resultant length (Fig 5.F.G). Thus we concluded that OXT reduces the entrainment of putative excitatory PIR cells to the respiration.

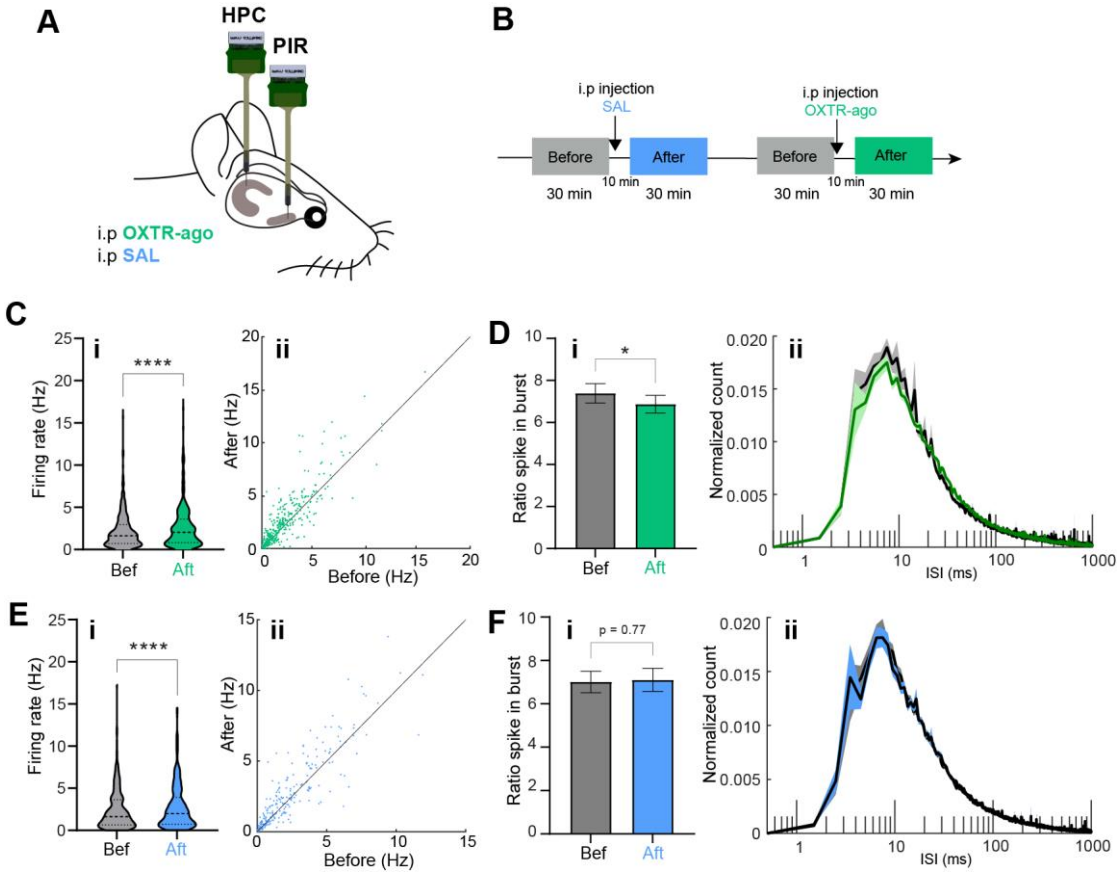

Figure 4 : Systemic oxytocin receptor agonist injection reduces the burstiness of putative excitatory neurons of the piriform cortex *in vivo*. A. Schematic of a mouse recorded *in vivo* in the CA1 region of the hippocampus (HPC), and piriform cortex (PIR) receiving intraperitoneal injections (i.p). **B.** Experimental protocol consisted of recording mice during spontaneous behavior. They were injected i.p with SAL and subsequently with the oxytocin receptor agonist (OXTR-ago), TGOT. 30 min intervals were analyzed before and after i.p injections. The 10 min post infusion were excluded to avoid the possible confounding effects of stress due to the i.p injection. **C.** Impact of systemic OXTR-ago injection on putative excitatory cells in the wake state. **(i,ii)** Mean firing rate is increased after (Aft) the injection compared to before (Bef) (Wilcoxon matched-pairs signed rank test: p<0.0001) (line = median, dashed lines = quartile) **D. (i)** Burstiness, as evaluated by the mean ratio of spikes in burst, is significantly decreased after the injection compared to before. Error bars are SEM (Wilcoxon matched-pairs signed rank test: p = 0.01) **(ii)** Normalized count of spikes with different inter spike intervals (ISI) **E.** Impact of systemic SAL injection on putative excitatory PIR cells in the wake state. **(i,ii)** Mean firing rate is increased after the injection compared to before (Wilcoxon matched-pairs signed rank test: p < 0.0001) (line = median, dashed lines = quartile) **F. (i)** Burstiness, as evaluated by the mean ratio of spikes in burst, is not significantly different before injection from after. Error bars are SEM. (Wilcoxon matched-pairs signed rank test: p = 0.77). **(ii)** Normalized count of spikes with different inter spike intervals. (Bef SAL: n = 245 neurons, n = 3 sessions, n = 3 mice; Aft SAL: n = 245 neurons, n = 3 sessions, n = 3 mice; Bef OXTR-ago: n = 377, n = 5 sessions, n = 4 mice; Aft OXTR-ago: n = 377, n = 5 sessions, n = 4 mice). *p<0.05, ****p<0.0001

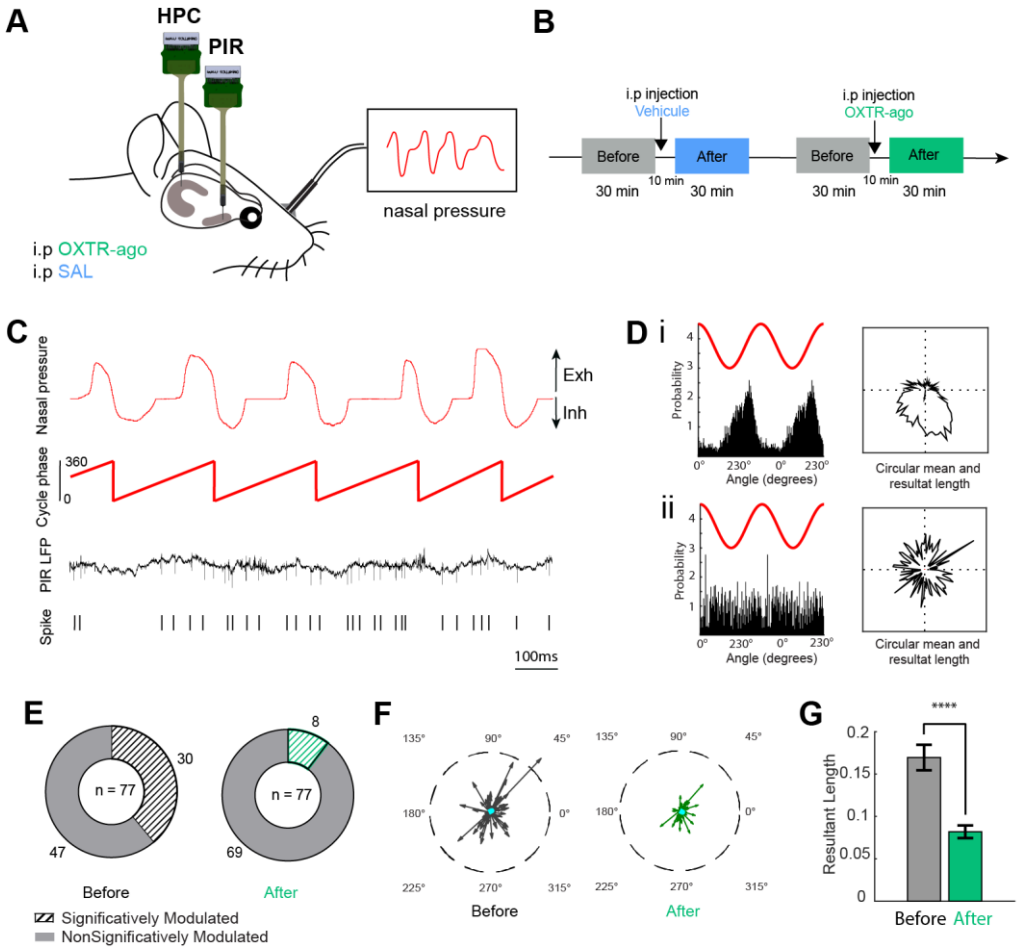

Figure 5 : Systemic oxytocin receptor agonist injection reduces the number and strength of the entrainment of putative excitatory neurons of the piriform cortex to the respiration *in vivo*. A. Schematic of a mouse recorded *in vivo* in the CA1 region of the hippocampus (HPC), piriform cortex (PIR) and nasal cavity for nasal pressure recording, receiving intraperitoneal injections (i.p). **B.** Experimental protocol consisted of recording mice during spontaneous behavior. Mice were injected i.p with SAL and subsequently with the oxytocin receptor agonist (OXTR-ago), TGOT. 30 min intervals were analyzed before and after the injections. The 10 min post infusion were excluded to avoid the possible confounding effects of injection stress. **C.** Raw traces of simultaneously recorded nasal pressure and PIR local field potential (LFP) together with schematic representation of cycle phase and PIR spike train. In the nasal pressure signal, upper variations indicate exhale (Exh), and lower variations indicate inhale (Inh). **D.** Example of one respiratory modulated cell **(i),** and non-modulated cell **(ii).** Examples show the probability of a neuron to fire at specific phases of the respiratory signal (left), and their circular mean and resultant length (right). **E.** Proportion of respiratory modulated putative excitatory cells in the PIR before (left) and after (right) OXTR-ago systemic injection is significantly different (Chi-square: $p < 0.0001$). **F.** Polar plots of individual neurons preferred phase and resultant length before (left), and after (right), OXTR-ago injection. **G.** Mean resultant length before and after OXTR-ago injection shows a significant decrease (Wilcoxon signed rank test: $p = 0.0009$). Error bars are SEM. (Before: n = 77 neurons, n = 3 sessions, n = 2 mice; After: n = 77 neurons, n = 3 sessions, n = 2 mice)**.** ****p<0.0001

Discussion.

In this study we have characterized the intrinsic properties of the two principal excitatory neurons of the PIR – the SP and SL cells -, in virgin female mice *in vitro*. As previously described (Suzuki and Bekkers 2006), SP cells were characterized by their initial action potential burst, and higher initial rheobase values; whereas SL cells had more regular firing pattern, were more excitable, and had higher after-hyperpolarisation amplitude.

We show that bath application of the OXTR agonist TGOT, blocked the burstiness of SP cells. It has previously been described that burstiness of PIR SL cells can be blocked by application of Ni^{2+}. This suggests that the channels involved in the generation of those burst are R-type or T-type calcium voltage-gated channels (Suzuki and Bekkers 2006). A very similar burst profile has been described in CA1 pyramidal cells, that like PIR SP neurons, present an afterdepolarization (ADP) (Suzuki and Bekkers 2006; Metz 2005). In CA1, a decrease in extracellular calcium diminishes the probability of bursting, while an increase in extracellular potassium increases it. Thus, these bursts seem to be underlined by calcium currents, while potassium currents oppose the mechanism for bursting (Metz 2005). The OXTR is a G-protein coupled receptor and induces Ca2+ influx through several calcium channels (Jurek and Neumann 2018). Hence, by modifying the calcium gradient, OXT could block the burstiness of PIR SP cells. It has also been described that OXT can activate inward rectifying potassium channels in neurons (Pekarek et al., 2020). Thus, another possible mechanism would be a change in the membrane potential of SP cells that would indirectly disrupt the burstiness of these cells in the presence of TGOT. Further experiments are necessary to confirm these findings and dissect the mechanisms underlying TGOT effects in PIR circuits.

We also show that OXTR agonist systemic injection *in vivo* induces a decrease in the burstiness of putative excitatory units, which is in line with our results *in vitro. In vivo* we do not have the precision to assign the cells we recorded to the SL or SP categories. However, a recent mouse line has been generated that seems to label specifically SL cells (Bolding et al. 2020; Nagappan and Franks 2021). Future experiments could be designed to identify those cells specifically in blind extracellular recordings using opto-tagging (Lima et al. 2009), and thus to distinguish between SL and SP cells *in vivo*, and confirm that this reduction in burstiness impacts SP cells specifically. It is likely

that the small size of the effect we uncovered here is due to the mixed populations of SL and SP included in the analysis. However, taking those subpopulation very probable differences apart, this decrease in burstiness due to OXTR activation is a novel finding. Indeed, in the brain, OXT has mainly been shown to depolarize interneurons (Zaninetti and Raggenbass 2000; Owen et al. 2013; Tirko et al. 2018; Nakajima et al., 2014). Only one recent study demonstrated that OXT impacts burstiness (Tirko et al. 2018). In this study, upon OXTR activation, pyramidal CA2 neurons increased their bursting activity. We found an opposite effect of OXTR activation on burstiness in the PIR. If our findings can be further confirmed, this would highlight the diversity of different effects that OXT can have on different cell types – interneurons, pyramidal neurons, but also astrocytes (Baudon et al. 2022) - and their differential effects depending on brain regions.

Finally, we have shown that OXTR activation reduces the entrainment of putative excitatory neurons of the PIR to the respiration. This could have strong effects both on the physiology of the PIR, but also on subsequent behavior. Indeed, respiration entrainment through the olfactory bulb has been shown to impact multiple brain regions (Tort et al., 2018) including the PIR. An hypothesis would be that respiration could orchestrate the coordination of distant neuronal circuits (Fontanini and Bower 2006; Karalis and Sirota 2022), by synchronizing their activity. If OXT reduces the entrainment of its excitatory neurons to respiration, this would imply that the PIR would decouple from this respiration entrained dialogue, and could thus be more sensitive to local computation at specific time points. Our findings, open the door for a more thorough investigation of the role of OXT in respiratory mediated activity.

References

Baudon, Angel, Etienne Clauss Creusot, Ferdinand Althammer, Christian P. Schaaf, and Alexandre Charlet. 2022. “Emerging Role of Astrocytes in Oxytocin-Mediated Control of Neural Circuits and Brain Functions.” *Progress in Neurobiology* 217 (October): 102328. https://doi.org/10.1016/j.pneurobio.2022.102328.

Bolding, Kevin A, Shivathmihai Nagappan, Bao-Xia Han, Fan Wang, and Kevin M Franks. 2020. “Recurrent Circuitry Is Required to Stabilize Piriform Cortex Odor Representations across Brain States.” *ELife* 9 (July): e53125. https://doi.org/10.7554/eLife.53125.

Buzsáki, György. 2015. “Hippocampal Sharp Wave-ripple: A Cognitive Biomarker for Episodic Memory and Planning.” *Hippocampus* 25 (10): 1073–1188. https://doi.org/10.1002/hipo.22488.

Fontanini, Alfredo, and James M. Bower. 2006. “Slow-Waves in the Olfactory System: An Olfactory Perspective on Cortical Rhythms.” *Trends in Neurosciences* 29 (8): 429–37. https://doi.org/10.1016/j.tins.2006.06.013.

Fontanini, Alfredo, PierFranco Spano, and James M Bower. n.d. “Ketamine–Xylazine-Induced Slow (Ↄ1.5 Hz) Oscillations in the Rat Piriform (Olfactory) Cortex Are Functionally Correlated with Respiration,” 9.

Grinevich, Valery, H. Sophie Knobloch-Bollmann, Marina Eliava, Marta Busnelli, and Bice Chini. 2016. “Assembling the Puzzle: Pathways of Oxytocin Signaling in the Brain.” *Biological Psychiatry* 79 (3): 155–64. https://doi.org/10.1016/j.biopsych.2015.04.013.

Grosmark, Andres D., Kenji Mizuseki, Eva Pastalkova, Kamran Diba, and György Buzsáki. 2012. “REM Sleep Reorganizes Hippocampal Excitability.” *Neuron* 75 (6): 1001–7. https://doi.org/10.1016/j.neuron.2012.08.015.

Hazan, Lynn, Michaël Zugaro, and György Buzsáki. 2006. “Klusters, NeuroScope, NDManager: A Free Software Suite for Neurophysiological Data Processing and Visualization.” *Journal of Neuroscience Methods* 155 (2): 207–16. https://doi.org/10.1016/j.jneumeth.2006.01.017.

Huber, Daniel, Pierre Veinante, and Ron Stoop. 2005. “Vasopressin and Oxytocin Excite Distinct Neuronal Populations in the Central Amygdala.” *Science* 308 (5719): 245–48. https://doi.org/10.1126/science.1105636.

Jurek, Benjamin, and Inga D. Neumann. 2018. “The Oxytocin Receptor: From Intracellular Signaling to Behavior.” *Physiological Reviews* 98 (3): 1805–1908. https://doi.org/10.1152/physrev.00031.2017.

Karalis, Nikolaos, and Anton Sirota. 2022. “Breathing Coordinates Cortico-Hippocampal Dynamics in Mice during Offline States.” *Nature Communications* 13 (1): 467. https://doi.org/10.1038/s41467-022-28090-5.

Knobloch, H. Sophie, Alexandre Charlet, Lena C. Hoffmann, Marina Eliava, Sergey Khrulev, Ali H. Cetin, Pavel Osten, et al. 2012. “Evoked Axonal Oxytocin Release in the Central Amygdala Attenuates Fear Response.” *Neuron* 73 (3): 553–66. https://doi.org/10.1016/j.neuron.2011.11.030.

Lima, Susana Q., Tomáš Hromádka, Petr Znamenskiy, and Anthony M. Zador. 2009. “PINP: A New Method of Tagging Neuronal Populations for Identification during In Vivo Electrophysiological Recording.” Edited by Michael N. Nitabach. *PLoS ONE* 4 (7): e6099. https://doi.org/10.1371/journal.pone.0006099.

Manabe, H., I. Kusumoto-Yoshida, M. Ota, and K. Mori. 2011. “Olfactory Cortex Generates Synchronized Top-Down Inputs to the Olfactory Bulb during Slow-Wave Sleep.” *Journal of Neuroscience* 31 (22): 8123–33. https://doi.org/10.1523/JNEUROSCI.6578-10.2011.

Marlin, Bianca J., Mariela Mitre, James A. D’amour, Moses V. Chao, and Robert C. Froemke. 2015. “Oxytocin Enables Maternal Behaviour by Balancing Cortical Inhibition.” *Nature* 520 (7548): 499–504. https://doi.org/10.1038/nature14402.

Metz, A. E. 2005. “R-Type Calcium Channels Contribute to Afterdepolarization and Bursting in Hippocampal CA1 Pyramidal Neurons.” *Journal of Neuroscience* 25 (24): 5763–73. https://doi.org/10.1523/JNEUROSCI.0624-05.2005.

Mitre, Mariela, Bianca J. Marlin, Jennifer K. Schiavo, Egzona Morina, Samantha E. Norden, Troy A. Hackett, Chiye J. Aoki, Moses V. Chao, and Robert C. Froemke. 2016. “A Distributed Network for Social Cognition Enriched for Oxytocin Receptors.” *The Journal of Neuroscience* 36 (8): 2517–35. https://doi.org/10.1523/JNEUROSCI.2409-15.2016.

Nagaeva, Elina, Ivan Zubarev, Carolina Bengtsson Gonzales, Mikko Forss, Kasra Nikouei, Elena de Miguel, Lauri Elsilä, et al. 2020. “Heterogeneous Somatostatin-Expressing Neuron Population in Mouse Ventral Tegmental Area.” *ELife* 9 (August): e59328. https://doi.org/10.7554/eLife.59328.

Nagaeva, Elina, Ivan Zubarev, and Esa Korpi. 2021. “Electrophysiological Properties of Neurons: Current-Clamp Recordings in Mouse Brain Slices and Firing-Pattern Analysis.” *BIO-PROTOCOL* 11 (12). https://doi.org/10.21769/BioProtoc.4061.

Nagappan, Shivathmihai, and Kevin M Franks. 2021. “Parallel Processing by Distinct Classes of Principal Neurons in the Olfactory Cortex.” *ELife* 10 (December): e73668. https://doi.org/10.7554/eLife.73668.

Nakajima, Miho, Andreas Görlich, and Nathaniel Heintz. 2014. “Oxytocin Modulates Female Sociosexual Behavior through a Specific Class of Prefrontal Cortical Interneurons.” *Cell* 159 (2): 295–305. https://doi.org/10.1016/j.cell.2014.09.020.

Oettl, Lars-Lennart, and Wolfgang Kelsch. 2017. “Oxytocin and Olfaction.” In *Behavioral Pharmacology of Neuropeptides: Oxytocin*, edited by Rene Hurlemann and Valery Grinevich, 35:55–75. Current Topics in Behavioral Neurosciences. Cham: Springer International Publishing. https://doi.org/10.1007/7854_2017_8.

Owen, Scott F., Sebnem N. Tuncdemir, Patrick L. Bader, Natasha N. Tirko, Gord Fishell, and Richard W. Tsien. 2013. “Oxytocin Enhances Hippocampal Spike Transmission by Modulating Fast-Spiking Interneurons.” *Nature* 500 (7463): 458–62. https://doi.org/10.1038/nature12330.

Pachitariu, Marius, Nicholas A Steinmetz, Shabnam N Kadir, Matteo Carandini, and Kenneth D Harris. n.d. “Fast and Accurate Spike Sorting of High-Channel Count Probes with KiloSort,” 9.

Pekarek, Brandon T., Patrick J. Hunt, and Benjamin R. Arenkiel. 2020. “Oxytocin and Sensory Network Plasticity.” *Frontiers in Neuroscience* 14 (January): 30. https://doi.org/10.3389/fnins.2020.00030.

Poo, Cindy, and Jeffry S. Isaacson. 2009. “Odor Representations in Olfactory Cortex: ‘Sparse’ Coding, Global Inhibition, and Oscillations.” *Neuron* 62 (6): 850–61. https://doi.org/10.1016/j.neuron.2009.05.022.

Rennaker, R. L., C.-F. F. Chen, A. M. Ruyle, A. M. Sloan, and D. A. Wilson. 2007. “Spatial and Temporal Distribution of Odorant-Evoked Activity in the Piriform Cortex.” *Journal of Neuroscience* 27 (7): 1534–42. https://doi.org/10.1523/JNEUROSCI.4072-06.2007.

Stark, Eran, Ronny Eichler, Lisa Roux, Shigeyoshi Fujisawa, Horacio G. Rotstein, and György Buzsáki. 2013. “Inhibition-Induced Theta Resonance in Cortical Circuits.” *Neuron* 80 (5): 1263–76. https://doi.org/10.1016/j.neuron.2013.09.033.

Suzuki, N., and J. M. Bekkers. 2006. “Neural Coding by Two Classes of Principal Cells in the Mouse Piriform Cortex.” *Journal of Neuroscience* 26 (46): 11938–47. https://doi.org/10.1523/JNEUROSCI.3473-06.2006.

Tan, Oliver, Hande Musullulu, Joel S. Raymond, Bianca Wilson, Mia Langguth, and Michael T. Bowen. 2019. “Oxytocin and Vasopressin Inhibit Hyper-Aggressive Behaviour in Socially Isolated Mice.” *Neuropharmacology* 156 (September): 107573. https://doi.org/10.1016/j.neuropharm.2019.03.016.

Terral, Geoffrey, Arnau Busquets-Garcia, Marjorie Varilh, Svein Achicallende, Astrid Cannich, Luigi Bellocchio, Itziar Bonilla-Del Río, et al. 2019. “CB1 Receptors in the Anterior Piriform Cortex Control Odor Preference Memory.” *Current Biology* 29 (15): 2455-2464.e5. https://doi.org/10.1016/j.cub.2019.06.041.

Tirko, Natasha N., Katherine W. Eyring, Ioana Carcea, Mariela Mitre, Moses V. Chao, Robert C. Froemke, and Richard W. Tsien. 2018. “Oxytocin Transforms Firing Mode of CA2 Hippocampal Neurons.” *Neuron* 100 (3): 593-608.e3. https://doi.org/10.1016/j.neuron.2018.09.008.

Tort, Adriano B.L., Jurij Brankačk, and Andreas Draguhn. 2018. “Respiration-Entrained Brain Rhythms Are Global but Often Overlooked.” *Trends in Neurosciences* 41 (4): 186–97. https://doi.org/10.1016/j.tins.2018.01.007.

Zaninetti, Marc, and Mario Raggenbass. 2000. “Oxytocin Receptor Agonists Enhance Inhibitory Synaptic Transmission in the Rat Hippocampus by Activating Interneurons in Stratum Pyramidale: Oxytocin Action in the Hippocampus.” *European Journal of Neuroscience* 12 (11): 3975–84. https://doi.org/10.1046/j.1460-9568.2000.00290.x.

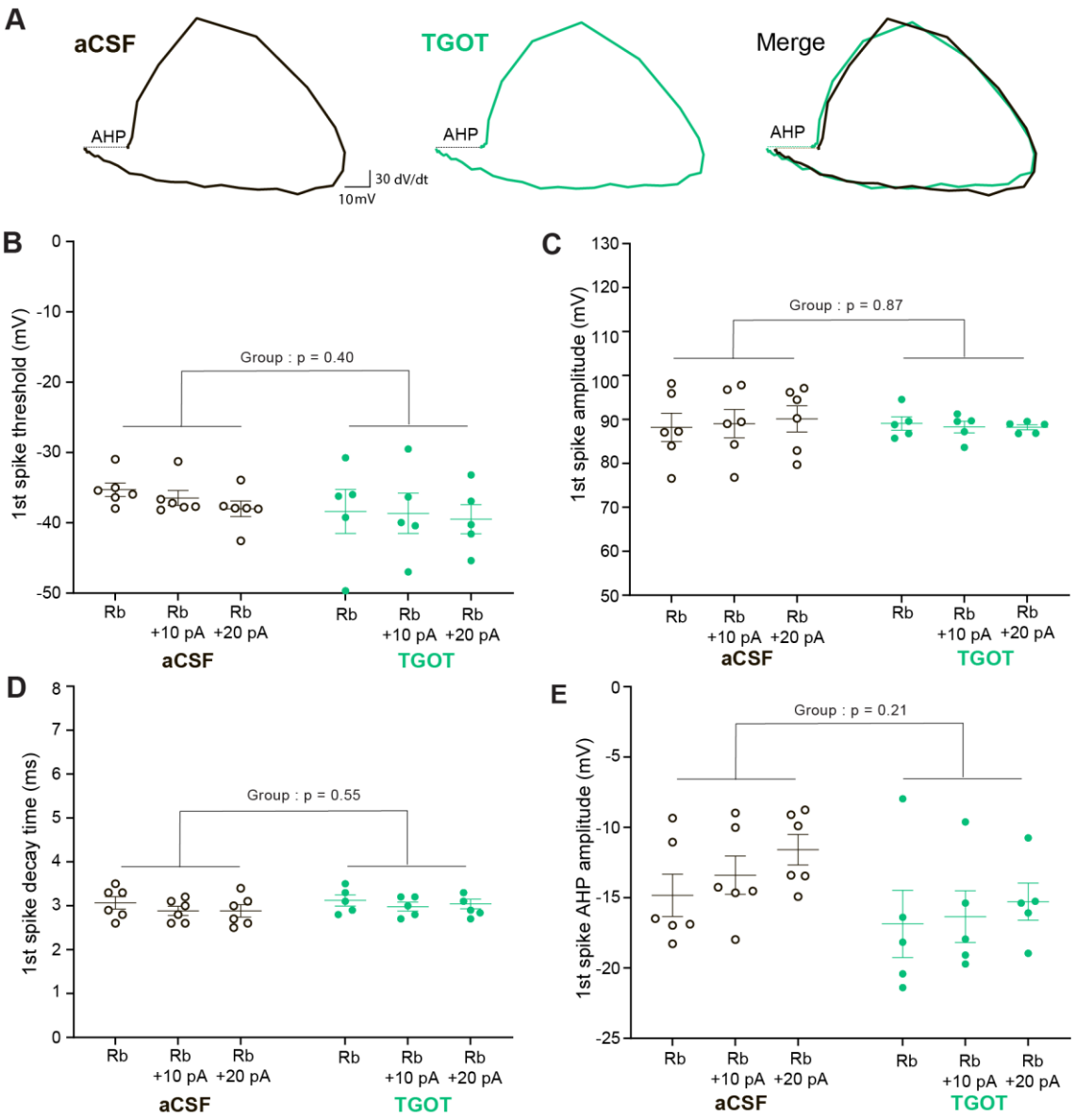

Supplementary 1 : Oxytocin receptor agonist TGOT does not affect the action potential shape of superficial pyramidal cells. A. Curves represent the derivative of the voltage over time (dV/dt), as a function of the voltage (mV) for the first action potential (AP) at the rheobase. Illustrative dV/dt x mV curves for a representative SP cell in aCSF condition (left) and TGOT condition (center). Merge (right) illustrates differences on AP shape. Curves are aligned on AP threshold. AHP represents after-hyperpolarization amplitude. **B.** Mean first spike threshold is not significantly different between aCSF and TGOT conditions (2-way ANOVA: Group effect, p = 0.40, Current effect, p = 0.06, Interaction, p = 0.52). **C.** Mean first spike amplitude is not different between aCSF and TGOT conditions (2-way ANOVA: Group effect, p = 0.87, Current effect, p = 0.64, Interaction, p = 0.19). **D.** Mean first spike decay time is not significantly different between aCSF and TGOT conditions (2-way ANOVA: Group effect, p = 0.55, Current effect, p = 0.02, Interaction, p = 0.58). **E.** Mean first spike after-hyperpolarization amplitude (AHP) is not significantly different in the two groups (2-way ANOVA: Group effect, p = 0.21, Current effect, p = 0.018, Interaction p = 0.48). SP-aCSF (n = 6 cells), SP-TGOT (n = 5 cells). Rb = rheobase,

Rb+10pA: sweep following the Rb; Rb+20pA: two sweeps following the rheobase. Error bars represent SEM.

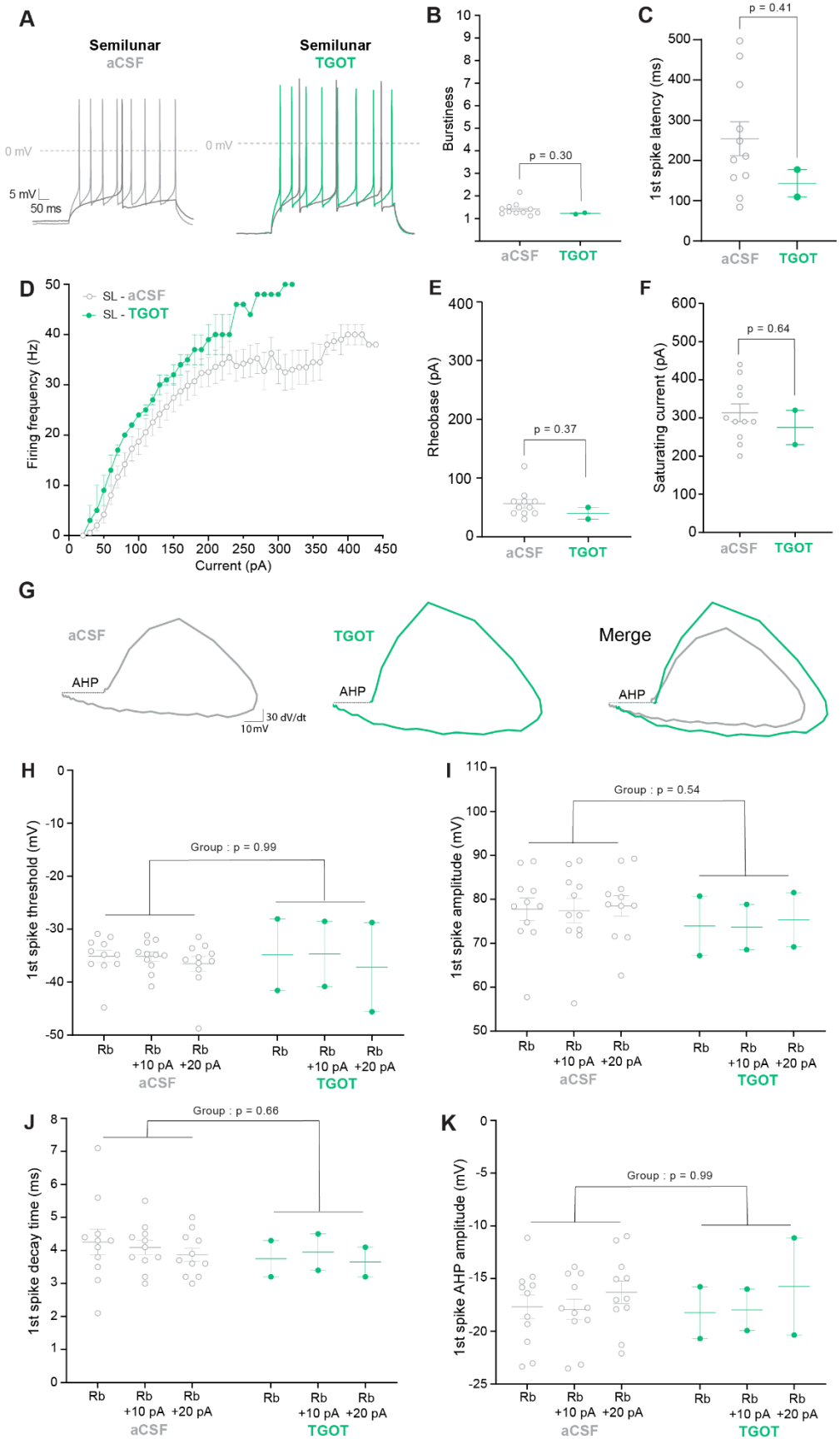
A
Semilunar
aCSF
Semilunar
TGOT
0 mV
0 mV
5 mV
50 ms
B
Burstiness
p = 0.30
aCSF
TGOT
C
1st spike latency (ms)
p = 0.41
aCSF
TGOT
D
SL - aCSF
SL - TGOT
Firing frequency (Hz)
Current (pA)
E
Rheobase (pA)
p = 0.37
aCSF
TGOT
F
Saturating current (pA)
p = 0.64
aCSF
TGOT
G
aCSF
AHP
30 dV/dt
10 mV
TGOT
AHP
Merge
AHP
H
1st spike threshold (mV)
Group : p = 0.99
Rb
Rb +10 pA
Rb +20 pA
aCSF
TGOT
I
1st spike amplitude (mV)
Group : p = 0.54
J
1st spike decay time (ms)
Group : p = 0.66
K
1st spike AHP amplitude (mV)
Group : p = 0.99

Supplementary 2 : Oxytocin receptor agonist TGOT does not affect burstiness or the action potential shape of semilunar cells. A. Illustrative recordings at rheobase (medium gray) or at current step with 8 action potentials (light gray or green) for SL cells in aCSF (left) or TGOT (right) condition. In this and all the following panels, data for SL- aCSF group is the same as shown in figure 1 and 2. **B.** Mean burstiness index is not significantly different for SL cells in the presence of TGOT compared to aCSF (Mann-Whitney test: p = 0.30) (aCSF: n = 11 cells, TGOT: n = 2 cells). **C.** Mean first spike latency is not significantly different between both conditions (Mann-Whitney test: p = 0.41). **D.** Mean frequency x injected current curves for SL cells in aCSF or TGOT conditions. Statistical analysis was not possible because of the low number of cells in TGOT conditions. **E.** Mean rheobase is not significantly different for SL cells in the two conditions (Mann-Whitney: p = 0.37). **F.** Mean saturating current is not significantly different for SL cells in the two conditions (Mann-Whitney: p = 0.64). **G.** Curves represent the derivative of the voltage over time (dV/dt), as a function of the voltage (mV) for the first action potential (AP) at the rheobase. Illustrative dV/dt x mV curves for a representative SL cell in aCSF condition (left) and TGOT condition (center). Merge (right) illustrates differences on AP shape. Curves are aligned on AP threshold. AHP represents after-hyperpolarization amplitude. **H.** Mean first spike threshold is not significantly different between aCSF and TGOT conditions (2-way ANOVA: Group effect, p = 0.99, Current effect, p = 0.04, Interaction, p = 0.73). **I.** Mean first spike amplitude is not different between aCSF and TGOT conditions (2-way ANOVA: Group effect, p = 0.54, Current effect, p = 0.27, Interaction, p = 0.92). **J.** Mean first spike decay time is not significantly different between aCSF and TGOT conditions (2-way ANOVA: Group effect, p = 0.66, Current effect, p = 0.43, Interaction, p = 0.72). **K.** Mean first spike after-hyperpolarization amplitude (AHP) is not significantly different in the two groups (2-way ANOVA: Group effect: p = 0.99, Current effect, p = 0.06, Interaction p = 0.82). SL-aCSF (n = 11 cells), SL-TGOT (n = 2 cells). Rb = rheobase, Rb+10pA: sweep following the Rb; Rb+20pA: two sweeps following the rheobase. Error bars represent SEM.

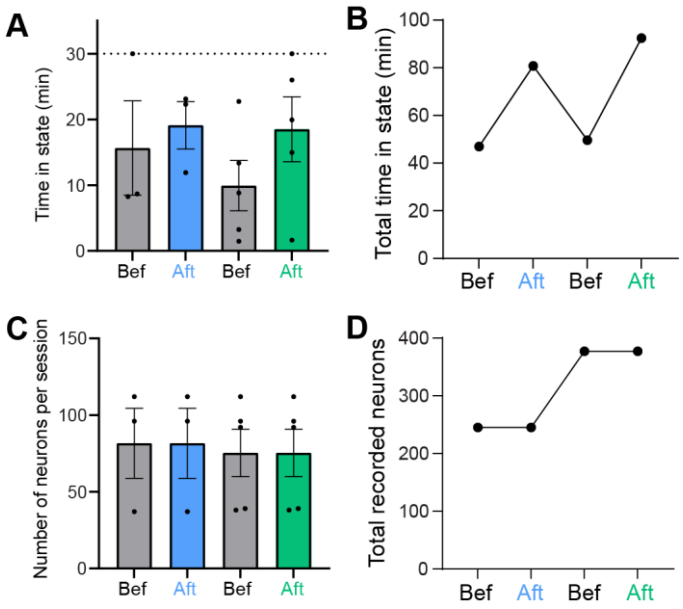

Supplementary 3 : Description of the data set used in Figure 4. A. Mean time spent in the wake state for each session before SAL injection (Bef), after SAL injection (Aft-blue), before OXTR-ago injection (Bef), and after OXTR-ago injection (Aft – green). Error bars are SEM. Note that the maximum time is 30 min because we retrained our analysis to 30min intervals. **B.** Total time in state corresponds to the sum of the durations in the wake state combining all sessions. **C.** Mean number of putative excitatory PIR neurons per session. Error bars are SEM. **D.** Total recorded neurons corresponds to the sum of the number of putative excitatory PIR neurons for all the sessions. (Bef SAL: n = 3 mice, Aft SAL: n = 3 mice, Bef OXTR-ago: n = 4 mice, Aft OXTR-ago: n = 4 mice)

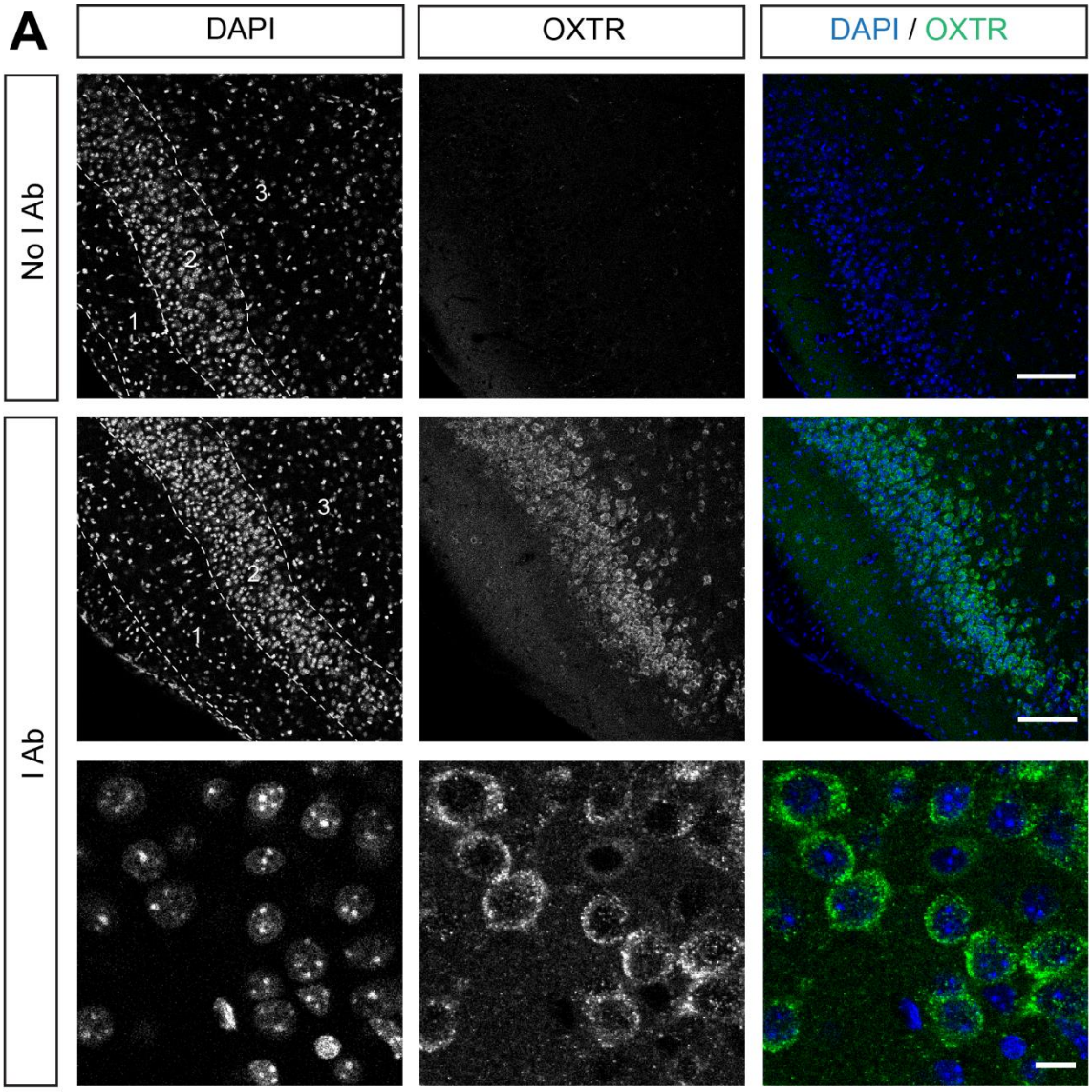
A
DAPI
OXTR
DAPI / OXTR
No I Ab
I Ab
1
2
3
B
OXTR / DAPI Mean Fluorescence Intensity
2.0
1.5
1.0
0.5
0.0
****
**
Female
Male
Layer 1
Layer 2
Layer 3

Supplementary 4 : Oxytocinergic receptor expression in the piriform cortex is layer specific in both sexes. (A) Lower panels: Illustrative oxytocin receptor (OXTR) labelling in the PIR using OXTR-2 specific antibody (gift from Froemke lab). Upper panels: Control without primary antibody. The dotted lines delimit the different PIR layers and numbers indicate cell layer number. Scale bar = 100 µm (low magnification) and 10 µm (high magnification). (B) Layer specific quantification of the mean fluorescence intensity of OXTR relative to DAPI staining in female (n=2/8 images) and male (n=1/8 images) C57bl6 mice. Data are expressed as mean +/- SEM. Friedman test for female **** P<0.0001 and for male ** P= 0.0024. Dunn's multiple comparisons: Layer 1 vs 2 **** P <0.0001 and ** P = 0.035 for female and male respectively.

DISCUSSION GENERALE

Impact de la respiration sur l'activité neuronale

La respiration reflète nos états cognitifs internes et constitue un puissant modulateur de l'activité cérébrale (Kepecs et al., 2007; Tort et al., 2018). Il a été proposé que le couplage de l'activité cérébrale avec la respiration, qui provient des mécanorécepteurs de l'épithélium olfactif (Grosmaitre et al. 2007), puisse régir la coordination longue-distance entre les réseaux neuronaux (Fontanini and Bower 2006; Moore et al. 2013; Buonviso et al. 2016; Heck et al. 2017; Tort et al., 2018; Girin et al. 2021). D'autre part, la fonction des circuits neuronaux *in vivo* est connue pour être orchestrée par différentes oscillations qui jouent un rôle central dans le transfert d'informations. Puisque de nombreuses études ont montré que la respiration entraîne les rythmes cérébraux à des fréquences similaires à celles du thêta (4-8Hz) (Tort et al., 2018) une question fondamentale est maintenant de comprendre l'interaction entre l'activité induite par la respiration et les rythmes thêta générés de façon interne (Tort et al., 2018). Ces rythmes, bien que générés par des mécanismes distincts, peuvent facilement être pris l'un pour l'autre (Tort et al., 2018), mais ils pourraient potentiellement se coordonner dans des conditions comportementales spécifiques (Moore et al. 2013). Outre les oscillations thêta, d'autres oscillations sont potentiellement modulées par la respiration : par exemple, il a été démontré que la respiration entraîne des *sharp wave ripples* dans la région CA1 de l'hippocampe et les potentiels de champ local du bulbe olfactif (qui reflètent fortement l'activité respiratoire) peuvent coordonner le rythme hippocampique lors d'une tâche olfactive (Martin et al., 2007). L'utilisation à plus large échelle de méthodes d'enregistrement de la respiration (Grimaud and Murthy 2018; Tort et al., 2018), comme le senseur de pression nasale que nous avons mis au point pour l'animal libre de ses mouvements (Résultats Partie 1), apportera des éléments de réponses à ces questions. Grâce à notre senseur, nous avons mis en évidence l'importance des pauses dans le signal respiratoire (Résultats Partie 1) qui n'est donc que partiellement oscillatoire. Il reste donc à comprendre comment les interactions entre la respiration et les rythmes cérébraux sont impactés par cette nouvelle vision du rythme respiratoire, et à découvrir comment le cerveau interprète cette information.

Impact de l'ocytocine sur l'entrainement du cortex piriforme par la respiration

Comme précisé ci-dessus, de nombreuses régions cérébrales sont entrainées par la respiration, dont notamment le PIR (Litaudon et al. 2003; Rennaker et al. 2007; Fontanini and Bower 2006; Poo and Isaacson 2009). Nous avons commencé à démontrer qu'une injection systémique de l'agoniste des OCTR entraine une diminution de la force d'entrainement des neurones excitateurs par la respiration dans le PIR. Quels sont les potentiels impacts de cette réduction de l'entrainement ? Pour émettre des hypothèses sur cette question il convient de rappeler, que l'un des rôles proposé de l'OCT est d'améliorer la *salience* des stimuli sociaux en modulant la transmission synaptique (Shamay-Tsoory and Abu-Akel 2016). Dans ce contexte, il est possible que la réduction de l'entrainement des neurones a la respiration agisse comme un filtre : seuls les neurones impliqués dans le traitement du stimulus olfactif socialement pertinent resteraient entrainés par la respiration, alors que la vaste majorité neurones non recrutés subiraient une forme de « découplage ».

Implication d'une étude du système ocytocinergique chez la femelle : le cycle ovarien

Une limite possible de notre étude est que nous avons travaillé avec des souris femelles vierges (Résultats Parties 2 et 3 pour *in vitro*), mais nous n'avons pas suivi l'état de leur cycle ovarien. En effet, même si l'expression de l'OCTR ne semble pas varier au cours du cycle ovarien, - au moins dans certaines régions du cerveau (NPV et cortex auditif) (Mitre et al. 2016) , il n'existe aucune information sur les niveaux d'OCTR dans le PIR et s'ils varient avec le cycle ovarien. Ce que l'on sait en revanche, c'est que les concentrations d'OCT varient au cours du cycle ovarien (Froemke and Carcea 2017) ce qui pourrait avoir des impacts à la fois sur les réponses physiologiques du PIR des cellules SP et SL, mais aussi sur le comportement de l'animal. En effet, il a été démontré que chez les souris femelles, le cycle ovarien influence les performances du test classique à trois chambres (Chari et al. 2020). Les souris femelles ont une préférence sociale pour les stimuli de même sexe pendant leur phase non réceptive, mais ne l'ont plus pendant leur phase sexuellement réceptive. Il serait donc recommandable à l'avenir de suivre le cycle ovarien de nos souris afin d'éviter tout élément confondant.

Méthodes d'études de la sociabilité

Au cours de notre étude comportementale, nous avons mis en évidence des différences sur la sociabilité de nos souris dans le Live Mouse Tracker (LMT), mais pas dans le test a trois chambres classique (Résultats Partie 2). Le test a trois chambre, bien qu'informatif, fournit une mesure assez grossière de la sociabilité. Notre première observation en utilisant ce type de test, est que la mesure du temps passé dans chaque compartiment n'est pas la mesure la plus adaptée pour mesurer la sociabilité de nos souris. En effet, même si c'est la mesure la plus directe, elle peut englober des moments de non-interaction, et donc entraine du bruit dans les données. Nous avons trouvé que la mesure du temps passé en contact « nez-nez » était plus informative, et plus fiable. L'inconvénient majeur de ce type de test, repose sur le fait qu'il limite le type d'interaction au contact « nez-nez » alors que les souris en interactions libres présentent une grande variété de types d'interactions (Chaumont et al. 2018). De plus ces mesures sont manuelles et donc sources d'erreurs ou de variabilité inter-experimentateur. Des options automatisées comme le LMT, ou DeepLabCut (Mathis et al. 2018) sont donc préférables dans le cadre d'études qui cherchent à distinguer des effets fins sur la sociabilité. Elles ont également l'avantage de pouvoir être performantes sur des très longues durées d'expériences et sur une variété de comportements.

Effets convergents de l'ocytocine et la vasopressine ?

L'OCTR et les récepteurs à la vasopressine (AVPR) partagent une forte homologie de séquence (Jurek and Neumann 2018). De ce fait, la vasopressine (AVP) se fixe sur l'OCTR et l'OCT se fixe sur les AVPR. L'homologie de structure des récepteurs est telle, que la vasopressine se fixe sur l'OCTR avec la même affinité que sur les AVPR (Stoop 2012). De plus, tout comme l'OCT, l'AVP est impliqué dans la régulation des comportements sociaux et est exprimée dans le système olfactif (Wacker and Ludwig 2019). Plus particulièrement, l'ARNm des sous-types d'AVPR - AVP1a et AVP1b - ont été détectés dans le PIR de rats mâles et femelles (Wacker and Ludwig 2019). Dans le cadre de nos études (Résultats Parties 2,3) nous avons utilisé des bloqueurs et des activateurs pharmacologiques spécifiques de l'OCTR pour nous concentrer sur les effets de la modulation des récepteurs ocytocinergiques exclusivement. Cependant, dans le cas du blocage (Résultats Partie 2), si de manière endogène l'AVP se lie à l'OCTR, on peut se demander si en présence d'antagonistes de l'OCTR, l'AVP

ne pourrait plus effectuer son rôle potentiel sur les OCTR du PIR. On ne peut donc pas totalement exclure que les effets reportés de l'OCT endogène ne soient pas en réalité dus à un effet synergique de l'OCT et de l'AVP qui agiraient conjointement sur les OCTR. Cette possibilité est d'autant plus plausible que la présence de fibres ocytocinergiques est remarquablement faible dans le PIR (Résultats Partie 2) et que la présence d'un autre activateur endogène des OCTR tel que l'AVP est donc envisageable. Afin de tester cette hypothèse, il serait intéressant de répliquer nos manipulations dans des souris KO pour le gène de l'AVP : si l'effet est maintenu, il serait alors possible d'écarter l'hypothèse d'une activation endogène des OCTR par l'AVP.

REFERENCES

A

Ache, Barry W., and Janet M. Young. 2005. “Olfaction: Diverse Species, Conserved Principles.” *Neuron* 48 (3): 417–30. https://doi.org/10.1016/j.neuron.2005.10.022.

Agapakis, Christina M, and Sissel Tolaas. 2012. “Smelling in Multiple Dimensions.” *Current Opinion in Chemical Biology* 16 (5–6): 569–75. https://doi.org/10.1016/j.cbpa.2012.10.035.

Apicella, A., Q. Yuan, M. Scanziani, and J. S. Isaacson. 2010. “Pyramidal Cells in Piriform Cortex Receive Convergent Input from Distinct Olfactory Bulb Glomeruli.” *Journal of Neuroscience* 30 (42): 14255–60. https://doi.org/10.1523/JNEUROSCI.2747-10.2010.

B

Bagur, Sophie, Julie M. Lefort, Marie M. Lacroix, Gaëtan de Lavilléon, Cyril Herry, Clara Billand, Hélène Geoffroy, and Karim Benchenane. 2018. “Dissociation of Fear Initiation and Maintenance by Breathing-Driven Prefrontal Oscillations.” Nature communication, https://doi.org/10.1038/s41467-021-22798-6

Bagur, Sophie, Julie M. Lefort, Marie M. Lacroix, Gaëtan de Lavilléon, Cyril Herry, Mathilde Chouvaeff, Clara Billand, Hélène Geoffroy, and Karim Benchenane. 2021. “Breathing-Driven Prefrontal Oscillations Regulate Maintenance of Conditioned-Fear Evoked Freezing Independently of Initiation.” *Nature Communications* 12 (1): 2605. https://doi.org/10.1038/s41467-021-22798-6.

Barnes, D. C., and D. A. Wilson. 2014. “Slow-Wave Sleep-Imposed Replay Modulates Both Strength and Precision of Memory.” *Journal of Neuroscience* 34 (15): 5134–42. https://doi.org/10.1523/JNEUROSCI.5274-13.2014.

Barnes, Dylan C, Rylon D Hofacer, Ashiq R Zaman, Robert L Rennaker, and Donald A Wilson. 2008. “Olfactory Perceptual Stability and Discrimination.” *Nature Neuroscience* 11 (12): 1378–80. https://doi.org/10.1038/nn.2217.

Barrios, Arthur W., Gonzalo Nunez, Pablo Sanchez Quinteiro, and Ignacio Salazar. 2014. “Anatomy, Histochemistry, and Immunohistochemistry of the Olfactory Subsystems in Mice.” *Frontiers in Neuroanatomy* 8 (July). https://doi.org/10.3389/fnana.2014.00063.

Bekkers, John M., and Norimitsu Suzuki. 2013. “Neurons and Circuits for Odor Processing in the Piriform Cortex.” *Trends in Neurosciences* 36 (7): 429–38. https://doi.org/10.1016/j.tins.2013.04.005.

Ben-Barak Yakov, Russel T. James, Whitnall H. Mark, Ozato keiko, Gainer Harold "Neurophysin in the hypothalamo-neurohypophysial system", The journal of neuosciences. Vol 5. No 1, 81-97 https://doi.org/10.1523/JNEUROSCI.05-01-00081.1985

Biskamp, Jonatan, Marlene Bartos, and Jonas-Frederic Sauer. 2017. “Organization of Prefrontal Network Activity by Respiration-Related Oscillations.” *Scientific Reports* 7 (1): 45508. https://doi.org/10.1038/srep45508.

Bolding, Kevin A, and Kevin M Franks. 2017. “Complementary Codes for Odor Identity and Intensity in Olfactory Cortex.” *ELife* 6 (April): e22630. https://doi.org/10.7554/eLife.22630.

Bolding Kevin A, Franks Kevin.M. 2019. “Recurrent Cortical Circuits Implement Concentration-Invariant Odor Coding,” Science, https://doi.org/10.1126/science.aat6904

Bouret, Sebastien, and Susan J. Sara. 2002. “Locus Coeruleus Activation Modulates Firing Rate and Temporal Organization of Odour-Induced Single-Cell Responses in Rat Piriform Cortex: Locus

Coeruleus Modulates Piriform Cortex Response." *European Journal of Neuroscience* 16 (12): 2371–82. https://doi.org/10.1046/j.1460-9568.2002.02413.x.

Brunjes, Peter C., Kurt R. Illig, and Elizabeth A. Meyer. 2005. "A Field Guide to the Anterior Olfactory Nucleus (Cortex)." *Brain Research Reviews* 50 (2): 305–35. https://doi.org/10.1016/j.brainresrev.2005.08.005.

Buck, Linda, and Richard Axel. 1991. "A Novel Multigene Family May Encode Odorant Receptors: A Molecular Basis for Odor Recognition," 13.

Buonviso, Nathalie, Corine Amat, and Philippe Litaudon. 2006. "Respiratory Modulation of Olfactory Neurons in the Rodent Brain." *Chemical Senses* 31 (2): 145–54. https://doi.org/10.1093/chemse/bjj010.

Buonviso, Nathalie, Mathias Dutschmann, Anne-Marie Mouly, and Daniel W. Wesson. 2016. "Adaptation and Plasticity of Breathing during Behavioral and Cognitive Tasks." *Neural Plasticity* 2016: 1–2. https://doi.org/10.1155/2016/2804205.

Burg, Erwin H van den, Julia Stindl, Thomas Grund, Inga D Neumann, and Olaf Strauss. 2015. "Oxytocin Stimulates Extracellular Ca2+ Influx Through TRPV2 Channels in Hypothalamic Neurons to Exert Its Anxiolytic Effects." *Neuropsychopharmacology* 40 (13): 2938–47. https://doi.org/10.1038/npp.2015.147.

Burkett, J. P., E. Andari, Z. V. Johnson, D. C. Curry, F. B. M. de Waal, and L. J. Young. 2016. "Oxytocin-Dependent Consolation Behavior in Rodents." *Science* 351 (6271): 375–78. https://doi.org/10.1126/science.aac4785.

Busnelli, Marta, Elisabetta Bulgheroni, Maurice Manning, Gunnar Kleinau, and Bice Chini. 2013. "Selective and Potent Agonists and Antagonists for Investigating the Role of Mouse Oxytocin Receptors." *Journal of Pharmacology and Experimental Therapeutics* 346 (2): 318–27. https://doi.org/10.1124/jpet.113.202994.

Busnelli, Marta, and Bice Chini. 2017. "Molecular Basis of Oxytocin Receptor Signalling in the Brain: What We Know and What We Need to Know." In *Behavioral Pharmacology of Neuropeptides: Oxytocin*, edited by Rene Hurlemann and Valery Grinevich, 35:3–29. Current Topics in Behavioral Neurosciences. Cham: Springer International Publishing. https://doi.org/10.1007/7854_2017_6.

Busnelli, Marta, Aude Saulière, Maurice Manning, Michel Bouvier, Celine Galés, and Bice Chini. 2012. "Functional Selective Oxytocin-Derived Agonists Discriminate between Individual G Protein Family Subtypes." *Journal of Biological Chemistry* 287 (6): 3617–29. https://doi.org/10.1074/jbc.M111.277178.

C

Calu, D. J., M. R. Roesch, T. A. Stalnaker, and G. Schoenbaum. 2007. "Associative Encoding in Posterior Piriform Cortex during Odor Discrimination and Reversal Learning." *Cerebral Cortex* 17 (6): 1342–49. https://doi.org/10.1093/cercor/bhl045.

Chapuis, Julie, and Donald A Wilson. 2012. "Bidirectional Plasticity of Cortical Pattern Recognition and Behavioral Sensory Acuity." *Nature Neuroscience* 15 (1): 155–61. https://doi.org/10.1038/nn.2966.

Chari, Trishala, Sophie Griswold, Nick A. Andrews, and Michela Fagiolini. 2020. "The Stage of the Estrus Cycle Is Critical for Interpretation of Female Mouse Social Interaction Behavior." *Frontiers in Behavioral Neuroscience* 14 (June): 113. https://doi.org/10.3389/fnbeh.2020.00113.

Chaumont, Fabrice de, Elodie Ey, Nicolas Torquet, Thibault Lagache, Stéphane Dallongeville, Albane Imbert, Thierry Legou, et al. 2018. "Live Mouse Tracker: Real-Time Behavioral Analysis of Groups of Mice." Preprint. Animal Behavior and Cognition. https://doi.org/10.1101/345132.

Chini, B, and M Manning. 2007. "Agonist Selectivity in the Oxytocin/Vasopressin Receptor Family: New Insights and Challenges." *Biochemical Society Transactions* 35: 5.

Choe, Han Kyoung, Michael Douglas Reed, Nora Benavidez, Daniel Montgomery, Natalie Soares, Yeong Shin Yim, and Gloria B. Choi. 2015. “Oxytocin Mediates Entrainment of Sensory Stimuli to Social Cues of Opposing Valence.” *Neuron* 87 (1): 152–63. https://doi.org/10.1016/j.neuron.2015.06.022.

Choi, Gloria B., Dan D. Stettler, Benjamin R. Kallman, Shakthi T. Bhaskar, Alexander Fleischmann, and Richard Axel. 2011. “Driving Opposing Behaviors with Ensembles of Piriform Neurons.” *Cell* 146 (6): 1004–15. https://doi.org/10.1016/j.cell.2011.07.041.

Courtiol, Emmanuelle, Laura LefÃ¨vre, Samuel Garcia, Marc ThÃ©venet, Belkacem Messaoudi, and Nathalie Buonviso. 2014. “Sniff Adjustment in an Odor Discrimination Task in the Rat: Analytical or Synthetic Strategy?” *Frontiers in Behavioral Neuroscience* 8 (May). https://doi.org/10.3389/fnbeh.2014.00145.

Courtiol, Emmanuelle, and Donald A. Wilson. 2017. “The Olfactory Mosaic: Bringing an Olfactory Network Together for Odor Perception.” *Perception* 46 (3–4): 320–32. https://doi.org/10.1177/0301006616663216.

Craven, Brent A, Eric G Paterson, and Gary S Settles. 2010. “The FLuid Dynamics of Canine Olfaction: Unique Nasal Airflow Patterns as an Explanation of Macrosmia.” *J. R. Soc. Interface*, 11.

Croy, I., S. Nordin, and T. Hummel. 2014. “Olfactory Disorders and Quality of Life--An Updated Review.” *Chemical Senses* 39 (3): 185–94. https://doi.org/10.1093/chemse/bjt072.

D

Dantzer, Robert, Abdou Tazi, and Rose-Marie Bluthé. 1990. “Cerebral Lateralization of Olfactory-Mediated Affective Processes in Rats.” *Behavioural Brain Research* 40 (1): 53–60. https://doi.org/10.1016/0166-4328(90)90042-D.

Diodato, Assunta, Marion Ruinart de Brimont, Yeong Shin Yim, Nicolas Derian, Sandrine Perrin, Juliette Pouch, David Klatzmann, Sonia Garel, Gloria B Choi, and Alexander Fleischmann. 2016. “Molecular Signatures of Neural Connectivity in the Olfactory Cortex.” *Nature Communications* 7 (1): 12238. https://doi.org/10.1038/ncomms12238.

Dluzen, Dean E., Shinichiro Muraoka, Mario Engelmann, Karl Ebner, and Rainer Landgraf. 2000. “Oxytocin Induces Preservation of Social Recognition in Male Rats by Activating α-Adrenoceptors of the Olfactory Bulb: Oxytocin and Olfactory Bulb Norepinephrine.” *European Journal of Neuroscience* 12 (2): 760–66. https://doi.org/10.1046/j.1460-9568.2000.00952.x.

Dölen, Gül, Ayeh Darvishzadeh, Kee Wui Huang, and Robert C. Malenka. 2013. “Social Reward Requires Coordinated Activity of Nucleus Accumbens Oxytocin and Serotonin.” *Nature* 501 (7466): 179–84. https://doi.org/10.1038/nature12518.

E

Ennis, Matthew, Adam C. Puche, Tim Holy, and Michael T. Shipley. 2015. “The Olfactory System.” In *The Rat Nervous System*, 761–803. Elsevier. https://doi.org/10.1016/B978-0-12-374245-2.00027-9.

F

Ferguson, Jennifer N., J. Matthew Aldag, Thomas R. Insel, and Larry J. Young. 2001. “Oxytocin in the Medial Amygdala Is Essential for Social Recognition in the Mouse.” *The Journal of Neuroscience* 21 (20): 8278–85. https://doi.org/10.1523/JNEUROSCI.21-20-08278.2001.

Ferguson, Jennifer N., Larry J. Young, Elizabeth F. Hearn, Martin M. Matzuk, Thomas R. Insel, and James T. Winslow. 2000. “Social Amnesia in Mice Lacking the Oxytocin Gene.” *Nature Genetics* 25 (3): 284–88. https://doi.org/10.1038/77040.

Ferretti, Valentina, Federica Maltese, Gabriella Contarini, Marco Nigro, Alessandra Bonavia, Huiping Huang, Valentina Gigliucci, et al. 2019. “Oxytocin Signaling in the Central Amygdala Modulates Emotion

Discrimination in Mice." *Current Biology* 29 (12): 1938-1953.e6. https://doi.org/10.1016/j.cub.2019.04.070.

Fontanini, Alfredo, and James M. Bower. 2006. "Slow-Waves in the Olfactory System: An Olfactory Perspective on Cortical Rhythms." *Trends in Neurosciences* 29 (8): 429–37. https://doi.org/10.1016/j.tins.2006.06.013.

Fontanini, Alfredo, PierFranco Spano, and James M Bower. 2003. "Ketamine–Xylazine-Induced Slow (Ↄ1.5 Hz) Oscillations in the Rat Piriform (Olfactory) Cortex Are Functionally Correlated with Respiration," 9.

Franks, Kevin M., Marco J. Russo, Dara L. Sosulski, Abigail A. Mulligan, Steven A. Siegelbaum, and Richard Axel. 2011. "Recurrent Circuitry Dynamically Shapes the Activation of Piriform Cortex." *Neuron* 72 (1): 49–56. https://doi.org/10.1016/j.neuron.2011.08.020.

Freeman, Sara M., and Larry J. Young. 2016. "Comparative Perspectives on Oxytocin and Vasopressin Receptor Research in Rodents and Primates: Translational Implications." *Journal of Neuroendocrinology* 28 (4). https://doi.org/10.1111/jne.12382.

Froemke, Robert C., and Ioana Carcea. 2017. "Oxytocin and Brain Plasticity." In *Principles of Gender-Specific Medicine*, 161–82. Elsevier. https://doi.org/10.1016/B978-0-12-803506-1.00037-1.

G

Ghosh, Sulagna, Stephen D. Larson, Hooman Hefzi, Zachary Marnoy, Tyler Cutforth, Kartheek Dokka, and Kristin K. Baldwin. 2011. "Sensory Maps in the Olfactory Cortex Defined by Long-Range Viral Tracing of Single Neurons." *Nature* 472 (7342): 217–20. https://doi.org/10.1038/nature09945.

Giessel, Andrew J, and Sandeep Robert Datta. 2014. "Olfactory Maps, Circuits and Computations." *Current Opinion in Neurobiology* 24 (February): 120–32. https://doi.org/10.1016/j.conb.2013.09.010.

Gimpl, Gerald, and Falk Fahrenholz. 2001. "The Oxytocin Receptor System: Structure, Function, and Regulation." *Physiological Reviews* 81 (2): 629–83. https://doi.org/10.1152/physrev.2001.81.2.629.

Girin, Baptiste, Maxime Juventin, Samuel Garcia, Laura Lefèvre, Corine Amat, Nicolas Fourcaud-Trocmé, and Nathalie Buonviso. 2021. "The Deep and Slow Breathing Characterizing Rest Favors Brain Respiratory-Drive." *Scientific Reports* 11 (1): 7044. https://doi.org/10.1038/s41598-021-86525-3.

Godoy, Maria, Richard Voegels, Fábio Pinna, Rui Imamura, and José Farfel. 2014. "Olfaction in Neurologic and Neurodegenerative Diseases: A Literature Review." *International Archives of Otorhinolaryngology* 19 (02): 176–79. https://doi.org/10.1055/s-0034-1390136.

Gottfried, Jay A. 2010. "Central Mechanisms of Odour Object Perception." *Nature Reviews Neuroscience* 11 (9): 628–41. https://doi.org/10.1038/nrn2883.

Grimaud, Julien, and Venkatesh N. Murthy. 2018. "How to Monitor Breathing in Laboratory Rodents: A Review of the Current Methods." *Journal of Neurophysiology* 120 (2): 624–32. https://doi.org/10.1152/jn.00708.2017.

Grinevich, Valery, H. Sophie Knobloch-Bollmann, Marina Eliava, Marta Busnelli, and Bice Chini. 2016. "Assembling the Puzzle: Pathways of Oxytocin Signaling in the Brain." *Biological Psychiatry* 79 (3): 155–64. https://doi.org/10.1016/j.biopsych.2015.04.013.

Grinevich, Valery, and Mike Ludwig. 2021. "The Multiple Faces of the Oxytocin and Vasopressin Systems in the Brain." *Journal of Neuroendocrinology* 33 (11). https://doi.org/10.1111/jne.13004.

Grinevich, Valery, and Inga D. Neumann. 2021. "Brain Oxytocin: How Puzzle Stones from Animal Studies Translate into Psychiatry." *Molecular Psychiatry* 26 (1): 265–79. https://doi.org/10.1038/s41380-020-0802-9.

Grinevich, Valery, and Ron Stoop. 2018. “Interplay between Oxytocin and Sensory Systems in the Orchestration of Socio-Emotional Behaviors.” *Neuron* 99 (5): 887–904. https://doi.org/10.1016/j.neuron.2018.07.016.

Grosmaitre, Xavier, Lindsey C Santarelli, Jie Tan, Minmin Luo, and Minghong Ma. 2007. “Dual Functions of Mammalian Olfactory Sensory Neurons as Odor Detectors and Mechanical Sensors.” *Nature Neuroscience* 10 (3): 348–54. https://doi.org/10.1038/nn1856.

H

Haberly, L. B. 2001. “Parallel-Distributed Processing in Olfactory Cortex: New Insights from Morphological and Physiological Analysis of Neuronal Circuitry.” *Chemical Senses* 26 (5): 551–76. https://doi.org/10.1093/chemse/26.5.551.

Haberly, Lewis B., and Joseph L. Price. 1977. “The Axonal Projection Patterns of the Mitral and Tufted Cells of the Olfactory Bulb in the Rat.” *Brain Research* 129 (1): 152–57. https://doi.org/10.1016/0006-8993(77)90978-7.

Hannum, Mackenzie, Margaret A Stegman, Jenna A Fryer, and Christopher T Simons. 2018. “Different Olfactory Percepts Evoked by Orthonasal and Retronasal Odorant Delivery.” *Chemical Senses* 43 (7): 515–21. https://doi.org/10.1093/chemse/bjy043.

Heck, Detlef H., Samuel S. McAfee, Yu Liu, Abbas Babajani-Feremi, Roozbeh Rezaie, Walter J. Freeman, James W. Wheless, et al. 2017. “Breathing as a Fundamental Rhythm of Brain Function.” *Frontiers in Neural Circuits* 10 (January). https://doi.org/10.3389/fncir.2016.00115.

Hegoburu, Chloé, Kiseko Shionoya, Samuel Garcia, Belkacem Messaoudi, Marc Thévenet, and Anne-Marie Mouly. 2011. “The RUB Cage: Respiration–Ultrasonic Vocalizations–Behavior Acquisition Setup for Assessing Emotional Memory in Rats.” *Frontiers in Behavioral Neuroscience* 5. https://doi.org/10.3389/fnbeh.2011.00025.

Hitti, Frederick L. Siegelbaum Steven A. “The Hippocampal CA2 Region Is Essential for Social Memory,” nature, doi:10.1038/nature13028

Huang, Huiping, Caterina Michetti, Marta Busnelli, Francesca Managò, Sara Sannino, Diego Scheggia, Luca Giancardo, et al. 2014. “Chronic and Acute Intranasal Oxytocin Produce Divergent Social Effects in Mice.” *Neuropsychopharmacology* 39 (5): 1102–14. https://doi.org/10.1038/npp.2013.310.

Huber, Daniel, Pierre Veinante, and Ron Stoop. 2005. “Vasopressin and Oxytocin Excite Distinct Neuronal Populations in the Central Amygdala.” *Science* 308 (5719): 245–48. https://doi.org/10.1126/science.1105636.

Hung, Lin W., Sophie Neuner, Jai S. Polepalli, Kevin T. Beier, Matthew Wright, Jessica J. Walsh, Eastman M. Lewis, et al. 2017. “Gating of Social Reward by Oxytocin in the Ventral Tegmental Area.” *Science* 357 (6358): 1406–11. https://doi.org/10.1126/science.aan4994.

Hurst, Jane L., Caroline E. Payne, Charlotte M. Nevison, Amr D. Marie, Richard E. Humphries, Duncan H. L. Robertson, Andrea Cavaggioni, and Robert J. Beynon. 2001. “Individual Recognition in Mice Mediated by Major Urinary Proteins.” *Nature* 414 (6864): 631–34. https://doi.org/10.1038/414631a.

Hutmacher, Fabian. 2019. “Why Is There So Much More Research on Vision Than on Any Other Sensory Modality?” *Frontiers in Psychology* 10 (October): 2246. https://doi.org/10.3389/fpsyg.2019.02246.

I

Igarashi, K. M., N. Ieki, M. An, Y. Yamaguchi, S. Nagayama, K. Kobayakawa, R. Kobayakawa, et al. 2012. “Parallel Mitral and Tufted Cell Pathways Route Distinct Odor Information to Different Targets in the Olfactory Cortex.” *Journal of Neuroscience* 32 (23): 7970–85. https://doi.org/10.1523/JNEUROSCI.0154-12.2012.

Ikemoto, Satoshi, and Jaak Panksepp. 1994. “The Relationship between Self-Stimulation and Sniffing in Rats: Does a Common Brain System Mediate These Behaviors?” *Behavioural Brain Research* 61 (2): 143–62. https://doi.org/10.1016/0166-4328(94)90155-4.

Imai, Takeshi. 2014. “Construction of Functional Neuronal Circuitry in the Olfactory Bulb.” *Seminars in Cell & Developmental Biology* 35 (November): 180–88. https://doi.org/10.1016/j.semcdb.2014.07.012.

Inoue, Kiyoshi, Charles L. Ford, Kengo Horie, and Larry J. Young. 2022. “Oxytocin Receptors Are Widely Distributed in the Prairie Vole (*Microtus Ochrogaster)* Brain: Relation to Social Behavior, Genetic Polymorphisms, and the Dopamine System.” *Journal of Comparative Neurology*, June, cne.25382. https://doi.org/10.1002/cne.25382.

Inoue, T, T Kimura, C Azuma, J Inazawa, M Takemura, T Kikuchi, Y Kubota, K Ogita, and F Saji. 1994. “Structural Organization of the Human Oxytocin Receptor Gene.” *Journal of Biological Chemistry* 269 (51): 32451–56. https://doi.org/10.1016/S0021-9258(18)31656-9.

Insel, Thomas R, 1991. “OXYTOCIN - A NEUROPEM’IDE FOR AFFILIATION: EVIDENCE FROM BEHAVIORAL, RECEPTOR AUTORADIOGRAPHIC, AND COMPARATIVE STUDIES,” 33.

Ito, J., S. Roy, Y. Liu, Y. Cao, M. Fletcher, L. Lu, J.D. Boughter, S. Grün, and D.H. Heck. 2014. “Whisker Barrel Cortex Delta Oscillations and Gamma Power in the Awake Mouse Are Linked to Respiration.” *Nature Communications* 5 (1): 3572. https://doi.org/10.1038/ncomms4572.

J

Jessberger, Jakob, Weiwei Zhong, Jurij Brankačk, and Andreas Draguhn. 2016. “Olfactory Bulb Field Potentials and Respiration in Sleep-Wake States of Mice.” *Neural Plasticity* 2016: 1–9. https://doi.org/10.1155/2016/4570831.

Johnson, Dawn M. G., Kurt R. Illig, Mary Behan, and Lewis B. Haberly. 2000. “New Features of Connectivity in Piriform Cortex Visualized by Intracellular Injection of Pyramidal Cells Suggest That ‘Primary’ Olfactory Cortex Functions Like ‘Association’ Cortex in Other Sensory Systems.” *The Journal of Neuroscience* 20 (18): 6974–82. https://doi.org/10.1523/JNEUROSCI.20-18-06974.2000.

Johnson, Zachary V., and Larry J. Young. 2017. “Oxytocin and Vasopressin Neural Networks: Implications for Social Behavioral Diversity and Translational Neuroscience.” *Neuroscience & Biobehavioral Reviews* 76 (May): 87–98. https://doi.org/10.1016/j.neubiorev.2017.01.034.

Jurek, Benjamin, and Inga D. Neumann. 2018. “The Oxytocin Receptor: From Intracellular Signaling to Behavior.” *Physiological Reviews* 98 (3): 1805–1908. https://doi.org/10.1152/physrev.00031.2017.

K

Karalis, Nikolaos, and Anton Sirota. 2022. “Breathing Coordinates Cortico-Hippocampal Dynamics in Mice during Offline States.” *Nature Communications* 13 (1): 467. https://doi.org/10.1038/s41467-022-28090-5.

Kawamata, Masaki, Yutaka Tonomura, Tadashi Kimura, Teruyuki Yanagisawa, and Katsuhiko Nishimori. 2004. “The Differential Coupling of Oxytocin Receptors to Uterine Contractions in Murine Estrous Cycle.” *Biochemical and Biophysical Research Communications* 321 (3): 695–99. https://doi.org/10.1016/j.bbrc.2004.07.019.

Kawasaki, Akiko, Koichi Hoshi, Michihiro Kawano, Haruo Nogami, Hiroyuki Yoshikawa, and Setsuji Hisano. 2005. “Up-Regulation of VGLUT2 Expression in Hypothalamic-Neurohypophysial Neurons of the Rat Following Osmotic Challenge.” *European Journal of Neuroscience* 22 (3): 672–80. https://doi.org/10.1111/j.1460-9568.2005.04240.x.

Kay, Leslie M, and Walter J Freeman. 1998. “Bidirectional Processing in the Olfactory-Limbic Axis During Olfactory Behavior,” 13.

Kepecs, Adam, Naoshige Uchida, and Zachary F. Mainen. 2007. “Rapid and Precise Control of Sniffing During Olfactory Discrimination in Rats.” *Journal of Neurophysiology* 98 (1): 205–13. https://doi.org/10.1152/jn.00071.2007.

Keverne, Eric B., and Keith M. Kendrick. 1992. “Oxytocin Facilitation of Maternal Behavior in Sheepa.” *Annals of the New York Academy of Sciences* 652 (1): 83–101. https://doi.org/10.1111/j.1749-6632.1992.tb34348.x.

Kim, Yongsoo, Kannan Umadevi Venkataraju, Kith Pradhan, Carolin Mende, Julian Taranda, Srinivas C. Turaga, Ignacio Arganda-Carreras, et al. 2015. “Mapping Social Behavior-Induced Brain Activation at Cellular Resolution in the Mouse.” *Cell Reports* 10 (2): 292–305. https://doi.org/10.1016/j.celrep.2014.12.014.

Kimura, Tadashi, Osamu Tanizawa, Kensaku Mori, Michael J. Brownstein, and Hiroto Okayama. 1992. “Structure and Expression of a Human Oxytocin Receptor.” *Nature* 356 (6369): 526–29. https://doi.org/10.1038/356526a0.

Knobloch, H. Sophie, Alexandre Charlet, Lena C. Hoffmann, Marina Eliava, Sergey Khrulev, Ali H. Cetin, Pavel Osten, et al. 2012. “Evoked Axonal Oxytocin Release in the Central Amygdala Attenuates Fear Response.” *Neuron* 73 (3): 553–66. https://doi.org/10.1016/j.neuron.2011.11.030.

L

Landgraf, Rainer, and Inga D. Neumann. 2004. “Vasopressin and Oxytocin Release within the Brain: A Dynamic Concept of Multiple and Variable Modes of Neuropeptide Communication.” *Frontiers in Neuroendocrinology* 25 (3–4): 150–76. https://doi.org/10.1016/j.yfrne.2004.05.001.

Linster, C. 2001. “Neuromodulation and the Functional Dynamics of Piriform Cortex.” *Chemical Senses* 26 (5): 585–94. https://doi.org/10.1093/chemse/26.5.585.

Litaudon, P., C. Amat, B. Bertrand, M. Vigouroux, and N. Buonviso. 2003. “Piriform Cortex Functional Heterogeneity Revealed by Cellular Responses to Odours: Piriform Cortex Heterogeneity in Response to Odours.” *European Journal of Neuroscience* 17 (11): 2457–61. https://doi.org/10.1046/j.1460-9568.2003.02654.x.

Liu, Jing-Jing, Katherine W. Eyring, Gabriele M. König, Evi Kostenis, and Richard W. Tsien. 2022. “Oxytocin-Modulated Ion Channel Ensemble Controls Depolarization, Integration and Burst Firing in CA2 Pyramidal Neurons.” *The Journal of Neuroscience*, September, JN-RM-0921-22. https://doi.org/10.1523/JNEUROSCI.0921-22.2022.

Liu, Yu, Samuel S. McAfee, and Detlef H. Heck. 2017. “Hippocampal Sharp-Wave Ripples in Awake Mice Are Entrained by Respiration.” *Scientific Reports* 7 (1): 8950. https://doi.org/10.1038/s41598-017-09511-8.

Lukas, Michael, Iulia Toth, Stefan O Reber, David A Slattery, Alexa H Veenema, and Inga D Neumann. 2011. “The Neuropeptide Oxytocin Facilitates Pro-Social Behavior and Prevents Social Avoidance in Rats and Mice.” *Neuropsychopharmacology* 36 (11): 2159–68. https://doi.org/10.1038/npp.2011.95.

Lukas, Michael, Iulia Toth, Alexa H. Veenema, and Inga D. Neumann. 2013. “Oxytocin Mediates Rodent Social Memory within the Lateral Septum and the Medial Amygdala Depending on the Relevance of the Social Stimulus: Male Juvenile versus Female Adult Conspecifics.” *Psychoneuroendocrinology* 38 (6): 916–26. https://doi.org/10.1016/j.psyneuen.2012.09.018.

M

Malnic, Bettina, Junzo Hirono, Takaaki Sato, and Linda B Buck. 1999. “Combinatorial Receptor Codes for Odors,” 11.

Marin, Concepció, Dolores Vilas, Cristóbal Langdon, Isam Alobid, Mauricio López-Chacón, Antje Haehner, Thomas Hummel, and Joaquim Mullol. 2018. “Olfactory Dysfunction in Neurodegenerative Diseases.” *Current Allergy and Asthma Reports* 18 (8): 42. https://doi.org/10.1007/s11882-018-0796-4.

Marlin, Bianca J., Mariela Mitre, James A. D'amour, Moses V. Chao, and Robert C. Froemke. 2015. "Oxytocin Enables Maternal Behaviour by Balancing Cortical Inhibition." *Nature* 520 (7548): 499–504. https://doi.org/10.1038/nature14402.

Martin, Claire, Jennifer Beshel, and Leslie M. Kay. 2007. "An Olfacto-Hippocampal Network Is Dynamically Involved in Odor-Discrimination Learning." *Journal of Neurophysiology* 98 (4): 2196–2205. https://doi.org/10.1152/jn.00524.2007.

Mathis, Alexander, Pranav Mamidanna, Kevin M. Cury, Taiga Abe, Venkatesh N. Murthy, Mackenzie Weygandt Mathis, and Matthias Bethge. 2018. "DeepLabCut: Markerless Pose Estimation of User-Defined Body Parts with Deep Learning." *Nature Neuroscience* 21 (9): 1281–89. https://doi.org/10.1038/s41593-018-0209-y.

Mazo, Camille, Julien Grimaud, Yasuyuki Shima, Venkatesh N. Murthy, and C. Geoffrey Lau. 2017. "Distinct Projection Patterns of Different Classes of Layer 2 Principal Neurons in the Olfactory Cortex." *Scientific Reports* 7 (1): 8282. https://doi.org/10.1038/s41598-017-08331-0.

McAfee, Samuel Stuart, Mary Cameron Ogg, Jordan M. Ross, Yu Liu, Max L. Fletcher, and Detlef H. Heck. 2016. "Minimally Invasive Highly Precise Monitoring of Respiratory Rhythm in the Mouse Using an Epithelial Temperature Probe." *Journal of Neuroscience Methods* 263 (April): 89–94. https://doi.org/10.1016/j.jneumeth.2016.02.007.

McGann, John P. 2017. "Poor Human Olfaction Is a 19th-Century Myth." *Science* 356 (6338): eaam7263. https://doi.org/10.1126/science.aam7263.

Menon, Rohit, Thomas Grund, Iulia Zoicas, Ferdinand Althammer, Dominik Fiedler, Verena Biermeier, Oliver J. Bosch, et al. 2018. "Oxytocin Signaling in the Lateral Septum Prevents Social Fear during Lactation." *Current Biology* 28 (7): 1066-1078.e6. https://doi.org/10.1016/j.cub.2018.02.044.

Mens, Wim B.J., Albert Witter, and Tjeerd B. Van Wimersma Greidanus. 1983. "Penetration of Neurohypophyseal Hormones from Plasma into Cerebrospinal Fluid (CSF): Half-Times of Disappearance of These Neuropeptides from CSF." *Brain Research* 262 (1): 143–49. https://doi.org/10.1016/0006-8993(83)90478-X.

Mitre, Mariela, Bianca J. Marlin, Jennifer K. Schiavo, Egzona Morina, Samantha E. Norden, Troy A. Hackett, Chiye J. Aoki, Moses V. Chao, and Robert C. Froemke. 2016. "A Distributed Network for Social Cognition Enriched for Oxytocin Receptors." *The Journal of Neuroscience* 36 (8): 2517–35. https://doi.org/10.1523/JNEUROSCI.2409-15.2016.

Miura, Keiji, Zachary F. Mainen, and Naoshige Uchida. 2012. "Odor Representations in Olfactory Cortex: Distributed Rate Coding and Decorrelated Population Activity." *Neuron* 74 (6): 1087–98. https://doi.org/10.1016/j.neuron.2012.04.021.

Miyamichi, Kazunari, Fernando Amat, Farshid Moussavi, Chen Wang, Ian Wickersham, Nicholas R. Wall, Hiroki Taniguchi, et al. 2011. "Cortical Representations of Olfactory Input by Trans-Synaptic Tracing." *Nature* 472 (7342): 191–96. https://doi.org/10.1038/nature09714.

Mombaerts, Peter, Fan Wang, Catherine Dulac, Steve K Chao, Adriana Nemes, Monica Mendelsohn, James Edmondson, and Richard Axel. 1996. "Visualizing an Olfactory Sensory Map," 12.

Moore, Jeffrey D., Martin Deschênes, Takahiro Furuta, Daniel Huber, Matthew C. Smear, Maxime Demers, and David Kleinfeld. 2013. "Hierarchy of Orofacial Rhythms Revealed through Whisking and Breathing." *Nature* 497 (7448): 205–10. https://doi.org/10.1038/nature12076.

Mucignat-Caretta, Carla, Marco Redaelli, and Antonio Caretta. 2012. "One Nose, One Brain: Contribution of the Main and Accessory Olfactory System to Chemosensation." *Frontiers in Neuroanatomy* 6. https://doi.org/10.3389/fnana.2012.00046.

Mutlu, K., J. Esquivelzeta Rabell, P. Martin del Olmo, and S. Haesler. 2018. "IR Thermography-Based Monitoring of Respiration Phase without Image Segmentation." *Journal of Neuroscience Methods* 301 (May): 1–8. https://doi.org/10.1016/j.jneumeth.2018.02.017.

N

Nagappan, Shivathmihai, and Kevin M Franks. 2021. “Parallel Processing by Distinct Classes of Principal Neurons in the Olfactory Cortex.” *ELife* 10 (December): e73668. https://doi.org/10.7554/eLife.73668.

Nagayama, Shin, Ryota Homma, and Fumiaki Imamura. 2014. “Neuronal Organization of Olfactory Bulb Circuits.” *Frontiers in Neural Circuits* 8 (September). https://doi.org/10.3389/fncir.2014.00098.

Nakajima, Miho, Andreas Görlich, and Nathaniel Heintz. 2014. “Oxytocin Modulates Female Sociosexual Behavior through a Specific Class of Prefrontal Cortical Interneurons.” *Cell* 159 (2): 295–305. https://doi.org/10.1016/j.cell.2014.09.020.

Natynczuk, Stephan E., and David W. Macdonald. 1994. “Scent, Sex, and the Self-Calibrating Rat.” *Journal of Chemical Ecology* 20 (8): 1843–57. https://doi.org/10.1007/BF02066226.

Neumann, I, E Koehler, R Landgraf, and J Summy-Long. 1994. “An Oxytocin Receptor Antagonist Infused into the Supraoptic Nucleus Attenuates Intranuclear and Peripheral Release of Oxytocin during Suckling in Conscious Rats.,” no. 1: 8.

Nguyen Chi, V., C. Muller, T. Wolfenstetter, Y. Yanovsky, A. Draguhn, A. B. L. Tort, and J. Branka k. 2016. “Hippocampal Respiration-Driven Rhythm Distinct from Theta Oscillations in Awake Mice.” *Journal of Neuroscience* 36 (1): 162–77. https://doi.org/10.1523/JNEUROSCI.2848-15.2016.

O

Oettl, Lars-Lennart, and Wolfgang Kelsch. 2017. “Oxytocin and Olfaction.” In *Behavioral Pharmacology of Neuropeptides: Oxytocin*, edited by Rene Hurlemann and Valery Grinevich, 35:55–75. Current Topics in Behavioral Neurosciences. Cham: Springer International Publishing. https://doi.org/10.1007/7854_2017_8.

Oettl, Lars-Lennart, Namasivayam Ravi, Miriam Schneider, Max F. Scheller, Peggy Schneider, Mariela Mitre, Miriam da Silva Gouveia, et al. 2016. “Oxytocin Enhances Social Recognition by Modulating Cortical Control of Early Olfactory Processing.” *Neuron* 90 (3): 609–21. https://doi.org/10.1016/j.neuron.2016.03.033.

Oliveira, Williara Queiroz de, Paulo Henrique Machado De Sousa, and Glaucia Maria Pastore. 2022. “Olfactory and Gustatory Disorders Caused by COVID-19: How to Regain the Pleasure of Eating?” *Trends in Food Science & Technology* 122 (April): 104–9. https://doi.org/10.1016/j.tifs.2022.01.022.

Owen, Scott F., Sebnem N. Tuncdemir, Patrick L. Bader, Natasha N. Tirko, Gord Fishell, and Richard W. Tsien. 2013. “Oxytocin Enhances Hippocampal Spike Transmission by Modulating Fast-Spiking Interneurons.” *Nature* 500 (7463): 458–62. https://doi.org/10.1038/nature12330.

P

Persson, Bjorn M., Veronika Ambrozova, Stephen Duncan, Emma R. Wood, Akira R. O’Connor, and James A. Ainge. 2022. “Lateral Entorhinal Cortex Lesions Impair Odor-context Associative Memory in Male Rats.” *Journal of Neuroscience Research* 100 (4): 1030–46. https://doi.org/10.1002/jnr.25027.

Pobbe, Roger L.H., Brandon L. Pearson, Erwin B. Defensor, Valerie J. Bolivar, W. Scott Young, Heon-Jin Lee, D. Caroline Blanchard, and Robert J. Blanchard. 2012. “Oxytocin Receptor Knockout Mice Display Deficits in the Expression of Autism-Related Behaviors.” *Hormones and Behavior* 61 (3): 436–44. https://doi.org/10.1016/j.yhbeh.2011.10.010.

Poo, Cindy, and Jeffry S. Isaacson. 2009. “Odor Representations in Olfactory Cortex: ‘Sparse’ Coding, Global Inhibition, and Oscillations.” *Neuron* 62 (6): 850–61. https://doi.org/10.1016/j.neuron.2009.05.022.

Popik, Piotr, Jerzy Vetulani, Adam Bisaga, and Jan M. van Ree. 1991. “RECOGNITION CUE IN THE RAT’S SOCIAL MEMORY PARADIGM.” *Journal of Basic and Clinical Physiology and Pharmacology* 2 (4). https://doi.org/10.1515/JBCPP.1991.2.4.315.

Premoli, Marika, Maurizio Memo, and SaraAnna Bonini. 2021. “Ultrasonic Vocalizations in Mice: Relevance for Ethologic and Neurodevelopmental Disorders Studies.” *Neural Regeneration Research* 16 (6): 1158. https://doi.org/10.4103/1673-5374.300340.

Q

Quintana, Daniel S., and Adam J. Guastella. 2020. “An Allostatic Theory of Oxytocin.” *Trends in Cognitive Sciences* 24 (7): 515–28. https://doi.org/10.1016/j.tics.2020.03.008.

R

Raam, Tara, Kathleen M. McAvoy, Antoine Besnard, Alexa H. Veenema, and Amar Sahay. 2017. “Hippocampal Oxytocin Receptors Are Necessary for Discrimination of Social Stimuli.” *Nature Communications* 8 (1): 2001. https://doi.org/10.1038/s41467-017-02173-0.

Ravel, Nadine, and Jeanne Pager. 1990. “Respiratory Patterning of the Rat Olfactory Bulb Unit Activity: Nasal versus Tracheal Breathing.” *Neuroscience Letters* 115 (2–3): 213–18. https://doi.org/10.1016/0304-3940(90)90457-K.

Reisert, Johannes, Glen J. Golden, Koichi Matsumura, Matt Smear, Dmitry Rinberg, and Alan Gelperin. 2014. “Comparing Thoracic and Intra-Nasal Pressure Transients to Monitor Active Odor Sampling during Odor-Guided Decision Making in the Mouse.” *Journal of Neuroscience Methods* 221 (January): 8–14. https://doi.org/10.1016/j.jneumeth.2013.09.006.

Rennaker, R. L., C.-F. F. Chen, A. M. Ruyle, A. M. Sloan, and D. A. Wilson. 2007. “Spatial and Temporal Distribution of Odorant-Evoked Activity in the Piriform Cortex.” *Journal of Neuroscience* 27 (7): 1534–42. https://doi.org/10.1523/JNEUROSCI.4072-06.2007.

Ressler, Kerry J., Susan L. Sullivan, and Linda B. Buck. 1993. “A Zonal Organization of Odorant Receptor Gene Expression in the Olfactory Epithelium.” *Cell* 73 (3): 597–609. https://doi.org/10.1016/0092-8674(93)90145-G.

Rinaldi, Andrea. 2007. “The Scent of Life: The Exquisite Complexity of the Sense of Smell in Animals and Humans.” *EMBO Reports* 8 (7): 629–33. https://doi.org/10.1038/sj.embor.7401029.

Roberts, Sarah A., Mark C. Prescott, Amanda J. Davidson, Lynn McLean, Robert J. Beynon, and Jane L. Hurst. 2018. “Individual Odour Signatures That Mice Learn Are Shaped by Involatile Major Urinary Proteins (MUPs).” *BMC Biology* 16 (1): 48. https://doi.org/10.1186/s12915-018-0512-9.

Rodriguez, I., and U. Boehm. 2008. “Pheromone Sensing in Mice.” In *Chemosensory Systems in Mammals, Fishes, and Insects*, edited by Sigrun Korsching and Wolfgang Meyerhof, 47:139–85. Results and Problems in Cell Differentiation. Berlin, Heidelberg: Springer Berlin Heidelberg. https://doi.org/10.1007/400_2008_8.

Roesch, M. R., T. A. Stalnaker, and G. Schoenbaum. 2006. “Associative Encoding in Anterior Piriform Cortex versus Orbitofrontal Cortex during Odor Discrimination and Reversal Learning.” *Cerebral Cortex* 17 (3): 643–52. https://doi.org/10.1093/cercor/bhk009.

Rojas-LÃ-bano, Daniel, Donald E. Frederick, Jose I. Egana, and Leslie M. Kay. 2014. “The Olfactory Bulb Theta Rhythm Follows All Frequencies of Diaphragmatic Respiration in the Freely Behaving Rat.” *Frontiers in Behavioral Neuroscience* 8 (June). https://doi.org/10.3389/fnbeh.2014.00214.

Roland, Benjamin, Thomas Deneux, Kevin M Franks, Brice Bathellier, and Alexander Fleischmann. 2017. “Odor Identity Coding by Distributed Ensembles of Neurons in the Mouse Olfactory Cortex.” *ELife* 6 (May): e26337. https://doi.org/10.7554/eLife.26337.

Root, Cory M., Christine A. Denny, René Hen, and Richard Axel. 2014. “The Participation of Cortical Amygdala in Innate, Odour-Driven Behaviour.” *Nature* 515 (7526): 269–73. https://doi.org/10.1038/nature13897.

Rozin, Paul. 1982. “‘Taste-Smell Confusions’ and the Duality of the Olfactory Sense.” *Perception & Psychophysics* 31 (4): 397–401. https://doi.org/10.3758/BF03202667.

Rydén, Gunnar, and Ingvar Sjöholm. 1969. “Half-Life of Oxytocin in Blood of Pregnant and Non-Pregnant Woman.” *Acta Obstetricia et Gynecologica Scandinavica* 48 (s3): 139–40. https://doi.org/10.3109/00016346909157733.

S

Sala, Mariaelvina, Daniela Braida, Daniela Lentini, Marta Busnelli, Elisabetta Bulgheroni, Valeria Capurro, Annamaria Finardi, et al. 2011. “Pharmacologic Rescue of Impaired Cognitive Flexibility, Social Deficits, Increased Aggression, and Seizure Susceptibility in Oxytocin Receptor Null Mice: A Neurobehavioral Model of Autism.” *Biological Psychiatry* 69 (9): 875–82. https://doi.org/10.1016/j.biopsych.2010.12.022.

Shamay-Tsoory, Simone G., and Ahmad Abu-Akel. 2016. “The Social Salience Hypothesis of Oxytocin.” *Biological Psychiatry* 79 (3): 194–202. https://doi.org/10.1016/j.biopsych.2015.07.020.

Shusterman, Roman, Matthew C Smear, Alexei A Koulakov, and Dmitry Rinberg. 2011. “Precise Olfactory Responses Tile the Sniff Cycle.” *Nature Neuroscience* 14 (8): 1039–44. https://doi.org/10.1038/nn.2877.

Small, Dana M., Johannes C. Gerber, Y. Erica Mak, and Thomas Hummel. 2005. “Differential Neural Responses Evoked by Orthonasal versus Retronasal Odorant Perception in Humans.” *Neuron* 47 (4): 593–605. https://doi.org/10.1016/j.neuron.2005.07.022.

Smear, Matthew, Roman Shusterman, Rodney O’Connor, Thomas Bozza, and Dmitry Rinberg. 2011. “Perception of Sniff Phase in Mouse Olfaction.” *Nature* 479 (7373): 397–400. https://doi.org/10.1038/nature10521.

Sofroniew, M.V. 1983. “Morphology of Vasopressin and Oxytocin Neurones and Their Central and Vascular Projections.” In *Progress in Brain Research*, 60:101–14. Elsevier. https://doi.org/10.1016/S0079-6123(08)64378-2.

Soloff, Melvyn S., Maria Alexandrova, and Martha J. Fernstrom. 1979. “Oxytocin Receptors: Triggers for Parturition and Lactation?” *Science* 204 (4399): 1313–15. https://doi.org/10.1126/science.221972.

Son, Seoyoung, Steffy B. Manjila, Kyra T. Newmaster, Yuan-ting Wu, Daniel J. Vanselow, Matt Ciarletta, Todd E. Anthony, Keith C. Cheng, and Yongsoo Kim. 2022. “Whole-Brain Wiring Diagram of Oxytocin System in Adult Mice.” *The Journal of Neuroscience* 42 (25): 5021–33. https://doi.org/10.1523/JNEUROSCI.0307-22.2022.

Sosulski, Dara L., Maria Lissitsyna Bloom, Tyler Cutforth, Richard Axel, and Sandeep Robert Datta. 2011. “Distinct Representations of Olfactory Information in Different Cortical Centres.” *Nature* 472 (7342): 213–16. https://doi.org/10.1038/nature09868.

Stettler, Dan D., and Richard Axel. 2009. “Representations of Odor in the Piriform Cortex.” *Neuron* 63 (6): 854–64. https://doi.org/10.1016/j.neuron.2009.09.005.

Stoop, Ron. 2012. “Neuromodulation by Oxytocin and Vasopressin.” *Neuron* 76 (1): 142–59. https://doi.org/10.1016/j.neuron.2012.09.025.

Stopka, Pavel, Katerina Janotova, and David Heyrovsky. 2007. “The Advertisement Role of Major Urinary Proteins in Mice.” *Physiology & Behavior* 91 (5): 667–70. https://doi.org/10.1016/j.physbeh.2007.03.030.

Strowbridge, Ben W. 2009. “Role of Cortical Feedback in Regulating Inhibitory Microcircuits.” *Annals of the New York Academy of Sciences* 1170 (1): 270–74. https://doi.org/10.1111/j.1749-6632.2009.04018.x.

Sullivan, Regina M., Donald A. Wilson, Nadine Ravel, and Anne-Marie Mouly. 2015. “Olfactory Memory Networks: From Emotional Learning to Social Behaviors.” *Frontiers in Behavioral Neuroscience* 9 (February). https://doi.org/10.3389/fnbeh.2015.00036.

Suzuki, N., and J. M. Bekkers. 2006. “Neural Coding by Two Classes of Principal Cells in the Mouse Piriform Cortex.” *Journal of Neuroscience* 26 (46): 11938–47. https://doi.org/10.1523/JNEUROSCI.3473-06.2006.

Suzuki N and J.M.Bekkers. 2011. “Two Layers of Synaptic Processing by Principal Neurons in Piriform Cortex.” *Journal of Neuroscience* 31 (6): 2156–66. https://doi.org/10.1523/JNEUROSCI.5430-10.2011.

Suzuki, Norimitsu, and John M Bekkers. 2007. “INHIBITORY INTERNEURONS IN THE PIRIFORM CORTEX.” *Clinical and Experimental Pharmacology and Physiology* 34 (10): 1064–69. https://doi.org/10.1111/j.1440-1681.2007.04723.x.

Suzuki, Norimitsu, and John M. Bekkers. 2010a. “Inhibitory Neurons in the Anterior Piriform Cortex of the Mouse: Classification Using Molecular Markers.” *The Journal of Comparative Neurology* 518 (10): 1670–87. https://doi.org/10.1002/cne.22295.

Suzuki N and J.M.Bekkers 2010b. “Distinctive Classes of GABAergic Interneurons Provide Layer-Specific Phasic Inhibition in the Anterior Piriform Cortex.” *Cerebral Cortex* 20 (12): 2971–84. https://doi.org/10.1093/cercor/bhq046.

Swanson, L W, and P E Sawchenko. 1983. “Hypothalamic Integration: Organization of the Paraventricular and Supraoptic Nuclei.” *Annual Review of Neuroscience* 6 (1): 269–324. https://doi.org/10.1146/annurev.ne.06.030183.001413.

T

Takayanagi, Yuki, Masahide Yoshida, Isadora F. Bielsky, Heather E. Ross, Masaki Kawamata, Tatsushi Onaka, Teruyuki Yanagisawa, et al. 2005. “Pervasive Social Deficits, but Normal Parturition, in Oxytocin Receptor-Deficient Mice.” *Proceedings of the National Academy of Sciences* 102 (44): 16096–101. https://doi.org/10.1073/pnas.0505312102.

Tan, Oliver, Hande Musullulu, Joel S. Raymond, Bianca Wilson, Mia Langguth, and Michael T. Bowen. 2019. “Oxytocin and Vasopressin Inhibit Hyper-Aggressive Behaviour in Socially Isolated Mice.” *Neuropharmacology* 156 (September): 107573. https://doi.org/10.1016/j.neuropharm.2019.03.016.

Tang, Yan, Diego Benusiglio, Arthur Lefevre, Louis Hilfiger, Ferdinand Althammer, Anna Bludau, Daisuke Hagiwara, et al. 2020. “Social Touch Promotes Interfemale Communication via Activation of Parvocellular Oxytocin Neurons.” *Nature Neuroscience* 23 (9): 1125–37. https://doi.org/10.1038/s41593-020-0674-y.

Tantirigama, Malinda L. S., Helena H.-Y. Huang, and John M. Bekkers. 2017. “Spontaneous Activity in the Piriform Cortex Extends the Dynamic Range of Cortical Odor Coding.” *Proceedings of the National Academy of Sciences* 114 (9): 2407–12. https://doi.org/10.1073/pnas.1620939114.

Terral, Geoffrey, Arnau Busquets-Garcia, Marjorie Varilh, Svein Achicallende, Astrid Cannich, Luigi Bellocchio, Itziar Bonilla-Del Río, et al. 2019. “CB1 Receptors in the Anterior Piriform Cortex Control Odor Preference Memory.” *Current Biology* 29 (15): 2455-2464.e5. https://doi.org/10.1016/j.cub.2019.06.041.

Tirko, Natasha N., Katherine W. Eyring, Ioana Carcea, Mariela Mitre, Moses V. Chao, Robert C. Froemke, and Richard W. Tsien. 2018. “Oxytocin Transforms Firing Mode of CA2 Hippocampal Neurons.” *Neuron* 100 (3): 593-608.e3. https://doi.org/10.1016/j.neuron.2018.09.008.

Tobin, V. A., G. Arechaga, P. J. Brunton, J. A. Russell, G. Leng, M. Ludwig, and A. J. Douglas. 2014. “Oxytocinase in the Female Rat Hypothalamus: A Novel Mechanism Controlling Oxytocin Neurones During Lactation.” *Journal of Neuroendocrinology* 26 (4): 205–16. https://doi.org/10.1111/jne.12141.

Tort, Adriano B.L., Jurij Brankačk, and Andreas Draguhn. 2018. “Respiration-Entrained Brain Rhythms Are Global but Often Overlooked.” *Trends in Neurosciences* 41 (4): 186–97. https://doi.org/10.1016/j.tins.2018.01.007.

Tribollet, E, S Charpak, A Schmidt, M Dubois-Dauphin, and Jj Dreifuss. 1989. “Appearance and Transient Expression of Oxytocin Receptors in Fetal, Infant, and Peripubertal Rat Brain Studied by Autoradiography and Electrophysiology.” *The Journal of Neuroscience* 9 (5): 1764–73. https://doi.org/10.1523/JNEUROSCI.09-05-01764.1989.

U

Uchida, Naoshige, and Zachary F Mainen. 2003. “Speed and Accuracy of Olfactory Discrimination in the Rat.” *Nature Neuroscience* 6 (11): 1224–29. https://doi.org/10.1038/nn1142.

V

Vanderwolf, C.H. 1992. “Hippocampal Activity, Olfaction, and Sniffing: An Olfactory Input to the Dentate Gyrus.” *Brain Research* 593 (2): 197–208. https://doi.org/10.1016/0006-8993(92)91308-2.

Verhagen, Justus V, Daniel W Wesson, Theoden I Netoff, John A White, and Matt Wachowiak. 2007. “Sniffing Controls an Adaptive Filter of Sensory Input to the Olfactory Bulb.” *Nature Neuroscience* 10 (5): 631–39. https://doi.org/10.1038/nn1892.

Vigneaud, Vincent du, Charlotte Ressler, John M. Swan, Carleton W. Roberts, and Panayotis G. Katsoyannis. 1954. “The Synthesis of Oxytocin [1].” *Journal of the American Chemical Society* 76 (12): 3115–21. https://doi.org/10.1021/ja01641a004.

W

Wachowiak, Matt. 2011. “All in a Sniff: Olfaction as a Model for Active Sensing.” *Neuron* 71 (6): 962–73. https://doi.org/10.1016/j.neuron.2011.08.030.

Wacker, Douglas, and Mike Ludwig. 2019. “The Role of Vasopressin in Olfactory and Visual Processing.” *Cell and Tissue Research* 375 (1): 201–15. https://doi.org/10.1007/s00441-018-2867-1.

Wahis, Jérôme, Angel Baudon, Ferdinand Althammer, Damien Kerspern, Stéphanie Goyon, Daisuke Hagiwara, Arthur Lefevre, et al. 2021. “Astrocytes Mediate the Effect of Oxytocin in the Central Amygdala on Neuronal Activity and Affective States in Rodents.” *Nature Neuroscience* 24 (4): 529–41. https://doi.org/10.1038/s41593-021-00800-0.

Welker, W.I. 1964. “Analysis of Sniffing of the Albino Rat 1).” *Behaviour* 22 (3–4): 223–44. https://doi.org/10.1163/156853964X00030.

Wesson, Daniel W, Ryan M Carey, Justus V Verhagen, and Matt Wachowiak. 2008. “Rapid Encoding and Perception of Novel Odors in the Rat.” Edited by Howard B Eichenbaum. *PLoS Biology* 6 (4): e82. https://doi.org/10.1371/journal.pbio.0060082.

Wesson, Daniel W., and Donald A. Wilson. 2011. “Sniffing out the Contributions of the Olfactory Tubercle to the Sense of Smell: Hedonics, Sensory Integration, and More?” *Neuroscience & Biobehavioral Reviews* 35 (3): 655–68. https://doi.org/10.1016/j.neubiorev.2010.08.004.

Wesson, Daniel W. 2013. “Sniffing Behavior Communicates Social Hierarchy.” *Current Biology* 23 (7): 575–80. https://doi.org/10.1016/j.cub.2013.02.012.

Williams, Jessie R., Thomas R. Insel, Carroll R. Harbaugh, and C. Sue Carter. 1994. “Oxytocin Administered Centrally Facilitates Formation of a Partner Preference in Female Prairie Voles (Microtus

Ochrogaster)." *Journal of Neuroendocrinology* 6 (3): 247–50. https://doi.org/10.1111/j.1365-2826.1994.tb00579.x.

Wilson, Donald A., and Regina M. Sullivan. 2011. "Cortical Processing of Odor Objects." *Neuron* 72 (4): 506–19. https://doi.org/10.1016/j.neuron.2011.10.027.

Y

Yom-Tov, Elad, Damien Lekkas, and Nicholas C. Jacobson. 2021. "Association of COVID19-Induced Anosmia and Ageusia with Depression and Suicidal Ideation." *Journal of Affective Disorders Reports* 5 (July): 100156. https://doi.org/10.1016/j.jadr.2021.100156.

Yoshida, M., Y. Takayanagi, K. Inoue, T. Kimura, L. J. Young, T. Onaka, and K. Nishimori. 2009. "Evidence That Oxytocin Exerts Anxiolytic Effects via Oxytocin Receptor Expressed in Serotonergic Neurons in Mice." *Journal of Neuroscience* 29 (7): 2259–71. https://doi.org/10.1523/JNEUROSCI.5593-08.2009.

Young, Larry J., Scott Muns, Zuoxin Wang, and Thomas R. Insel. 1997. "Changes in Oxytocin Receptor MRNA in Rat Brain During Pregnancy and the Effects of Estrogen and Interleukin-6." *Journal of Neuroendocrinology* 9 (11): 859–65. https://doi.org/10.1046/j.1365-2826.1997.00654.x.

Young, Larry J, Zuoxin Wang, and Thomas R Insel. 1998. "Neuroendocrine Bases of Monogamy," 5.

Young, W. Scott, and June Song. 2020. "Characterization of Oxytocin Receptor Expression Within Various Neuronal Populations of the Mouse Dorsal Hippocampus." *Frontiers in Molecular Neuroscience* 13 (March): 40. https://doi.org/10.3389/fnmol.2020.00040.

Youngentob, Steven L., Maxwell M. Mozell, Paul R. Sheehe, and David E. Hornung. 1987. "A Quantitative Analysis of Sniffing Strategies in Rats Performing Odor Detection Tasks." *Physiology & Behavior* 41 (1): 59–69. https://doi.org/10.1016/0031-9384(87)90131-4.

Z

Zaninetti, Marc, and Mario Raggenbass. 2000. "Oxytocin Receptor Agonists Enhance Inhibitory Synaptic Transmission in the Rat Hippocampus by Activating Interneurons in Stratum Pyramidale: Oxytocin Action in the Hippocampus." *European Journal of Neuroscience* 12 (11): 3975–84. https://doi.org/10.1046/j.1460-9568.2000.00290.x.

Zhao, K. 2004. "Effect of Anatomy on Human Nasal Air Flow and Odorant Transport Patterns: Implications for Olfaction." *Chemical Senses* 29 (5): 365–79. https://doi.org/10.1093/chemse/bjh033.

Zhou, Xiao-Bo, Susanne Lutz, Frank Steffens, Michael Korth, and Thomas Wieland. 2007. "Oxytocin Receptors Differentially Signal via Gq and Gi Proteins in Pregnant and Nonpregnant Rat Uterine Myocytes: Implications for Myometrial Contractility." *Molecular Endocrinology* 21 (3): 740–52. https://doi.org/10.1210/me.2006-0220.